Signal Processing Approaches for Cardio-Respiratory Biosignals with an Emphasis on Mobile Health Applications

PAR

Leila MIRMOHAMADSADEGHI

EPFL

ÉCOLE POLYTECHNIQUE
FÉDÉRALE DE LAUSANNE

Suisse
2017

Abstract

We humans are constantly preoccupied with our health and physiological status. From precise measurements such as the 12-lead electrocardiograms recorded in hospitals, we have moved on to mobile acquisition devices, now as versatile as smart-watches and smart-phones. Established signal processing techniques do not cater to the particularities of mobile biomedical health monitoring applications. Moreover, although our capabilities to acquire data are growing, many underlying physiological phenomena remain poorly understood.

This thesis focuses on two aspects of biomedical signal processing. First, we investigate the physiological basis of the relationship between cardiac and breathing biosignals. Second, we propose a methodology to understand and use this relationship in health monitoring applications.

Part I of this dissertation examines the physiological background of the cardio-respiratory relationship and indexes based on this relationship. We propose a methodology to extract the respiratory sinus arrhythmia (RSA), which is an important aspect of this relationship. Furthermore, we propose novel indexes incorporating dynamics of the cardio-respiratory relationship, using the RSA and the phase lag between RSA and breathing. We then evaluate, systematically, existing and novel indexes under known autonomic stimuli. We demonstrate our indexes to be viable additions to the existing ones, thanks to their performance and physiological merits.

Part II focuses on real-time and instantaneous methods for the estimation of the breathing parameters from cardiac activity, which is an important application of the cardio-respiratory relationship. The breathing rate is estimated from electrocardiogram and imaging photoplethysmogram recordings, using two dedicated filtering schemes, one of which is novel. Our algorithm measures this important vital rhythm in a truly real-time manner, with significantly shorter delays than existing methods. Furthermore, we identify situations, in which an important assumption regarding the estimation of breathing parameters from cardiac activity does not hold, and draw a road-map to overcome this problem.

In Part III, we use indexes and methodology developed in Parts I and II in two applications for mobile health monitoring, namely, emotion recognition and sleep apnea detection from cardiac and breathing biosignals. Results on challenging datasets show that the cardio-respiratory indexes introduced in the present thesis, especially those related to the phase lag between RSA and breathing, are successful for emotion recognition and sleep apnea detection. The novel indexes reveal to be complementary to previous ones, and bring additional insight into the physiological basis of emotions and apnea episodes.

To summarize, the techniques proposed in this thesis help to bypass shortcomings of previous approaches in the understanding and the estimation of cardio-respiratory coupling in real-life mobile health monitoring.

Keywords: electrocardiogram, respiratory sinus arrhythmia, heart rate variability, breathing rate, phase lag, phase lag variability, phase lag synchronization, time-varying filter, notch filter, band-pass filter, altitude acclimatization, sleep apnea, emotion, imaging photoplethysmography.

Résumé

L'être humain a toujours été préoccupé par sa santé et sa physiologie. Des mesures électrocardiographiques précises à 12 dérivations, nous sommes passés à présent aux dispositifs mobiles, tels que les dénommés smart-phones, ou encore les textiles électroniques et les "vêtements intelligents". Les méthodes de traitements de signaux conventionnelles ne répondent pas aux besoins de ces nouvelles applications. De plus, en dépit de nos avancées technologiques sur les méthodes d'acquisition, les phénomènes physiologiques sous-jacents n'en demeurent pas moins peu élucidés.

Ce travail de thèse porte sur deux aspects du traitement de signaux biomédicaux. Dans un premier temps, nous examinons les bases physiologiques de la relation entre les activités cardiaque et respiratoire. Ensuite, nous proposons une méthodologie pour comprendre et utiliser cette relation.

La première partie de cette thèse traite la relation cardio-respiratoire et les indices basés sur celle-ci. Nous proposons une méthodologie pour extraire l'arythmie sinusale respiratoire, un élément important de cette relation. De plus, nous proposons de nouveaux indices reflétant la dynamique de la relation cardio-respiratoire, basés sur l'arythmie sinusale et son déphasage par rapport à la respiration. Nous évaluons ensuite de manière systématique les nouveaux indices, ainsi que les indices conventionnels avec des stimuli connus liés au système nerveux autonome. Nous démontrons que nos indices constituent des additions avantageuses aux indices existants de par leurs bonnes performances et leur interprétabilité physiologique.

La deuxième partie de cette dissertation est dédiée à l'estimation du rythme respiratoire à partir du rythme cardiaque, une application importante de la relation cardio-respiratoire. Le rythme respiratoire est estimé en utilisant l'électrocardiogramme et des mesures de vidéo-photo-plethysmogramme, avec deux méthodes de filtrage dédiées, dont une novatrice. Notre algorithme mesure ce rythme vital important en temps réel, avec des retards plus bas que les méthodes existantes. De plus, nous identifions les limitations d'une hypothèse importante lors de l'estimation des paramètres respiratoires avec les méthodes conventionnelles, et proposons une solution pour y remédier.

Dans la troisième partie de ce travail, nous utilisons les indices et la méthodologie des deux premières parties pour des applications de surveillance de la santé, en particulier, la reconnaissance des émotions et les apnées du sommeil. Les résultats sur des données complexes démontrent que les indices cardio-respiratoires proposés dans cette thèse, en particulier ceux liés au déphasage entre l'arythmie sinusale et la respiration, sont utiles pour la reconnaissance d'émotions et d'apnées du sommeil. Ces indices novateurs se révèlent complémentaires aux indices existants et offrent un aperçu nouveau sur la physiologie de ces phénomènes.

En résumé, les techniques proposées dans cette thèse peuvent permettre de combler les lacunes des méthodes existantes pour la compréhension et l'estimation du couplage cardio-respiratoire dans les applications de surveillance de la santé de la vie réelle.

Mots-clés : électrocardiogramme, arythmie sinusale respiratoire, variabilité du rythme cardiaque, rythme respiratoire, déphasage, variabilité de déphasage, synchronisation de déphasage, filtre variable dans le temps, filtre coupe-bande, filtre passe-bande, acclimatation à l'altitude, apnée du sommeil, émotion, vidéo-photoplethysmographie.

Remerciements

Un travail de doctorat ne s'effectue jamais seul. Je tiens à remercier :

Contents

II Estimation of Breathing Parameters using the RSA 53

List of Acronyms

k-NN	*k*-Nearest Neighbors
ANS	autonomic nervous system
AR	autoregressive
BB	β-blocker
BL	baseline
bpm	beats-per-minute
BR	breathing rate
brpm	breaths-per-minute
CAF	caffeine
ECG	electrocardiogram
EEG	electroencephalogram
EMD	empirical mode decomposition
EMG	electromyogram
FIR	finite impulse response
GSR	galvanic skin response
HF	high frequency
HR	heart rate
HRV	heart rate variability
IIR	infinite impulse response
IMF	intrinsic mode function
iPPG	imaging photoplethysmography
IR	infrared
LF	low frequency
LMS	least mean squares
PL	phase lag
PLS	phase lag synchronization
PLV	phase lag variability

PPG	photoplethysmography
PSD	power spectral density
PSG	polysomnography
PTT	pulse transit time
RPA	R-peak amplitudes
RSA	respiratory sinus arrhythmia
sb	spontaneous breathing
SNR	signal to noise ratio
SSA	singular spectrum analysis
STD	standard deviation
STFT	short time Fourier transform
SVM	support vector machine
SWASVD	sliding window adaptive singular value decomposition

List of Tables

List of Figures

Introduction

<div style="text-align: right; font-size: 3em;">**1**</div>

1.1 Motivation and problem statement

We, as humans, have always been curious about our health and possible ways to preserve it. Technological advances have helped us become more acquainted with our physiology. Precise measuring techniques, such as 12-lead electrocardiography, have allowed us to observe and understand many physiological phenomena and to make major breakthroughs in medicine. Today, with modern sensors, data processing and storage, we are capable of recording and processing large amounts of health-related data. We use smart-phones and wearables such as smart watches and smart shirts, which increasingly accompany us in our daily life and record continuous physiological data, not only when we are sick, but also when are healthy. Monitoring at-risk situations increases the chances of identifying and addressing health-problems in early stages and helps people to pursue a healthy lifestyle. Furthermore, the availability of longer-term data has allowed us to study our health in a different manner, taking into account variations over longer periods of time. With these devices, we have a growing number of means to record a vast amount of data about our physiology and health. We rely on signal processing tools and methods to transform this data into knowledge.

The focus of the present thesis is on signal processing techniques for cardiac and breathing biosignals, particularly designed for real-life applications, such as health-monitoring with wearables. We place a special emphasis on the cardio-respiratory relationship.

Indeed, most of the physiological signals we record reflect information about the heart. It is understandable, as the diseases of this vital organ are the leading cause of mortality in humans. In conventional cardiac signal processing, aside from the obvious direct monitoring of the heart function, changes in the heart rhythm are used as a surrogate to study the autonomic nervous system (ANS). The ANS is an important part of our nervous system, managing key involuntary functions of the body. The indirect monitoring of ANS activity is preferred, as it avoids the burden of monitoring nerve traffic in-vivo. Heart rate variability (HRV) analysis has attempted to study the mechanisms of ANS regulation, and its relation to different stimuli and even to pathology. In conventional HRV analysis, the spectrum of the heart inter-beat intervals is divided into several pre-defined frequency bands, each linked in the past to the activations of different ANS branches through observational studies [1]. Recently, these measures have been contested, because they are largely based on general assumptions, with little physiological justification, and have experimentally been proven ill-conceived [2, 3]. Furthermore, frequency-based analysis provides only mean values and important information from transitions may be lost.

Heart function is closely linked to the pulmonary breathing function through the ANS [4].

Respiratory sinus arrhythmia (RSA) is an element of HRV defined as the modulation of the heart inter-beat intervals concomitant with breathing [5, 6]. Its measurement is linked to conventional HRV analysis and is performed generally within the HRV framework. Although there is a vigorous debate on the flaws of the current methodology [2, 3], HRV indexes, and especially the RSA, are increasingly used to assess a number of different physiological and psychological occurrences. By virtue of their link to the ANS, HRV indexes are widely accepted physiological markers and have been shown to be altered by clinical conditions, psycho-behavioral predicaments and in a larger sense, any external or internal stimulus affecting the ANS [1, 7].

Despite the open methodological questions and disputes, the advent of mobile health monitoring with user-friendly wearables and portable devices has further fueled the rapid rise in popularity of ANS indexes based on the cardio-respiratory relationship, while introducing new complications [8–12]. These easy-to-use devices acquire signals in a continuous manner in a variety of real-world applications and present two main challenges from the signal processing viewpoint. First, the current technology requires a compromise between ease-of-use and signal quality. For example, the breathing signal acquired with an impedance belt embedded in a smart-shirt textile is usually of a poorer quality than one acquired in a laboratory, while the subject wears an airflow mask. Indeed, the smart-shirt may move, the subject may run, change posture, temperatures and humidity may change, the subject may sweat, etc. Second, in mobile health-monitoring applications, the user may need/wish to follow the outcome of the measurement in a real-time manner. Although signals are acquired in real-time, the vast majority of signal processing techniques rely on established methodologies, which were not designed to cater to real-time conditions. An example is the estimation of physiological rhythms, such as the heart rate or the breathing rate. The most popular choice in estimating the frequency of an oscillation is spectral analysis. Spectral analysis is achieved through power spectral density (PSD) estimation, or time-frequency analysis. PSD analysis is unsuitable for non-stationary data as the temporal dimension of the spectral information is lost. As a result, the estimated values are representative of a time-window and not a time-instant, and do not produce a real-time instantaneous result when considered for a health-monitoring application. Time-frequency analysis, such as short-term Fourier transform (STFT), provides a mapping of a signal frequency content over time. However, it requires further non-trivial processing among other drawbacks. Spectral methods, in general, suffer from the well-known time-frequency resolution trade off, as computations are performed on a block-by-block basis.

It is increasingly important to adapt conventional signal processing methods to the particular conditions of signals acquired with portable devices. Furthermore, for regulated medical devices, any processing method should be interpretable from a physiological viewpoint, by an expert physician, for its outcome to be medically salient.

To summarize, two aspects of cardio-respiratory signal processing are the focus of this thesis. First, the physiological basis of measurements and measurement techniques are investigated. Second, the convenience of the methods from the viewpoint of complexity and timing is held at high importance. For mobile health monitoring, it is not only important for methods to be real-time, or near real-time, but also that they reflect adequately the underlying processes and especially transitions and fast changes.

1.2   Objectives

Despite the recent years' rise in awareness about cardio-respiratory health and our ability to monitor it, we are not coming closer to an exact knowledge on many of the underlying physiological mechanisms, as apparent from the diverging opinions of experts. Furthermore, existing methods do not answer to many of the modern health-monitoring particularities. There is, therefore, an unmet need for methods with physiological validation, that, at the same time, adhere to

the requirements of emerging health-monitoring applications.

The present dissertation is aimed at investigating existing and novel HRV indexes related to the RSA, as autonomic markers, and to apply them in several mobile health-monitoring applications. To do so, a primary aim is to study existing HRV indexes in the context of known autonomic stimuli, and to re-evaluate the methodology to define the RSA, and RSA-related indexes. One important application of the RSA is the estimation of breathing parameters. Therefore, a second, but equally important goal, is to re-visit breathing rate estimation from the RSA, in a truly real-time and instantaneous manner. We aim to apply an existing algorithm and to evaluate and overcome its shortcomings with respect to the particular needs of real-time processing. A related goal is the estimation of the breathing rate by using the RSA acquired with heart monitoring technologies other than the electrocardiogram. Finally, one last goal is to apply the methodology and indexes developed in the present thesis to monitoring applications.

To summarize, the main objectives of this thesis are:
- to define the instantaneous RSA in a generalized manner,
  - to re-evaluate the potential of RSA as an HRV marker,
- to define novel means and indexes to assess the autonomic balance from the HRV,
  - to evaluate these novel indexes in real conditions,
- to provide a methodology for robust real-time estimation of breathing parameters from the HRV,
- to investigate the potential of the novel HRV measures in monitoring applications.

1.3   Organization

This dissertation is divided into three parts. The first part is focused on the physiology of the RSA and its relationship to breathing. The second part is dedicated to the estimation of breathing parameters from cardiac signals. The third part consists of two applications for novel cardio-respiratory indexes. The three parts are described in more detail as follows.

Part I: Physiological Study

This part consists of theoretical background and several studies on RSA characterization. Chapter 2 introduces the concept of HRV, RSA and considerations on autonomic activity in relation with the regulation of cardiac and breathing functions. We describe conventional means for the measurement of RSA, and discuss its clinical and psycho-behavioral utility. In Chapter 3, we present a methodology for RSA extraction and novel cardio-respiratory indexes and apply them, along with conventional HRV measures, to a set of measurements performed under known autonomic stimuli. In Chapter 4, we explore the autonomic particularities of exposure to altitude using measures introduced in Chapter 3.

Part II: Estimation of Breathing Parameters using the RSA

This part is centered on one of the well-known practical applications of the cardio-respiratory relationship, namely, estimating the breathing rate from the breathing modulation of cardiac activity. In Chapter 5, we propose two algorithms for the estimation of the instantaneous breathing rate from the RSA, as measured from the electrocardiogram (ECG), in real-time. We then apply one of the algorithms to estimate the instantaneous breathing rate from the RSA, but using the novel contact-less imaging-based photoplethysmography technique in Chapter 6. As the two previous chapters rely on assumptions about the recording conditions, in Chapter 7, we propose a generalized scenario for the estimation of breathing parameters from ECG recordings.
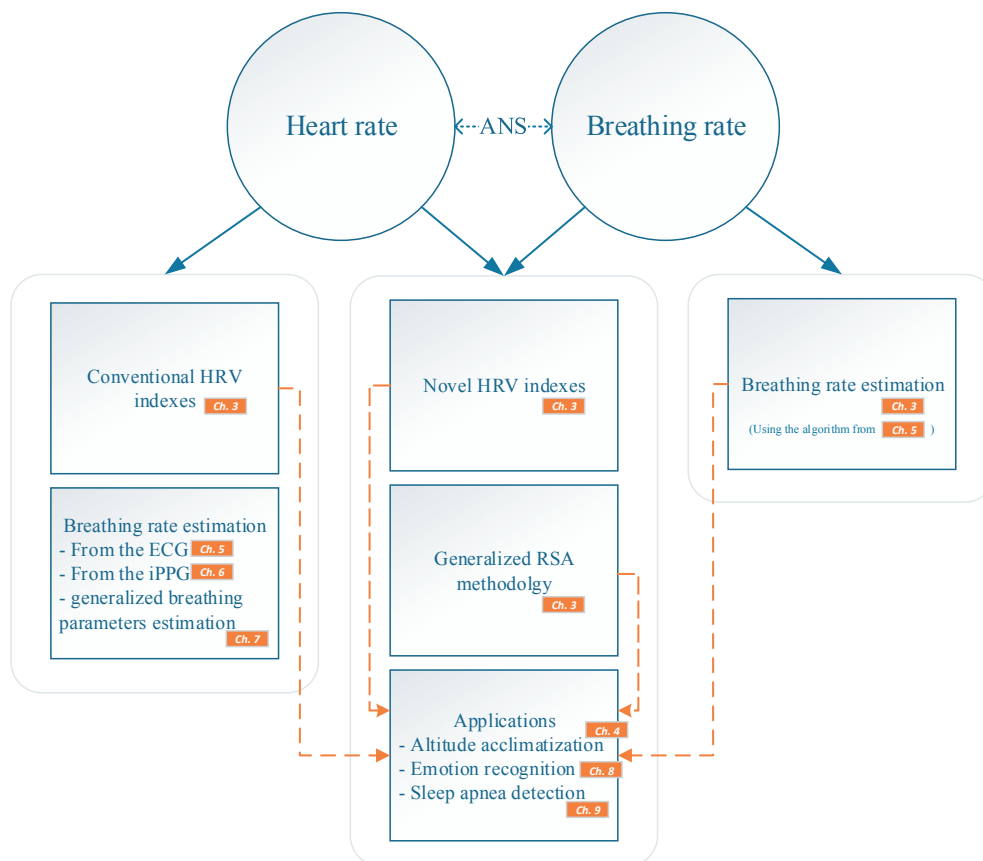
Figure 1.1: Illustration of the links between the chapters of the present dissertation. ANS: autonomic nervous system; HRV: heart rate variability; ECG: electrocardiogram; iPPG: imaging photoplethysmogram; RSA: respiratory sinus arrhythmia.

Part III: Applications

This part contains two applications for the methodology presented in parts I and II. In Chapter 8, we explore the applicability and accuracy of the cardio-respiratory indexes introduced in this dissertation for the task of automatic emotion recognition. In Chapter 9, we explore the cardio-respiratory correlates of these indexes with sleep apnea conditions and delves into the automatic screening of such events using wearables and real-time signal processing methods.

Chapter 10 concludes this dissertation with a summary of achievements and perspectives. There are four appendices in this dissertation. Appendix A contains several relevant definitions, while the other three enclose further results related to several chapters.

Figure 1.1 illustrates the links between the chapters of the present dissertation.

1.4   Original contributions

The main contributions of this work are [1]:

- **Physiological study**
  - Formulation of a generalized methodology to define the instantaneous RSA.
  - Design of novel indexes to study autonomic influences on the HRV based on the cardio-respiratory relationship.
  - Introduction of these indexes to improve existing means of ANS assessment in particular cases such as known autonomic conditions, exposure to altitude, ANS correlates of emotions, and ANS particularities of sleep apnea.

- **Estimation of breathing parameters**
  - Application of an existing frequency estimation algorithm for estimating the instantaneous breathing rate from the breathing modulation of cardiac activity in real-time.
  - Development of a novel instantaneous and real-time capable frequency estimation algorithm to overcome shortcomings of the previous method.
  - Application of the proposed methodology to estimating the breathing rate from the novel cardiac monitoring technique of imaging photoplethysmography.

- **Applications**
  - Application of novel HRV indexes and RSA methodology for emotion recognition from cardiac and breathing signals.
  - Application of novel HRV and RSA indexes to aid in sleep apnea detection with cardiac and breathing signals acquired in non-laboratory conditions.

---

1. See also a list of the publications at the end of this manuscript (p. 179)

Part I

Physiological Study

Respiratory Sinus Arrhythmia (RSA)

2

This chapter explores the physiological background on the variations in the heart rhythm in Section 2.1, and in particular the breathing-related variations in Section 2.2. The quantification and measurement of these variations is covered in Section 2.3, and finally, Section 2.4 gives a brief overview of the importance and applications of these measurements.

2.1 Heart rate regulation

Every heartbeat starts with electrical impulses generated by the sinoatrial node. The sinoatrial node is a cluster of cells with particular electrical properties, located in the right atrium of the heart. These cells have no resting potential and therefore "fire" in a regular manner, making the sinoatrial node the natural pacemaker of the heart. These electrical impulses spread throughout the atria and cause them to contract, thereby filling the ventricles with their content in blood. The impulses are then transfered to the ventricles, causing them to contract and pump blood out to the entire body. The sinoatrial node generates impulses thanks to the properties of its cells. However, the rate of firing is controlled by the nervous system and in particular the autonomic nervous system (ANS) [13]. As seen on Figure 2.1, the human nervous system receives sensory inputs and provides motor control. The motor control division has two main branches, the somatic system, associated with voluntary muscle control and the ANS, unconsciously maintaining the functions of internal organs. The ANS is further divided into the parasympathetic and sympathetic systems. The parasympathetic system maintains rest-and-digest functions such as the regulation of the heart rate and the breathing rate, while the sympathetic system is involved in fight-or-flight responses. Each of these branches exert control via their specific nerves, receptors and organic chemicals (hormones) [14].

Both the sympathetic and parasympathetic branches of the ANS innervate various parts of the heart as illustrated in Figure 2.2. Both innervate in particular the sinoatrial node, and affect how it generates electrical impulses and thus affect the heart rate. The sympathetic nerves also innervate the ventricles, exerting control on the contraction of the ventricles. They innervate the atrioventricular node as well, thereby controlling the conduction between the atria and the ventricles. The parasympathetic nervous system, slows the heart rate by slowing the rhythm of the sinoatrial node and by slowing the transmission of the impulses generated by it from the atria into the ventricles, all by releasing a specific hormone, acetylcholine [4]. The vagus nerve and its subsequent branches, the vagi, carry parasympathetic messages. On the other hand, in response to external or internal stimuli, the sympathetic nervous system increases the heart rate to accelerate the responses of the body. By releasing the hormone norepinephrine, it increases

9
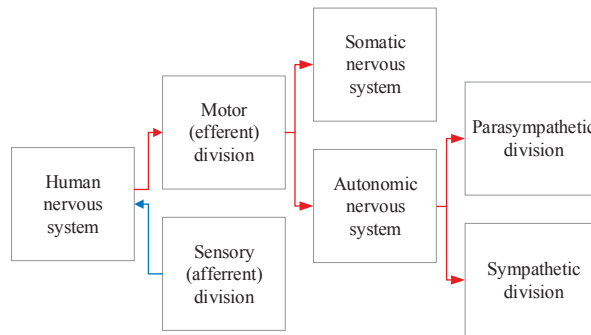
Figure 2.1: The human nervous system.
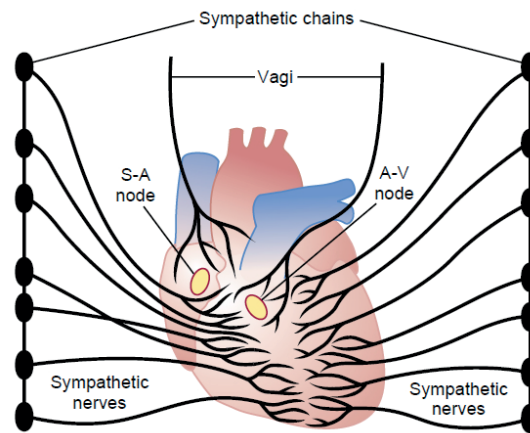
Figure 2.2: Parasympathetic and sympathetic innervation of the heart. The S-A node is the sinoatrial node, where electrical impulses generating each heartbeat originate from. The A-V node is the atrioventricular node, which transfers the electrical impulses originating in the sinoatrial node from the atria to the ventricles. Image from [15] with permission, © Elsevier 2006.

the rate of discharge in the sinoatrial node, increases the conduction between the atria and the ventricles and increases the contraction force in the cardiac muscles [4]. The combination of these events leads to an increased heart rate.

The baroreflex mechanism is an important element controlling the sympathetic and parasympathetic drive to the heart [4]. Stretch receptors located in the carotid arteries and in the aorta react to changes in blood pressure. If blood pressure is too high, causing the vessels to stretch, the baroreceptors communicate this event to the brainstem by firing action potentials at a faster-than-normal rate. As a response, the parasympathetic system action is increased and the sympathetic action is inhibited. Consequently, the heart rate is decreased, peripheral vessels are dilated and the blood pressure is quickly decreased. If the blood pressure falls (for example after assuming an orthostatic position), the baroreceptors sense the drop and fire at a slower rate than normal. The sensing of this event in the brain triggers an increase in the sympathetic nervous system activity and a decrease in that of the parasympathetic system. Thus, the heart rate is increased, vessels are constricted and the blood pressure increases.

The study of heart rate variability (HRV), i.e. the variations of the heart inter-beat intervals, in a systematic and widespread manner, started and was further facilitated with the emergence of the electrocardiogram (ECG) in the twentieth century even though heart rhythm variations were observed and documented in the eighteenth and nineteenth centuries through auscultation.

In the second half of the twentieth century, with the advent of precise monitoring techniques and digital data processing, the study of HRV flourished. HRV has been studied in part to uncover its underlying physiological mechanisms. In particular, the exact autonomic events triggering HRV have been a matter of interest, as monitoring nerve signals directly is a cumbersome endeavor and HRV was early-on linked with the ANS and the brainstem. On the other hand, physicians linked HRV events to medical and pathological conditions, and psychophysiologists linked HRV with psychophysiological and behavioral conditions.

2.2   What is RSA?

Respiratory sinus arrhythmia (RSA) is the naturally occurring change in the interval between heartbeats in relation to the pulmonary breathing [5, 6]. The heartbeats occur nearer each other upon inspiration, and during expiration their distance lengthens. This phenomenon exists in all vertebrates and is linked to pulmonary gas exchange, optimizing the transport of oxygen to the body via the circulatory system [16–18] and energy exchange [6, 19]. The RSA is illustrated in Figure 2.3, as seen in the electrical activity of the heart (ECG).
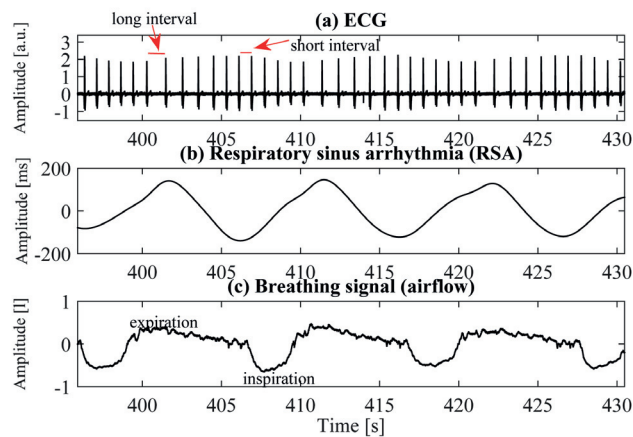
Figure 2.3: Illustration of the RSA. (a) the ECG, (b) RSA and (c) reference breathing signal.

The RSA has been observed, described and studied since at least over a century ago. Fast and shallow breathing produces a smaller variation than slow and deep breathing [6]. However, the exact mechanisms and physiological origins of RSA remain unknown. There are two much-debated theories, one associating it with a central mechanism, another with a blood volume and baroreflex mechanism [20–22]. According to the central-mechanism theory, a central breathing gating of vagal motoneuron responses entirely explains the RSA, based on the observation that vagal cardiac motoneuron membrane potentials fluctuate at breathing frequencies [21]. The shortening of the heart beat intervals during inspiration would be due to the inhibition of the vagal control of the heart concurrent with lung inflation. During expiration, the vagal nerve activity reaches its maximum and thus lengthens the interval between heartbeats [17, 18]. For this reason, the RSA is often used as a parasympathetic marker. The dependence of the kinetics of the heart sinoatrial node on body posture and breathing enforces this view [21]. However, the

perpetuation of RSA, although in a reduced form, after blockade of the receptors of both sympathetic and vagal systems and even after a vagotomy indicates there must be different or additional mechanism involved [14, 23].

According to the baroreflex-mechanism theory (blood volume), RSA is mainly a reflex mechanism [20]. It is assumed that breathing induces blood pressure changes, which in turn translate into heart rate changes because of the baroreflex. In other words, the RSA stabilizes blood pressure [24]. However, there is debate on whether latencies related to the breathing-related fluctuations in the heart rate are physiologically plausible within the baroreflex framework [21]. On the other hand, fetal RSA has been recorded at a gestational age of 36 weeks [18], when there are no breathing fluctuations so to speak of. Similarly, RSA persists during apnea and coincides with diaphragm activity, even in the absence of oxygen intake [25].

The above-mentioned mechanisms have each their advocates and critics, however, it has been suggested that they may be involved in parallel in the generation of the RSA, especially given that they are both "central" in that both are operated from the brainstem [19, 25]. Other inputs may have been overlooked in these theories, such as feedback from the lungs and atrial stretch receptors [26].

To summarize, cardiac vagal traffic seems to have a role in the RSA formation, although it is not the only contributing factor [6]. The RSA is therefore often used as an index of vagal activity. It has been suggested that the RSA reflects vagal tone because of evidence for the central mechanism although it must not be considered synonymous with vagal activity as breathing affects the RSA, presumably through baroreflex mechanisms.

2.3   RSA measurement techniques

The RSA is measured in the context of HRV analysis. Most often, the inter-beat intervals are measured from the ECG. The R-peak of the ECG, as indicated in Figure 2.4, represents the heartbeat, with the QRS complex reflecting the heart ventricular re-polarization [27].
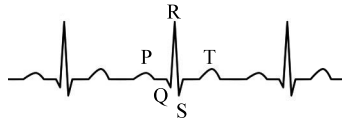
Figure 2.4: Three heartbeats in a normal ECG. The R-wave represents the heartbeat.

The RSA has been defined in the following manners:

(a) The power of the R-R intervals occurring at the breathing rate, in which case the RSA is expressed in terms of squared time units:

The time differences between successive R-peaks constitutes the R-R intervals time series. However, the values of this time series, i.e. the intervals between heartbeats, are variable and therefore the time series is naturally unequally sampled. Most commonly, the midpoint of each interval is selected as time-index for that interval, as illustrated in Figure 2.5. Then the time series is re-sampled uniformly at 4 Hz through cubic spline interpolation [28] [1]. Since the normal breathing rate of humans is most often in the range of 10-30 breaths-per-minute, the RSA is often defined as the HRV occurring in those frequency ranges through spectral analysis [1, 18, 24, 29–51]. More precisely, the breathing bandwidth is designated by the high frequency (HF) range, defined as the fixed range of 0.15 -0.4 Hz [1], illustrated in Figure 2.6, which is assumed to contain the breathing. Such values are conventionally computed in 60-120 s windows of data according to

---

1. Several interpolation techniques are discussed in Appendix A
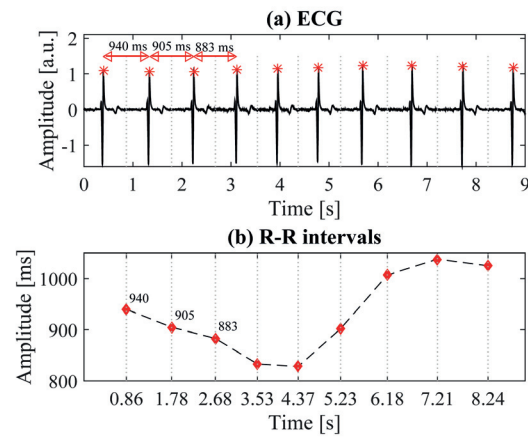
Figure 2.5: R-R intervals time series illustration. (a) The ECG and the R-peaks. (b) The R-R intervals constituted from the time-differences between consecutive R-peaks.

the guidelines [1]. There have been propositions to adjust the bandwidth of interest in special cases to include lower and higher breathing frequencies, for example to 0.12- 1 Hz [32, 52–54].
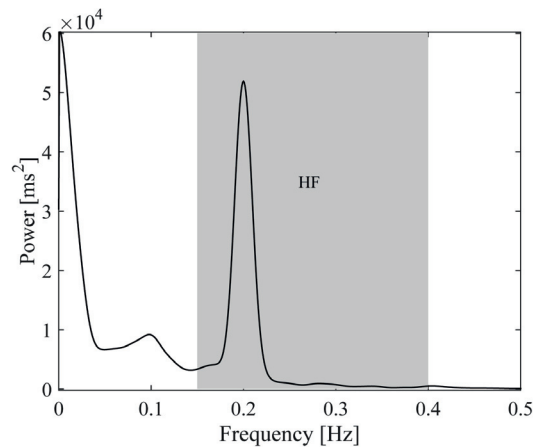
Figure 2.6: The power spectral density of an R-R intervals time series from a 10-minute recording in supine position, while the subject was breathing constantly at 0.2 Hz with the aid of an auditory signal (metronome). The HF frequency band is highlighted.

(b) The average difference between the shortest and longest R-R intervals, in time units, for example in milliseconds:

Given that spectral analysis only captures the mean values of the RSA, different methods for the breath-by-breath or second-by-second analysis of the RSA have been proposed. In breath-by-breath analysis, the RSA is the difference in heart rate between peak and trough [32, 55–57], or the difference between the shortest inter-beat interval during inspiration and the longest during expiration [58]. Second-by-second characterization of the RSA has also been performed via vector-autoregressive modeling [59]. The square root of mean successive differences between ECG R-waves has also been used as an index of the RSA [60].

(c) The RSA waveform, containing the breathing-related oscillation of the R-R intervals as illustrated in Figure 2.3 (b), represented by amplitudes on a time scale, such as milliseconds:

The RSA waveform has been extracted form the R-R intervals in several ways such as adaptive filtering [61], principal component analysis [62], phase-rectified signal averaging [63–65], autoregressive modeling [66], orthogonal subspace projection [67, 68], and mathematical modeling of the relationship between the cardiac autonomic regulation and breathing [19, 69, 70].

Other points of view in characterizing the RSA involve the approximate entropy of the R-R intervals time-series [32], Poincaré plots [18, 71], time-frequency analysis [72, 73], and symbolic analysis [74]. Recently, the cross-correlation between the breathing waveform and the R-R intervals series was also proposed as a means to quantify the RSA [75].

The HRV and the RSA can also be measured from other cardiac signals apart from the ECG, such as photopletysmographs [76–78], which derive from the blood volume changes in the vessels due to heartbeats. They have also been measured with non-contact measurement techniques, such as imaging photoplethysmography [79] and Doppler radar cardiopulmonary remote sensing [80, 81].

2.4   Usefulness of RSA

RSA can be acquired in a relatively easy and non-invasive manner and is believed to reflect, at least partly, the ANS function as it has been related to the parasympathetic nervous system. It is therefore a very widely used descriptor and has long been considered a clinical and psycho-physiological indicator [7, 82, 83]. It is often used as a clinical marker for a given health-related condition or as a means to characterize response to a given stimuli. Although the neuro-physiological basis of the link between autonomic regulation of the heart and psycho-behavioral traits is not completely understood, RSA and other HRV parameters have been observed to have specific trends with pathological and psycho-physiological processes. Changes in these indexes are thought to aid in elucidating changes in the autonomic function related to pathological and psychological states [1, 84, 85]. This section enumerates some recent studies (2011-2016) involving RSA analysis, and is meant to give an overview of the wide range of clinical and psycho-physiological utility of cardio-respiratory indexes and in particular the RSA. It is by no means a comprehensive review.

Cardiac health

Because of its (at least partly) cardiac vagal origin, the RSA has been used to study particular aspects of cardiac health [86]. Several HRV indexes, including the HF power have been used to study autonomic regulation in relationship with myocardial infarction [47]. Several HRV indexes, in particular the RSA, have been used in the early detection of cardiac iron accumulation before myocardial dysfunction [87]. The RSA has also been employed in studying autonomic particularities of the postural tachycardia syndrome in children [88].

Response to disease

The RSA, as measured with the HRV HF power, was used in the prediction of the levels of inflammatory markers [89]. It has also been used to study autonomic dysfunction in breast cancer patients [43].

Mental health

As the ANS function may reflect on other cerebral functions given the inter-linked nature of the human nervous system, several HRV measures pertaining to the cardio-respiratory relationship have been employed to analyze autonomic particularities of schizophrenia [38] and other mental illnesses [90].

Stress

Given its (at least partly) autonomic origins, the RSA is thought to reflect on the mental state. It has been shown, for instance, to be affected by mental stress [34, 67]. The RSA defined as the HF power of the HRV has been linked to anxiety and attention control [91], response to worry [44], and the prediction of preoperative stress [92], and post-deployment post-traumatic stress disorder [93]. The RSA has also been used to study maternal prenatal anxiety in relation with infant negative affectivity [94] and maternal depressive symptoms in relation to toddler sleep quality [95]. RSA levels have also been used as markers in studying the link between socioeconomic status and self-reported stress [96]. They have also been used to assess social adaptations mechanisms in maltreated children [97].

The RSA reactivity, i.e. the change in RSA in response to task demands, has been linked to internalization and externalization symptoms [52, 98, 99] and also to the relation between aggression and internalization symptoms in children [100, 101]. The RSA reactivity has also been used as a measure in self-regulation and effortful control in children [57, 102].

Emotions

The HF HRV power has been used to assess autonomic changes in response to musci-induced emotions [103]. The RSA has been used as a marker in understanding children with neurobehavioral disinhibition [54]. Greater RSA has been observed during the experience of compassion [104]. RSA levels have been measured in studying attachment insecurity in adolescents [105]. In a biofeedback context, the success of the voluntary upregulation of the RSA predicted altruistic behavior [49].

The RSA levels of students exaggerating their grade averages were used to study their anxiety about academic performance [106].

RSA levels have been shown to be affected with the experience of transient emotions [107]. They have also been used as markers in studying emotion regulation [37, 48, 108–111].

Sleep

The RSA and its relationship to other cardiac variables has been used in the study of sleep stages [55, 112] and sleep apnea [75]. RSA levels have been linked to sleep quality [35], and the effects of obesity on sleep quality [113].

Long-stating psycho-physiological conditions

The RSA has also been studied in relation to long-standing mental states, such as personality traits in general [114] or disorders, for example in the prediction of depressive symptoms [40, 45, 46, 51]. Changes in the RSA were shown to be potentially useful in the analysis and diagnosis of autism spectrum disorder [36, 53, 115, 116], and borderline personality disorder [117]. The RSA has also been used to study long-term physiological correlates of emphatic behavior [118] and Internet gaming addiction [119].

Variations of the RSA over time have been linked to psycho-physiological synchrony in husband-wife dyads [42]. RSA levels have been investigated in the context of the relationship

between marital conflicts and children's sleep [41]. The RSA has been used to predict eating disorder symptoms and their relationship to parenting [120]. The co-regulation of the RSA in romantic partners has been studied in the context of the association between relationship and health [121]. The RSA was also measured to study cardio-respiratory synchronization of choir singers [122].

RSA levels have been used for the prediction of the quality of life of breast cancer survivors [60].

Mental tasks

The phase synchronization between the RSA and the breathing waveform was reduced during mental tasks such as arithmetic calculations [34, 123]. The RSA has been used in the prediction of implicit learning [124].

Autonomic-mediated responses to non-pathological stimuli

The RSA was shown to increase when viewing a green urban scene in comparison with a built urban setup, placing emphasis on the positive influence of green scenes on the parasympathetic tone and the autonomic regulation [58, 125, 126].

Autonomic reactivity, as measured by changes in the RSA, was found to be associated with narrative-aligned behavior, in particular in the context of appeal for charitable giving [39].

The phase relationship between the RSA and the breathing waveform has been used to study the autonomic responses during food ingestion [50, 127].

The RSA defined as the HF power of the HRV has also been used to assess autonomic changes occurring with athletic training [128].

Breathing-related parameters of the HRV, such as the HF power have been used to characterize autonomic particularities of altitude exposure [129–135], which is of importance in the prediction of mountain sickness [136, 137].

The RSA has been used to derive the breathing rate in a convenient and non-invasive manner, as conventional breathing monitoring requires cumbersome apparatus [28, 138, 139].

Characterization of the RSA and the Autonomic Balance

<div style="float:right; font-size:4em; font-weight:bold;">3</div>

This chapter describes the non-invasive assessment of ANS function using the HRV and RSA. Mapping RSA alterations to known ANS stimuli is discussed by examining the existing literature and by reporting results of new experiments. Elements of the methods and results reported in this chapter were presented as a conference paper [140].

3.1 Non-invasive assessment of the autonomic balance

Changes in ANS responsiveness to an excitatory stimulus are hypothesized to be related to pathological conditions [128]. There is considerable interest to track changes in the ANS activity in a non-invasive manner, as probing for nerve signals requires delicate invasive methods. As discussed in Chapter 2, the heart rhythm is controlled by the ANS. Therefore, HRV analysis is a choice means to assess changes in the ANS [141, 142].

In HRV analysis, the low frequency (LF) power of the inter-beat intervals, the high frequency (HF) power, and the ratio of the LF/HF powers are often used as autonomic indexes [1, 2, 143]. The LF power, between 0.04 Hz and 0.15 Hz is believed to reflect the activation of the sympathetic and parasympathetic branches of the ANS [1]. In humans, there are particular oscillations in the LF band at around 0.1 Hz. These oscillations have been linked to functions of the baroreflex loop [144, 145], and also seem related to the sympathetic innervation of the baroreflex, as they are attenuated by the blockade of sympathetic receptors [145]. As these oscillations constitute an important part of the LF power, the LF power and the power ratio LF/HF are used as markers of sympathetic activation [2, 146]. The HF power, between 0.15 Hz and 0.4 Hz is believed to reflect the parasympathetic branch of the ANS and is related to breathing as discussed in Chapter 2. The underlying physiological justifications of these autonomic indexes remain a matter of debate [20–22]. One avenue into the exploration of the relation of these indexes to autonomic states, is to observe their responses to particular autonomic stimuli. As such, the links between autonomic events and these indexes can be studied in a cause-and-effect manner, and consolidated or challenged.

3.1.1 Body posture alteration of the autonomic balance

Changing one's body posture is an easy an rapid manner of inducing autonomic changes [128]. When one is in the supine position, blood circulation occurs in a horizontal manner as the height difference between the heart and major body parts is small. When one stands up, this height difference increases. It has been reported that standing increases (up to 10-fold) the LF power

as compared to the supine position, while decreasing the HF power [88, 128, 147–149]. The increase in LF power in the orthostatic position is hypothesized to be either due to increased blood pressure fluctuations causing increased beat-to-beat interval fluctuations, or increased baroreflex control of the blood pressure.

3.1.2   Effects of controlled breathing on the autonomic balance

Often, the RSA has been studied under controlled breathing, which involves controlling the breathing rate or volume or both [150]. Doing so reduces variations due to spontaneous breathing and facilitates the identification of the RSA. However, the process of controlling the breathing parameters induces changes to the physiological state because of the mental effort involved in addition to the disruption of the bi-directional interaction between cardiac control and breathing function control [151]. It has been hypothesized that the mental processes required to control one's breathing entail an increase of sympathetic activity, which reduces the breathing fluctuations on the cardiac rhythm [150]. However, in a ramped breathing protocol, the muscle sympathetic nerve activity was found to be lower during controlled breathing compared to spontaneous breathing [152].

Studies investigating the effect of controlled breathing on RSA magnitude (most frequently as measured by the HF power of the HRV) have found very different results, ranging from a nearly 50% decrease to no change, to nearly 90% increases in the RSA amplitude induced by the breathing mode [56, 150, 153, 154]. In studies reporting a large increase in RSA magnitude, high breathing rates such as 0.25 Hz and 0.33 Hz were imposed. Studies in which no differences were found, either normalized the RSA amplitude using the tidal volume or used a frequency close to that of each subject's spontaneous breathing for controlling the breathing rate [56, 150].

Regarding the adjustment of the breathing volume, when the breathing rate is controlled, subjects automatically modify their tidal volume, such that in one study, the investigators found no noticeable differences between the actual inspired volume when the tidal volume was not controlled and when the tidal volume was controlled to maintain normal alveolar ventilation regardless of breathing rate [155].

Combining an increase in respiratory frequency and a decrease in the respiratory volume induced a larger decrease in the HF power than each maneuver alone [156].

3.1.3   Pharmacological altering of the autonomic balance

To study the ANS responses to specific autonomic conditions, it is possible, by administering drugs, to artificially modify the ANS control on the heart. Specific drugs block the receptor sites related to each of the ANS branches. The β-blockers are a class of drugs that block the receptors of the norepinephrine hormone involved in the sympathetic nervous system activation [157]. By blocking the receptor sites of the norepinephrine hormone, the sympathetic influence over the heart rhythm is effectively null.

If, as is believed, the LF band was mediated by both the sympathetic and parasympathetic systems, and the HF band was mostly mediated by parasympathetic activity, blockade of the sympathetic system would reduce power in the LF band while leaving the HF band unchanged. Indeed, after β-blocker ingestion, the sympathetic nerve activity has been observed to decrease [23]. However, what has been generally reported in literature after the ingestion of a β-blocker compound such as propranolol, is mostly an increase of the HF power with little decrease or no influence on the LF power [143, 157, 158].

The parasympathetic branch of the ANS can also be blocked by administering an acetylcholine receptor antagonist for example by atropine injection [23, 159].

On the other hand, artificial activation of the sympathetic nervous system in particular, is thought to provide insights into the functioning of ANS in healthy and pathological condi-

tions [160]. One widely used stimulant is caffeine, which has been reported to increase sympathetic nerve activity [161, 162]. The exact effect of caffeine on the ANS is not completely understood yet, although one important event is the inhibition of adenosine receptors [163]. Adenosine, which occurs naturally in the body, is an important vasodilatator [164]. Vasodilatation refers to the widening of the veins and arteries. When blood vessels widen, blood flow is increased and blood pressure decreases. Therefore, caffeine ingestion affects the normal dilatation of the veins and arteries, affecting blood pressure and eliciting sympathetic activation [161].

Caffeine ingestion stimulates the ANS, however with conflicting effects. For example, its reported effects on the heart rate range from decrease to no change to increase [162, 165–167]. Regular ingestion of caffeine was reported to increase HRV as measured by the standard deviation of the normal inter-beat intervals, with no significant effect on the LF and HF powers and their ratio [160]. In another study, punctual intake of caffeine was reported to increase the HF power with no effect on the LF power [168].

3.1.4 Motivation and contribution

The LF-HF partitioning and the use of the LF/HF marker are widely contested [2, 3, 62, 169–171], in part because there is evidence against a clear linear separability of the activations of the two branches of the ANS, but also due to the influence of breathing on HRV [2, 3, 62]. The conventional LF-HF partitioning assumes that the breathing rate is between 0.15 Hz and 0.4 Hz. However, in practice, the influence of breathing can extend to the LF band, when the breathing rate is below 0.15 Hz or 9 breaths-per-minute (brpm) [3, 170]. For instance, people with athletic training for example often have low resting breathing rates [3, 172]. Furthermore, breathing rates higher than 24 breaths-per-minute (0.4 Hz) are also likely to occur, especially during exercise, in children, or in pathological conditions [173]. There have been propositions to adjust the bandwidth of interest in special cases, for example to 0.12- 1 Hz [32, 52–54]. Breathing may occur in the LF or the HF band, or jump from one to the other within a given experimental protocol, and since it has a large influence on the power of the inter-beat intervals, it cannot be ignored when performing HRV analysis [174]. Furthermore, tasks such as speech shift the breathing frequency into the LF band [175]. Some researchers have proposed to analyze the breathing-related and breathing-unrelated HRV [62], while others propose to center the HF band on the breathing rate and to adjust the LF boundary accordingly [169].

RSA extraction

RSA is a widely used physiological marker related to the HF power as reported in Chapter 2. If extracted by taking into account the reference breathing waveform instead of fixed bandwidth-filtering the inter-beat intervals based on general assumptions, the RSA has the advantage of always being related to breathing and the parasympathetic branch of the ANS in contrast to the limitations of the standard LF-HF partitioning. Existing methods to extract the RSA according to the breathing waveform have many limitations when considering real-time health monitoring applications. Phase-rectified signal averaging and projection methods are based on analyzing fixed-length segments of data [62–65, 67, 68]. Adaptation to real-time processing requires empirical choices on the length of data to be analyzed. Filtering-based methods seem to perform poorly in the presence of wide-band spontaneous breathing [66]. Mathematical modeling of the cardio-respiratory relationship aims at uncovering the RSA generation mechanisms and have not been intended to provide a "functional" RSA waveform, for instance to study RSA responses to particular autonomic stimuli [19, 69, 70].

Given the growing interest in real-time processing, for example in mobile health monitoring applications, the automatic extraction of the RSA from the inter-beat interval times series is

achieved by local filtering of the HRV with the true breathing rate measured from the breathing waveform.

Phase relationship between the RSA and the breathing waveforms

Furthermore, the relationship and the synchronization between the RSA and the breathing waveforms are of particular interest, as it may bring valuable information about the autonomic control of the cardio-respiratory system [176–178]. The breathing and the RSA waveforms are mostly in phase opposition, as inspiration coincides with the shortening of R-R intervals (minimum of RSA) [34, 63, 64, 179]. The autonomic effects on this relationship have not been widely studied, although it has been reported that β-blocker ingestion did not modify this phase lag [179]. Postural changes on the other hand, affected this phase difference between the cardio-vascular and breathing signals [180]. This phase relationship has also been studied in the context of the autonomic characterization of mental stress [34, 177], altitude exposure effects [133], cardio-respiratory synchronization of choir singers [122], the autonomic effects of age and coronary artery disease [181] and sleep stage and sleep apnea characterization [55, 112, 182].

The phase relationship is most often studied by using the signal instantaneous phases, as measured with the Hilbert transform [34, 112, 133, 177, 180]. The Hilbert transform is an important linear operator in signal processing. It derives from a given input, its analytic representation, extended into the complex plane. The instantaneous phase of the signal is then derived from the phase of the analytic signal [183]. However, for the Hilbert transform to yield meaningful results, the input needs to be narrow-band [184–186].

Once the phase of the RSA has been defined, it can be further employed to characterize various aspects of the cardio-respiratory relationship. In particular, the ratio of heart beats to breathing cycles, deduced visually from the cardio-respiratory synchrogram, has often been used to characterize the cardio-respiratory relationship [55, 112, 133, 181, 187].

The synchronization of the phase lag between the RSA and breathing waveforms, reported as the mean angular dispersion of the phase differences in the complex space, is another parameter used sometimes to describe the cardio-respiratory relationship [34, 122].

Mapping HRV and RSA indexes to autonomic conditions using known autonomic stimuli

In the present chapter, changes in the RSA and the autonomic control of the heart are studied in the supine and orthostatic body positions, assumed to elicit parasympathetic and sympathetic dominance, respectively. They are also studied under the influence of β-blocker drugs (sympathetic blockade) and caffeine (sympathetic activation), for both spontaneous and controlled breathing.

The RSA and several aspects of the relationship between breathing and the RSA are investigated and compared to the conventional autonomic indexes of the LF and HF power and the LF/HF ratio. The relationship between breathing and the RSA is assessed with the phase lag between them, as well as its variability and its synchronization. The variation of the phase lag was used as an index in [188] to assess the relationship of the fundamental and first harmonic of specific biosignals, and thus their regularity, which is reflected in their phase difference [189].

3.2   Materials and methods

3.2.1   Data acquisition

Young healthy volunteers were recruited. The single-lead ECG and breath-by-breath airflow were recorded simultaneously with an in house ECG device and the Medgraphics spirometer (Medgraphics, CPX, St. Paul, MN, USA) respectively. The two data streams were acquired with

a sampling frequency of 1000 Hz using an analogue-to-digital converter (PowerLab 16/30, ADInstruments, Bella Vista, Australia) and recorded with commercially available software (LabChart v.7.2 ADInstruments, Bella Vista, Australia) [1].

Study 1- Autonomic alterations induced by body posture

Data were recorded from 21 healthy volunteers (16 men, age 34 ± 8 years, weight 78 ± 17 kg, height 178 ± 9 cm). Recordings were performed while the subjects lay supine for 8 minutes and then stood in the orthostatic position for 7 minutes breathing spontaneously. An example of the acquired signals is shown in Figure 3.1. All the study procedures were in accordance with the Declaration of Helsinki, and the study was approved by the Canton de Vaud ethical committee (#2016-00308). The subjects gave informed consent prior to participation.
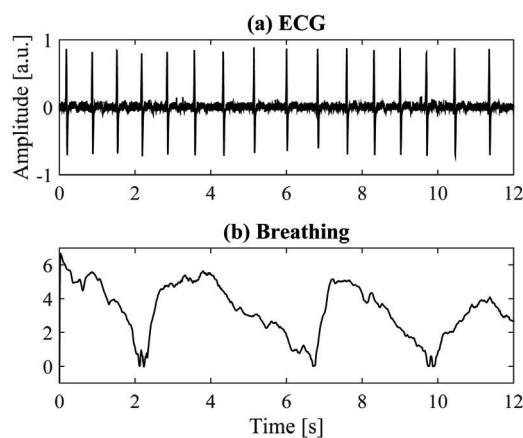
Figure 3.1: The (a) ECG and (b) breathing waveform for one subject in supine position.

Study 2- Autonomic alterations induced by controlled breathing and pharmacological manipulations

Data were recorded from 17 healthy volunteers (10 men, age 33 ± 9 years, weight 78 ± 22 kg, height 175 ± 10 cm). The recordings were performed over two days for each subject. The subjects were asked to refrain from coffee, alcohol and tobacco use on the days of the experiment. One day the subjects underwent recording 45 minutes after the ingestion of a β-blocker drug (propranolol, 0.2 mg/kg, administered by pills [179]) and the other day (random order), they underwent recording 45 minutes after the ingestion of caffeine (6 mg/kg, administered by pills [190, 191]). Each recording session consisted of a 10-minute spontaneous breathing (sb) segment, a 10-minute segment breathing at 9 brpm, with the help of a metronome and a 10-minute segment breathing at 12 brpm, also with the help of a metronome (in a random order). On each day, baseline recordings were performed before the subjects ingested the drugs in all three breathing modes (in the same breathing-mode order). All recordings were performed in a laboratory setting, with a temperature of 25 ± 2 °C and 44 ± 7% humidity. All the study procedures were in accordance with the Declaration of Helsinki, and the study was approved by the Canton de Vaud ethical committee (#451/14). The subjects gave informed consent prior to participation and filled a medical questionnaire.

---

1. The data acquisition was coordinated by Nicolas Bourdillon, from the Institute of Sport Science of the University of Lausanne.

3.2.2 Data processing

The ECG R-peaks were extracted. The maxima of the signal were identified with a local extrema detection method, adjusting the maxima detection constraints based on the autocorrelation of the ECG in a 30-second window. All the extractions were manually inspected and artifacts were removed. The R-R intervals series was then created and re-sampled uniformly at 4 Hz using cubic spline interpolation[2], by setting the time index of each interval to its midpoint as described in Section 2.3. The breathing signal was re-sampled similarly to the R-R intervals time series. Both signals were filtered with a Butterworth filter (order 18) between 0.06 and 1 Hz to remove drift and high frequency artifacts. The heart rate in beats-per-minute (bpm) was computed from the inverse of the R-R intervals.

The RSA was extracted from the pre-processed R-R intervals by bandpass filtering the latter with a time-varying filter with the transfer function H described in (3.1) centered on the breathing rate f_{br}. In (3.1), $\beta = 0.95$ defines the filter bandwidth as narrow and selective (as illustrated in Figure B.1 in Appendix B).

$$H(z; n) = \frac{1 - \beta}{2} \frac{1 - z^{-2}}{1 - \cos(2\pi f_{br})(1 + \beta)z^{-1} + \beta z^{-2}}. \tag{3.1}$$

Using H, with the pre-processed R-R intervals series as input, the RSA is extracted as:

$$
\begin{aligned}
RSA[n] &= \cos(2\pi f_{br}[n])(\beta + 1)RSA[n-1] - \beta RSA[n-2] \\
&+ 0.5(1 - \beta)(RR[n] - RR[n-2]),
\end{aligned} \tag{3.2}
$$

where $RSA[2] = RSA[1] = RR[1]$ for $n > 2$.

The breathing rate f_{br} was estimated from the re-sampled breathing signal by using a notch filter bank estimation algorithm (see Section 5.2.2). Briefly, this method consists in identifying the dominant frequency of a signal by probing the outputs of a bank of FIR notch filters spaced equally over a given bandwidth. The instantaneous frequency of the signal is estimated as the weighted sum of the notch frequencies, where the weights are computed using the inverse of the filter output powers.

The outcome, $RSA[n]$, was subtracted from the R-R intervals to produce the breathing-unrelated component of the R-R intervals:

$$RR_{non-br} = RR - RSA. \tag{3.3}$$

The RSA power (P_{RSA}) was measured from its power spectral density (PSD) estimate (Welch method) over 60-second-long windows with 50% overlap. The breathing-unrelated power of the R-R intervals (P_{non-br}) was computed from RR_{non-br} in a similar manner.

The phase lag (PL) between the RSA and the breathing signal was computed by using the spacing between the successive maxima of the two signals similarly to [178]. Given a reference signal $s1$, the phase lag of another signal $s2$ is computed for each sample n by identifying two successive maxima of the reference signal $p1(s1)$ and $p2(s1)$ and one maximum of the second signal $p1(s2)$ as follows:

$$PL[n] = 2\pi \frac{t_{p1(s2)} - t_{p1(s1)}}{t_{p2(s1)} - t_{p1(s1)}} \quad t_{p1(s1)} < n \le t_{p1(s2)}. \tag{3.4}$$

As illustrated in Figure 3.2, when the phase lag between the two signals is π and the signals are in exact phase opposition, the distance between the maxima of the two signals is half the period of the reference signal, in other words $t_{p1(s2)} - t_{p1(s1)}$ is the half of $t_{p2(s1)} - t_{p1(s1)}$ and the phase lag is correctly computed as π.

---

2. described in Appendix A
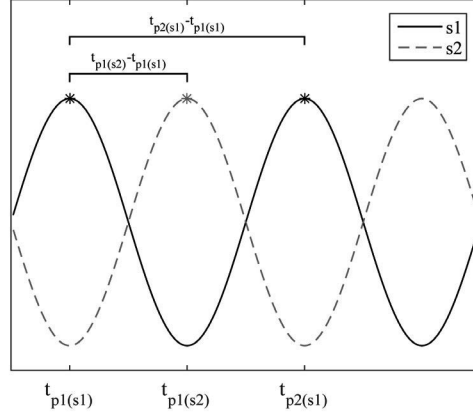
Figure 3.2: Illustration of the phase lag between two signals. The phase lag of $s2$ with respect to $s1$ is computed using the ratio of the time-difference between successive maxima of $s2$ and $s1$ ($t_{p1(s2)} - t_{p1(s1)}$) and two successive maxima of $s1$ ($t_{p2(s1)} - t_{p1(s1)}$). The maxima $p1(s1)$, $p1(s2)$ and $p2(s1)$ are marked with asterisks. In this particular case, given that $t_{p1(s2)} - t_{p1(s1)}$ is half $t_{p2(s1)} - t_{p1(s1)}$, the phase lag is computed as π.

The maxima of each signal were extracted by using a conventional window-based extrema detection method. This window length was empirically set as $2/(3f_{resp})$.

The PL variability (PLV), was assessed by the standard deviation of the slope of the PL [192], computed as:

$$PL_{slope}[n] = \frac{PL[n + L/2] - PL[n - L/2]}{L + 1},\tag{3.5}$$

where $L = 16$ (equivalent to 4 s at the 4 Hz sampling rate chosen here) is the computation window size. This value was empirically chosen to capture an average breathing period and experimentally proved to be adequate. The variation of the slope, i.e. PLV, was computed by calculating the standard deviation of the latter in a sliding window of length $W = 40$ (equivalent to 10 s at the 4 Hz sampling rate chosen here):

$$PLV[n] = STD(PL_{slope}[n - W/2 : n + W/n])\tag{3.6}$$

The phase lag synchronization (PLS), which is the mean angular dispersion of the phase differences in a complex space, was computed as in [34]:

$$PLS[n] = \left| \frac{1}{W} \sum_{j=n-W/2}^{n+W/2} e^{(iPL[j])} \right|^2,\tag{3.7}$$

where $W = 40$ (equivalent to 10 s at the 4 Hz sampling rate chosen here) is the computation sliding window. PLS values range from 0, in the case of randomly distributed phase lags, to 1, if the PL is always constant.

The conventional HRV LF and HF powers were computed in 60-second-long windows with 50% overlap as well as their normalized versions (with respect to the total peak-to-peak intervals power minus the very low frequency band, below 0.04 Hz), nLF and nHF. The LF/HF ratio was also computed.

The power in the breathing-corrected LF and HF bands, denoted as the cLF and cHF powers, were computed from the R-R interval PSD by setting the LF-HF boundary according to the

breathing rate, as $min(f_{br} - \delta f, 0.15)$, where two values of 0.05 and 0.1 Hz were investigated for δf. Their normalized versions ncLF and ncHF were computed similarly to the nLF and nHF powers.

Comparisons were made between the different conditions by directional hypothesis testing using the Mann-Whitney U-test, which does not make assumptions on the distribution of the data.

3.3 Results

3.3.1 Body posture alteration

Results using data from *study 1* are reported in this section. Comparisons were made between the supine (sup.) and orthostatic (orth.) positions and the significance of the p-values for the directional hypothesis testing are reported for the two significance levels of 5% and 10% (trend). There were no significant differences between the instantaneous frequency of the RSA and the instantaneous breathing rate, meaning that the RSA extraction was correct for all subjects. The breathing rates of 12 subjects (57%) were below the LF upper boundary of 0.15 Hz. For six of these subjects (28%), it was close to the baroreflex frequency (0.1 Hz).

Figure 3.3 shows the R-R intervals series for one subject in the supine and orthostatic positions. Figure 3.4 illustrates the PSD of these R-R intervals series. Visually, the breathing influence on the R-R intervals, seen in the main oscillation, is more prominent in the supine position. In both graphs of Figure 3.4, a peak can be seen around 0.1-0.11 Hz because the breathing rate of this subject for both recordings was 0.11 Hz, which is close to the baroreflex frequency. In this case, the HF power does not represent breathing activity at all, and the LF power contains both breathing-related and baroreflex-related power. This case illustrates the need for taking into account the true breathing rate in HRV analysis.
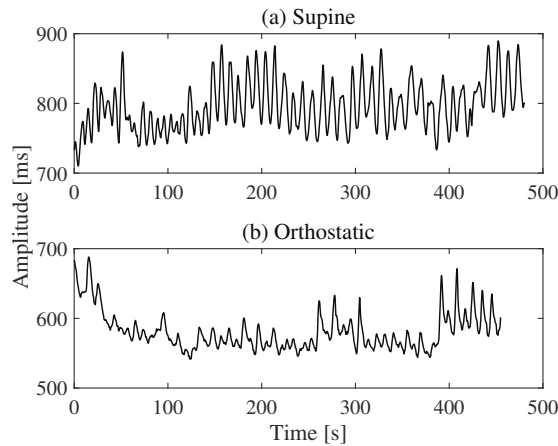
Figure 3.3: The R-R intervals for one subject: (a) in the supine and (b) in the orthostatic positions.

Figure 3.5 reports the heart rates and breathing rates of all subjects in the supine and orthostatic positions. They both increased ($p < 0.05$ for the HF difference and $P < 0.1$ for the BR difference) in the orthostatic position.

Figure 3.6 shows the RSA power and the breathing-unrelated power of the R-R intervals. Both were larger in the supine position although the differences were relatively small ($p < 0.05$ for the RSA power, while the breathing-unrelated power differences were not significant). Figure 3.7
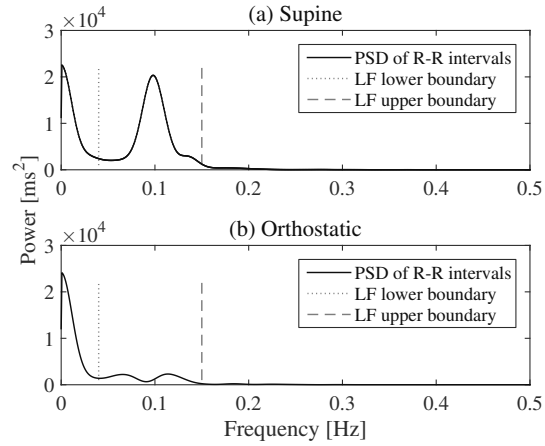
Figure 3.4: The PSD of the R-R intervals in Figure 3.3: (a) in the supine and (b) in the orthostatic positions. In both cases, the breathing frequency was in the LF band, making the usual LF-HF separation meaningless.
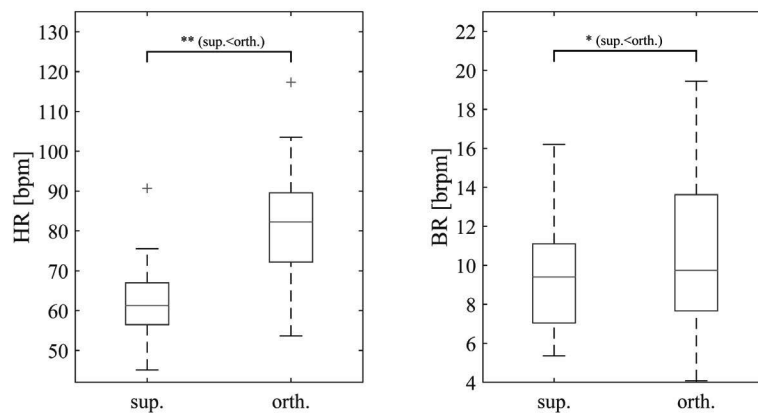
Figure 3.5: The heart rate (HR) and breathing rate (BR) in the supine and orthostatic positions for all 21 subjects. $*p < 0.1$; $**p < 0.05$.

reports the normalized versions of the RSA and breathing-unrelated powers. Differences between the two positions were more visible in the normalized parameters. The normalized RSA power was significantly smaller ($p < 0.05$) in the orthostatic position, while the normalized breathing-unrelated power was significantly larger ($p < 0.05$).
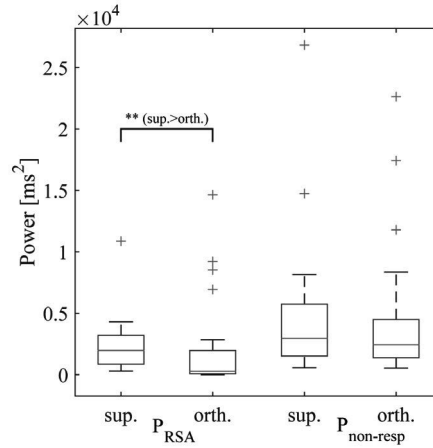
Figure 3.6: The RSA and breathing-unrelated powers in the supine and orthostatic positions for all 21 subjects. $**p < 0.05$.
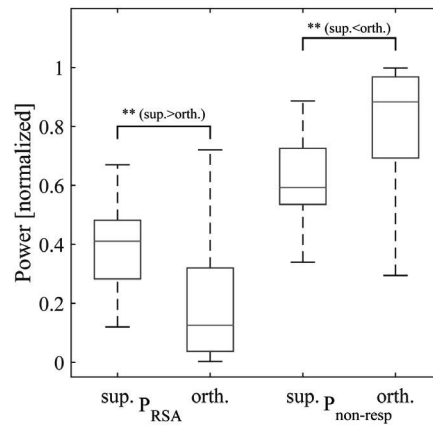
Figure 3.7: The normalized RSA and breathing-unrelated powers in the supine and orthostatic positions for all 21 subjects. $**p < 0.05$.

Figure 3.8 reports the phase-related RSA-breathing synchronization parameters. The PLV was significantly larger ($p < 0.05$) in the orthostatic position while the PLS was significantly smaller ($p < 0.05$). Furthermore, the values of both parameters were more diverse in the orthostatic position. The PL and PL_{slope} did not show any significant differences in the two positions as reported in Appendix B, Figure B.2.

Figure 3.9 reports the LF and HF powers as well as the breathing-corrected cLF and cHF powers over all 21 subjects in the supine and orthostatic positions for $\delta f = 0.05$ Hz. For $\delta f = 0.1$ Hz, the cLF could not be computed for several subjects, as for low breathing rates, the cLF effectively became null. There were no significant differences between the supine and orthostatic
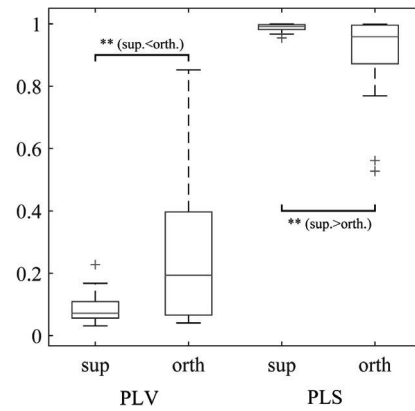
Figure 3.8: The synchronization measures between the RSA and breathing signals in the supine and orthostatic positions for all 21 subjects. $**p < 0.05$.

positions for the LF and cLF powers but the HF and cHF powers were significantly larger (p < 0.05) in the supine position. The cLF was smaller than the LF and the cHF was larger than the HF because the cLF, in contrast to the LF, does not contain any breathing-related power, and the cHF, contrary to the HF, always contains the breathing-related power. The normalized versions reported in Figure 3.10 reveal that the nLF and ncLF powers were significantly larger (p < 0.05) in the orthostatic position. The total R-R intervals power was slightly larger in the supine position as seen in Figure 3.11. The LF/HF and cLF/cHF were also larger (p < 0.1) in the orthostatic position, however the difference is smaller in the case of the breathing-corrected index as seen in Figure 3.12.
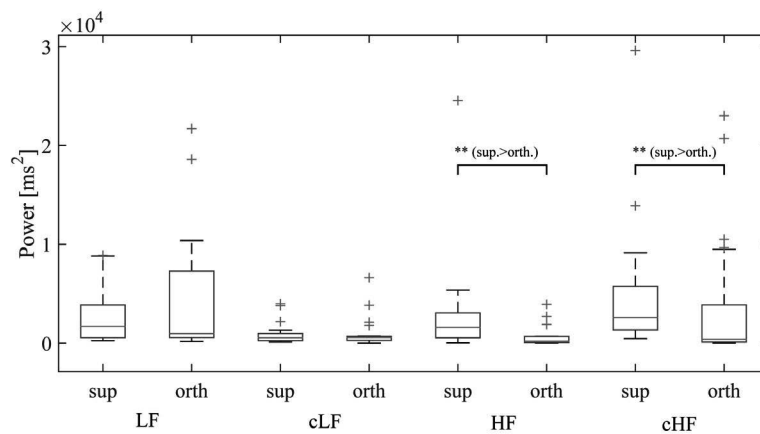
Figure 3.9: The LF, HF, cLF and cHF powers in the supine and orthostatic positions for all 21 subjects. $**p < 0.05$.
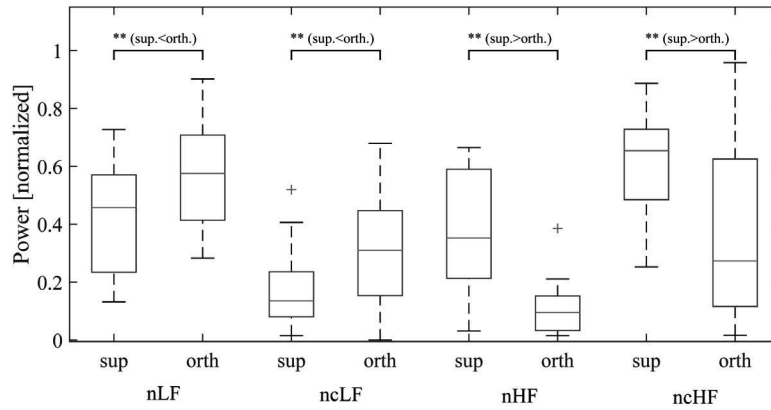
Figure 3.10: The nLF, nHF, ncLF and ncHF powers in the supine and orthostatic positions for all 21 subjects. $**p < 0.05$.
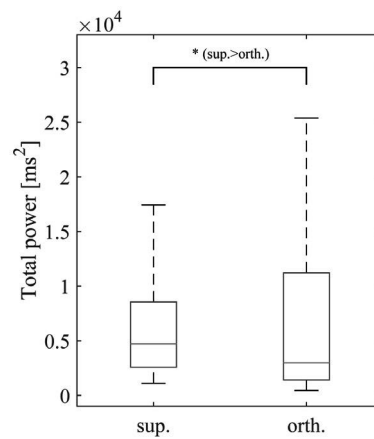
Figure 3.11: The total R-R intervals power in the supine and orthostatic positions for all 21 subjects. $*p < 0.1$.
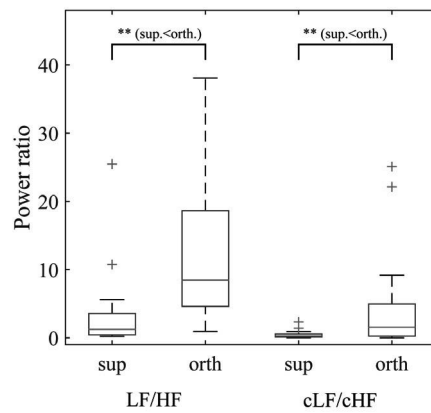
Figure 3.12: The LF/HF index and the breathing-corrected cLF/cHF in the supine and orthostatic positions for all 21 subjects. **$p < 0.05$.

3.3.2 Controlled breathing and pharmacological alteration

Results on data from all subjects in *study 2* are reported here. Comparisons were made between the breathing modes: spontaneous breathing (sb) vs 9 brpm, sb vs 12 brpm and 9 vs 12 brpm at baseline (BL) and between the baseline and each condition, i.e, the β-blocker (BB) and caffeine (CAF) conditions for each breathing mode (BL vs BB or CAF). The significance of the p-values for the directionals hypothesis testing are reported for the two significance levels of 5% and 10% (trend). There were no significant differences between the instantaneous frequency of the RSA and the instantaneous breathing rate, meaning that the RSA extraction was correct for all subjects.

Figure 3.13 reports the breathing rates of all the subjects in the spontaneous breathing sessions (baseline and under β-blocker influence and caffeine influence). The spontaneous breathing rate was below the LF-HF boundary of 0.15 Hz in 34% of all sb records.
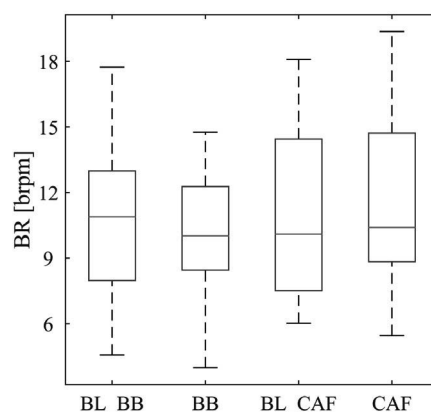
Figure 3.13: The breathing rates during the sb sessions for all 17 subjects. BL: baseline, BB: β-blocker case, CAF: caffeine case.

Figure 3.14 reports the RSA power for all three breathing modes at baseline and under β-

blocker influence. The RSA power was significantly higher under β-blocker influence regardless of the breathing mode. Figure 3.15 reports the same results for the caffeine case. Under caffeine influence, there were no significant differences expect for an increase after caffeine ingestion when breathing at 9 brpm ($p < 0.1$). The only influence of the breathing mode on baselines values, which was observed over the two days of the experiment, was a significant increase in the RSA power when breathing at 9 brpm compared to breathing at 12 brpm.

Figures 3.16 and 3.17 report the normalized RSA powers for the β-blocker and caffeine cases, respectively. The differences observed between baseline and β-blocker influence during spontaneous breathing were not reproduced after normalization. There were no differences between baseline conditions and caffeine ingestion. However, the differences in the baseline values between the breathing modes were maintained for both the β-blocker and caffeine cases.

Figures 3.18 and 3.19 illustrate the breathing-unrelated power in the β-blocker and caffeine cases, respectively. Under β-blocker influence, the breathing-unrelated power was significantly larger than at baseline for all breathing modes. Under caffeine influence, it was significantly larger only during the 9 brpm breathing mode. There were no significant differences or trends between the breathing modes at baseline present in both cases.

Figures 3.20 and 3.21 report the normalized non respiratory power. After β-blocker ingestion, the power decreased in the 9 brpm ($p < 0.1$) and 12 brpm ($p < 0.05$) breathing modes. Caffeine did not have an influence on this parameter. In both cases, at baseline, the power was larger during spontaneous breathing and 12 brpm breathing than 9 brpm breathing.
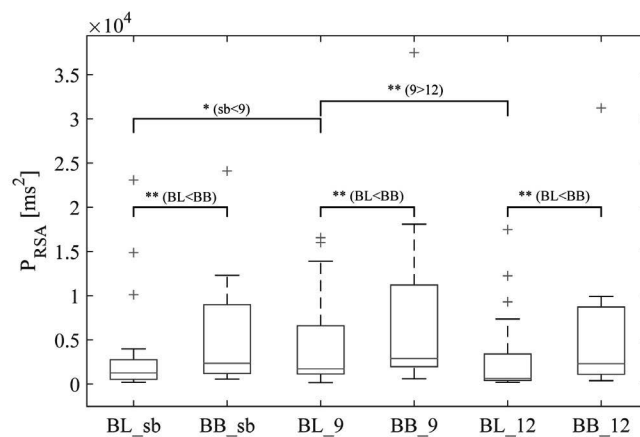
Figure 3.14: The RSA power for the three breathing modes in the β-blocker case for all 17 subjects. BL: baseline, BB: β-blocker influence. *$P < 0.1$; **$P < 0.05$.

Figure 3.22 presents the PL values at baseline and under β-blocker influence in the three breathing modes. During controlled breathing, the PL was smaller under β-blocker influence. There were no significant differences in its values during spontaneous breathing. There were no significant changes in the PL value under caffeine influence compared to baseline as seen in Figure 3.23. There were no significant differences in the baseline values between the different breathing modes consistent in both days.

The analysis of the other phase-related parameters, the PL slope, PLV and PLS did not yield consistent differences. The results pertaining to these parameters are reported in Figures B.3 - B.8, in Appendix B.

The LF power was significantly larger after β-blocker ingestion in all three breathing modes as reported in Figure 3.24. However, the nLF only displayed an increase ($p < 0.1$) in the 9 brpm mode as seen in Figure B.9 in Appendix B. Caffeine changed neither the LF nor nLF values,
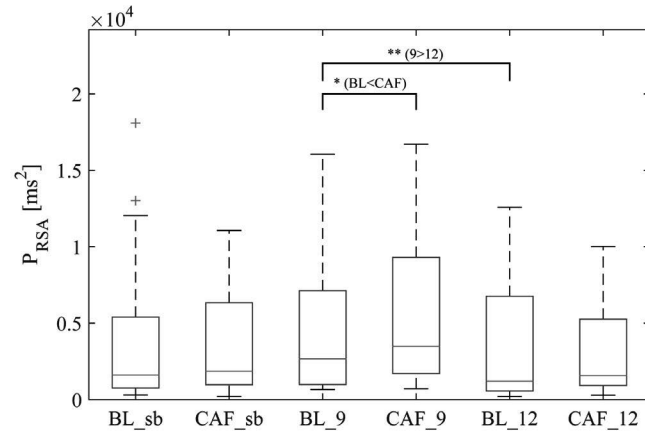
Figure 3.15: The RSA power for the three breathing modes in the caffeine case for all 17 subjects. BL: baseline, CAF: caffeine influence. $*P < 0.1$; $**P < 0.05$.
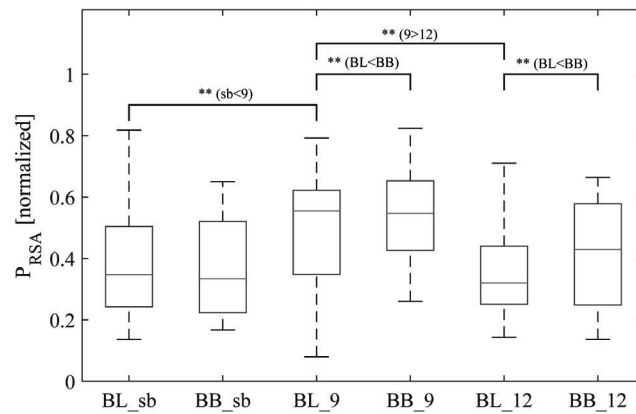
Figure 3.16: The normalized RSA power for the three breathing modes in the β-blocker case for all 17 subjects. BL: baseline, BB: β-blocker influence. $**P < 0.05$.
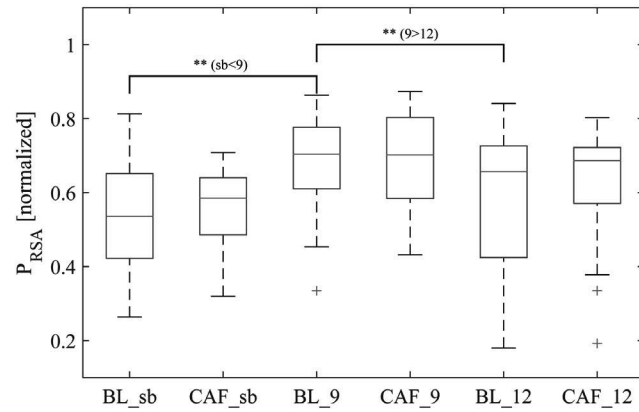
Figure 3.17: The normalized RSA power for the three breathing modes in the caffeine case for all 17 subjects. BL: baseline, CAF: caffeine influence. $**P < 0.05$.
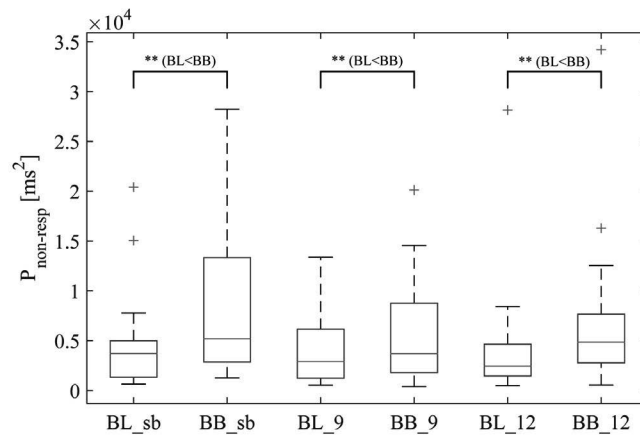
Figure 3.18: The breathing-unrelated power for the three breathing modes in the β-blocker case for all 17 subjects. BL: baseline, BB: β-blocker influence. $**P < 0.05$.
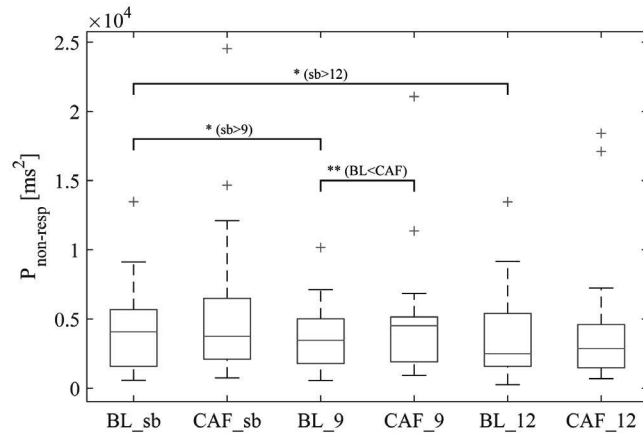
Figure 3.19: The breathing-unrelated power for the three breathing modes in the caffeine case for all 17 subjects. BL: baseline, CAF: caffeine influence. $*P < 0.1$; $**P < 0.05$.
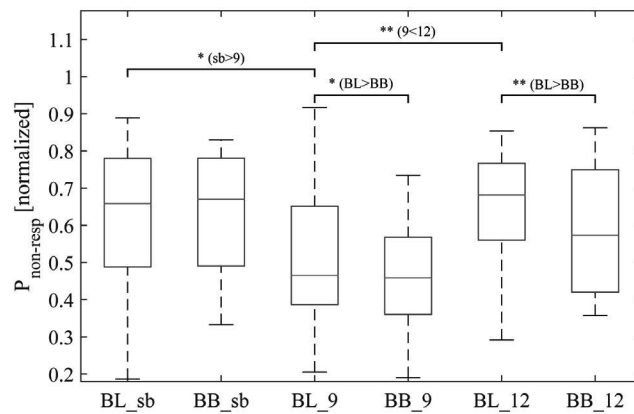
Figure 3.20: The breathing-unrelated power for the three breathing modes in the β-blocker case for all 17 subjects. BL: baseline, BB: β-blocker influence. $*P < 0.1$; $**P < 0.05$.
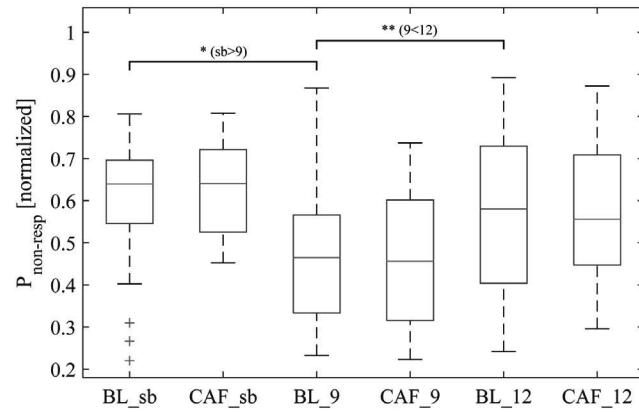
Figure 3.21: The breathing-unrelated power for the three breathing modes in the caffeine case for all 17 subjects. BL: baseline, CAF: caffeine influence. $*P < 0.1$; $**P < 0.05$.
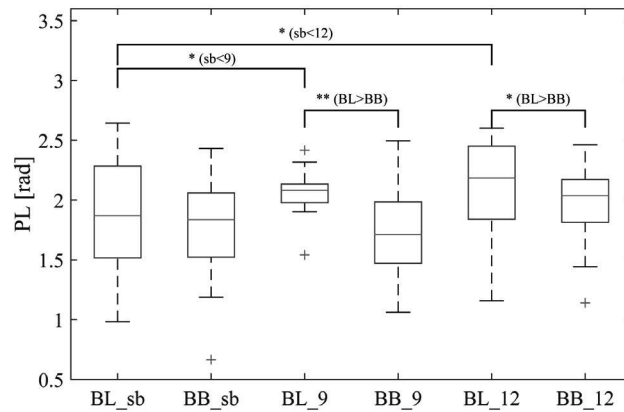
Figure 3.22: The PL for the three breathing modes in the β-blocker case for all 17 subjects. BL: baseline, BB: β-blocker influence. $*P < 0.1$; $**P < 0.05$.
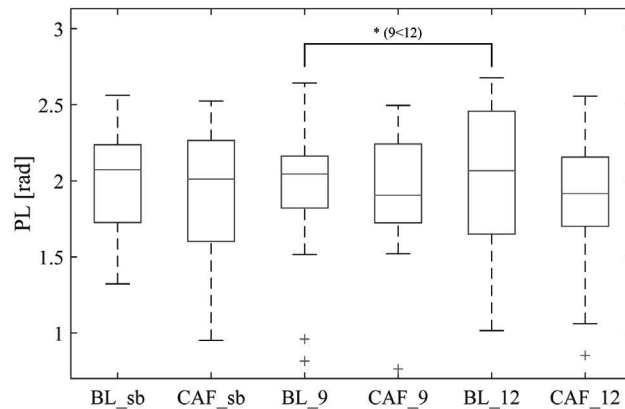
Figure 3.23: The PL for the three breathing modes in the caffeine case for all 17 subjects. BL: baseline, CAF: caffeine influence. *$P < 0.1$.

except for producing a trend towards decrease at 9 brpm. The LF and nLF powers were smaller during breathing at 12 brpm compared to 9 brpm or spontaneous breathing during the two days of the experiment. This observation is not surprising, as only at 12 brpm the breathing was never in the LF band.
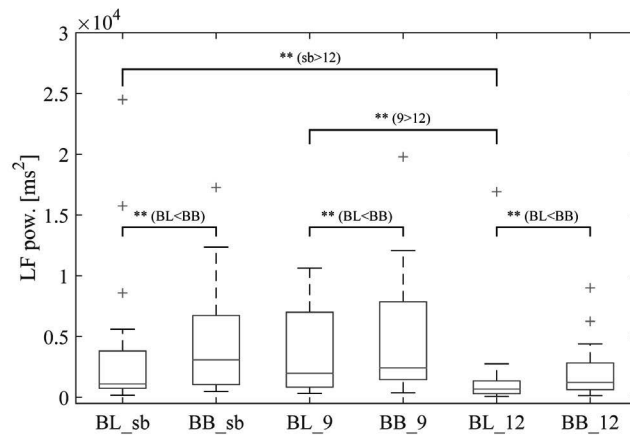
Figure 3.24: The LF power for the three breathing modes in the β-blocker case for all 17 subjects. BL: baseline, BB: β-blocker influence. **$P < 0.05$.

The HF power was significantly larger after β-blocker ingestion in all three modes as seen in Figure 3.26. Caffeine ingestion increased the HF power as well, but only during the 9 brpm breathing mode as seen in Figure 3.27. The nHF power did not exhibit a significant difference between the baseline and the β-blocker cases in spontaneous breathing as seen in Figure B.11 in Appendix B. The differences in the HF power and the nHF power between the three breathing modes were not reproduced over the two days and were not consistent in the HF and the nHF cases.

Figures 3.28 and 3.29 report the total power for the three breathing modes in the β-blocker and caffeine cases. β-blocker ingestion increased the total power regardless of the breathing
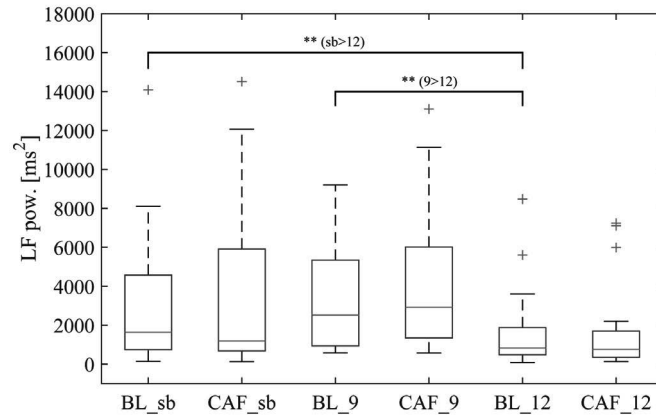
Figure 3.25: The LF power for the three breathing modes in the caffeine case for all 17 subjects. BL: baseline, CAF: caffeine influence. $**P < 0.05$.
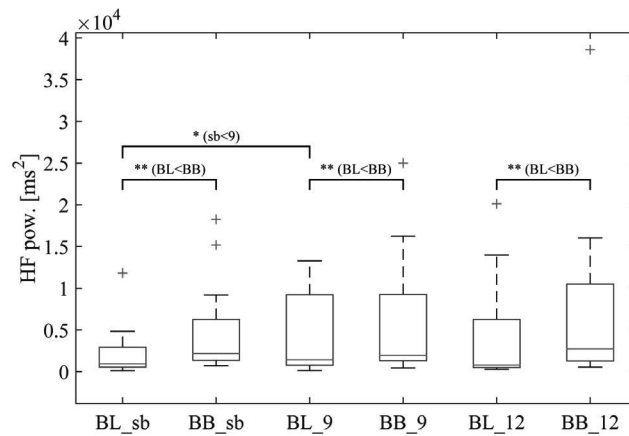
Figure 3.26: The HF power for the three breathing modes in the β-blocker case for all 17 subjects. BL: baseline, BB: β-blocker influence. $*P < 0.1$; $**P < 0.05$.
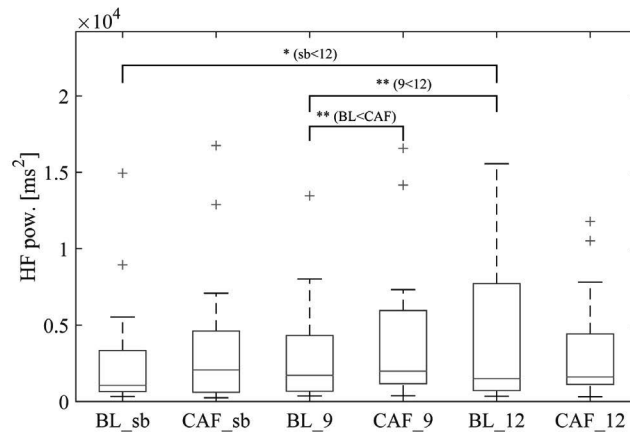
Figure 3.27: The HF power for the three breathing modes in the caffeine case for all 17 subjects. BL: baseline, CAF: caffeine influence. *$P < 0.1$; **$P < 0.05$.

mode while caffeine increased its value only for the 9 brpm breathing mode. There were no significant differences in the total power between the breathing modes, consistent over the two days of the experiment.
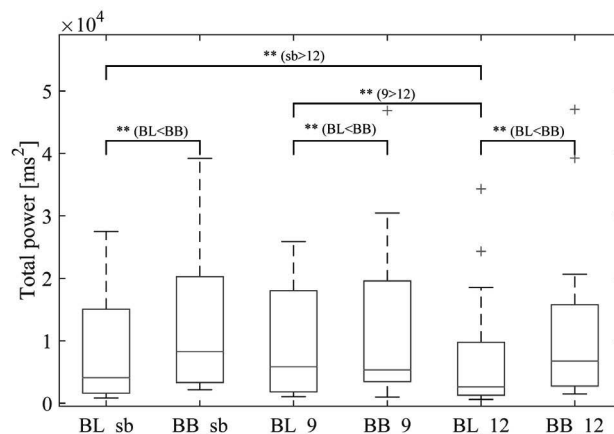
Figure 3.28: The total power for the three breathing modes in the β-blocker case for all 17 subjects. BL: baseline, BB: β-blocker influence. **$P < 0.05$.

Figure 3.30 reports the LF/HF index for the three breathing modes during baseline and under β-blocker influence. The index significantly decreased under β-blocker influence at 9 brpm. In that breathing mode, it also significantly increased after caffeine ingestion as seen in Figure 3.31. No other significant differences were observed. Regarding the differences in the index at baseline between the breathing modes, it was observed that in both days, the LF/HF was smallest during the 12 brpm breathing mode than the two other modes, similarly to the LF and nLF powers.

The results are summarized in Table 3.1.
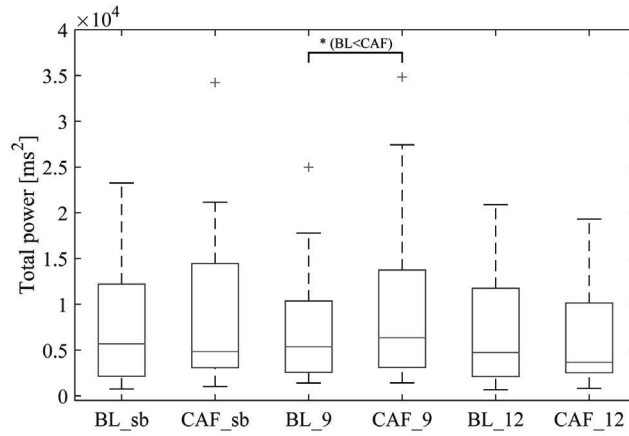
Figure 3.29: The total power for the three breathing modes in the caffeine case for all 17 subjects. BL: baseline, CAF: caffeine influence. *$P < 0.1$.
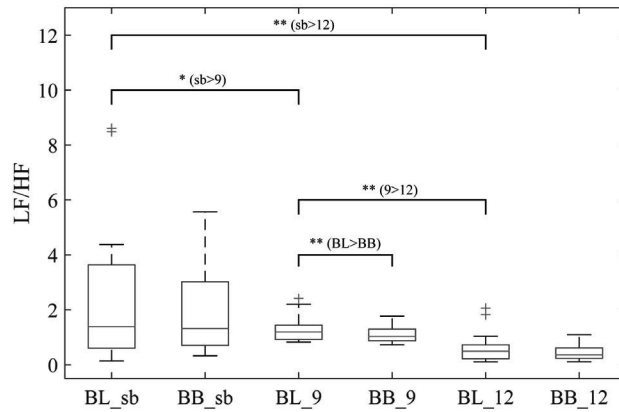
Figure 3.30: The LF/HF index for the three breathing modes in the β-blocker case for all 17 subjects. BL: baseline, BB: β-blocker influence. *$P < 0.1$; **$P < 0.05$.

Table 3.1: Summary of parameters in response to controlled breathing and autonomic altering.

	BB	CAF	Breathing mode
P_{RSA}	larger than BL for all	larger than BL only for 9 brpm	larger for 9 brpm than 12 brpm
nP_{RSA}	larger than BL only for 9 brpm and 12 brpm	-	larger for 9 than sb and 12 brpm
$P_{non\text{-}resp}$	larger than BL for all	larger than BL only at 9 brpm	-
$nP_{non\text{-}resp}$	smaller than BL for 9 brpm and 12 brpm	-	larger for sb and 12 brpm than 9 brpm
PL	larger than BL for 9 brpm and 12 brpm	-	-
PL_{slope}	-	larger than BL only for sb	-
PLV	larger than BL only for 12 brpm	larger than BL only for sb	-
PLS	-	smaller than BL only for sb	-
LF	larger than BL for all	-	larger for sb and 9 brpm than 12 brpm
nLF	larger than BL only for 9 brpm	smaller than BL only for 9 brpm	larger for and 9 brpm than 12 brpm
HF	larger than BL for all	larger than BL only for 9 brpm	-
nHF	larger than BL only for 9 brpm and 12 brpm	larger than BL only for 9 brpm	larger for 12 brpm than sb and 9 brpm
Total pow.	larger than BL for all	larger than BL only for 9 brpm	-
LF/HF	smaller than BL only for 9 brpm	smaller than BL only for 9 brpm	larger for sb and 9 brpm than 12 brpm
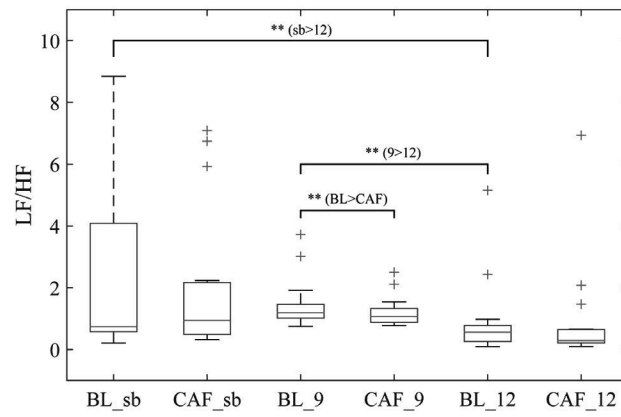
Figure 3.31: The LF/HF index for the three breathing modes in the caffeine case for all 17 subjects. BL: baseline, CAF: caffeine influence. **$P < 0.05$.

3.4   Discussion and conclusion

3.4.1   Body posture

It is unanimously reported in literature that the orthostatic position elicits larger LF and smaller HF power than the supine position [88, 128, 147–149]. The results reported in this chapter are in accordance with literature.

The breathing-corrected cLF power was generally lower than the LF power, as it was computed on the same or a narrower frequency bandwidth that did not contain any breathing-related power. By the same reasoning the cHF power was larger than the HF power, especially with respect to the normalized parameters (Figures 3.9 and 3.10). It is therefore important to consider the true breathing rate, as it may contribute to producing erroneous values, even though trends exist between different autonomic conditions. However, one problem with the modification of the boundary was the arbitrary nature of the new boundary. The LF band was highly dependent on the distance of the boundary from the actual breathing rate as demonstrated by the sensitivity of the results to the boundary parameter δf. For a large δf, when the actual breathing rate was low, the LF or breathing-unrelated band was non-existent.

The RSA power showed the same patterns as the conventional and corrected HF powers, its value decreasing in the orthostatic position (Figures 3.6 and 3.7). On the other hand, the breathing-unrelated power was larger in the orthostatic position. These differences were emphasized in the normalized powers, highlighting again the importance of normalization. As the breathing-unrelated power is mostly low-frequency power, the RSA and breathing-unrelated power can be used as physiologically interpretable alternatives to the conventional LF and HF powers.

The relationship between breathing and RSA, as measured using the variability and the synchronization of their phase lag, was significantly affected by the change in posture from supine to orthostatic, in spite of the phase lag itself not being affected (Figures 3.8 and B.2). The increase in variability and decrease in synchronization of the phase lag indicate that the relationship between the RSA and the breathing was less stable in the orthostatic position. Given the sympathetic dominance in the orthostatic position, the activation of this branch of the ANS can be associated with a decrease in the stability in the RSA-breathing relationship compared to the parasympathetic dominance of the supine position.

3.4.2   Controlled breathing

Breathing modes did not seem to affect the total power and the HF power, as no consistent differences were observed over the two days (Figures 3.26 - 3.29). The LF power and LF/HF index were lowest at 12 brpm, which is expected since at this breathing rate, the breathing activity did not appear in the LF band (Figures 3.24, 3.25, 3.30 and 3.31). Normalized nLF and nHF powers showed the same differences more clearly (Figures B.9 to B.12). In summary, the differences observed in these conventional indexes were expected.

The RSA power on the other hand was not significantly different in spontaneous and controlled breathing except in its normalized form (Figures 3.14 - 3.17). It was however larger in 9 brpm than in 12 brpm controlled breathing. The absence of difference between the spontaneous and controlled breathing may be due to the fact that, in spontaneous breathing, the breathing rates of the subjects had a wide range as seen in Figure 3.13, and therefore no distinctive trend was apparent. On the other hand, since the controlled breathing rate was relatively close to the natural breathing rates of the subjects, our results are in concordance with reports of no change in the RSA when the controlled breathing rate is close to the natural breathing rate [56, 150].

The phase-related indexes were not affected by the breathing modes.

3.4.3 Pharmacological alteration

Blockade of the sympathetic nervous system influence on the cardiac rhythm regulation with β-blocker ingestion increased the LF, HF and total power for all breathing modes (Figures 3.24, 3.26 and 3.28). When normalized, some trends in the LF and HF powers during the spontaneous breathing mode were no longer visible (Figures B.9 and B.11). Activation of the sympathetic nervous system with caffeine ingestion resulted in an increase in the total power but only during the 9 brpm breathing mode (Figure 3.29). Several trends were present in the LF, HF powers and their normalized versions, but all were related to the 9 brpm breathing mode (Figures 3.25, 3.27, B.10, B.12). The LF/HF index was smaller under the influences of both the β-blocker and caffeine, only for the 9 brpm mode (Figures 3.30 and 3.31). In this mode the assumption that the breathing occurs in the HF mode does not hold, in which case the observed trends can be incorrectly attributed to the influence of breathing.

The RSA power was larger after β-blocker ingestion for all breathing modes (Figure 3.14). This observation held for its normalized version, except during spontaneous breathing (Figure 3.16). The breathing-unrelated power was also larger after β-blocker ingestion, however its normalized version revealed the opposite trend, except during spontaneous breathing (Figures 3.18 and 3.20). The absence of difference during spontaneous breathing in the normalized RSA and breathing-unrelated powers may be attributed to the large differences in the breathing rates of the subjects, such that no overall trend exists over the population. Both the RSA and breathing-unrelated powers were increased after caffeine ingestion, while their normalized versions were unchanged (Figures 3.15, 3.17, 3.19 and 3.21). Given the absence of any real effect of caffeine on the indexes believed to report the sympathetic activation (the cLF power and the cLF/cHF index) [1, 2, 146], the absence of significant differences in the normalized breathing-unrelated power after caffeine ingestion is not surprising. This index reported correctly on the sympathetic dominance of the orthostatic posture in Section 3.4.1. The differences observed in the absolute value of the index at 9 brpm (Figure 3.19) can be attributed to the total power (Figure 3.29). The absence of change in the RSA power may indicate that caffeine has no effect on the breathing power and parasympathetic activation, as expected.

The phase lag between RSA and breathing was increased after β-blocker ingestion only during controlled breathing (Figure 3.22). During spontaneous breathing, the changes in breathing rate may themselves introduce phase shifts and the phase relationship of the RSA and the breathing may be less stable. The fact that no change was detected after β-blocker ingestion in this breathing mode may be attributed to this instability. Indeed, even at baseline, the relationship was somewhat instable. The slope of the phase lag and its synchronization showed no differences between baseline and β-blocker influence (Figures B.3 and B.7). Caffeine ingestion had no effect on the phase lag (Figure 3.23) but induced changes in the slope, variability and synchronization of the phase lag, however, only during spontaneous breathing (Figures B.4, B.6 and B.8). All changes were in the direction of decreased stability after caffeine ingestion. The absence of differences during controlled breathing may be due to the fact that artificial imposition of a pattern on the breathing, in conjunction with the effects of caffeine, hinders the natural relationship between the latter and the RSA, and yields an abnormally stable relationship.

The increase in the total power and in the RSA power observed in this study with β-blocker ingestion (Figures 3.28 and 3.14) confirms the previous reports of increases of the breathing-related power [143, 157, 158]. Our results show that the breathing rate must be considered, as the occurrence of the breathing in the LF band leads to erroneous measurements. In several cases, only measurements at 9 brpm showed significant differences in the parameters between the breathing modes and the autonomic conditions. At this frequency, breathing occurs partly in the LF band. Furthermore, some subjects reported that the auditory signal at this breathing rate was rather difficult to follow, which may have induced stress on them, and thus bias in the recordings during this mode. However, even after taking into account the breathing rate, none of

the investigated parameters reflected changes thought to be caused by the caffeine ingestion with its subsequent increase in sympathetic tone.

When normalized, after β-blocker ingestion, some of the effects observed on the absolute LF and HF powers were no longer visible, which leads to believe that the normalization aids in the observation of the theoretical effects, i.e., no change in LF or HF powers. However, with respect to the effects of caffeine ingestion, the normalization changed nothing in the HF results but caused an increase in LF power at 9 brpm. Given that at this rate, the breathing occurs within the LF band, it is deduced that the observed change is related to the respiratory and parasympathetic tone.

3.5   Conclusion

Although the conventional measures of the autonomic balance, namely the LF and HF powers and the LF/HF index sometimes may seem to report autonomic changes, they are difficult to interpret on a physiological basis.

The real breathing rate must be measured and taken into account as the breathing is not confined to the conventional 0.15-0.4 Hz bandwidth in many people.

Correcting the conventional LF-HF boundary of 0.15 Hz for the breathing rate is a solution, however lacking in robustness.

The RSA and breathing-unrelated powers report changes in the autonomic condition which are physiologically interpretable. The RSA power is related to the parasympathetic dominance and the breathing-unrelated power increases when sympathetic dominance increases. Measuring them always requires the real breathing rate.

The breathing-unrelated power reflected the expected autonomic changes because of posture change and in particular the increase in sympathetic tone in the orthostatic position. However, it did not reflect the expected changes in the sympathetic tone due to caffeine ingestion. As none of the conventional indexes were affected by caffeine ingestion either, our results confirm those in the literature reporting an absence of increase in sympathetic tone due to caffeine ingestion [160, 168].

As stated in previous works, normalization is necessary to avoid the inclusion of changes in the baseline values of the parameters. For example, in the orthostatic position, the heart rate tends to be higher. Therefore changes in the heart rate are higher than the same changes occurring in the supine position, where the heart rate is lower.

Characterization of the RSA upon Exposure to Altitude

4

In this chapter, the ANS response to altitude exposure is investigated. The HRV indexes introduced in Chapter 3 are employed to study ANS responses to an acute exposure to altitude as well as to acclimatization to altitude.

4.1 The RSA in studying the effects of altitude exposure

HRV indexes, such as the LF and HF powers, the LF/HF index and the RSA were introduced as non-invasive measures of autonomic activity in Chapter 3. One of the applications of these indexes is the analysis of the changes occurring in the human ANS upon exposure to altitude, often with the end goal of studying the acclimatization to altitude and predicting mountain sickness [136, 137].

Hypoxia is the condition of decreased concentration of the air oxygen (11% at 5000 m vs. 21% at sea level). Hypoxia exposure to achieve altitude acclimatization is somewhat popular in athletic training, as it has been shown that living at a high altitude, e.g. above 5000 m and training in low altitudes improves athletes performance at sea-level [193]. There is evidence that the increased athletic performance following this so-called "live high, train low" regime of training would be due to an increased red cell mass, increased muscle buffer capacity and increased mechanical efficacy. Given that access to high altitude is geographically inconvenient in many countries, simulated altitude, in a normobaric chamber, has also been studied within this training technique. Since the "live high, train low" regime may possibly have undesired autonomic effects, it has become important to study the effects of altitude exposure on cardiac autonomic control.

Given these motivations, there have been works on the characterization of HRV parameters at high altitudes by studying changes due to exposure to real altitude and exposure to artificial hypoxia, for example in a hypoxic chamber.

4.1.1 Effect of real altitude on the RSA

Early studies on HRV parameters at high altitudes above or near 5000 m reported decreases in the HF power [194, 195], sometimes with increases in the LF power [196, 197]. Other studies reported decreases in both LF and HF powers but with increases in the LF/HF index [131, 198–201]. Some works pointed to decreases in the total power and the HF power with no change in the LF/HF index [202]. There has even been a report on the increase in HF power upon exposure to altitude [203]. Some of these works on HRV and hypoxia were summarized in [129], and

the authors concluded that their findings imply that "acute exposure to hypoxia causes decreased parasympathetic and increased sympathetic tone and during acclimatization there is a progressive shift toward still higher sympathetic tone."

More recent studies also show a variety of patterns: one study reported no changes in HRV parameters above 5000 m compared to their sea-level values [204]. Another study reported a decrease in the HF and total power, and an increase in the LF power and LF/HF indexes [205].

To summarize, consistent with the findings reported in [129], it seems that at altitude, the sympathetic activity increases while the parasympathetic tone decreases.

4.1.2   Effect of artificial hypoxia on the RSA

Due to differences in heart rate and physiology in normobaric hypoxia (hypoxia in a hypobaric chamber at sea level with a pressure of 760 mmHg) and hypobaric hypoxia (hypoxia at natural altitude with a pressure < 760 mmHg) [206, 207], studies reporting information related to normobaric hypoxia (simulated altitude) are reported here, separately from studies at real altitude.

Acute hypoxia has been shown to affect the sympathetic nerve activity in animals such as rats and dogs [129]. In dogs, the RSA has been observed to be attenuated with hypoxia [17].

Regarding the traditional HRV parameters, one study found that the exposure during 8 hours to normobaric hypoxia reduced total HRV power, LF and HF powers, while the LF/HF index increased [130]. Another also reported a general decrease in HRV power during hypoxia when subjects were exposed to intermittent hypoxia episodes [135]. There is also a report of no change in the HF power [132].

One study reported an increase in the LF power, LF/HF index and total power upon exposure to a normobaric hypoxic air mixture and after the withdrawal of the hypoxic factor, the HF power increased and the LF/HF decreased [134]. The authors concluded that sympathetic tone prevails in hypoxic conditions, while immediately after their withdrawal, the parasympathetic tone increases.

The LF/HF index has been reported to increase upon exposure of the subjects to a hypobaric chamber set for 4000 m, which were confirmed by measurements when the subjects were actually at an altitude of 2700 m [208].

Similarly to the studies at real altitude, under artificial hypoxia it seems that there is an increase in the sympathetic activity and a decrease in parasymathetic tone.

4.1.3   Motivation and contribution

As described in Section 3.1.4, the conventional LF and HF power indexes and the LF/HF index do not accurately take into account the breathing influence on the autonomic sate. Previous studies on the characterization of the autonomic effects of altitude, although mostly coherent, have sometimes reported contradictory changes in the LF, HF and total HRV powers, ranging from increases to decreases, and including no change upon exposure to the subject to real or simulated hypoxia. Most studies report an increase in sympathetic activity and a decrease in parasympathetic tone at real or simulated altitude.

On the other hand, the RSA, extracted using the reference breathing waveform as described in Section 3.2.2, as well as its phase relationship with breathing were introduced as promising descriptors for the autonomic state in Chapter 3. They have not been widely investigated in relation to the autonomic changes induced by altitude exposure, while the cardio-respiratory phase coupling has been shown to be affected after exposure to hypobaric hypoxia conditions in a hypoxic chamber [133]. In the present study, the changes in the RSA and its relationship to breathing were analyzed upon acute exposure to altitude (> 5000 m) and after acclimatization to that altitude for 16 days.

4.2   Materials and methods

4.2.1   Data

The data used in this study were the arterial blood pressure (ABP) and breathing waveform (%O_2 in airflow) acquired in the framework of the "AltitudeOmics" project [209]. This project was designed to study several aspects of human acclimatization to altitude and its data were very extensive. The subset of the "AltitudeOmics" data used in the present study consists of: resting-state recordings of 16 subjects (nine male, age 20 ± 1 years, height 175 ± 7 cm, weight 70 ± 8 kg) at sea-level (baseline recordings), upon acute exposure to an altitude of 5260 m at Mt Chacaltaya, Bolivia (ALT1), and after 16 days of acclimatization at that same altitude (ALT16). Both signals were acquired with a sampling rate of 200 Hz. An example of the raw signals for a baseline recording is shown in Figure 4.1. A heart rate estimate was also provided. Most subjects had a 6-minute recording for all three conditions. However, in ALT1, one subject only had 2 minutes and in the ALT16, two subjects had about 3 minutes only.
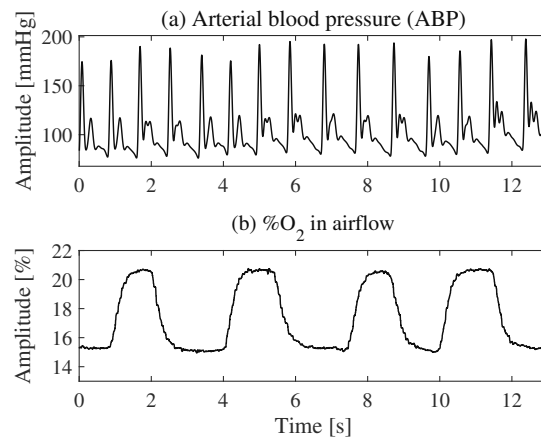
Figure 4.1: Sample signals from the "AltitudeOmics" project: (a) The ABP; (b) the % O_2 in airflow.

4.2.2   Data processing

The maxima of the ABP signal were identified with a local extrema detection method, using the available heart rate estimate as reference. The extracted peaks were manually inspected to ensure their correctness. The inter-beat intervals series was then created and re-sampled uniformly at 4 Hz using cubic spline interpolation[1], by setting the time index of each interval to its midpoint. The %O_2 in airflow was re-sampled similarly to the ABP inter-beat intervals time series. It must be noted that the ABP inter-beat intervals are not exactly equivalent to the heart R-R intervals, which are normally used to derived the RSA, as in Chapter 3. Given that the aortic valve opening, the beginning of the increase in the ABP signal, coincides with the end of the ECG S-wave (see Figure 2.4 for ECG waves), the ABP peak location is somewhere in the T-wave, meaning the ABP maximum has a delay of about 200 ms with respect to the ECG R-peak (see Figure C.2 in Appendix C). At a sampling rate of 4 Hz, this delay is less than one sampling period. Therefore, in the analysis below, the ABP inter-beat intervals were considered to be a surrogate for the heart inter-beat intervals.

---

1. described in Appendix A

The RSA was extracted from the inter-beat intervals according to (3.2) described in Section 3.2.2. The RSA power and its normalized version were computed as described in Section 3.2.2. The breathing rate (BR) was computed from the airflow signal using the notch filter bank method described in Section 5.2.2. The portion of the inter-beat intervals power unrelated to breathing, as well as its normalized version, were also computed as described in Section 3.2.2.

The phase lag (PL) between the RSA and breathing waveforms, the phase lag variability (PLV) and the phase lag synchronization (PLS) index, were computed as described in Section 3.2.2, in particular by using (3.4) and (3.7).

The conventional HRV LF and HF powers were measured, as well as their normalized versions nLF and nHF, as described in Section 3.2.2.

4.3   Results

An example of the RSA and breathing waveforms (normalized for visualization purposes) for the three cases of baseline, ALT1 and ALT16 are depicted in Figure 4.2 for one subject. It can be seen that, in this example, at baseline, the delay of the RSA with respect to the breathing waveform is smaller than after exposure to altitude and acclimatization.
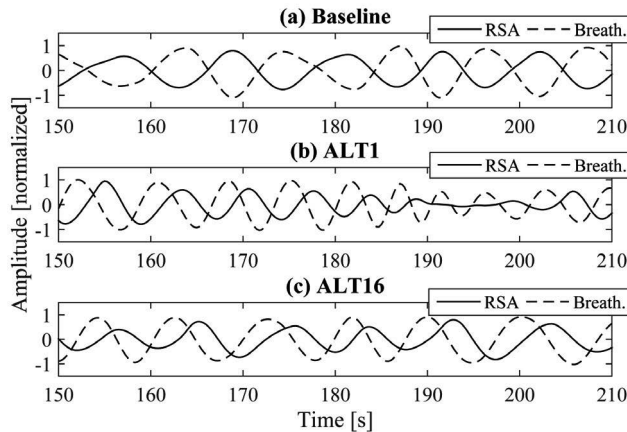
Figure 4.2: The RSA and breathing signals at (a) baseline, (b) after acute exposure to altitude (ALT1) and (c) after acclimatization (ALT16) for one subject.

Figure 4.3 reports the RSA power in the three conditions. This power was significantly reduced after exposure to altitude, and stayed reduced during acclimatization. There was no significant difference between the power at acute exposure and after acclimatization. The breathing-unrelated power followed the same pattern as the RSA power as seen in Figure 4.4. Although the normalized RSA power followed mostly the same pattern as the RSA power (Figure 4.6), the normalized breathing-unrelated power differences were inverted as observed in Figure 4.7. It was smallest at baseline, and increased upon acute exposure. It slightly decreased after acclimatization. As reported in Figure 4.5, the total power was also largest at baseline, which may account partly for the differences observed in the absolute values of the RSA and breathing-unrelated powers.

Figure 4.8 shows the PL of the RSA with respect to the breathing waveform. The PL was significantly larger upon exposure and after acclimatization to altitude than at baseline. The PL slope did not change significantly as seen in Figure C.1 in Appendix C.
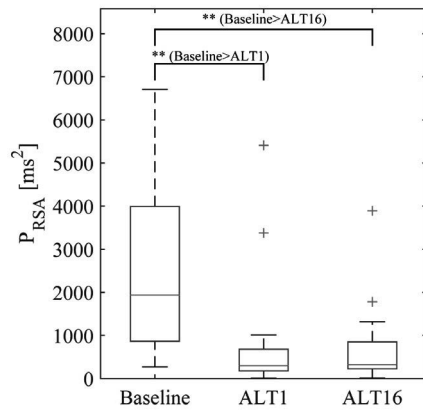
Figure 4.3: The RSA power at baseline and after exposure to altitude for all 16 subjects. **p<0.05.
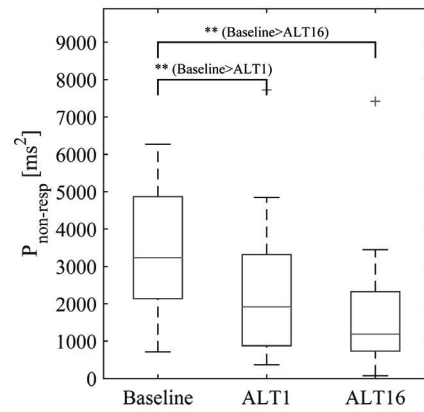
Figure 4.4: The breathing-unrelated power at baseline and after exposure to altitude for all 16 subjects. $**p < 0.05$.
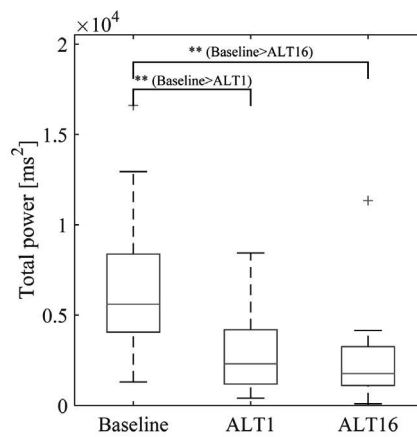
Figure 4.5: The total inter-beat intervals power at baseline and after exposure to altitude for all 16 subjects. $**p < 0.05$.
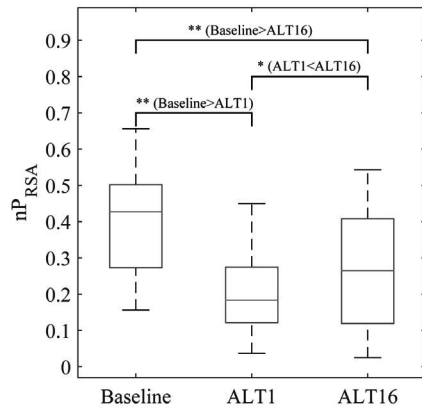
Figure 4.6: The normalized RSA power at baseline and after exposure to altitude for all 16 subjects. $**p < 0.05$.
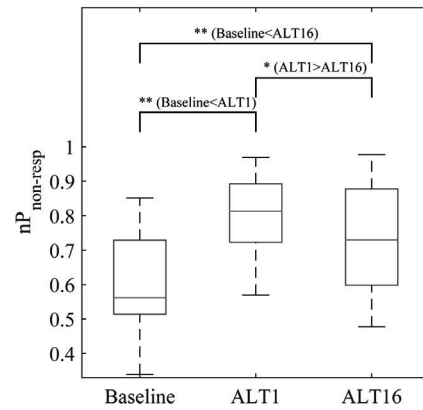
Figure 4.7: The normalized breathing-unrelated power at baseline and after exposure to altitude for all 16 subjects. $**p < 0.05$.
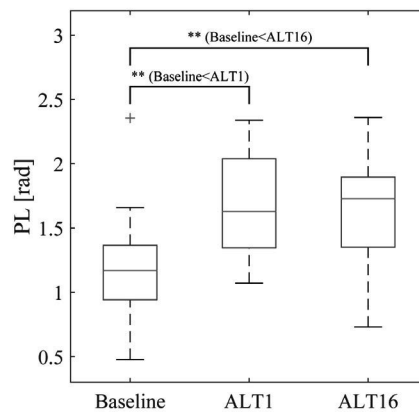
Figure 4.8: The PL at baseline and after exposure to altitude for all 16 subjects. $**p < 0.05$.

Figure 4.9 reports the PLV at baseline, after acute exposure to altitude and after acclimatiza-
tion. The PLV was significantly larger upon exposure and after acclimatization than at baseline.

Figure 4.10 shows the PLS for the three cases. The PLS was significantly smaller upon
exposure to altitude, but it did not significantly change further after acclimatization.
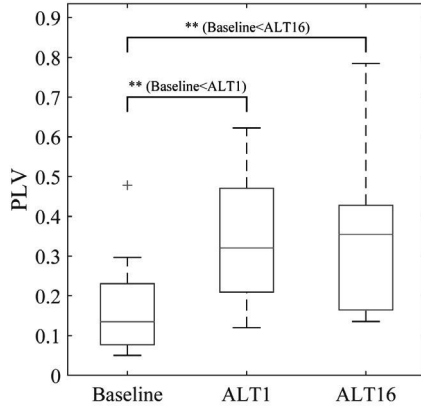
Figure 4.9: The PLV at baseline and after expo-
sure to altitude for all 16 subjects. $**p < 0.05$.
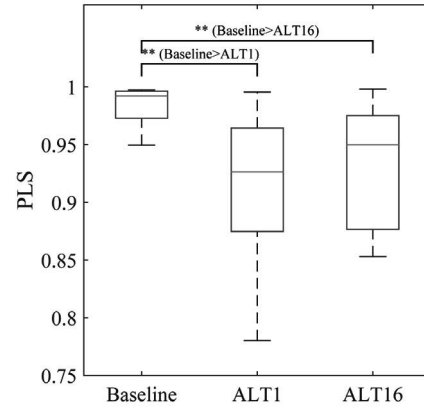
Figure 4.10: The PLS at baseline and after expo-
sure to altitude for all 16 subjects. $**p < 0.05$.

Figures 4.11 and 4.12 report the BR and HR values of the subjects. In each of the baseline,
ALT1 and ALT16 sessions, two subjects (12.5% of the population) had BR values below the LF-
HF boundary of 0.15 Hz. BR and HR values were significantly higher in the altitude recordings,
but they were not significantly different after acute exposure and after acclimatization.
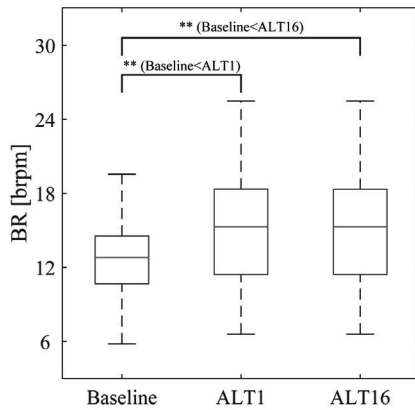
Figure 4.11: The breathing rate at baseline and
after exposure to altitude for all 16 subjects.
$**p < 0.05$.
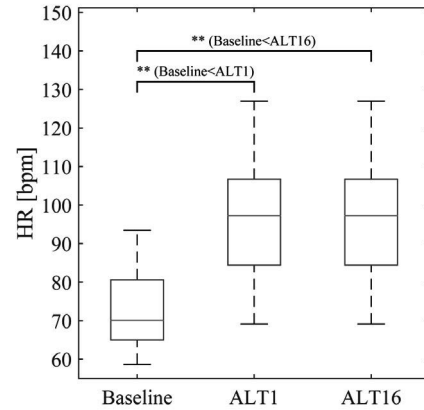
Figure 4.12: The heart rate at baseline and after
exposure to altitude for all 16 subjects. $**p <
0.05$.

Figures 4.14 and 4.13 show the conventional LF and HF powers at baseline, upon exposure
to altitude and after acclimatization. Both the LF and HF powers were significantly larger at
baseline, however this may be due to the total power as seen in Figure 4.5, as the differences

were visible in the normalized nHF, although less prominent, and no longer visible in the nLF power as seen in Figures 4.15 and 4.16. There were no significant differences in the LF/HF index at baseline or in either of the altitude conditions as reported in Figure 4.17.
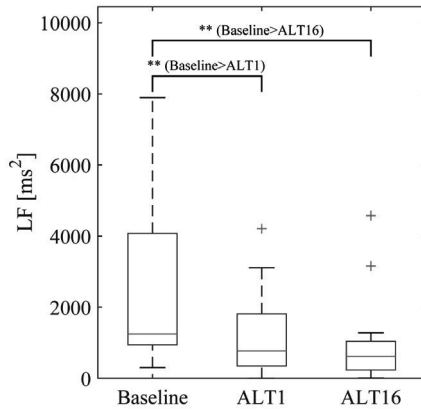
Figure 4.13: The LF power at baseline and after exposure to altitude for all 16 subjects. $**p < 0.05$.
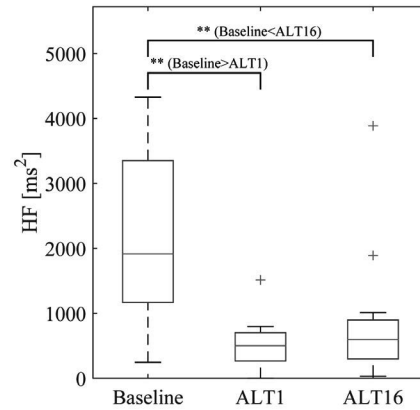
Figure 4.14: The HF power at baseline and after exposure to altitude for all 16 subjects. $**p < 0.05$.
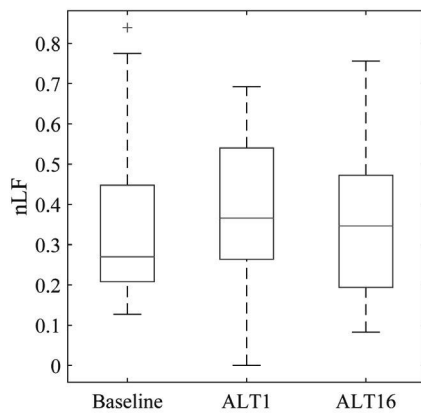
Figure 4.15: The nLF power at baseline and after exposure to altitude for all 16 subjects.
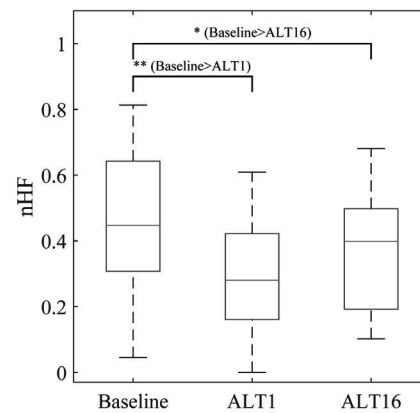
Figure 4.16: The nLF power at baseline and after exposure to altitude for all 16 subjects. $*p < 0.1$; $**p < 0.05$.

4.4 Discussion

When analyzing the RSA and breathing-unrelated power of the inter-beat intervals, it was apparent that normalization by the total power was necessary, as the inter-beat intervals total power was affected by the altitude conditions as seen in Figure 4.5 as a result of the change in heart rate (Figure 4.12). The normalized RSA power decreased in altitude (acute exposure
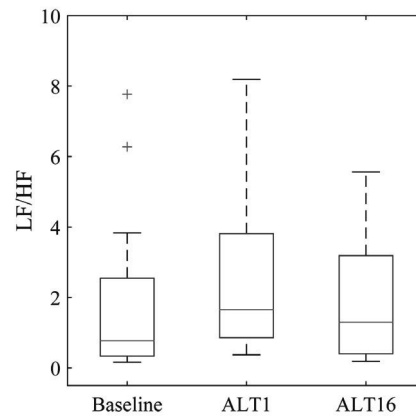
Figure 4.17: The LF/HF index at baseline and after exposure to altitude for all 16 subjects.

and acclimatization) compared to baseline, and between acute exposure and acclimatization, it slightly increased as seen in Figure 4.6. The normalized breathing-unrelated power increased in altitude compared to baseline, however it slightly decreased after acclimatization compared to its value after acute exposure as reported in Figure 4.7. It seems that acclimatization brings the values of these parameters slightly closer to their baseline values. The increase of the breathing-related power and decrease of the breathing-unrelated power in altitude is consistent with the conclusion made to the decrease in parasympathetic tone and increase in sympathetic tone with altitude [129].

The total power and both the LF and HF powers decreased in the altitude conditions (Figures 4.13 and 4.14). The normalized LF power did not reveal any trends at all, while the normalized HF power showed the same trends as the HF power, however less marked. These observations are consistent with those reported in [202] and partly consistent with those in [131, 198, 200, 201].

It has been reported in literature, that the normalization of the power indexes with respect to the total power is necessary, as the latter is also affected by the autonomic state [143]. The observations made in the present study on the RSA and breathing-unrelated power confirm the need for normalization.

In light of the importance of the normalization, the normalized LF and HF indexes do not adequately reflect changes in the autonomic state, which are better reflected by the breathing-related and unrelated powers of the inter-beat intervals.

The phase lag between the RSA and the breathing waveform, its variability and its synchronization were all significantly affected by exposure to altitude. The increase in phase lag, and its variability and the decrease in its synchronization attest to the fact that upon exposure to altitude, the relationship between the RSA and the breathing waveform becomes less stable and somewhat more erratic. It can be deduced that the sympathetic activation decreases the stability of the RSA-breathing relationship. This is in accordance with finding on ANS responses to body posture changes reported in Section 3.4.1 and in particular, the decrease of the stability of the RSA-breathing relationship in the orthostatic position (sympathetic activation). After acclimatization, these phase-related parameters did not change significantly from their values after acute exposure to altitude.

To summarize, our findings of decreased RSA power (or increased breathing-unrelated power), along with the increase in the instability in the relationship between the RSA and breathing, report on an increase sympathetic activation and decreased parasympathetic tone, similarly to most

previous studies on the effects of altitude on cardiac autonomic indexes.

4.5   Conclusion

The conventional LF and HF indexes have been widely used in literature to assess the autonomic state upon exposure to altitude. However, the absolute values of these indexes may present differences attributable to the underlying inter-beat interval power related to the heart rhythm. Their normalized versions, carrying relative information, reported effects partially in accordance with the literature. The breathing-related and unrelated power of the inter-beat intervals, on the other hand, reported physiologically interpretable effects upon exposure to altitude. Their reported effects were in accordance with theoretical considerations accepted in the literature. The phase relationship between breathing and the RSA revealed changes in the relationship between the two, which is also related to the autonomic state. These changes reflect aspects of the cardio-respiratory relationship which are not revealed by the LF and HF powers or even their breathing-related and unrelated counterparts and may offer new avenues into the exploration of the autonomic system role in altitude exposure and acclimatization.

Part II

Estimation of Breathing Parameters using the RSA

Estimation of the Breathing Rate from the ECG

5

In this chapter, two algorithms are studied for the estimation of the breathing rate (BR) from the ECG. One is an existing algorithm and the other a novel technique designed to overcome shortcomings of the existing method. Section 5.1.1 provides background on the estimation of the BR from the ECG and the RSA in particular. Section 5.1.2 discusses frequency estimation in general, and Section 5.1.3 gives the motivation behind the work presented in this chapter as well as a summary of contributions. The algorithms are described in detail in Sections 5.2.1 and 5.2.2. Section 5.2.3 describes the creation of a reference for the evaluation of the algorithms. Section 5.3 outlines evaluation scenarios. Results are presented in Section 5.4 and discussed in Section 5.5. Conclusions are drawn in Section 5.6. Elements of this chapter have been published in two journal articles and presented in several conferences [210–214].

5.1 Introduction

5.1.1 Breathing rate estimation from the RSA

The BR is one of the human vital signs that need to be monitored in clinical and non-clinical applications for diagnosis and control purposes [173, 215, 216]. It is currently difficult to accurately and continuously monitor the BR, as the apparatus and devices are intrusive, expensive and uncomfortable for the patient [217]. It is therefore of great interest to provide easy and inexpensive means for accurate, continuous and convenient monitoring of the BR. The breathing and heart activities are linked through physiological processes. As discussed in Chapter 2, the RSA is a waveform containing the breathing modulation of the heart rate. Furthermore, the filling and emptying of the lungs during breathing causes a rotation of the electrical axis of the heart and a change in the impedance of the thorax, which yield changes in the ECG beat morphology [28]. As a result, the R-peak amplitudes are also modulated by the breathing activity. A waveform can be extracted from the ECG representing this modulation, which is referred to as the R-peak amplitudes (RPA). In the last twenty years, many researchers have investigated the possibility of deriving the BR by exploiting the influence of breathing on the heart rate or ECG beat morphology by using either the RSA or RPA waveforms.

The BR is traditionally computed from the spectra of the the RSA or the RPA [28, 218, 219]. For instance, windowed spectral analysis has been applied to extract the BR from the RSA waveform [220]. Windowed temporal analysis using peak count was also applied to estimate the BR from the RSA waveform [215, 220–222] as well as from the RPA waveform [221]. Correlation analysis [220, 223] and Kalman filtering have also been applied to this task [224].

55

In a pioneering work, Orphanidou *et al.* fused spectral information form ECG-derived RSA and RPA waveforms in order to derive the BR [138]. The most dominant peak was selected from the autoregressive (AR)-estimated spectra of the RSA and RPA waveforms according to several criteria as representing the BR. Vehkaoja *et al.* also used the RSA and RPA signals simultaneously and combined their temporal maxima and minima counts after ad-hoc filtering to estimate the BR [225].

Generally speaking, the problem of instantaneous BR estimation from the RSA or the RPA is a problem of tracking the instantaneous frequency of these waveforms.

5.1.2   Estimating the instantaneous frequency of an oscillatory signal

The instantaneous frequency of an oscillatory signal is an important attribute defined as the derivative of its instantaneous phase [226].

By definition, the instantaneous frequency is difficult to measure and determine exactly, especially when a signal contains several oscillations and other components. In theory, the instantaneous frequency can be computed by deriving the instantaneous phase of the signal, as given by the Hilbert transform [227]. However, for the Hilbert transform to yield a meaningful result, the oscillation must be narrow-band [184]. The Hilbert-Huang transform tackles this problem by extracting the main oscillation of the signal with the empirical mode decomposition [185, 186, 228]. Other methods, such as Kalman filters [229] and energy tracking operators [227] can also be used to estimate the instantaneous frequency of a signal. In real cases, particularly in biomedical applications, the above-mentioned methods do not seem to have found a widespread use because of their complexity and lack of robustness.

In practice, the frequency of a signal is commonly computed via its spectrum with the short-term Fourier transform. However, this method does not provide a truly instantaneous estimate and two major drawbacks are the well-known time-frequency resolution trade-off and the delay, which is half the length of the computation window.

Adaptive filters represent another family of approaches to track the instantaneous frequency of a signal. Adaptive notch filters have been proposed, but suffer from a convergence-bias trade-off [230–232]. Adaptive band-pass filters, such as the weighted multi-signal oscillator-based adaptive band-pass filter (*W-OSC*) have been used in biomedical applications to track an oscillation in one signal or in several signals carrying the same oscillatory component [233]. However, a major shortcoming of adaptive methods is the inherent and signal-dependent adaptation delay, which needs further attention. Indeed, when an IIR band-pass filter is employed, the output is delayed due to the long response of the recursive filter. An interesting property of this type of algorithm on the other hand is its versatility with respect to the number of signals from which the target frequency is estimated. This aspect is of particular interest in biomedical applications as one oscillatory phenomenon could modulate several recordings. For example, the breathing modulates the heart rhythm and the heart-beat magnitude [28]. Using this modulation is of growing interest in health monitoring, as recording the breathing waveform directly requires cumbersome apparatus as discussed in the previous section.

5.1.3   Motivation and contribution

None of the existing BR estimation methods using ECG-derived breathing waveforms offer a real-time and robust instantaneous (sample-by-sample) estimate. With the advent of portable health monitoring devices and the general growing interest in real-time systems, it is increasingly important to be able to measure basic physiological rhythms, such as the BR, in a real-time manner.

Conscious of the growing interest in real-time processing and motivated by the recent contribution of Orphanidou *et al.* to fuse breathing-related information from the RSA and RPA

waveforms extracted from the ECG [138], the estimation of the BR from the RSA and the RPA is addressed with two different real-time-capable methods in the present chapter.

In a first step, the instantaneous real-time BR was estimated using an adaptive band-pass filter method, the *W-OSC* algorithm [233], to track the common oscillatory component present in the RSA and RPA waveforms. This multi-signal frequency tracking method operates recursively on several signals, simultaneously, to track a common oscillatory component. This method has been shown to successfully track a common oscillatory component in biomedical signals such as electroencephalogram signals [234]. Furthermore, it is instantaneous and provides an automatic approach to BR estimation from the RSA and RPA, in contrast to the *ad hoc* processing proposed in [138]. Therefore, it can be implemented in a real-time setting to estimate the BR continuously without the need for any subject-dependent adjustment. The performance of this tracking method was assessed using the single-lead ECG recordings of the PhysioNet "Fantasia" data set.

In a second step, a novel algorithm is introduced, which is a real-time and low-delay frequency tracking algorithm to estimate the instantaneous frequency of one signal, or the common instantaneous frequency of several signals, particularly designed for biomedical applications such as estimating the BR. It uses a bank of length-3 FIR notch filters over a range of discrete frequencies to filter the algorithm inputs. The output powers are then used in a recursive scheme to compute weights for the discrete notch frequencies. The weighted sum of the notch frequencies yields an estimate of the dominant frequency of the inputs at each sample. To the best of our knowledge, this scheme is original. The proposed algorithm was tested on synthetic data with one or two inputs. It was then applied to the estimation of the BR from the RSA and the RPA and compared to the *W-OSC* algorithm on the "Fantasia" data set. The novel algorithm was further tested on signals acquired during physical activity.

5.2 Materials and Methods

5.2.1 The *W-OSC* algorithm

The *W-OSC* algorithm is an adaptive band-pass filter with an oscillator-based mean-square error update algorithm [233]. This algorithm can track a common frequency, which is present in M signals $\{u_m\}$, $m = 1, \ldots, M$ of the form:

$$u_m[n] = s_m[n] + b_m[n], \tag{5.1}$$

where the $s_m[.]$ are oscillations at the time-varying frequency $\omega[.]$ and the $b_m[.]$ are additive white noises. All M signals are filtered with the same filter and the tracking quality of the outcome is used to weigh the contribution of each signal to the filter update in order to track a common oscillation $\omega[.]$ in the signals. The transfer function of the filter is:

$$H_{band-pass}(z; n) = \frac{1 - \beta}{2} \frac{1 - z^{-2}}{1 - \alpha[n](1 + \beta)z^{-1} + \beta z^{-2}}, \tag{5.2}$$

where $0 < \beta < 1$ defines the bandwidth of the filter and $\alpha[.] = cos(\omega[.])$ is the central frequency coefficient of the filter. The output of the filter for signal m is:

$$y_m[n] = (1 + \beta)\alpha[n]y_m[n - 1] - \beta y_m[n - 2] + \frac{1 - \beta}{2}(u_m[n] - u_m[n - 2]). \tag{5.3}$$

Since the breathing modulation is oscillatory, it is desired that the filter output follows the oscillator model, i.e., that the filter output, $y_m[.]$, is locally as close as possible to a sinusoid:

$$d[n] = 2\alpha_0 d[n - 1] - d[n - 2]. \tag{5.4}$$

In order to update the filter such that the output follows (5.4), the following cost function is minimized:

$$J_m[n] = E\{(y_m[n] - 2\alpha[n + 1]y_m[n - 1] + y_m[n - 2])^2\} \tag{5.5}$$

with $E\{.\}$ denoting the mathematical expectation. The minimization of J_m yields the optimal $\alpha[n + 1]$ as:

$$\alpha[n + 1] = \frac{E\{y_m[n - 1](y_m[n] + y_m[n - 2])\}}{2E\{y_m^2[n - 1]\}}. \tag{5.6}$$

In practice, the expectations in the expression of $\alpha[n+1]$ cannot be computed and are replaced by time recursive estimates such that:

$$\alpha[n + 1] = \frac{Q_m[n]}{2P_m[n]} \tag{5.7}$$

with

$$
\begin{aligned}
Q_m[n] &= \delta Q_m[n - 1] \\
&\quad + (1 - \delta)y_m[n - 1](y_m[n] + y_m[n - 2]) \\
P_m[n] &= \delta P_m[n - 1] + (1 - \delta)y_m^2[n - 1]
\end{aligned}
\tag{5.8}
$$

where $0 < \delta < 1$ is the update coefficient. If the frequency of a unique signal is estimated, (5.7) describes the update of the filter. If the common frequency of M signals is estimated, it is natural to weigh the contribution of each signal to update the filter central frequency. The M signals do not necessarily have the same signal to noise ratio (SNR), therefore a set of weights $\{W_m \mid \sum_{m=1}^{M} W_m = 1\}$ is sought based on the estimates of the SNRs that minimize the variance of the linear combination of the updates [233]:

$$W_m = \frac{1/\sigma_m^2}{\sum_{i=1}^{M} 1/\sigma_i^2}. \tag{5.9}$$

These weights are proportional to the inverse of the variances σ_m^2 of each signal, in order to maximize the effect of signals with high SNR and to minimize the effect of signals with low SNR. It is assumed that the variances in (5.9) are proportional to:

$$\sigma_m^2 \propto \frac{J_m}{S_{u_m}} \tag{5.10}$$

where J_m is defined in a recursive manner as:

$$J_m[n] = \lambda J_m[n - 1] + (1 - \lambda)|y_m[n] - 2\alpha[n + 1]y_m[n - 1] + y_m[n - 2]|^2 \tag{5.11}$$

and S_{u_m} is the variance of the input u, which in its recursive estimate form is:

$$S_{u_m}[n] = \lambda S_{u_m}[n - 1] + (1 - \lambda)u_m^2[n] \tag{5.12}$$

with $0 < \lambda < 1$. The weights in (5.9) are therefore obtained as:

$$W_m[n] = \frac{S_{u_m}[n]/J_m[n]}{\sum_{i=1}^{M} S_{u_i}[n]/J_i[n]}. \tag{5.13}$$

The inclusion of the weighting process yields:

$$\alpha[n + 1] = \sum_{m=1}^{M} W_m[n]\frac{Q_m[n]}{2P_m[n]}. \tag{5.14}$$

The instantaneous frequency is computed as:

$$f[n + 1] = \arccos(\alpha[n + 1])/2\pi. \tag{5.15}$$

The BR was expressed as $f_{estim} = f \times f_s \times 60$ brpm, where f_s is the sampling rate of the inputs.

5.2.2   The *NFB* algorithm

One input signal: A notch filter output is smallest when its input is an oscillation at the notch frequency. The notch filter bank (*NFB*) algorithm is based on this fact and uses a bank of notch filters to probe the input signal for its main frequency. Given the output powers of a bank of notch filters with notch frequencies ranging over a certain band, the main frequency of the input is close to the notch frequency of the filter resulting in the smallest output. It is possible to design short FIR notch filters, so estimating the input frequency with a small delay with such a scheme is feasible. The *NFB* algorithm is, accordingly, based on a bank of length-3 FIR notch filters characterized by a pair of complex-conjugate zeros defined by the transfer function H_{notch}:

$$H_{notch}(z) = 1 - 2z^{-1}\cos(2\pi f_i) + z^{-2}, \tag{5.16}$$

where f_i is a discrete frequency from a given range $[f_1, f_F]$, with F the number of discrete frequencies. An example is shown in Figure 5.16. At sample n, the output of such a filter is $y_i[n]$:

$$y_i[n] = u[n] - 2u[n-1]\cos(2\pi f_i) + u[n-2], \ n = 3, 4, ..., \tag{5.17}$$

where u is the input signal.

If the dominant frequency of the input u is close to f_i, then the output y_i is small. The input u is filtered with all the filters of the bank. For each filter, the output-to-input power is computed as:

$$P_i[n] = \frac{Y_i[n]}{U[n]}, \tag{5.18}$$

with

$$Y_i[n] = \delta Y_i[n-1] + (1-\delta)y_i^2[n], \tag{5.19}$$

$$U[n] = \delta U[n-1] + (1-\delta)u^2[n], \tag{5.20}$$

which are the estimates of the mean squared values of the filter outputs and the input, initialized to $Y_i[2] = U[2] = 0.5(u^2[1] + u^2[2])$ with a forgetting factor $0 \ll \delta < 1$.

The set of P_i for $i = 1, ..., F$ are then used to compute a set of weights such that the weighted sum of the notch frequencies estimates the input dominant frequency. It is necessary to scale the weights in such a way as to give more importance to the small powers (where the notch frequency is close to the input dominant frequency) and little-to-no importance to the larger powers. An exponential weight dissociation scheme is employed to create large differences between the weights. The weights are thus computed as:

$$W_i[n] = \exp(-\gamma P_i[n]), \tag{5.21}$$

where γ is a weight dissociation parameter. It is computed as $\gamma = [min_{i=1,...,F}(P_i[n])]^{-1}$, for the smallest output power to yield the largest weight. The final frequency estimate is computed as the weighted sum of the notch frequencies of the filter bank:

$$f[n] = \frac{\sum_{i=1}^{F} W_i[n]f_i}{\sum_{i=1}^{F} W_i[n]}. \tag{5.22}$$
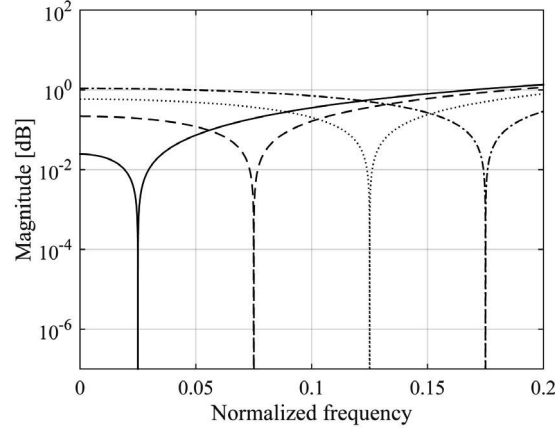
Figure 5.1: FIR notch filters with transfer functions according to (5.16).

Multiple input signals: By using vectors to represent the input, the outputs of the bank of filters and the weight computation, a single implementation is used regardless of the number of input signals containing the oscillation of interest. If there are multiple inputs with a common dominant frequency, then u becomes a vector signal $\mathbf{u}$. For each column of $\mathbf{u}$, i.e., $\mathbf{u}[n, j]$, for $j = 1, ..., S$ with S the number of input signals, (5.18) yields one set of $\{\mathbf{P_i}[n, j]\}$ for the notch frequencies. In order to obtain a single weight per frequency f_i, a weighted sum of the $\mathbf{P_i}[n, j]$ is computed across the inputs $j = 1, ..., S$:

$$W_i[n] = \exp(-\gamma \frac{1}{S} \sum_{j=1}^{S} \mathbf{R}[n, j]\mathbf{P_i}[n, j]),$$ (5.23)

where $\gamma = [min_{i=1,...,F}(\mathbf{R}[n, j]\mathbf{P_i}[n, j])]^{-1}$ and the $\mathbf{R}[n, j]$ for $j = 1, ..., S$ are a set of weights related to the input signals. These weights are introduced to emphasize signals with a clearer manifestation of the oscillation. In an application, one may be in presence of several measurements differing in noise level and/or modulation strength. It is useful to take into account how well multiple inputs present the oscillation of interest. One possible indication is the power remaining in each input after the suppression of the oscillation at the estimated frequency. Therefore, the $\mathbf{R}$ weights are defined as the signal-to-output power ratios of the input signals for a notch filter centered on the target frequency. Emphasis is therefore placed on the signal or signals with a smaller output and thus containing a stronger manifestation of the estimated frequency. This quality is assessed for each input by using its output $\mathbf{y_f}$ from a notch filter, according to (5.16), centered at the estimated frequency of the previous sample:

$$\mathbf{y_f}[n, j] = \mathbf{u}[n, j] - 2\mathbf{u}[n - 1, j] \cos(2\pi f[n - 1]) + \mathbf{u}[n - 2, j],$$ (5.24)

with $f[n - 1]$ being the previously estimated frequency (initialized to $f[2] = f_1$). The mean squared value of the input is estimated in (5.20) and that of the output $\mathbf{y_f}$ is assessed recursively as:

$$\mathbf{O}[n, j] = \delta\mathbf{O}[n - 1, j] + (1 - \delta)\mathbf{y_f}^2[n, j],$$ (5.25)

initialized to $\mathbf{O}[2] = (\mathbf{u}[3] - 2\mathbf{u}[2] \cos(2\pi f_1) + \mathbf{u}[1])^2$. The signal-to-output ratios are computed and normalized to create a set of weights $\mathbf{R}$ for the S inputs as:

$$\mathbf{R}[n, j] = \frac{\mathbf{U}[n, j]/\mathbf{O}[n, j]}{\sum_{j=1}^{S} \mathbf{U}[n, j]/\mathbf{O}[n, j]}.$$ (5.26)

After the weights related to the input signals are combined and scaled in (5.23), the frequency is computed as in (5.22). The BR is expressed as $f_{estim} = f \times f_s \times 60$ brpm.
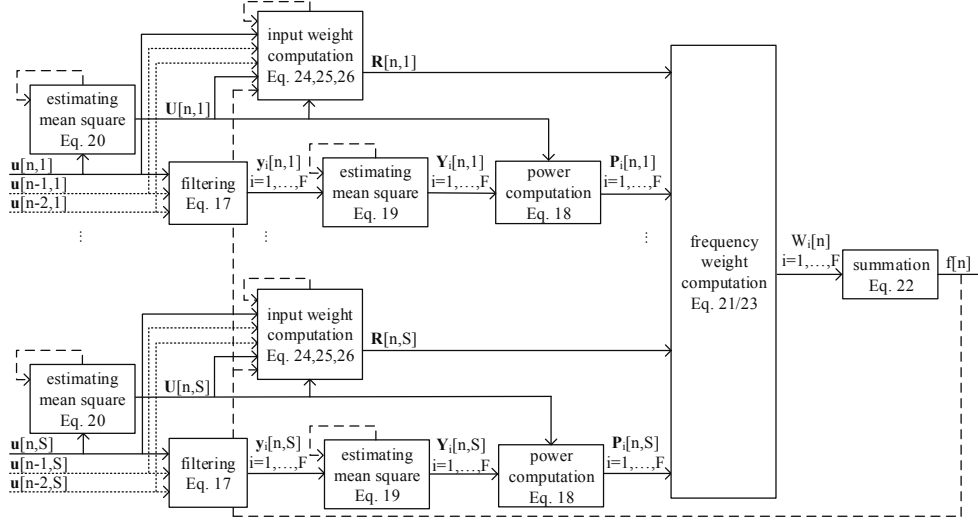
Figure 5.2: Flowchart of the *NFB* method with multiple inputs.

5.2.3 Estimation of the reference BR

To evaluate the BR estimated from the RSA and RPA waveforms, one needs to compare the estimate with the true BR. However, deriving the BR from a real breathing signal is a challenging problem as the breathing signal derived from thoracic volume changes (measured with impedance pneumography) or nasal/oral airflow is neither stationary nor band limited. It also contains many artifacts and noise due to the acquisition process. Many methods have been proposed until today, but no single automated technique exists to reliably compute the BR from this signal in a window or instantaneously. In fact, deriving the instantaneous BR from the breathing waveform poses the same challenges as deriving the BR from an ECG-derived breathing waveform.

One could apply the *W-OSC* or the *NFB* algorithms of course, but for evaluation purposes, it is chosen not to introduce a bias due to the method.

A common practice to estimate the BR from the breathing waveform is to compute the power spectrum in a sliding window and to consider the frequency of its dominant peak as the BR [28]. The power spectrum can be computed using either a non-parametric or a parametric estimator. AR modeling [138] and extrema detection [235] have been previously used to estimate a reference BR.

In this chapter, eight frequency estimation algorithms were used to estimate the BR from the reference breathing signal. The various frequency-domain and time-domain estimates were then combined to provide a robust estimate, to be used as reference BR. The majority of the selected methods are instantaneous.

Prior to the reference BR estimation process, the breathing signal was re-sampled at 4 Hz using cubic spline interpolation [1]. In addition, a high pass filter with a cutoff frequency of 0.01 Hz was applied to the re-sampled breathing signal in order to remove its baseline wander.

---

1. described in Appendix A.

1. Short term Fourier transform maximum frequency estimate: In order to determine the frequency content of a non-stationary signal using its spectrum, the short term Fourier transform (STFT) can be used. The STFT of a signal u windowed by a given window w (e.g., Hamming window) of length L is:

$$X(n,k) = \sum_{m=0}^{L-1} u[m]w[n-m]e^{-j2\pi km/L}.$$ (5.27)

Using the STFT, the instantaneous frequency was computed as the pulsation corresponding to the local maximum in the magnitude of the Fourier transform as:

$$\omega[n] = \arg \max_{k} [|X(n,k)|^2].$$ (5.28)

The instantaneous BR was computed as the normalized frequency corresponding to ω for L set to 75 s. This window length was empirically found to allow for necessary frequency resolution based on several trials.

2. Frequency estimate using the Hilbert-Huang transform: The Hilbert transform allows to generate, from a real signal, a complex signal, termed the analytic signal with separable amplitude and phase components [236]. However, for the Hilbert transform to be meaningful, the input signal must be narrow band [184]. Empirical mode decomposition (EMD) is a data analysis method that decomposes the signal into a set of intrinsic mode functions (IMFs) based on the extraction of energy from different intrinsic time scales [228]. EMD is used to extract a component of the breathing signal, which contains the BR and is narrow band such that the Hilbert transform outcome is meaningful. This method is referred to as the Hilbert-Huang transform [185, 186, 228]. When the EMD was applied to the breathing signal, the first IMF was generally observed to contain oscillations within the range of the BR. The instantaneous frequency was obtained by differentiating the phase of the analytic representation of the first IMF.

The Hilbert transform generates, from a real signal u, a complex valued signal, termed the analytic signal u_a, with instantaneous amplitude a and instantaneous phase ϕ such that:

$$u_a[n] = a[n]e^{j\phi[n]}.$$ (5.29)

The instantaneous phase of the analytic signal is

$$\phi[n] = arg\{u_a[n]\},$$ (5.30)

and the instantaneous frequency is computed by differentiating the phase:

$$\omega[n] = \phi[n] - \phi[n-1].$$ (5.31)

An IMF represents an oscillation mode embedded in the signal. Oscillation modes are identified based on their characteristic time scales (time lapse between one maximum and one minimum) empirically using local extrema and zero-crossing detections. The decomposition of the signal into IMFs uses the upper and lower envelopes defined by the local maxima and minima, respectively. The mean envelope is computed and subtracted from the signal. The same procedure is repeated for the difference signal, and so on, till a stopping criterion, such as a limitation on the standard deviation of two difference waves, is met. This sifting process has the effect of eliminating riding waves and making the oscillation more symmetric and results in the first IMF component of the data. Once an IMF component is obtained, it is subtracted from the original signal and the sifting process is applied to the residue in order to extract the next IMF, and so on. This iterative process extracts the oscillations in the order of the finest scale (shortest period) to the largest, the finest being extracted as the first IMF component. The method is summarized

in Algorithm 5.1 and an example of its application is illustrated in Figure 5.3. The process ends when a stopping criterion such as a limitation on the amplitude of the residue r_{mode} is met [237].

Algorithm 5.1 empirical mode decomposition (EMD).

---

1. Identify extrema of u.
2. Interpolate between maxima to obtain the upper envelope e_{max} and interpolate between minima to obtain the lower envelope e_{min}.
3. Compute mean of envelopes $m[n] = (e_{max}[n] + e_{min}[n])/2$.
4. Compute the residual $r[n] = u[n] - m[n]$.
5. Iterate steps 1-4 on $u = r$ until the residual is an IMF according to stopping criteria: $r = c_{mode}$. The residual is $r_{mode}[n] = u[n] - c_{mode}[n]$.
6. Iterate steps 1-5 on residual $u = r_{mode}$ to obtain the next IMF.

IMFs are extracted from the signal such that the number of extrema and zero crossings are equal (or at most, differ from each other by one) and the mean of the upper and lower envelopes is zero or close to zero. Due to their definition, IMFs have well-behaved Hilbert transforms, from which the instantaneous frequency can be derived. The first IMF is selected as the main breathing component of the signal.
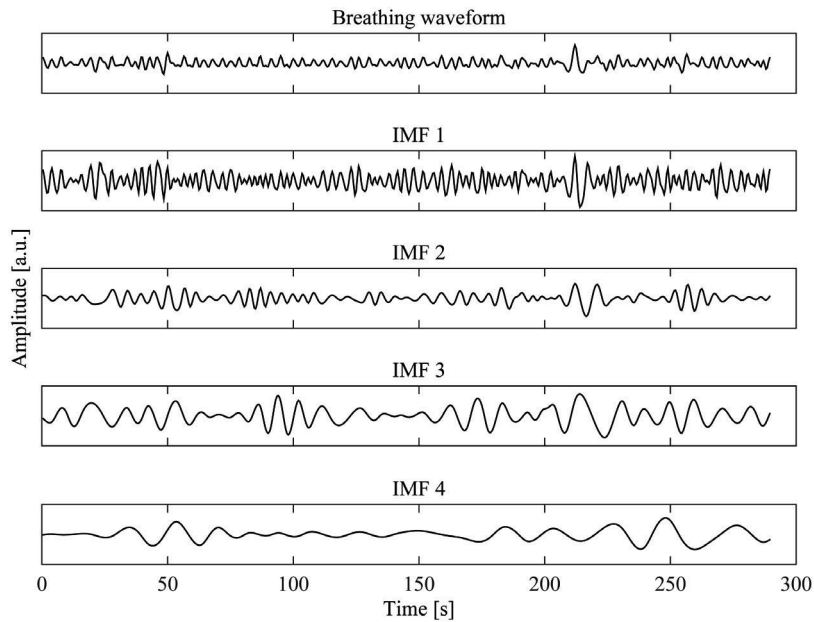
Figure 5.3: The decomposition of a signal into IMFs with the EMD. The first four IMFs were extracted through EMD from a sample breathing signal. The first IMF contains the main breathing-related oscillation.

3. Frequency estimate based on the breathing cycle: The time difference between two breathing peaks is interpreted as a breathing cycle. The peaks were extracted by local maxima detection. The time series of their differences, attributed to the time index of the second peak, was created and inversed in order to estimate the instantaneous BR. The resulting BR was

re-sampled at 4 Hz using cubic spline interpolation [2].

4. Frequency estimate based on the number of peaks per windows: The number of local maxima in a window determines the number of breathing cycles in that window. The BR was estimated as the ratio of the number of breathing cycles in the window by the length of the window. A 20-s-long sliding window was chosen based on several trials. Respiratory peaks were extracted by local maxima detection.

5. Frequency estimate based on the Teager-Kaiser energy tracking operator: The Teager-Kaiser energy tracking operator estimates the energy required to generate a given amplitude and frequency modulated signal, which is then used to separate the amplitude and frequency components [227]. The operator is defined for a discrete-time signal u as:

$$\Psi_d\{u[n]\} = u^2[n] - u[n-1]u[n+1]. \tag{5.32}$$

When the nonlinear operator Ψ_d is applied to an signal u defined as:

$$u[n] = a[n]\cos(\phi[n]) \tag{5.33}$$

with envelope $|a[n]|$ and instantaneous frequency $\omega_i[n] = \frac{d\phi}{dn}[n]$, it can estimate the squared product of the amplitude and frequency:

$$\Psi_d\{u[n]\} \approx a^2[n]\sin^2[(\omega[n]). \tag{5.34}$$

When Ψ_d is applied to both u and its backward difference $y[n] = u[n] - u[n-1]$, the instantaneous frequency of u can be separated following the energy operator separation algorithm according to [227] as

$$\omega_i[n] \approx \arccos(1 - \frac{\Psi_d\{y[n]\} + \Psi_d\{y[n+1]\}}{4\Psi_d\{u[n]\}}). \tag{5.35}$$

6. Frequency estimate based on the modified covariance method: The modified covariance method is a recursive frequency tracking algorithm derived from the linear prediction property of sinusoids [238]. For a signal u in the form of:

$$u[n] = s[n] + b[n], \tag{5.36}$$

where s is a sinusoid expressed as $s[n] = cos(\omega_0[n] + \phi)$, and b is additive white noise, the linear prediction expresses the recurrence of the signal such that:

$$s[n] = 2cos(\omega)s[n-1] - s[n-2]. \tag{5.37}$$

The prediction error is thus:

$$e[n] = u[n] - 2cos(\omega)u[n-1] + u[n-2], \tag{5.38}$$

where ω is the estimation of ω_0. The modified covariance method minimizes the sum of the squares of e, which leads to:

$$\omega[n] = \arg\min_\lambda\{\sum_{n=3}^{k}e^2[n]\} = cos^{-1}(\frac{A_k}{2B_k}), \tag{5.39}$$

where

---

2. described in Appendix A.

$$A_k = \sum_{n=3}^{k} u[n-1](u[n] + u[n-2]),$$

$$B_k = \sum_{n=3}^{k} u^2[n-1], \tag{5.40}$$

with k the number of available samples. A_k and B_k can be approximated in an instantaneous manner such that:

$$A_k = \lambda A_{k-1} + u[k-1](u[k] + u[k-2]),$$
$$B_k = \lambda B_{k-1} + u^2[k-1], \tag{5.41}$$

where $0 < \lambda < 1$ is the forgetting factor. The empirical value of $\lambda = 0.65$ was used here based on several trials.

7. Frequency estimate based on AR modeling: The BR was extracted as the largest peak, within a 20-s-long sliding window, of the spectrum estimated using an AR model fit to the data [28]. The window length was found to be optimal based on several trials. A Yule-Walker 10-th order autoregressive model was used. In [138], an AR model of order 8 was used to estimate the spectrum of the breathing signal. However, several trials showed that increasing the order to 10 yields more detailed BR estimates. The signal is expressed in terms of an autoregressive model such that:

$$u[n] = -a_1 u[n-1] - \ldots - a_P u[n-p] + b[n], \tag{5.42}$$

where p is the model order and b is a white noise. The model transfer function is:

$$H_{ar}(e^{jk}) = \frac{b}{\sum_{l=0}^{p} a_l e^{-jkl}}. \tag{5.43}$$

The power spectrum is:

$$P(e^{jk}) = \frac{|b|^2}{\sum_{l=0}^{p} a_l e^{-jkl}}. \tag{5.44}$$

The largest peak within a given window is chosen as the BR within that window:

$$\omega_{window} = \arg \max_{k} [P(e^{jk})]. \tag{5.45}$$

8. Frequency estimate based on Prony's method: Prony's method is a technique for modeling a discrete-time signal as a linear combination of exponentials. It extends Fourier analysis by directly estimating frequency, damping, strength and relative phase of modal components present in a signal [239]. In the original approach, a model is fit to the data. Using this model, the frequency and other signal attributes are computed. Later, a modified instantaneous linear-prediction-based version of Prony's frequency estimator was proposed [240], which uses five data points to directly estimate the instantaneous frequency of a sinusoidal signal u:

$$\omega[n] = acos(\frac{(u[n-1]u[n+2] - u[n-2]u[n+1]) + (u[n]u[n+1] - u[n-1]u[n+2])}{4(u[n]^2 - u[n-1]u[n+1])}). \tag{5.46}$$

Reference BR: At each time index, the three closest estimates to the median of the eight afore-mentioned estimates were chosen as the three most accurate BRs. The reference BR was computed as the mean of the three retained estimates. This combination method is robust to outliers and allows to take into account different estimates, some of which are spectral and some other temporal. Estimates *1*, *4* and *7* were computed in windows and estimates *2*, *3*, *5*, *6* and *8* were instantaneous. A low-pass Butterworth filter with a cutoff frequency of 0.8 Hz (48 brpm) was used to filter the estimates *2*, *5*, *6*, *7* and *8* in order to smooth sudden changes due to the imperfection of the breathing signal with respect to the assumptions of each algorithm. The final reference BR was filtered as well. In the filtering operations mentioned, forward-backward filtering was used in order to avoid phase shifts. The BR was expressed as $f_{ref} = 2\pi\omega_{ref} \times f_s \times 60$ brpm.

5.3 Evaluation

Three separate evaluation tasks were performed: 1) The bias and variance of the *NFB* were evaluated on synthetic data. 2) The performance of the *W-OSC* and the *NFB* methods was evaluated on a set of real data pertaining to the resting state. 3) The performance of the *NFB* method was evaluated on signals acquired during physical exercise.

5.3.1 The bias and variance of the *NFB* algorithm

The bias and variance of the *NFB* algorithm output were evaluated using Monte-Carlo simulations. 1000-sample sinusoids were generated with a normalized time-varying frequency with a sinusoidal pattern (one period of the sine was generated over the 1000 samples) ranging between two values drawn randomly in the interval $[0.02, 0.1]$ and with random initial phases. A Gaussian white noise was added to the sinusoids with several SNR values ranging from 0 to 5 dB. The bias (relative) and variance of the frequency estimates were computed over the length of the test signals and averaged over 1000 runs. The algorithm was tested with one input and with two inputs. The sensitivity of the algorithm to its parameters F (number of filters) and δ (forgetting factor of the recursion) was assessed by recording the estimation bias and variance for different values of each parameter. F was varied between 10 and 100 and δ was varied between 0.8 and 0.99.

5.3.2 Application of the *W-OSC* and *NFB* algorithms to data at rest

The PhysioNet "Fantasia" data set [241, 242] was used to evaluate the algorithms in this study. This data set provides 120-minute recordings of simultaneously acquired single-lead ECG and spontaneous breathing signals (thought to be recorded through impedance pneumography according to [138]) from 20 young (21-34 years of age) and 20 elderly (68-85 years of age) subjects. The subjects were healthy and lay supine watching the movie "Fantasia". Both sets of signals were digitized with a sampling rate of 250 Hz.

The test data are off-line recordings. However, given the interest in real-time processing in monitoring systems, both the *W-OSC* and the *NFB* algorithms were implemented to support real-time processing. In the particular case of BR estimation from the ECG, a pipeline was designed to process immediately each heartbeat in chronological order. The overall implementation is therefore a beat-to-beat implementation. Regardless, the frequency estimation methods were implemented to process one sample at a time, while keeping in memory the internal variables and parameters necessary for the processing.

After each new heartbeat, the RSA and the RPA were extracted from the ECG. The R-peaks of the ECG were identified with a conventional extrema detection method. The R-R intervals time series was created and re-sampled uniformly at 4 Hz using sample-and-hold interpolation [28]

as described in Section A.1. The resulting re-sampled waveform contains steps and must be low-pass filtered. This type of interpolation was chosen because of its truly real-time (with one beat delay) nature. The resulting samples were concatenated with those in memory and band-pass filtered (causal filtering) within the breathing frequencies, i.e., between 0.08 Hz and 0.8 Hz, equivalent to 4.8 to 48 brpm using an order 18 Butterworth filter to yield the RSA waveform. The R-peak amplitudes were re-sampled and filtered similarly to yield the RPA waveform.

In [138] it was noted that in the "Fantasia" data set, the baroreflex activity (occurring around the frequency of 0.1 Hz)[3] was sometimes very strong and could be confused for a low BR. The authors therefore used a filter with a higher cutoff frequency of 0.2 Hz (12 brpm) in addition to the wider breathing-range filtering. In an additional processing step, they combined the various filter outputs. Similarly, in the present study, a narrow-band version of the RSA was created (the RPA is not assumed to contain baroreflex activity) by filtering the inter-beat intervals between 0.2 Hz and 0.8 Hz. The narrow-band version was fed as input to the algorithm in addition to its wider-band counterpart. It was hypothesized that in the case of a high BR, as both versions contain the high frequency breathing oscillation, there was less chance that the low-frequency baroreflex oscillation would be extracted by the algorithm. In the case of a low BR, two out of the three inputs (the narrow-band RSA, the wide-band RSA and the RPA) would contain the common modulation, which should be sufficient for a valid estimation. After filtering, the new samples were fed to the frequency estimation algorithm. It must be noted that, at most, one-minute worth of data was retained in memory. Figure 5.4 displays the flowchart of the implementation.
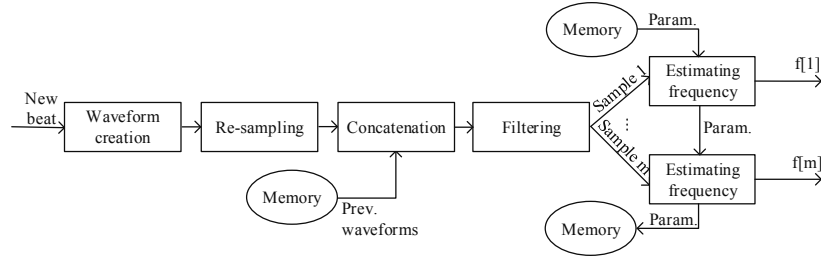
Figure 5.4: Flowchart of the beat-to-beat BR estimation from the ECG.

The algorithms were tested with one or two inputs. In the single-input case, either the RSA (wide-band) or the RPA was used by the algorithms. In the two-input case, both the RSA (narrow-band and wide-band) and the RPA were used, meaning that in fact, the algorithms ran with three inputs. The fixed range of $[f_1, ..., f_F] = [0, ..., 0.2]$ equivalent to 0 to 0.8 Hz (given the 4 Hz sampling rate) or BRs ranging from 0 to 48 brpm, was used to define the filter bank.

The *W-OSC* algorithm was applied with the parameter set $\beta = 0.95$ (band-pass filter bandwidth), $\delta = \lambda = 0.95$ (forgetting factors) [233]. Given that the *W-OSC* has already been extensively tested on simulated and real data in [233], its performance is reported here only for this set of default parameters.

The mean absolute error was computed as:

$$error = \frac{1}{N} \sum_{i=1}^{N} \left| f_{estim} - f_{ref} \right|, \tag{5.47}$$

where N is the length of the signals. f_{estim} is the estimated BR and f_{ref} is the reference BR.

---

3. see Section 2.1 for a brief explanation on the baroreflex mechanism.

In order to assess the delays of the frequency estimates, the correlation of the estimates with the reference BR was computed using the Pearson correlation coefficient for lag values ranging from 1 to 200 samples. The lag yielding the highest correlation was chosen as the estimation delay.

The statistical significance of the differences between the errors and delays of the two algorithms for the two age groups was assessed with student's T-test or the Mann-Whitney U-test, depending on the normality of the data. The normality of the data was tested using the Anderson-Darling test.

5.3.3   Application of the *NFB* algorithm to physical activity signals

To test the *NFB* algorithm on challenging signals with extreme BR values, we used signals acquired from two subjects (healthy young males, moderately trained) during a VO$_2$ max test (incremental exercise test to assess maximum oxygen uptake) on an ergo-cyclometer (i.e., 3 minutes of rest followed by 3 minutes of cycling with no load followed by load increments of 30 W/min every 2 s until exhaustion). The inter-beat intervals were recorded with a Polar® belt and the breathing waveform was acquired with a spirometer[4]. The signals were re-sampled at 4 Hz with cubic spline interpolation[5]. The RSA (only wide-band, filtered between 0.1 and 1.5 Hz, equivalent to 6 to 90 brpm, because of the plausibility of high BRs during exercise) was extracted from the inter-beat intervals as described for the "Fantasia" signals. The BR was estimated from the RSA with the *NFB* algorithm with $[f_1, ..., f_F] = [0, ..., 1.5]$ Hz.

5.4   Results

5.4.1   The bias and variance of the *NFB*

The bias and variance of the frequency estimates of one and two inputs are shown in Figure 5.5 for two values of F with $\delta = 0.9$ (mid-range). Figure 5.6 shows the estimation bias and variance for one and two inputs for two values of δ with $F = 50$ (mid-range). It can be seen that the benefit of a second input is the reduction of the bias and especially the variance, particularly at low SNR values. Over the test range, F did not appear to have a notable effect on the bias or the variance. A smaller δ resulted in a smaller bias and larger variance, especially at low SNR values.

Table 5.1 summarizes the bias and variance of the estimates for several combinations of the algorithm parameters F and δ for the single-input and two-input cases over 1000 runs for an SNR value of 5 dB. It can be seen that the benefit of a second input is the reduction of the bias and the variance by up to 50%.

5.4.2   The performance of the *W-OSC* and *NFB* algorithms on data at rest

An example of the RSA and RPA waveforms from the "Fantasia" data set is shown in Figure 5.7 together with the simultaneously recorded breathing waveform. An oscillatory component corresponding to breathing can be observed in both the RSA and RPA waveforms.

An example of the BR estimates using the *W-OSC* and the *NFB* algorithms with both the RSA and the RPA as inputs is presented along with the reference BR in Figure 5.8. It can be seen that, generally, the estimate using the *NFB* algorithm is closer to the reference compared to that of the *W-OSC*. It also follows the reference with less delay in time.

---

4. The raw signals were provided thanks to Dr Fabio Borrani from the Institute of Sport Science, University of Lausanne, Switzerland.

5. described in Appendix A.
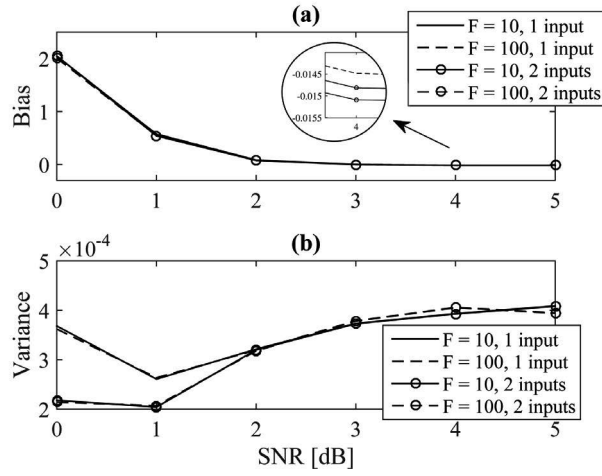
Figure 5.5: The estimation bias (a) and variance (b) of the the *NFB* method for different values of the parameter F with $\delta = 0.9$ (mid-range).
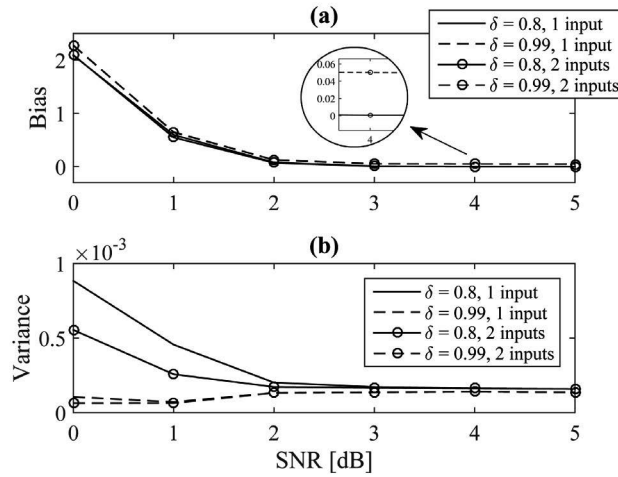
Figure 5.6: The estimation bias (a) and variance (b) of the *NFB* method for different values of the parameter δ with $F = 50$ (mid-range).

Table 5.1: The estimation bias (relative) and variance of the *NFB* algorithm for several combinations of F and δ. SNR = 5 dB.

		bias	variance
single-input	$F = 10, \ \delta = 0.8$	-2.03×10^{-2}	4.08×10^{-4}
	$F = 10, \ \delta = 0.99$	8.54×10^{-2}	3.17×10^{-4}
	$F = 100, \ \delta = 0.8$	3.53×10^{-4}	1.49×10^{-4}
	$F = 100, \ \delta = 0.99$	4.10×10^{-2}	1.22×10^{-4}
two-input	$F = 10, \ \delta = 0.8$	-2.03×10^{-2}	4.08×10^{-4}
	$F = 10, \ \delta = 0.99$	8.54×10^{-2}	3.17×10^{-4}
	$F = 100, \ \delta = 0.8$	1.33×10^{-4}	1.48×10^{-4}
	$F = 100, \ \delta = 0.99$	4.07×10^{-2}	1.19×10^{-4}
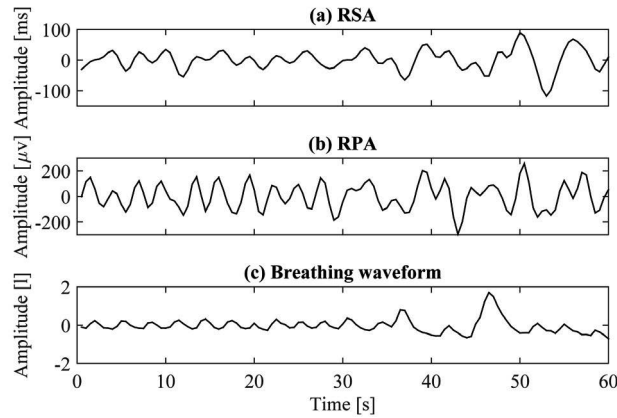
Figure 5.7: An example of the RSA, RPA and the breathing waveforms from the "Fantasia" data set: (a) RSA waveform; (b) RPA waveform; (c) breathing signal.

Table 5.2 reports the estimation errors and delays of the *NFB* algorithm over the entire data set for different combinations of the algorithm parameters F and δ. It can be seen that a larger F reduces the estimation error with a plateau at $F = 50$. However, F does not seem to have a uni-directional relationship with the delay. A smaller δ reduces the estimation delay, but the value of δ does not have a uni-directional relationship with the error. Therefore for a small error and a small delay, both parameters need to be chosen from their mid-range values. The average reference BR over the entire data set was 17.34 brpm.

Table 5.2: The mean (STD) of the error (brpm) and the delay (s) of the *NFB* algorithm with several combinations of F and δ over the "Fantasia" data set using both the RSA and the RPA. The values in bold highlight the smallest errors and delays achieved.

$F \setminus \delta$		0.8	0.9	0.99
10	error	2.32 (1.18)	2.29 (1.12)	2.51 (1.04)
	delay	**11.89 (7.37)**	13.58 (7.33)	30.04 (12.09)
50	error	2.23 (1.15)	**2.20 (1.11)**	2.32 (1.08)
	delay	12.88 (8.13)	13.41 (7.98)	27.93 (10.66)
100	error	2.23 (1.15)	**2.20 (1.11)**	2.32 (1.08)
	delay	13.42 (8.40)	13.89 (8.04)	28.13 (11.91)

Table 5.3 reports the errors of the *W-OSC* and the *NFB* ($F = 50$ and $\delta = 0.9$) algorithms with only the RSA or the RPA, or both as inputs. In all cases, the differences between the errors of the young population and those of the elderly were not significant. For both the young and the elderly, the errors of the *NFB* algorithm were significantly smaller ($p < 0.05$) than those of the *W-OSC* method. In line with intuition and simulation results, using both the RSA and the RPA yielded more accurate estimates than using each signal alone. The number of inputs did not seem to have a unique effect on the estimation delay.

In order to check the estimation delay, the mean delay for each algorithm was introduced and the errors were re-computed. The corrected errors are reported in Table 5.4. It can be seen that as expected, the errors were smaller than when no delay correction was performed. In this setting also, the errors of the *NFB* algorithm were significantly smaller ($p < 0.05$) than those of the *W-OSC*.
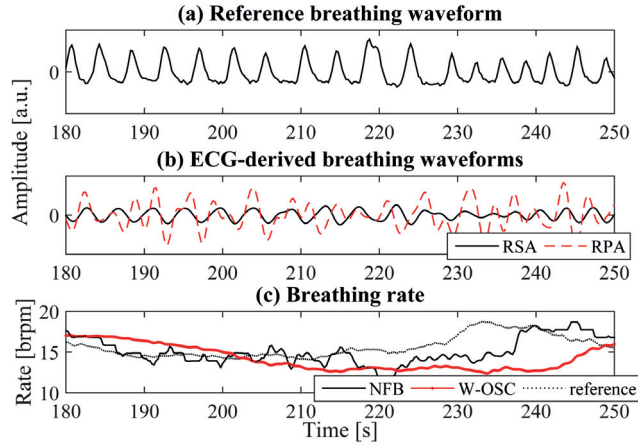
Figure 5.8: Breathing rate estimation with the *W-OSC* and *NFB* algorithms: (a) the reference breathing waveform; (b) the RSA and RPA waveforms; (c) the BR estimates of the *NFB* method and the *W-OSC*, and the reference BR.

Table 5.3: The mean (STD) of the estimation error (brpm) and delay (s) of the *W-OSC* and the *NFB* algorithms over the "Fantasia" data set. The errors and delays of the *NFB* algorithm were significantly smaller (p < 0.05) than those of the *W-OSC* for all categories. The values in bold highlight the smallest errors and delays achieved.

			Young	Elderly	All
W-OSC	RSA	error	3.50 (1.57)	4.31 (1.74)	3.91 (1.71)
		delay	24.33 (9.52)	27.33 (11.49)	25.76 (10.61)
	RPA	error	3.50 (1.68)	3.27 (1.25)	3.38 (1.49)
		delay	23.08 (9.60)	24.44 (8.94)	23.74 (9.32)
	both	error	2.42 (1.28)	2.84 (1.11)	2.63 (1.22)
		delay	24.45 (9.92)	26.29 (9.95)	25.30 (9.98)
NFB	RSA	error	3.41 (1.59)	3.59 (2.00)	3.50 (1.81)
		delay	14.68 (10.19)	12.08 (8.15)	13.45 (9.37)
	RPA	error	2.43 (1.09)	2.56 (1.18)	2.50 (1.14)
		delay	14.25 (11.57)	12.85 (7.26)	13.55 (9.69)
	both	error	**2.02 (0.94)**	**2.38 (1.25)**	**2.20 (1.11)**
		delay	**11.98 (4.97)**	**14.84 (9.93)**	**13.41 (7.98)**

Table 5.4: The delay-corrected errors (brpm) of the *NFB* and the *W-OSC* algorithm over the "Fantasia" data set using both the RSA and the RPA. The errors and delays of the *NFB* algorithm were significantly smaller (p < 0.05) than those of the *W-OSC*. The values in bold highlight the smallest errors and delays achieved.

	Young	Elderly	All
W-OSC	1.77	2.17	1.97
NFB	**1.72**	**2.03**	**1.87**

Figure 5.9 shows the sensitivity of the *W-OSC* and the *NFB* algorithms to variation in the parameter δ ($\lambda = \delta$ for the *W-OSC* here) over the "Fantasia" data set (δ is a parameter similar in both algorithms). The algorithms were tested in the two-input case. The *NFB* algorithm was used with $F = 50$ and the *W-OSC* with $\beta = 0.95$ and $\lambda = \delta$ (λ is also a forgetting factor). It can be seen that the *NFB* algorithm presented mean errors and delays which were less variable with respect to δ compared to the *W-OSC*. For example, for $\delta = [0.8, 0.95]$, the error and delay of the *NFB* algorithm estimates were 2.20 ± 0.02 brpm and 14.12 ± 1.69 s respectively, whereas the error and delay of the *W-OSC* estimates were 2.99 ± 0.47 brpm and 20.58 ± 4.78 s, respectively.
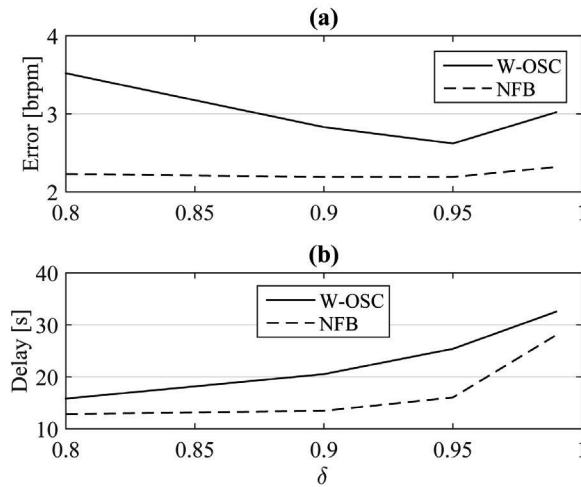
Figure 5.9: The sensitivity of the *W-OSC* and the *NFB* algorithms to their respective forgetting factors δ (a) in terms of error and (b) in terms of delay.

5.4.3 Performance of the *NFB* method on physical activity data

Figures 5.10 and 5.11 illustrate the reference BR and the estimated BR ($F = 50$ and $\delta = 0.9$) from the inter-beat intervals of the two subjects during the entire length of the exercise. It can be seen from the two figures that the *NFB* generally tracked the BR well with average errors of 1.61 brpm and 3.71 brpm over the length of the records. It must be noted that there is a large deviation of the estimated frequency for subject 2 between 500 s and 700 s, but a time-frequency analysis of the inter-beat intervals revealed that the algorithm was in fact truthful to their variation.

5.5 Discussion and benchmarking

5.5.1 The bias and variance of the *NFB*

On simulated data, the *NFB* algorithm yielded estimates with bias and variance approaching zero with increasing input SNR values. The simulations showed that the sensitivity of the *NFB* algorithm to its parameters (i.e., the filter bank resolution F and the forgetting factor δ) depends on the input SNR. A second input to the *NFB* algorithm reduced the estimation bias and variance by up to 50% compared to using a single input with a larger effect on the bias than on the variance.
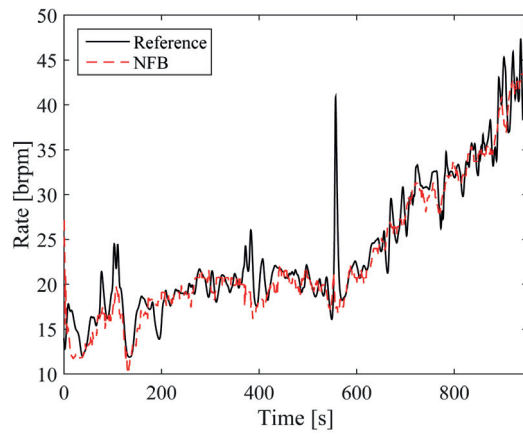
Figure 5.10: The reference and *NFB* estimate BRs for Subject 1 during exercise. The mean absolute error over the length of the record was 1.61 brpm.
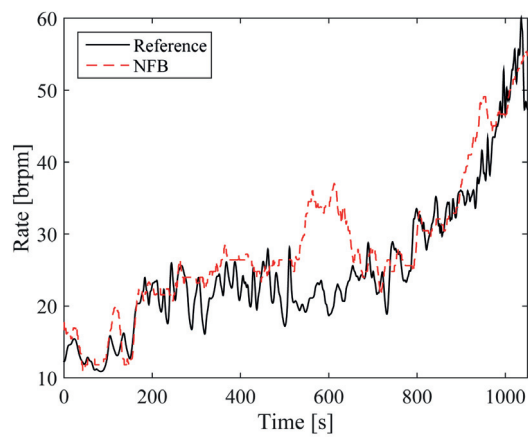
Figure 5.11: The reference and *NFB* estimate BRs for Subject 2 during exercise. The mean absolute error over the length of the record was 3.71 brpm.

5.5.2 The performance of the *W-OSC* and *NFB* algorithms on resting data

Both the *W-OSC* and the *NFB* methods yielded instantaneous BR estimates in a continuous and automatic manner, without requiring special adjustments based on subject characteristics. Furthermore, sudden changes in the BR estimate because of abnormal beats or bad quality segments in the recordings were rectified within a limited number of iterations due to the recursiveness of both methods, thus no special data-dependent pre-processing was needed.

Since the number of input signals in the *W-OSC* and *NFB* algorithms is not limited, the breathing-related waveforms extracted from more than one ECG lead can be used to estimate the BR. In fact, other inputs containing the breathing modulation can be used as well. In particular, the RSA extracted from photoplethysmogram (PPG) recordings and the pulse transit time (PTT) are candidates as seen from their power spectral densities (PSD) in Figure 5.12. They both contain the breathing modulation of the heart rate similarly to the RSA and RPA of ECG. PPG waveforms are somewhat popular for the estimation of the cardiac and breathing parameters in a non-invasive and easy manner [139, 219] and the PTT can be derived by using ECG and PPG recordings, and also carries the breathing modulation of the cardiac rhythm [243]. Figure 5.13 shows a snapshot of a demonstration created for the startup company Leman Micro Devices [6] in a collaborative project. In this demonstration, the BR was estimated from the ECG RSA and RPA, RSA from PPG signals acquired in red and infrared (IR) illuminations, the PTT and several combinations of them.
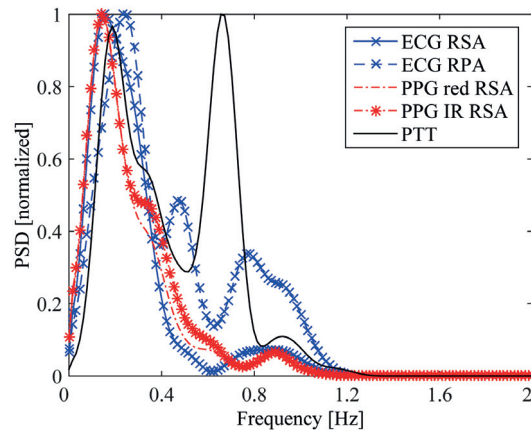
Figure 5.12: The PSD of the ECG and PPG RSA and the PTT. All contain the breathing modulation as seen in the peak at around 0.2 Hz.

From real ECG data, the *NFB* estimated the BR with a smaller error and less delay (nearly half less) than the *W-OSC* method. When the mean delay was introduced in the estimates, the errors were smaller for both algorithms, as expected.

On the ECG data, the estimation error of the *NFB* method was consistent with the results of the simulations in terms of variations with respect to the parameter choice and the number of inputs. The estimation delay appeared to be directly related to δ. On the other hand, the resolution (F) did not seem to have a specific relationship with the delay, but it had an effect on the complexity of the algorithm. A mid-range value of the two parameters provided an acceptable error-delay compromise. Nonetheless, over the range of tested values, the error varied at most by 0.31 brpm, which is not a large variation considering that the reference BR was on average 17.34 brpm. In comparison with the *W-OSC*, the *NFB* algorithm showed a considerably smaller sensitivity to its

---

6. www.leman-micro.com/site/
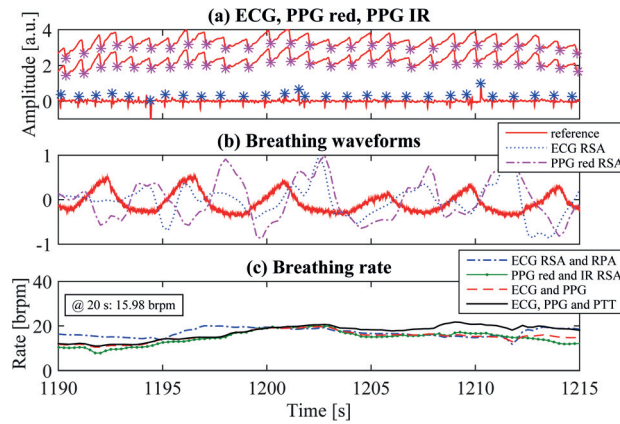
Figure 5.13: Estimating the BR from several ECG and PPG breathing modulations: (a) The PPG and ECG and the heart beats; (b) the reference breathing waveform and the RSA extracted from the ECG and the PPG; (c) The BR estimated with the *W-OSC* method.

parameter choice. This property is especially beneficial in real biomedical applications, in which there is a large variability in the signals between individuals and even within one individual. It is therefore beneficial to use a method, which does not require much adjustment of its parameters.

Using the RSA and RPA, separately, was also by far not as good as using both together, which shows the importance of the additional information. The RPA alone yielded better results than the RSA alone. This result is not in line with other studies [138]. In [138], all the inputs were narrow-band filtered to avoid the baroreflex oscillation. However, in the event of a low BR (lower than 0.2 Hz equivalent to 12 brpm), the breathing-related component would not be correctly extracted. The results were good regardless, because in the "Fantasia" data set, the BR is always above 12 brpm. The filtering operation removed the unwanted baroreflex influence without removing breathing-related oscillations. It seems that indeed, in the present study, the large baroreflex amplitude interferes with the identification of the breathing-related component of the RSA (wide-band). It is important to note that without prior knowledge about the BR, which is normally the case in an application, one cannot justify using only the narrow-band RSA. In a spirit of objectivity, we respected this condition in this study.

Results obtained in the present study can be compared to those of Orphanidou *et al.* [138], which were also presented on the "Fantasia" data set. It must be noted that the others used the same AR-based frequency estimation method on both the ECG-derived breathing waveform and the breathing signal to derive estimated BRs and reference BRs. A degree of correlation may therefore exist between the derived BRs. Furthermore, a validity criterion was used to exclude up to 35% of the data. In the present study, the *W-OSC* tracking method was excluded for reference estimation in order to avoid bias in the results. Due to the unavoidable differences in methodology and the different reference BR, the *W-OSC* and *NFB* estimates are not directly comparable to Orphanidou *et al.*'s. However, the order of magnitude of the errors in the present study are similar, despite using the entire data set, and not imposing restrictive bandwidths in the filtering processes.

Unlike the AR-based method of Orphanidou *et al.*, both the *W-OSC* and the *NFB* methods are automatic and instantaneous, robust to abnormal beats and segments of bad quality data. The delay in the estimates of Orphanidou *et al.* is half the window length, which is 30 s. Both methods in this chapter were implemented in a truly real-time manner, such that heart beats were processed in chronological order, and the BR estimates were updated with information from each

new beat.

5.5.3   The performance of the *NFB* method on physical activity data

On the data acquired during physical activity, the *NFB* method was robust and tracked the rapidly varying BR accurately and with no need for any special adjustments compared to its application to resting-state signals, except for a slightly larger application bandwidth.

It must be noted that the *W-OSC* method was also applied to the task of etimating the BR during exercise. The results were similar to those of the *NFB* with a larger estimation delay, as expected. Due to the small amount of data available, we chose not to carry out an extensive analysis on the exercise data.

5.5.4   Limitations

On the real data, i.e. the "Fantasia" data set and the VO2MAX data, the reference BR was computed with automated methods. Despite our best care and intentions, the automatic reference could be influenced by noise and artifacts and does not fully represent a ground-truth.

As discussed in Chapter 3, in the supine position, the RSA is generally the largest component of the R-R intervals. In the orthostatic position, the baroreflex activity influence is larger than at supine, and may be confused for the breathing-related component. This problem even occurred in the "Fantasia" supine data in [138]. Other studies have also highlighted that estimating the BR in positions other than supine or seated is more difficult [224]. Most of the results presented in this chapter were also on supine data. It must be noted that estimating the BR regardless of the position my be more challenging than on supine resting data. However, interestingly, on the exercise data, this problem did not arise. This could be due to the more prominent breathing patterns and the autonomic particularities of exercise.

5.6   Conclusions

Two algorithms were applied to the case of estimating the BR from the ECG and in particular the RSA. The *W-OSC* method is an established algorithm and the other, the *NFB* algorithm, is a novel technique, attempting to overcome a shortcoming of the *W-OSC* method, namely its estimation delay.

Both were successful in estimating the BR with the same accuracy as other existing methods, however in a truly real-time manner and with a lower estimation delay. These algorithms can be applied to the estimation of the BR from various modalities (such as the PPG [139]) and to combinations (e.g. ECG and PPG).

Estimation of the Breathing Rate using Imaging Photoplethysmography

6

The direct measurement of BR requires a mask or an impedance belt. Measuring the BR using the RSA from the ECG requires at least one ECG lead, with electrodes placed sufficiently apart on the body. However, it is of increasing interest to monitor the heart rate and the BR in an entirely contactless manner. For example, for monitoring new born infants, devices with cables or transmission capabilities are considered cumbersome and unreliable.

In Chapter 5, the BR was estimated from the ECG and in particular from the RSA, in a real-time manner with two different algorithms. As the main necessity for these methods is the heart inter-beat intervals, other signals representing the cardiac activity, from which the inter-beat intervals can be derived, are also useful for the goal of estimating the BR from the RSA. This chapter explores the BR estimation from imaging photoplethysmography using one of the methods described in Chapter 5, namely the notch filter bank (*NFB*) method. Imaging photo-plethysmography is a novel technique to capture heartbeats via blood volume changes, reflected in skin tone changes observable in a video sequence of a person's face. Elements of this chapter were presented at a conference [244].

6.1   Introduction

6.1.1   What is imaging photoplethysmography (iPPG)?

Photoplethysmography (PPG) is a non-invasive technique to measure blood volume varia-tions by placing a small illumination and detection probe on the surface of the skin [245]. PPG systems produce a waveform representing blood volume changes caused by heartbeats by mea-suring reflectance or transmittance of a light source placed in contact with the skin. This method has many medical uses in the measurement of cardio-vascular features such as heart rate (HR), blood volume, oxygen saturation and even the BR [219, 245].

Recently, it has been demonstrated that PPG signals can be acquired in an entirely contactless manner, bringing forth the imaging photoplethysmography (iPPG) [246, 247]. In iPPG systems, a visible-light or infrared video camera is placed in front of the subject at a distance of about 1 m, and captures skin tone changes (often in the face) in visible red, green, blue or infrared channels [248, 249]. Figure 6.1 shows colormaps of the face, under visible and infrared illumi-nations, highlighting regions of the face where the HR is visible from images acquired with a

video camera. The variation of skin tone in time is then extracted from the pixels of each frame to produce the iPPG waveform.
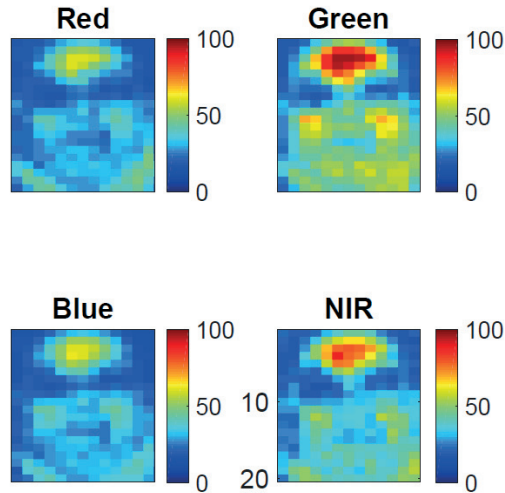
Figure 6.1: Colormaps of the face representing HR-related power captured with a video-camera. The green channel captures the most HR-related information. Figure from [249] with permission.

6.1.2   BR estimation from the iPPG

The BR has previously been estimated from conventional PPG waveforms [139, 235, 250–254]. iPPG waveforms have also been used to estimate the breathing-related information directly [248, 255] or indirectly through the RSA. The latter is usually measured as the HF component of the HRV [256]. These studies employ conventional spectral estimation and fixed bandwidths (drawbacks of which have been discussed in Chapter 3) or EMD, which requires analyzing fixed-length segments of the iPPG waveforms.

6.1.3   Motivation and contribution

The goal of the present chapter is to estimate the BR from the iPPG signal (acquired in a contactless manner) using the RSA in real-time. As with the estimation of the BR from the ECG in Chapter 5, the instantaneous and real-time *NFB* algorithm introduced in Section 5.2.2 was applied to track the main frequency component of the iPPG HRV, in other words, the iPPG RSA. The BR estimates were compared to an estimate computed from the simultaneously recorded ECG and to the reference BR, computed from the signal recorded by the impedance belt.

6.2   Materials and methods

6.2.1   Data acquisition

Data were acquired from 12 subjects with two different protocols: breathing-protocol and isometric hand-grip exercise. The subjects were supine, facing a RGB camera (20 frames-per-second, with artificial light) at a distance of 1 m and wore ECG and impedance belt (for the breathing waveform) Biopac® sensors. The breathing protocol included a short apnea (10-15 seconds) and an increase in the BR from 5 to about 20 brpm. The handgrip protocol alternated

between rest and contraction periods of 15 to 30 seconds. Both protocols induced changes in the HR of the subjects [257]. All the subjects gave informed consent. In total, 96 minutes of data were acquired. All procedures were in accordance with the Declaration of Helsinki [1].

6.2.2 Data processing

iPPG waveform creation

The iPPG waveform was obtained from the consecutive frames of the video by averaging pixels, in a region-of-interest extracted from the forehead of the subjects as illustrated in Figure 6.2. The forehead has been shown to be an optimal location to capture blood volume changes in iPPG waveforms [249]. The video was acquired with a frame-rate of 20 frames-per-second, therefore the resulting iPPG waveform was sampled at 20 Hz. The waveforms were extracted [2] for each of the red, green and blue (RGB) channels separately [257], and subsequently band-pass filtered between 0.6 and 4 Hz. An illustration is provided in Figure 6.3. Figure 6.5 shows an example of the ECG, iPPG (green channel only) and the reference breathing signals for a duration of 50 seconds during the hand-grip protocol.
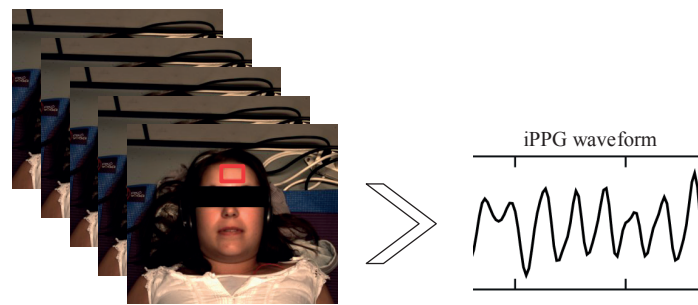
iPPG waveform

Figure 6.2: The creation of the iPPG waveform from a video sequence. The region-of-interest is highlighted with a red rectangle.

RSA extraction

The instantaneous HR was computed using the *NFB* algorithm with the three channels as simultaneous inputs. The mean heart rate was used to compute an appropriate inter-beat estimate for an extrema detection method to identify the heartbeats in each channel. Given the rather low sampling rate of the iPPG waveform (20 Hz), it was necessary to locally interpolate the value around the identified maxima to correct for the lack of time-resolution. The local neighborhood of the maxima were interpolated linearly to equivalent of 500 Hz.

The inter-beat intervals time series were created for each channel and all three series were re-sampled uniformly at a sampling rate of 4 Hz using linear interpolation [3]. The re-sampled series was then band-pass filtered between 0.09 and 1 Hz, considered to be a large breathing band comprising rates from 5.4 to 60 brpm. Given the challenging protocol and the large variations in the BR, this wide frequency band was necessary to correctly estimate the BR.

---

1. The data were acquired thanks to Virginie Moser and Fabian Brown from the Swiss Center for Electronics and Microtechnology (CSEM) in Neuchâtel, and Sibylle Fallet from EPFL-ASPG.
2. The iPPG waveform extraction was performed by Sibylle Fallet from EPFL-ASPG
3. described in Appendix A.
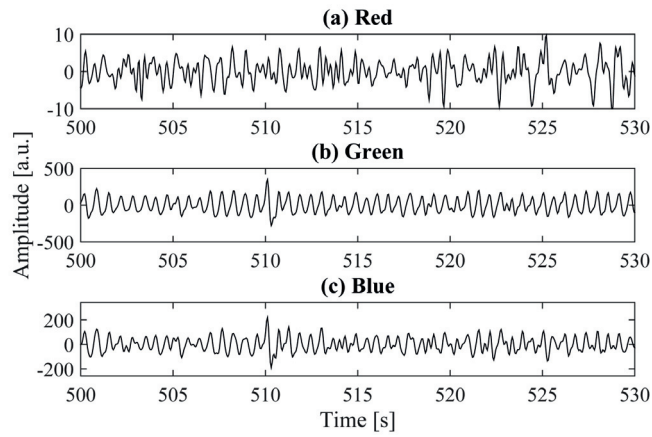
Figure 6.3: The iPPG waveforms in the (a) red, (b) green and (c) blue channels during the breathing protocol.
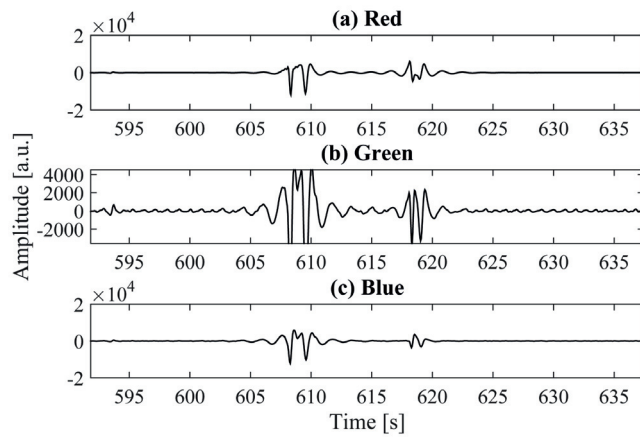
Figure 6.4: The iPPG waveforms in the (a) red, (b) green and (c) blue channels during the handgrip protocol.
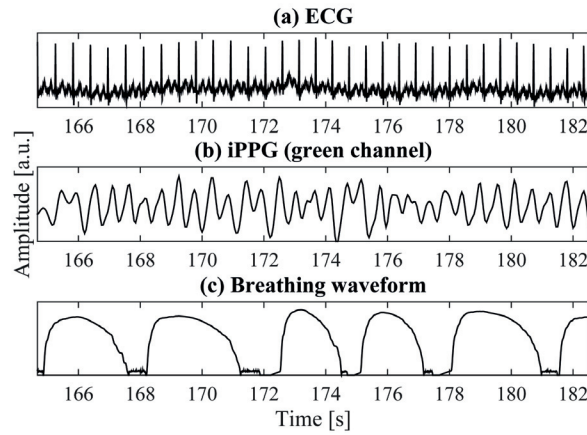
Figure 6.5: The (a) ECG, (b) iPPG and (c) reference breathing signals for one subject during the handgrip protocol.

The wide-band filtered RSA poses a major problem with frequency estimation methods such as the *NFB* method (presented in Section 5.2.2). It was therefore necessary to locally filter the RSA further. However, given the fast-changing nature of the BR in the study protocol, and given the sample-by-sample nature of the *NFB* method, we chose to filter the RSA in an adaptive manner using local information from the signal at each sample. The BR was therefore estimated using a modified version of the *NFB* algorithm with each of the three filtered iPPG inter-beat intervals as input. This modified version comprises an extra pre-processing step, in which the principal oscillation of the R-R intervals series is enhanced. Two schemes were considered to identify the oscillatory components of the RSA:

- Singular spectrum analysis (SSA) [258, 259]: This method decomposes a time series $s[n]$ of N samples into trend, periodic components and noise. It is based on the singular value decomposition of a trajectory matrix X, which is a multi-dimensional mapping of the one-dimensional time-series s. This matrix is created by stacking segments of length L of the time-series with $L-1$ overlaps as $X = [\mathbf{s}[1] : \mathbf{s}[k] : \mathbf{s}[K]]$ with $\mathbf{s}[k] = (s[k]\ s[k+1]...s[k+L-1])^T$ and $K = N - L + 1$. The parameter $2 \le L \le N - 1$ determines the size of the trajectory matrix. The L columns of the matrix are L time-adjacent observations of the underlying process of the original time-series. This matrix X is then decomposed as $X = \sum_{i=1}^{r} X_i$, where r is the rank of X and $X_i = \sigma_i U_i V_i^T$ via singular value decomposition. The σ_i are the non-zero singular values of X and the $(U_1, V_1)\ ...(U_r, V_r)$ the singular vectors. The diagonals of $U_i V_i^T$ are averaged. The decomposition yields L components or sources of s. The selection of L is crucial, it depends on the structure of s and in particular its periodicity [259]. There is no generalized accepted scheme to optimally select L [260]. The empirical value of $L = 10$ was used in the present chapter. The selection of L is also discussed later in Section 7.2.

- Sliding window adaptive singular value decomposition (SWASVD) [261]: This method is an adaptation of the conventional eigenvalue decomposition of a square matrix to perform the decomposition in a sliding window in an adaptive manner without having to perform the full decomposition at every sample. The algorithm is based on a bi-orthogonal iteration of the conventional SVD. Orthogonal basis are derived using QR decompositions [4] at every time step. The projection of the data on this basis and subsequent decomposition yields a set of final components representing, in this case, prominent oscillations of the input. This

---

4. The A=QR decomposition of matrix A yields an orthogonal basis Q and an upper triangular matrix R.

algorithm is described in Figure 6.6 and was implemented in [257] [5] for the estimation of the instantaneous HR from iPPG signals [257]. Experimentally, it proved not to be directly applicable to estimate the BR from the RSA. A 30-second sliding window was used here.

Figure 6.6: The sliding window adaptive SVD algorithm. Two iterative QR decompositions are performed. After the projection of the input data ($x(t)$) onto the first decomposition of the previous step (Q_A), a decomposition is performed to yield another basis (Q_B). The projection of the input data onto this basis yields the basis for the next step and also a set of components. Image from [261], © 2004 IEEE.

The above-mentioned methods are based on identifying the eigenvalue-eigenvector pairs from a matrix created from samples of the RSA. As such, by choosing the first eigenvalue-eigenvector pair, the most prominent oscillation of the input is selected. The dominant frequency of the component was estimated through its Fourier-based spectrum. The RSA was then locally filtered with the band-pass filter described in (3.2) in Section 3.2.2. The bandwidth of the local filter was set to $\beta = 0.8$ for the filter to be rather wide-band (as illustrated in Figure B.1 in Appendix B). In effect, the RSA extraction in the present chapter is similar to the extraction described in Section 3.2.2, but instead of the reference BR (f_{resp} in (3.2)), the dominant frequency of the first oscillatory component of the RSA was used.

BR estimation

The instantaneous BR was estimated from the filtered RSA with the *NFB* method presented in Section 5.2.2. For comparison purposes, the BR was estimated in a similar manner from the inter-beat intervals of the ECG.

Reference BR

The reference BR was computed from the reference breathing recorded with the impedance belt. This signal was re-sampled at 4 Hz and filtered similarly to the iPPG and ECG inter-beat intervals. Its instantaneous frequency was then estimated in three ways: (1) by identifying the largest peak of the Welch PSD in a sliding window, (2) using the *NFB*, and (3) the average of (1) and (2).

---

5. By Sibylle Fallet.

Evaluation

The correlations between the iPPG and ECG inter-beat intervals were computed with Pearson's correlation coefficient. The errors of their smoothed (4 second-long windows) estimates were computed as the mean absolute difference, in brpm, between the estimates and the smoothed (4 s-long windows) reference rate as described in (5.47) in Section 5.3.1. However, due to large artifacts in the iPPG, it was necessary to develop a quality index to identify portions of sufficient quality and to consider errors only in good quality segments. Indeed, in practice, one would prefer to know that the signals are of poor quality rather than being presented with a bad estimate. Therefore, an empirical quality index based on the amplitude of the iPPG signals was developed. To compute this quality index, an amplitude index was computed as the squared amplitude of the signal, divided by its variance (computed in a sliding window). The quality index was set to 1 where the amplitude index was smaller than ten times its interquartile range (computed in a sliding window) and 0 elsewhere. Portions with a quality index of 1 were retained when computing the correlations and the errors.

6.3 Results

The evaluation was performed on the entire length of the recordings where the quality index was equal to 1. Among the three iPPG channels, the green channel yielded the inter-beat intervals most similar to the ECG R-R intervals with an average correlation of 0.65 ± 0.27 (all per-record correlations were significant with $p < 0.05$). The red and blue channels intervals yielded correlations with the ECG R-R intervals below 0.5 as reported in Table 6.1. Therefore, only the green channel was retained for BR estimation.

Table 6.1: The mean correlations (STD) between the inter-beat intervals of the three iPPG channels and the ECG R-R intervals over all subjects.

	iPPG red	iPPG green	iPPG blue
ECG	0.04 (0.11)	0.65 (0.27)	0.38 (0.24)

RSA extraction

As expected, the SSA pre-processing step was computationally expensive. The SWASVD was much faster as the matrix was not required to be entirely decomposed at every iteration. An example of the filtered versions of the RSA for the green channel are shown for the two pre-processing schemes in Figure 6.7. As the pre-processing scheme involves already a frequency estimation step, one could imagine stopping the operation at this point. However, as illustrated in Figure 6.8, the two estimates only roughly narrow-down the RSA bandwidth, and do not directly constitute a good BR estimate.

BR estimation

Figures 6.9 and 6.10 illustrate, respectively, the iPPG and ECG BR estimates and the reference for two subjects during the breathing protocol. The iPPG quality index is displayed as well. It can be seen that both estimates follow the steep increase in the reference for the two subjects.

The errors between the estimates and the reference are reported in Table 6.2 for the ECG and the iPPG with the SSA pre-processing. The difference between the ECG and iPPG estimates was 3.05 ± 1.69 brpm. Table 6.3 shows the iPPG and ECG-based estimation errors for the SWASVD pre-processing. The difference between the ECG and iPPG estimates is 3.96 ± 2.02 brpm.

The results were obtained on 88% of the data selected as having sufficient iPPG quality.
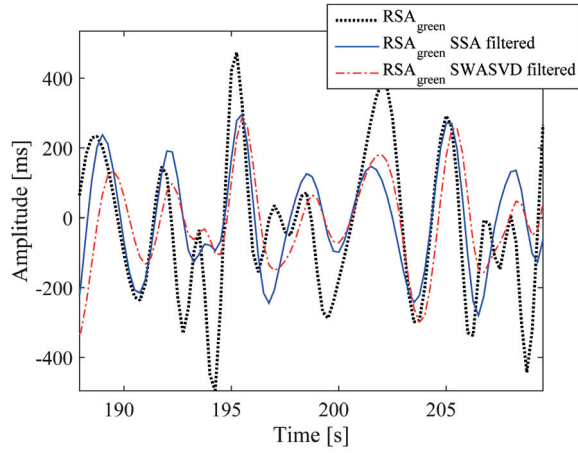
Figure 6.7: An example of the pre-processing of the RSA with the SSA and SWASVD schemes.
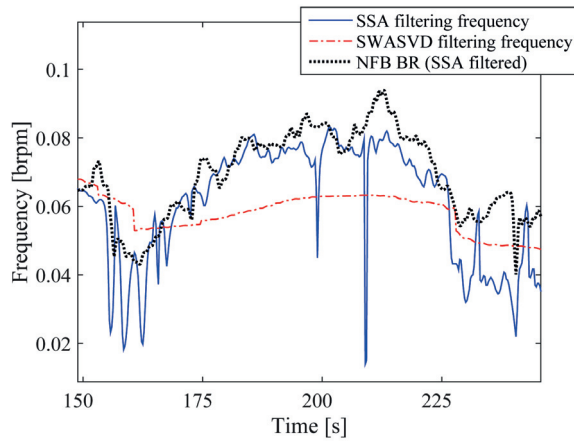
Figure 6.8: An example of the estimated BR and the pre-processing frequencies from the two SSA and SWASVD schemes.

Table 6.2: The mean error (STD) in brpm of the ECG and iPPG green BR estimates over all subjects with the SSA pre-processing.

	Welch (1)	NFB (2)	mean (3)
ECG	3.22 (3.25)	2.94 (3.38)	2.93 (3.3)
iPPG	4.56 (2.06)	4.23 (2.10)	4.26 (2.08)

Table 6.3: The mean error (STD) in brpm of the ECG and iPPG green BR estimates compared to the reference over all subjects with the SWASVD pre-processing.

	Welch (1)	NFB (2)	mean (3)
ECG	3.18 (2.94)	2.86 (3.67)	2.74 (3.25)
iPPG	4.06 (1.88)	3.49 (2.32)	3.52 (1.99)
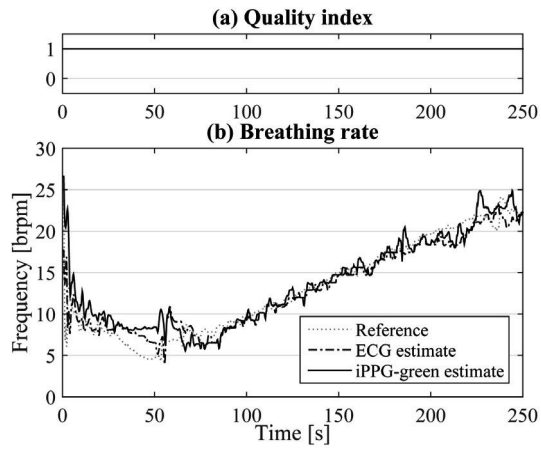
Figure 6.9: BR estimation (SWASVD pre-processing) from the iPPG- subject 1. (a) Displays the quality index and (b) the BR estimated from the iPPG and the ECG and the reference.
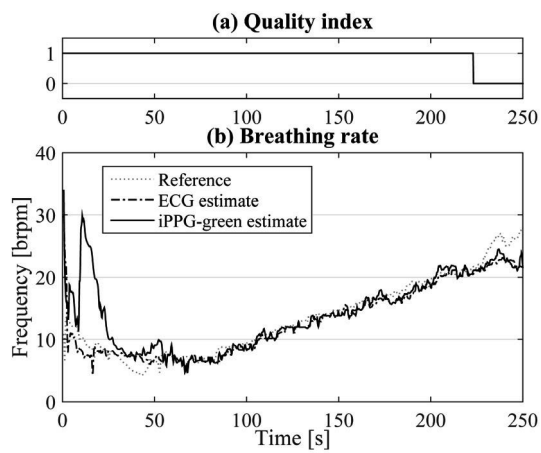
Figure 6.10: BR estimation (SWASVD pre-processing) from the iPPG- subject 2. (a) Displays the quality index and (b) the BR estimated from the iPPG and the ECG and the reference.

6.4   Discussion

6.4.1   Accuracy

The iPPG green channel yielded the inter-beat intervals most similar to those of the ECG, which corroborates with other works stating that the green wavelength is more suitable than red and blue to capture skin tone differences due to blood circulation, because of its better absorption by hemoglobin [247, 249]. The accuracy of the iPPG estimates was slightly less than that of ECG estimates. However, considering the challenging conditions of the iPPG acquisition and processing, the errors are still comparable to errors reported in the literature for estimating the BR from the ECG or the PPG [138, 219].

The two RSA processing schemes were proven to be necessary in extracting a narrow-band RSA, without using restrictive bandwidths based on general assumptions. The SWASVD scheme yielded in more accurate estimates and was also computationally less expensive than the SSA scheme.

It has been shown that the breathing influence on the inter-beat intervals subsists in a weaker form even without the breathing act [262], which means that apneas cannot be detected reliably via the inter-beat intervals. Therefore, the subject of apnea detection with iPPG-derived inter-beat intervals was not addressed in the present study.

This kind of estimation can be combined with other modes of estimating the BR from videos, for example by using breathing-induced motion [263, 264], as performed recently in [265].

6.4.2   Limitations

In the present study, the subjects were in a supine position. In this case, most often, the breathing influence on the HRV is much stronger than the baroreflex activity, occurring at 0.1 Hz[6]. Therefore, the main component of the HRV in all but one subject was the breathing oscillation. However, in the orthostatic position, the baroreflex activity would be larger than that of the breathing and the previous assumption would not hold.

The iPPG waveform contained a large amount of artifacts and noise, in part due to the video capture, but also due to the waveform extraction procedure. Slight illumination changes and the movement of the subjects contributed to these artifacts. This modality remains a challenging one even for HR estimation [257], let alone BR estimation from HRV.

6.5   Conclusion

In this study, real-time BR was estimated from the inter-beat variations of the contactless iPPG waveform, acquired in visible light with a commercial video-camera. The estimation errors are comparable to commonly reported errors for BR estimation from the ECG and the conventional contact-based PPG. Moreover, the data were recorded with varying BRs, which is challenging. These findings are encouraging in the use of iPPG for real-time contactless BR monitoring.

---

6. see Section 2.1 for a brief explanation on the baroreflex mechanism.

Estimation (and Removal) of the Breathing Oscillation from the Inter-Beat Intervals

7

As discussed in Chapter 2, one major influence on the HRV is the RSA, originating from the breathing. It is of much interest to separate the waveform containing the breathing influence, i.e. the RSA, from the inter-beat intervals, to either study it alone, for example for the purpose of estimating the breathing rate as in Chapter 5, or to study breathing-unrelated influences on HRV as in Chapters 3 and 4. In Chapter 5, breathing was assumed to be the most dominant influence on the inter-beat intervals due to the particular conditions of the experiments (supine posture). However, this assumption does not hold in more general conditions. Current methods to identify the RSA in a generalized scenario, such as those in Chapters 3 and 4, rely on using a reference breathing waveform. However, in some situations, a breathing waveform cannot be acquired directly, or historical and retroactive data must be analyzed. The present chapter introduces an automatic methodology to decompose the inter-beat intervals of a given subject without using a reference breathing waveform and to classify the components as being related to breathing-related or not, based on a training set composed of data from independent subjects. An article based on this study is in preparation.

7.1   Introduction

7.1.1   Identification of the RSA without the reference breathing waveform

As discussed in Chapter 3, the LF and HF powers of the inter-beat intervals time series are widely used indexes of the autonomic state. However, these indexes rely on an assumption on the breathing rate (BR), which often does not hold. In Chapter 3, by taking into account the breathing signal, several avenues for assessing the autonomic state with modified and novel HRV parameters were explored. These approaches hinge on the identification of the RSA using the reference breathing waveform.

However, in some applications, in which the cumbersome apparatus for the recording of a breathing signal cannot be used, such as during athletic training, for practical reasons (e.g., the inter-beat intervals can be easily recorded with a heart rate monitor [266], while the breathing signal is less accessible); or applications in which historical or retroactive data must be analyzed, the reference breathing waveform may not be available. In such cases, it is necessary to deduce the RSA from the HRV by only using inter-beat intervals. In the seated or supine positions, this may not be a challenge, as the largest influence on the inter-beat intervals is that of breathing

as discussed in Chapters 3 and 5. However, in the orthostatic (standing) position, the baroreflex control of the blood pressure fluctuations greatly influence the inter-beat intervals. Indeed, as compared to the supine position, assuming an upright position induces a decrease in the blood pressure, which triggers baroreflex mechanisms to stabilize the latter. This influence may be equal to or larger than that of breathing.

Current methods to identify and separate the RSA waveform are divided into data-driven and model-based methods. Data-driven methods use a reference breathing waveform to identify the RSA, and then proceed to subtracting it to obtain the breathing-unrelated portion of the intervals [68, 267]. These methods are based on techniques such as adaptive filtering [61, 70], independent component analysis [268], autoregressive modeling [66], principal component analysis [62], and subspace projection [68]. Model-based methods describe the relationship between the inter-beat intervals and the breathing waveform [69].

One method developed to identify the RSA, without using a reference breathing waveform (to the best of our knowledge), is to analyze the HRV spectrum and to choose plausible breathing-related peaks in a decision-based manner [269]. Another, designed to study the RSA during sleep, derived the RSA by decomposing the inter-beat intervals into their oscillatory components and choosing the first one as the RSA [267].

7.1.2   Motivation and contribution

There is a need for a methodology to efficiently identify the RSA without the use of restrictive bandwidths and without the reference breathing in general conditions. The method presented in [269] does not seem to have found practical application and has not been validated, possibly due to the lack of robustness in the decision-making step. The method presented in [267] is dependent on a number of assumptions about the inter-beat intervals during sleep, which may not hold globally. During sleep, one is presumably in the supine position and the baroreflex oscillation is not amplified by sympathetic stimulation. It is reasonable to assume that, during sleep, the largest influence on the inter-beat intervals is that of breathing. In the present chapter, we decomposed the inter-beat intervals into a set of (mostly oscillatory) constituents using singular spectrum analysis (SSA) [258, 259]. A scheme for component grouping and selection was applied to retain possibly breathing-related components. These components were then classified with a support vector machine (SVM) scheme as being breathing-related or breathing-unrelated based on a training set composed of recordings acquired from other subjects, where the reference breathing (airflow) was available. The experiments were performed in the supine and orthostatic body postures. These two postural conditions were investigated to include a wide range of autonomic conditions elicited by body posture, as described in Chapter 3. We tested the hypothesis that removing the estimated breathing leads to similar results as when the reference breathing waveform is used.

7.2   Materials and Methods

7.2.1   Data

The data from *Study 1*- Body posture autonomic alteration, described in Section 3.2 were used in this chapter.

7.2.2   Processing

The ECG R-peaks were extracted using a conventional extrema detection method and manually inspected for artifacts. The R-R intervals were then created by setting the time index of each interval at its midpoint. There are three distinct steps in the proposed processing: first,

the decomposition (and component grouping) of the R-R intervals, then the identification of the breathing component (the RSA) and finally its removal from the R-R intervals. The removal of the estimated breathing influence was compared to the removal using the reference breathing waveform. Figure 7.1 illustrates this process.
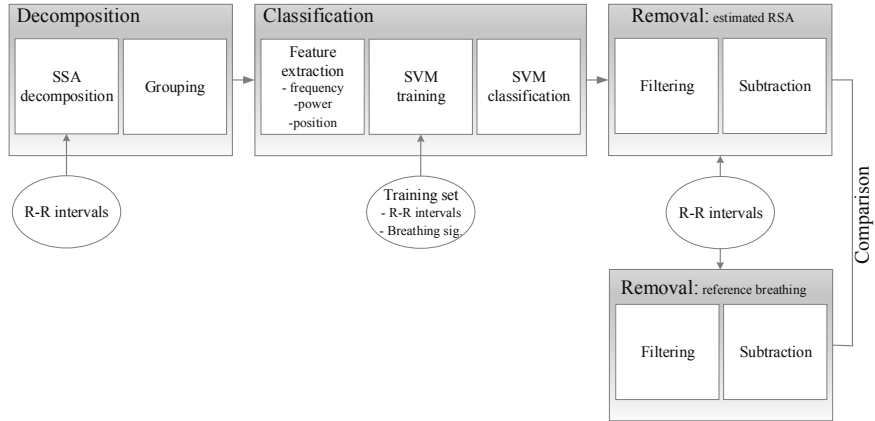
Figure 7.1: Diagram of the proposed processing chain to estimate the RSA.

Decomposition of the R-R intervals

The R-R intervals and the reference breathing were re-sampled at 4 Hz using cubic spline interpolation [1]. They were band-pass filtered using an order-18 Butterworth filter between 0.06 Hz and 1 Hz (equivalent to 3.6 to 60 brpm).

The SSA technique [258, 259] was used to decompose the band-pass filtered R-R intervals. This method was described in Section 6.2. The parameter L, which determines the size of the trajectory matrix ($L \times K$) is a crucial factor [260, 270]. L depends on the structure of the time-series and in particular its periodicity. If L is equal to the number of sources which create a given mixed-source time series, and the sources are independent, then the eigenvectors of the trajectory matrix will point to the sources [270]. The primary dilemma is the presupposition on the number of sources. There are studies suggesting to select L based on the position and location of the peaks of the autocorrelation of the time series [270], which introduces further parameters required for the selection process and seems counterproductive. In the present chapter, several values of L were investigated.

After this decomposition, it may be necessary to group similar components and to retain the pertinent ones. Indeed, in the case of a large value of L, the SSA decomposition may yield several components for a given frequency. With a hierarchical-tree grouping, similar components were grouped [271]. This method starts by assigning a class to each component and then clustering the two (distinct) most similar components to the same class and so on. The similarity criterion was the cross-correlation between components. Care was taken to group only components with similar frequencies. It must be noted that for small values of L, it was observed that this grouping scheme had little effect, but it was necessary for large values of L. After this refinement step, the five most powerful components were retained.

In summary, for each subject, the R-R intervals were decomposed into five components for each of the two cases of supine and orthostatic recordings. The order of extraction of each of the

---

1. described in Appendix A.

five components reveals its importance (from the power point of view [271]) and is referred to as the SSA component rank. The estimation and removal of the breathing influence is based on identifying which one of these five components is breathing-related in each case.

For each component, three attributes were considered: 1) its power, computed in the time-domain; 2) its dominant frequency, as estimated by the frequency of the peak of its power spectrum; 3) its correspondence to the supine or orthostatic body posture.

Identification of the breathing influence

The SSA components were classified using an SVM classifier as being breathing-related or breathing-unrelated on the basis of the three attributes described previously. To construct a reference for the training and the evaluation of the classifier, the components were labeled manually as being breathing-related or not, according to the reference BR. The reference BR was computed from the breathing signal with the *NFB* method introduced in Chapter 5.

For each subject, the classifier was trained with the data from all other 20 subjects (there were 21 subjects in the data set). All 10 components of the test subject were then classified. This leave-one-subject-out cross validation scheme was adopted to assess how well the results would generalize to an independent set as our data set was not large enough to be split into training and testing sets. Polynomial orders from 2 to 6 were considered for the SVM kernel. The components identified as breathing-related by the classifier were summed to create the estimated $RSA_{estim,raw}$.

Removal of the breathing influence

Because of classification errors, $RSA_{estim,raw}$ may be composed of several components and may not be narrow band. It is therefore necessary to refine it. To this end, an approximate BR was estimated from $RSA_{estim,raw}$, which was then used to locally filter the R-R interval series to extract the RSA as in Chapter 3. The $RSA_{estim,raw}$ was therefore treated as the breathing waveform in the procedures reported in Section 3.2.2. More specifically, in Equation (3.2), f_{br} was replaced by $f_{rsa,raw}$. The instantaneous frequency of $RSA_{estim,raw}$, $f_{rsa,raw}$, was computed with the *NFB* method. The outcome of Equation (3.2) is RSA_{estim}, which was then subtracted from the R-R intervals, as described by Equation (3.3) to yield $RR_{non-br,estim}$, the R-R intervals, devoid of the estimated RSA. For reference, the same procedure was applied by using the BR obtained from the reference breathing waveform, in other words, f_{br} and obtaining $RR_{non-br,ref}$, the R-R intervals devoid of the true breathing influence through Equations (3.2) and (3.3).

7.2.3   Evaluation

Two aspects were evaluated: the identification of the breathing influence on the R-R intervals and the impact of its removal from the R-R intervals on the power of the latter.

The identification was evaluated from the outcome of the SVM classification with the conventional identification measures of sensitivity, specificity and accuracy, defined in (7.1), (7.2) and (7.3). The sensitivity or the true positive rate (TPR) reflects the proportion of correctly identified breathing-related components, the specificity or the true negative rate (TNR) reflects the proportion of correctly identified breathing-unrelated components, and the accuracy (ACC) reports the proportion of all true results [2].

$$TPR = \frac{TP}{TP + FN} \tag{7.1}$$

$$TNR = \frac{TN}{TN + FP} \tag{7.2}$$

---

2. Appendix A, Section A.2 expands on classification measures.

$$ACC = \frac{TP + TN}{TP + TN + FP + FN} \tag{7.3}$$

The impact of the removal of the estimated breathing influence was evaluated by measuring the remaining power in the R-R intervals after its application, and by comparing it to the remaining power after removal by using the reference breathing signal. In other words, comparing $power(RR_{non-br,estim})$ to $power(RR_{non-br,ref})$. The power was measured in 120-second long segments with 50% overlap, resulting in 6-7 segments per recording. The values were then averaged for each recording.

7.3 Results

The reference BRs for all recordings are reported in Fig 7.2. Thirteen subjects (62%) had BRs below 0.16 Hz (The LF upper limit is 0.15 Hz).
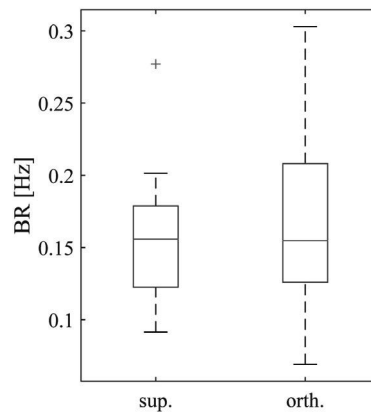
Figure 7.2: The reference BR for all recordings.

7.3.1 Decomposition of the R-R intervals

Figures 7.3 and 7.4 illustrate the decomposition of supine R-R interval time series into their five main components with $L = 8$ (L is the length of the SSA trajectory matrix). In one example, the first component is breathing-related, and in the other, the second component is the breathing-related oscillation. Figure 7.5 illustrates the decomposition of R-R intervals acquired in the orthostatic position. Generally, The most prominent components of the R-R intervals were the breathing and the baroreflex (occurring around 0.1 Hz) activities. The lower frequency components had larger powers and were retrieved in the first SSA ranks. Small values of L (≤ 10) yielded very dissimilar components. Larger values such as $L = 60$ resulted in many extra components in addition to the breathing and the baroreflex activities. Values of $L = 5$ to $L = 60$ were further considered for systematic evaluation.

Table 7.1 reports the number of manually labeled breathing-related components based on their rank in the SSA. With $L = 5, 8, 10$, the breathing-related component was always either the first or the second most prominent component of the R-R intervals. For supine recordings, the breathing-related component was often the first component. For orthostatic recordings, it was often second after the baroreflex component. In some orthostatic recordings, the breathing-related oscillation was not extracted as a component at all (the rank is reported as "none" in Table
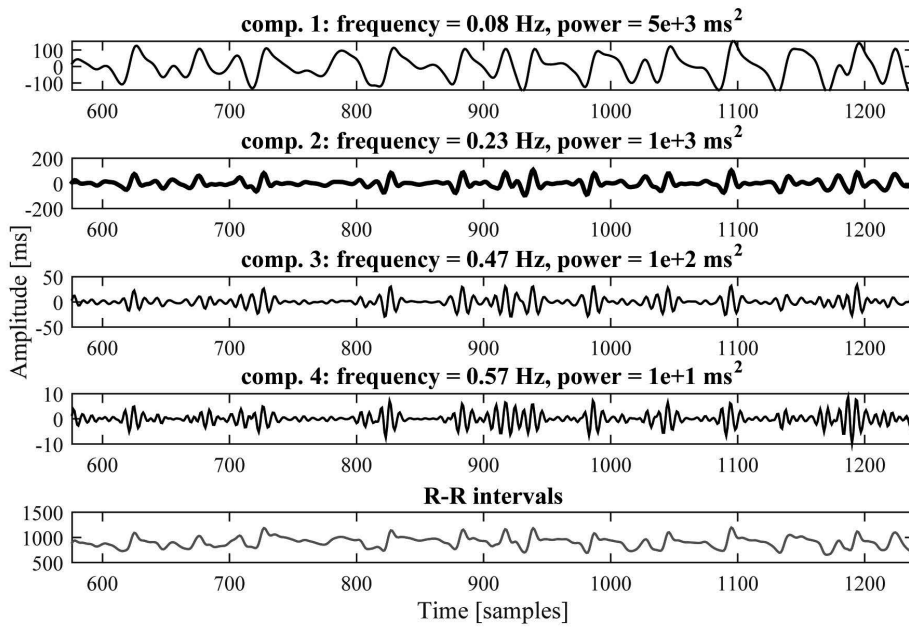
Figure 7.3: The decomposition of the R-R intervals of a supine recording. The component 1 is the breathing-related component ($L = 8$).
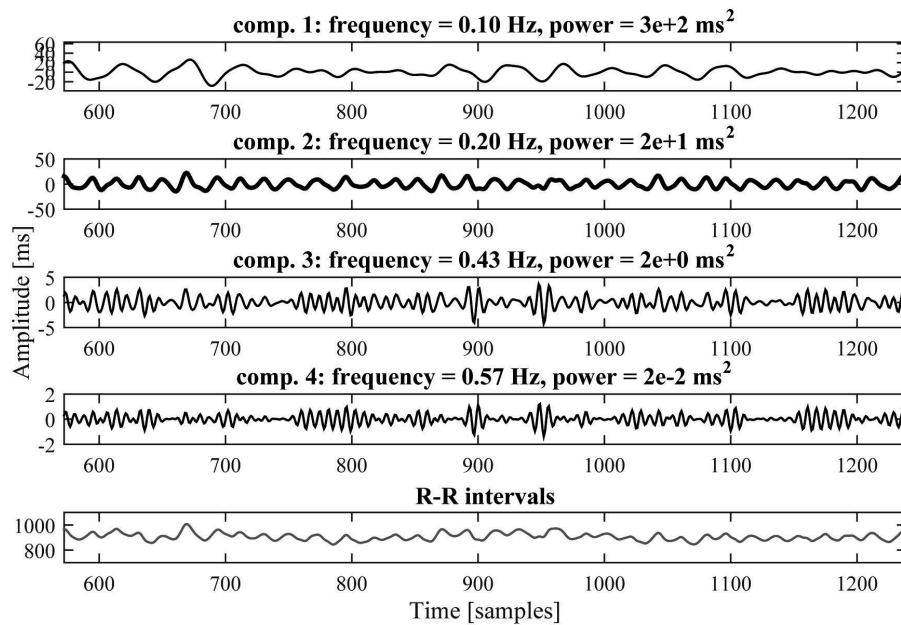
Figure 7.4: The decomposition of the R-R intervals of a different supine recording than that of Figure 7.3. The component 2 is the breathing-related component ($L = 8$).
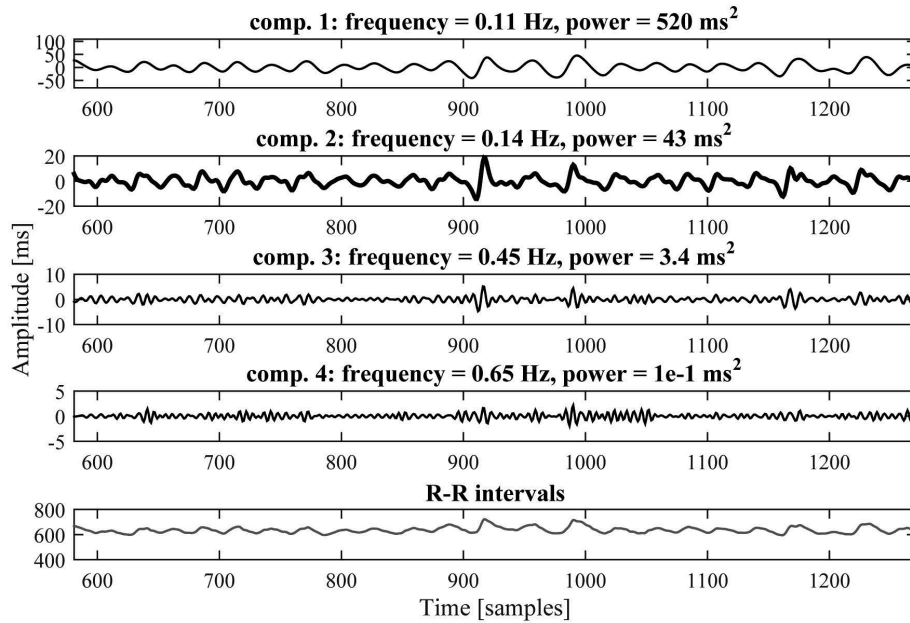
Figure 7.5: The decomposition of the R-R intervals of an orthostatic recording. The component 2 is the breathing-related component ($L = 8$).

7.1). For example, for $L = 8$, for six recordings, no breathing-related component was extracted. Larger values of L (≥ 20) extracted more often a breathing-related component. However, it was not necessarily in the first or second rank. For $L = 60$, a breathing-related component was always extracted, however, it was positioned in various SSA ranks, up to the fifth, meaning it had a reduced importance in the decomposition. In 9 recordings (21% of recordings), the BR of the subjects was close to the baroreflex oscillation frequency of 0.1 Hz. In these cases, the breathing-related and baroreflex activities were extracted as one single component, as it is difficult to separate frequencies that close.

Table 7.1: The number of the occurrence of the breathing-related component per SSA rank. There were 21 recordings (subjects) for each of the supine and orthostatic cases.

	SSA rank\L	5	8	10	20	60
Supine	1	19	19	17	19	17
	2	2	2	4	1	4
	none	0	0	0	1	0
Orthostatic	1	6	6	6	8	7
	2	10	9	11	8	7
	3	0	0	0	3	2
	4	0	0	0	0	1
	5	0	0	0	0	4
	none	5	6	4	2	0

7.3.2   Identification of the RSA

Figure 7.6 shows the separability of the breathing-related and breathing-unrelated components based on their power and frequency features. It can be seen that, generally, the component spaces of the two conditions are well separated. Breathing-related components are within a certain frequency range and have rather large powers.
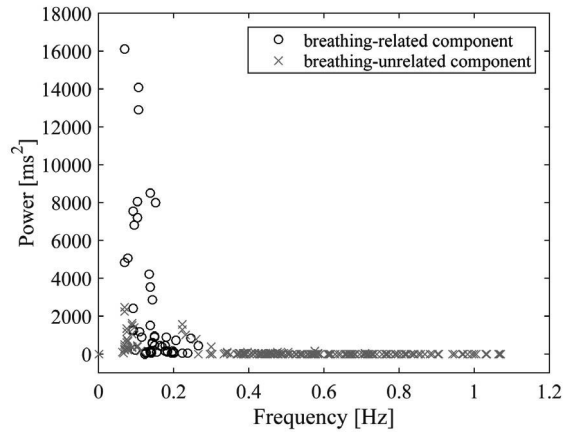
Figure 7.6: The R-R intervals breathing-related and breathing-unrelated components separability. The frequency (Hz) vs. power (ms^2) of the breathing-related and breathing-unrelated components over all subjects ($L = 8$).

Figures 7.7, 7.8 and 7.9 illustrate the sensitivity, specificity and accuracy of the classification, respectively, for values of the SSA trajectory matrix length $L = 5$ to $L = 60$ and SVM kernel polynomial orders 2 to 6. It can be seen that small values of L such as 5 and large values such as 20 and 60 were not as good as the intermediate values of 8 and 10. Higher order polynomial kernels yielded in a higher specificity but lower sensitivity, while lower order polynomials resulted in the inverse. Therefore to evaluate the removal of the respiratory influence, the outcome of classification with $L = 8$ and an SVM kernel of order 4 was retained.
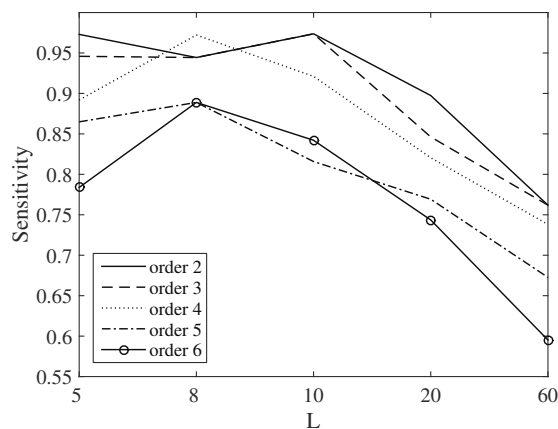
Figure 7.7: The sensitivity of the breathing-related/unrelated R-R interval component classification as a function of L and the SVM kernel order.
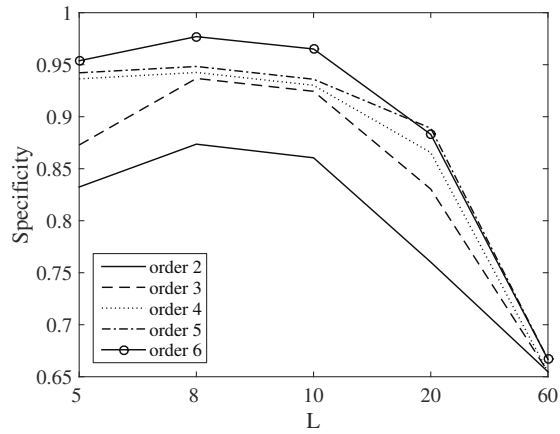
Figure 7.8: The specificity of the breathing-related/unrelated R-R interval component classification as a function of L and the SVM kernel order.
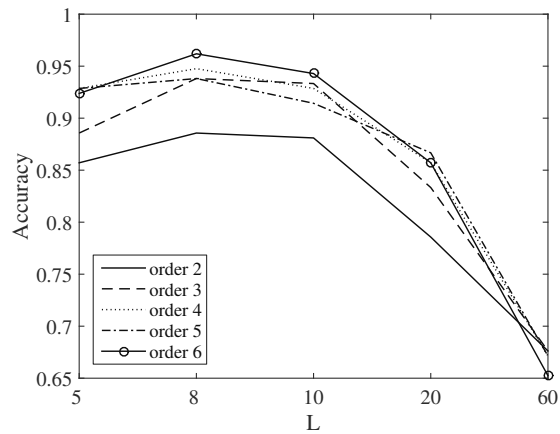
Figure 7.9: Accuracy of the breathing-related/unrelated R-R interval component classification as a function of L and the SVM kernel order.

7.3.3   Removal of the breathing influence

Figure 7.10 shows the power of the R-R intervals, after the removal of the breathing influence using the RSA or the reference breathing waveform. Removal using the estimated RSA is compared to removal using the reference breathing waveform. It can be observed, that in the supine position, the distributions are similar. In the orthostatic position, the power seemed larger after the removal of the estimated rather than the reference breathing waveform, which could be due to the six recordings in which the breathing-related activity was not extracted as a component form the R-R intervals at all. However, a hypothesis test (paired t-test) did not reveal statistical differences in either posture. Furthermore, Fig. 7.11 illustrates the relative difference of $RR_{non-br,ref}$ and $RR_{non-br,estim}$, i.e., the difference between the two respiration-corrected tachograms, where the breathing influence was removed either with the estimation or with the reference. It can be seen that on average, the difference was below 20%.
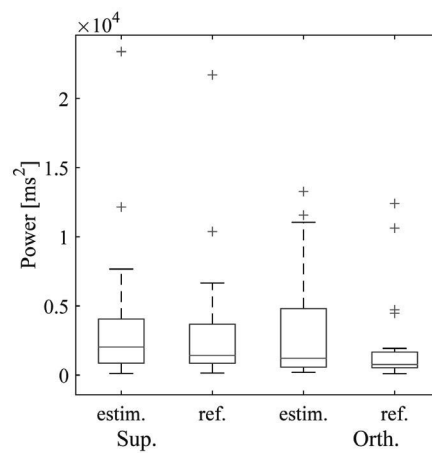
Figure 7.10: The breathing-unrelated R-R interval power, after removal using the estimated RSA (estim.) and the reference breathing signal (ref.).
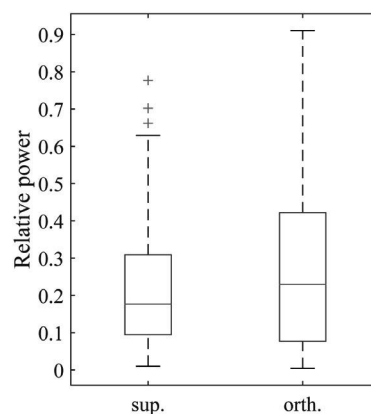
Figure 7.11: The relative power of the difference of the breathing-corrected tachograms, when the estimated and the reference breathing waveforms were used.

7.4   Discussion

In the orthostatic posture, due to the changes occurring in the blood pressure, the baroreflex activity is heightened and is more prominent than in the supine posture. Therefore, it is not surprising that the breathing-related oscillation was not the most prominent component of the R-R intervals in this posture. In 62% of the subjects, the resting breathing rate was close to, or below the usual LF band upper limit. Conventional HRV analysis would clearly not reflect expected autonomic influences. These elements contribute to the difficulties of identifying the breathing influence on the R-R intervals in generalized conditions.

The existence and importance (SSA rank) of the breathing-related component of the R-R intervals was dependent on the SSA trajectory matrix length L as seen in Table 7.1. When L was small (e.g. 8), the decomposition of 14% of the records did not yield a breathing-related component. All these cases were related to the orthostatic position and in most of them, the BR was high, leading to a reduced power of the breathing-related component [272]. Therefore, the absence of a clear breathing-related component in the decomposition is not surprising in these cases. For $L \leq 10$, 100% of the breathing-related components in the supine position and 71-81% of the breathing-related components in the orthostatic position were extracted in the SSA first and second ranks. For $L = 60$ the decomposition always yielded a breathing-related component. However, it was ranked in the first or second only in 66% of the orthostatic records. This means that the breathing-related component was not always the most important component. In the remaining records, its rank was more scattered as third, fourth or fifth, which increased the difficulty of the classification, as no distinctive trend existed. As a result, the classification performance was better for $L = 8$, 10 than for $L = 60$ as seen in Figures 7.7, 7.8 and 7.9.

The SVM classifier identified the vast majority of the breathing-related components. However, the order of the kernel polynomial affected the performance. It was found that the third and fourth order polynomials yielded good overall results as seen in Figures 7.7, 7.8 and 7.9.

The refinement process of the identified component may not seem straightforward. It is not an absolutely crucial step and in some applications, the raw estimate as identified with the classifier may be sufficient. A number of different schemes could be employed to refine the estimate, such as a second SSA pass or EMD. The proposed solution, however, is less computationally expensive than both the aforementioned options.

Of course, once the RSA is identified, estimating the BR is only one step away. In fact, a rough BR estimate was computed and utilized in the RSA refinement process. However, given the SSA decomposition (and to a lesser extent the classification), this entire methodology does not allow to estimate the BR in a truly real-time manner. The application of the SWASVD decomposition introduced in Chapter 6 may be a route to rendering the process instantaneous.

Globally, the R-R interval powers were similar whether the reference breathing oscillation or estimated RSA was used for the removal of the breathing influence as shown in Figure 7.10. The relative difference was smaller in the supine posture as seen in Figure 7.11. Deeper investigation into the results revealed that most of the records in which the removal yielded significantly different results compared to the reference, were from subjects whose BRs were near the baroreflex frequency (0.1 Hz). In this case, it is indeed difficult to separate the breathing influence from that of the baroreflex and the correction removes all or part of the baroreflex influence. These subjects represented 24% of our sample, which contained 61% subjects with athletic training. It would be of interest to investigate the percentage of these subjects in a larger population.

The results for different values of L showed that the choice of L is crucial for the success of such a scheme. In the present chapter, the value of L was maintained for all recordings and all subjects. A closer look showed, however, that the optimal value of L was different for different recordings and different subjects. This chapter did not uncover a theoretical justification for such differences, and given the nature of the SSA decomposition, such justification would presumably not be straightforward. One way of choosing a value for each recording would be to do so based

on the outcome of the decomposition rather than a rule on the input, such as correlation-based selections of L proposed in literature [260, 270]. One could decompose the input with several values of L, and based on a quality derived from the decomposition outputs, chose the best value. Such a scheme would avoid a general sub-optimal pre-selection.

The posture, i.e., supine or orthostatic position adopted during the recordings was a feature in the recognition of the breathing-related oscillation. However, if the posture is not known, one could imagine a similar classification scheme using the power and dominant frequency to recognize the posture from training data, as a first step before identifying the breathing influence.

In view of the results of the leave-one-out cross validation, the classifier can be used for a subject when it has been trained with data from other subjects. Indeed, in the case of retroactive or historical data, one may not have access to the same subjects and the same conditions, so one could construct a training set for the classifier from a completely different set of subjects. However, we believe that training subjects similar to the test ones in their general characteristics (age, height, weight, sex), and more importantly their level of athletic training, would yield a more accurate model for identification of the breathing influence.

In summary, the identification and removal of the breathing-related influence, without the use of the reference breathing waveform, with the aid of a training set proves to be accurate except when the subject breathes at a frequency close to the baroreflex mechanism oscillation.

7.5   Conclusion

In the present study, the possibility of identifying the RSA without using a reference breathing signal was investigated. We found that classifying constituting SSA components of the R-R intervals of a given subject was accurate in identifying the breathing influence on the basis of a training set constructed from data of 20 other subjects. Furthermore, we found that removal of the identified breathing-related oscillation yielded similar results, in terms of breathing-corrected R-R intervals power, to R-R intervals from which the RSA was removed using the reference breathing waveform. This work is promising in improving HRV analysis in cases where it is not possible to acquire a breathing signal or when historical and retroactive data are processed.

Part III

Applications

Emotion Recognition using RSA and Breathing Signals

8

Recognizing human emotions automatically has received much interest in many clinical and non-clinical fields, such as personality disorders monitoring, multimedia applications with recommendation and personalization, and improvement of mutual sympathy in human-machine interactions, to cite a few [273–276]. The present chapter explores the automatic recognition of emotions using the RSA and breathing signals. Elements of this chapter were presented as a conference paper [277].

8.1 Introduction

8.1.1 What are emotions?

Human emotions, such as happiness, sadness, serenity and anger among others, are mental states originating from the cortex and subcortical regions in the brain, which affect various systems in the body [274]. The exact definition of emotion is a subject for debate. However, according to one well cited source "emotion is defined as an episode of interrelated, synchronized changes in the states of all or most of the five organismic subsystems in response to the evaluation of an external or internal stimulus event as relevant to major concerns of the organism" [278].

There are many models to characterize emotions, to facilitate their quantification and use. In most models, dimensions and intensities are assigned to emotions and emotions are organized on bipolar scales. One widely used model is the circumplex model, characterized by the two dimensions of arousal and valence [279], in which arousal is related to inner activation (excited vs. calm) and valence describes the experienced pleasantness. Emotions are organized in this two-dimensional space as illustrated in Figure 8.1.

8.1.2 Emotion recognition using physiological signals

The central nervous system is among the many physiological systems affected by emotions [273, 280]. Analyzing brain activity recorded using the electroencephalogram (EEG) has previously been proposed in emotion recognition [281, 282]. Changes in the EEG are related to the central nervous system (controlled from the brain) and are a logical avenue to capture emotions even though the exact neurophysiological mechanisms of emotions remain unknown [273]. However, due to the cumbersome apparatus and large number of electrodes necessary for its recording, the EEG cannot be considered for most mobile applications.
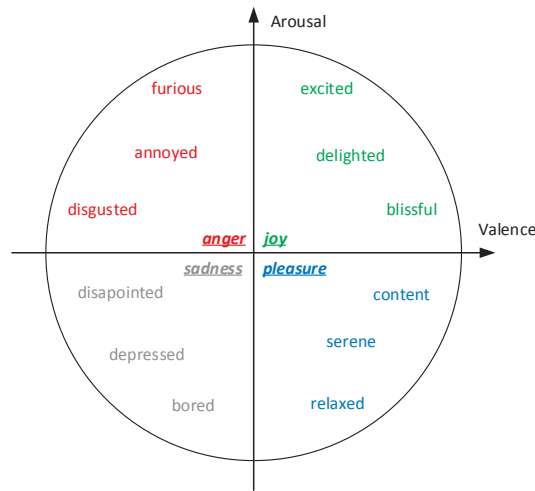
Figure 8.1: The circumplex model of emotions.

Another physiological system affected by emotions is the autonomic nervous system (ANS) [103]. Brain imaging has identified several brain regions, which are involved in emotional responses, and present correlations with the ANS [283]. Emotions affect many physiological signals because the ANS controls a number of body functions with visible and recordable effects. The cardiac and breathing functions are affected for instance. In addition, sweating in relation with emotions changes the electrical properties of skin. There is a body of literature investigating emotion recognition through physiological signals affected by the ANS such as the ECG, breathing, blood pressure and galvanic skin response (GSR), to cite those most often used [103, 273, 284, 285]. The correlates of emotions with ANS indexes such as the RSA have also been investigated, for example in [29, 107], in which the directionality of changes in the RSA magnitude during positive and negative emotional experience were studied. Decrease in the RSA following the experience of high-arousal emotions has been reported [29] as well as a generalized (non-significant) decrease in the RSA with the experience of emotion, irrespective of its kind [107]. These changes may be dependent on gender and other subject-related factors [107]. Some studies have investigated the RSA as a marker for emotional regulation, for example in relation with cognitive performance or Internet addiction [30, 48]. Abnormal RSA levels have been observed in impaired emotional regulation [37, 37, 108, 110, 111]. Breathing-related parameters have also been reported to contribute to RSA responses and it has been suggested to control for breathing volume among other things when using the RSA in emotion recognition [107].

Several emotion recognition systems based solely on the ECG have been proposed, as this modality is easy to acquire and process. In these systems, linear and nonlinear features are typically extracted from the ECG and then classified as corresponding to an emotional state with SVM or neural network schemes [285–287]. However, the ECG has been shown to be less reactive to emotions than other modalities such as the GSR [287]. The breathing signal alone has also been used to recognize distinct emotional states [288]. Using features from several physiological modalities has been proposed as well, and advocated as being superior to a single modality alone [281, 289, 290]. The correlations between different modalities has also been employed in the context of emotion recognition [291].

One of the predicaments in studying emotions is that they have to be artificially elicited in

the subjects. To this effect, in such studies, stimuli are first chosen and the subjects are exposed to them. Most of the above-mentioned studies used image stimuli to elicit emotions, and not always in a random emotional order. Some used music to elicit emotions [273] and others used films [291]. It has been noted that the type of stimulus and the order of presentation have a rather large effect on the performance of a given system [273, 286, 287].

8.1.3 Motivation and contribution

With the increasing volume of available multimedia content, especially music video clips, many diffusion services attempt to recommend personalized contents to users [292]. This recommendation can be based on the emotions of the user, i.e., the arousal and valence. For instance, a user might seek exciting and/or pleasant content. Moreover, the recommender can take into account whether the subject likes the content. Indeed, it is possible that a user likes content with low arousal and/or negative valence. With this possible application in mind and given the fact that music video clip stimuli have only attained limited success in emotion recognition [281], this chapter aims to investigate automatic emotion recognition from the RSA and breathing signals, as well as their interaction and combination when using music video clips as emotional stimuli. It is hypothesized that, as both the heart function and breathing are affected by the ANS, the synchronization of the two is an additional revealing aspect. Furthermore, previous work has highlighted the need to consider the breathing when using the RSA to study emotions [107]. Features from the RSA and the breathing waveforms, and their interaction are extracted and classified as related to a particular emotional state with an SVM scheme.

8.2 Methods

8.2.1 Data
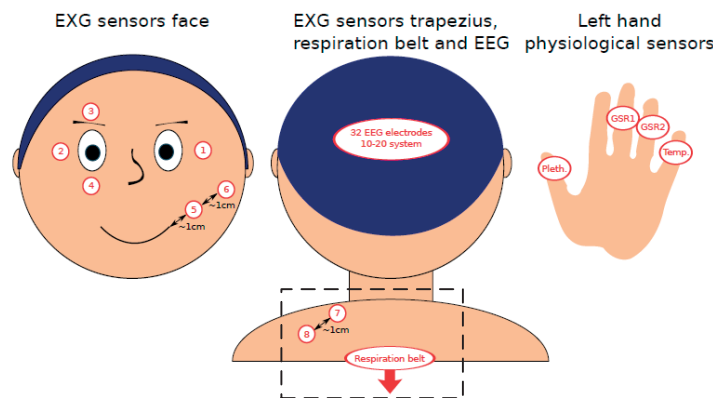
Figure 8.2: The sensors used in the acquisition of the DEAP data set. The signals acquired with the sensors in the dashed rectangle were used in the present chapter. Sensors 7 and 8 were used to acquired the EMG on the Trapezius muscle, employed as an ECG in the present chapter and the impedance belt acquired the reference breathing signal. Image from [281], © 2012 IEEE.

The publicly available Database for Emotion Analysis using Physiological Signals (DEAP)

[281] was used in the present chapter. This dataset contains EEG, and thirteen peripheral physiological signals, including GSR, blood volume pressure, breathing (impedance belt), skin temperature, electromyogram (EMG) and electro-oculogram recordings from 32 healthy subjects (50% female) aged between 19 and 37 years (mean age 27 years). The subjects watched, in laboratory conditions, in the seated position, in random order, 40 one-minute video clips with emotional content, and rated them on liking, arousal and valence from 1 (negative/low) to 9 (positive/high). All signals were sampled at 512 Hz. Figure 8.2 illustrates the sensors used to acquire the DEAP data.

One of the EMG recordings, acquired from the Trapezius muscle (on the shoulder), contains ECG activity due to the proximity of the electrode location to the heart. In the present chapter, to infer heart rhythm information, this EMG signal was used instead of the blood volume pressure signal, as the latter was corrupted for subjects 24 through 32 and of poorer quality than the EMG signal for at least two other subjects. This EMG signal is hereafter referred to as the ECG signal. Figure 8.3 illustrates a typical example of the raw ECG (EMG) and breathing signals, which were used in the present chapter.
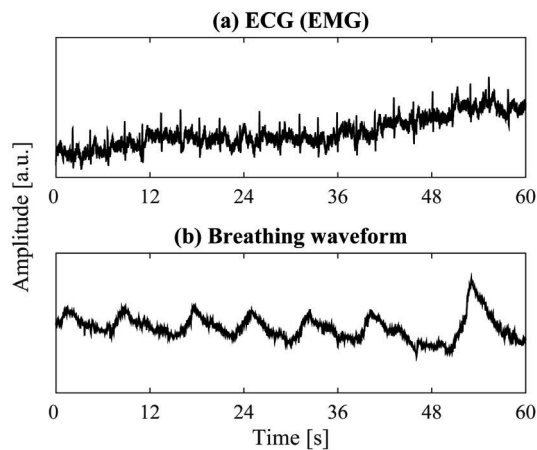
Figure 8.3: An example of the raw DEAP signals. (a) ECG; (b) Breathing waveform.

8.2.2   Feature extraction

Extracting the breathing-related oscillations
The first step of the processing chain was to extract the RSA. This was done using the reference instantaneous breathing rate (BR) to locally filter the R-R intervals as described in Chapter 3, Section 3.2.2. The breathing waveform was also re-sampled at 4 Hz and locally filtered similarly to the RSA. This refined breathing waveform is referred to as the breathing oscillation.

Features
The instantaneous heart rate (HR) was computed from the inverse of the R-R intervals. The LF and HF power of the R-R interval series were computed in a 25 s-long sliding window by integrating the Welch PSD over the concerned frequency bounds. The power of the RSA signal was also computed in a 25-s-long sliding window. The instantaneous RSA frequency and the BR were estimated from the respective signals using the notch filter bank (*NFB*) method introduced in Chapter 5, Section 5.2.2. The difference between the two frequencies was computed as well. It is hypothesized that, although this value should be small, it varies with changes in the relative phases of the two signals and thus could be an indicator of their synchronization.

The instantaneous amplitudes of the RSA and the breathing oscillation were extracted using the Hilbert transform (the parameter a in (5.29) in Section 5.2.3). Their ratio was also computed as it is hypothesized to carry information about the relative importance of the RSA amplitude. The phase lag (PL) between the two signals was assessed as described in (3.4) in Section 3.2.2. The slope of the PL (PL_{slope}) and its variability (PLV) were also computed as in Section 3.2.2.

To summarize, a total of 13 features were extracted from the signals acquired from each subject for each video, of which the following ones are cardiac: the HR, the R-R interval LF and HF powers, the RSA power, the RSA instantaneous frequency and the RSA amplitude; the following are breathing-related features: the instantaneous BR and breathing amplitude; and the following features are jointly from the breathing and the RSA waveforms: the amplitude ratio of the RSA to the breathing oscillation, the difference in frequency between RSA and breathing, the PL of the RSA with respect to the breathing waveform, the PL_{slope} and PLV.

Statistical analysis

To assess the relevance of the various features to emotional states, for each subject, the following statistical analysis was performed:

- the features corresponding to videos with a liking score ≥ 5 were compared to those corresponding to videos with liking scores < 5.
- the features corresponding to videos with an arousal score ≥ 5 were compared to those corresponding to videos with arousal scores < 5.
- the features corresponding to videos with a valence score ≥ 5 were compared to those corresponding to videos with valence scores < 5.

A Mann-Whitney U test was used for directional hypothesis testing in all the above cases as it does not require any assumption on the distribution of the data, and can compare sets with different sizes.

8.2.3 Classification

Three different binary classifiers were build: low/high liking, low/high arousal and positive/negative valence. To this end, the subjects' ratings by self-assessment during the experiment were used as the ground truth. The ratings for each of these scales were thresholded at mid-scale into two classes (low/high or negative/positive). The signals corresponding to each video were broken down into 12-s-long non-overlapping windows. 12 seconds is long enough to contain an entire period of even the slowest BR (5.4 brpm). These windows are hereafter referred to as single trials. Therefore, for each video, a total of 5 single trials were created. In order to perform the final classification of signals corresponding to each video, a majority voting on the results of single-trial classification was performed as depicted in Figure 8.4. An SVM classifier with a multilayer perceptron kernel was used for the classification of single trials. In order to evaluate classification performance, a leave-one-video-out cross-validation approach was used. More precisely, for each subject, all single trials of a given video were left out and the SVM was trained using the single trials from the remaining (39) video clips. This was repeated for all videos. The rationale for this cross-validation is that the single trials of a video were not used both as training and test samples in the cross-validation. Therefore, for testing each video, the training was performed using 195 trials (5 single trials × 39 videos). It was subsequently labeled according to the majority voting scheme on its single trials. To quantify the classification accuracy, the accuracy (ACC), true positive rate (TPR), true negative rate (TNR), false positive rate (FPR) and false negative rate (FNR) values are reported. These measures were defined in Chapter 7, Section 7.2.3 [1]. An ACC value of 0.8 for classifying a subject's valence, for instance,

---

1. Appendix A, Section A.2 further expands on classification measures.

would indicate that for 80% of the video clips (32 out of 40 video clips), the signal-based classified valence values match the subject's self-assessments. Similarly, a TPR of 0.8 means that 80% of positive-valence videos were correctly classified as such. A TNR of 0.8 means that 80% of negative-valence videos were correctly labeled as such. An FPR of 0.2 means that 20% of negative-valence videos were incorrectly labeled as being positive-valence. An FNR of 0.2 means that 20% of positive-valence videos were incorrectly labeled as being negative-valence.
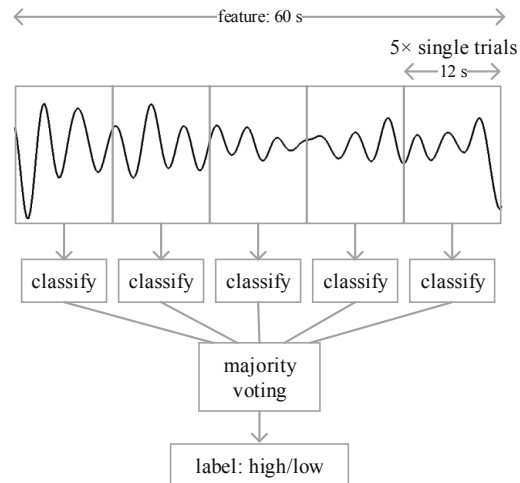
Figure 8.4: The classification of the emotion elicited by one video with 5 single trials using any given feature.

8.3 Results

8.3.1 Features and statistical analysis

Figure 8.5 shows an example of the RSA and breathing oscillations for one subject, for one video she/he liked and one video she/he disliked. It can be seen that the signals related to the video that the subject liked differ considerably in amplitude and frequency from those related to the video that the subject disliked. In this particular case, the RSA and breathing related to the liked video were of lower amplitude and frequency than those pertaining to the disliked video.

Figures 8.6 and 8.7 illustrate the difference in frequency between RSA and breathing for one subject, for liked and a disliked video, respectively. In these two examples, when the subject liked the content, the RSA and breathing waveforms displayed more erratic behavior than when the subject disliked the content. Hence, the RSA-breathing frequency difference was less variable for the disliked video.

Figure 8.8 shows an example of the phase lag between the RSA and the breathing oscillation, as well as its slope, for one subject, for one video she/he liked and for another she/he disliked. It can be seen that the features related to video-clips the subject liked differ considerably in amplitude and variation from those related to video-clips the subject disliked. Both features were more uniform for video-clips the subject disliked. Similar differences were observed between videos with low vs. high arousal and positive vs. negative valence.
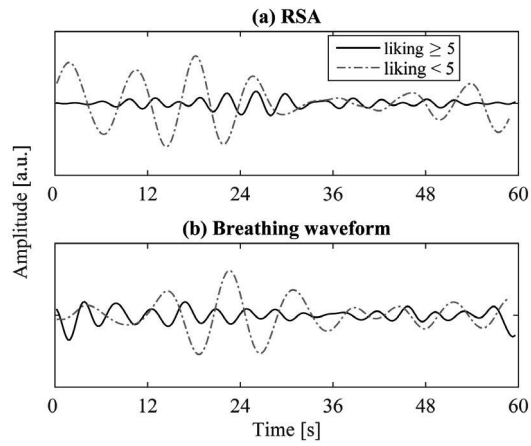
Figure 8.5: The RSA (a) and breathing signal (b) for a liked and a disliked video.
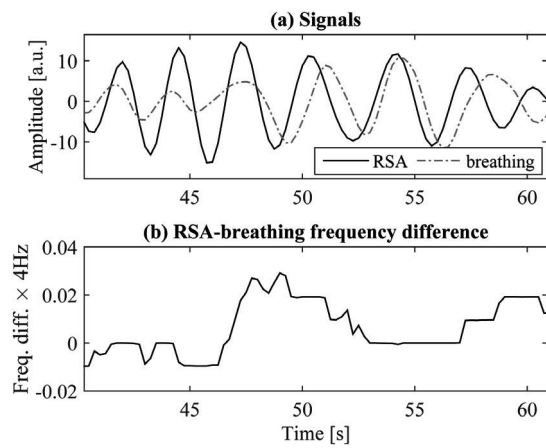
Figure 8.6: (a) The RSA and breathing signals; (b) difference in their instantaneous frequency-liked video.
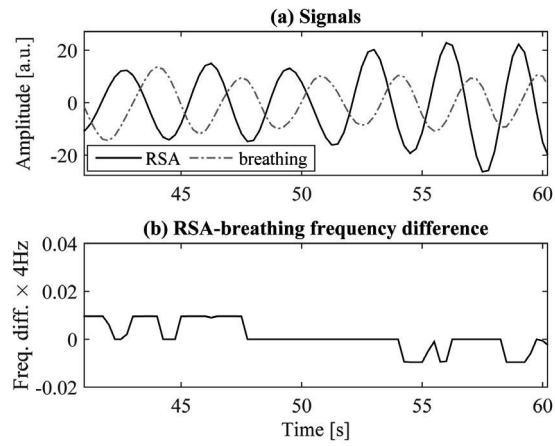
Figure 8.7: (a) The RSA and breathing signals; (b) difference in their instantaneous frequency-disliked video.
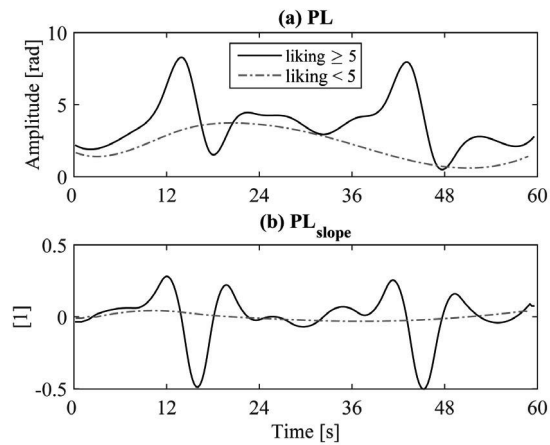
Figure 8.8: The PL (a) and PL$_{\text{slope}}$ (b) for a liked and a disliked video.

The directionality of the feature trends were not similar for all subjects. For some subjects, the RSA amplitude was larger when they disliked the content as shown in Figure 8.9 for one subject. In others, it was the inverse as depicted in Figure 8.10 for another subject. Similarly, in some subjects, the RSA and breathing frequencies were larger in the case of videos they liked as in Figures 8.11 and 8.13, but in others they were larger when they disliked the videos as in Figures 8.12 and 8.14. The frequency difference exhibited opposite trends depending on the emotion as shown in Figures 8.15 and 8.16 for two different subjects.
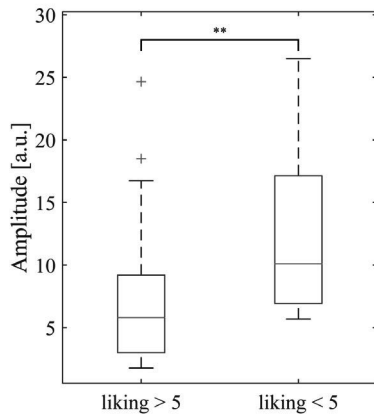
Figure 8.9: The RSA amplitude for liked and disliked videos, for one subject. **p < 0.05.
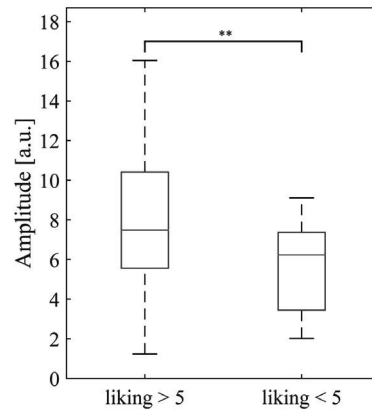
Figure 8.10: The RSA amplitude for liked and disliked videos, for another subject than in Figure 8.9. **p < 0.05.
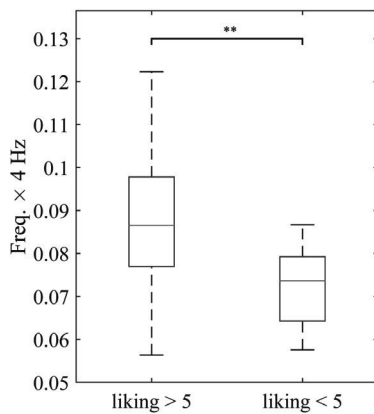
Figure 8.11: The RSA frequency for liked and disliked videos, for one subject. **p < 0.05.
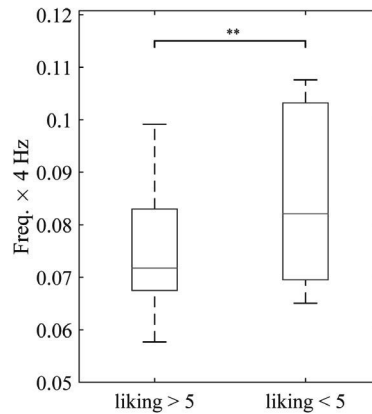
Figure 8.12: The RSA frequency for liked and disliked videos, for another subject than in Figure 8.11. **p < 0.05.

Table 8.1 reports the statistical relevance of the features. For each feature, the number of subjects for whom the feature was statistically different in each of the three scenarios of 1) low vs. high liking, 2) low vs. high arousal and 3) positive vs. negative valence, are reported. The features showing the largest trends across the subjects were the HR, the HF power, the RSA and
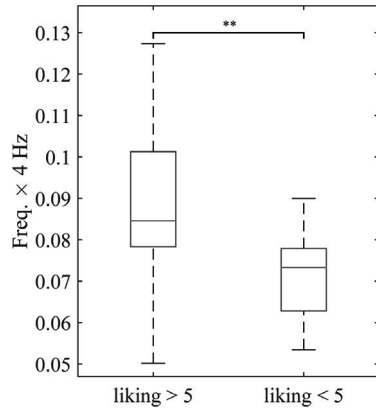
Figure 8.13: The BR for liked and disliked videos, for one subject. **$p < 0.05$.
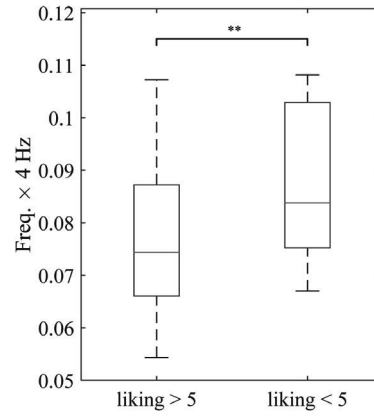
Figure 8.14: The BR for liked and disliked videos, for another subject than in Figure 8.13. **$p < 0.05$.
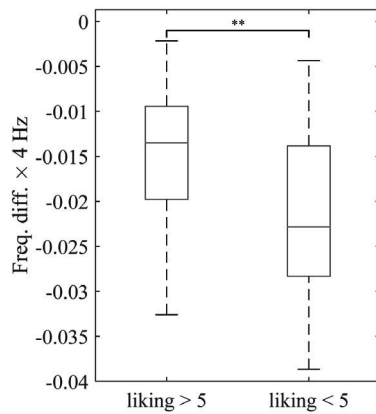
Figure 8.15: The frequency difference of the RSA and the breathing signals for liked and disliked videos, for one subject. **$p < 0.05$.
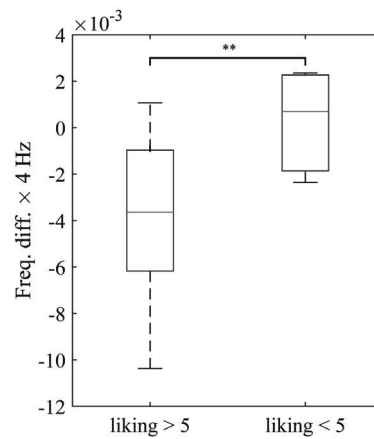
Figure 8.16: The frequency difference of the RSA and the breathing signals for liked and disliked videos, for another subject than in Figure 8.15. **$p < 0.05$.

breathing frequencies and their difference.

Table 8.1: Statistical relevance of cardiac and breathing-related features for emotion recognition. The number of subjects for whom there was a significant difference ($p < 0.1$) between the feature for videos with high vs. low liking, high vs. low arousal and positive vs. negative valence are reported for each feature. The most relevant features are reported in bold.

feature	liking	arousal	valence
HR	**12**	**10**	**13**
R-R LF power	11	8	8
R-R HF power	**12**	**15**	**6**
LF/HF	5	7	9
RSA amplitude	10	9	9
RSA power	9	11	8
RSA frequency	**10**	**9**	**18**
Breathing amplitude	9	6	12
BR	**13**	**7**	**15**
RSA-breathing frequency difference	**11**	**10**	**8**
RSA/breathing amplitude ratio	9	6	13
PL	7	3	6
PL_{slope}	7	4	7
PLV	7	9	12

8.3.2   Classification

Each of the 13 features was used alone in each of the three classification scenarios (low/high liking, low/high arousal and positive/negative valence). The impact of each feature was assessed by its average ACC over all subjects. The features resulting in the highest ACC values across all three classification scenarios were then employed together in classification schemes involving the best two and the best four features. Table 8.2 summarizes the ACC values for each feature alone, as well as for several feature combinations. The best classification was obtained with the frequency difference of the RSA and the breathing waveforms and with the RSA frequency. The accuracy was slightly lower when combining the best two or the best four features and even all 13 features.

Table 8.3 reports the average (over all subjects) performance metrics using the difference in frequency between RSA and breathing. The TPR was higher than the TNR, and the FPR was higher than the FNR.

8.4   Discussion

The directionality and intensity of the changes occurring in the RSA and other features with emotions were not uniform over the subjects. Opposite trends were even observed as seen in Figures 8.9 and 8.10 for example. This observation is coherent with the heterogeneous changes in the RSA with emotions reported in [107] and the accepted notion that there is no unique correspondence between physiological states and emotional states across different individuals [273]. It is therefore beneficial for the recognition system to be personalized for each subject.

It is interesting to note that conventional features, such as the HR and the HF power of the R-R intervals, although statistically relevant, were not the most discriminant features based on

Table 8.2: Emotion classification with cardiac and breathing-related features. Average ACC (STD) values for classification with each feature.

feature	liking	arousal	valence
HR	0.69 (0.11)	0.71 (0.10)	0.72 (0.09)
R-R LF power	0.67 (0.16)	0.63 (0.17)	0.67 (0.09)
R-R HF power	0.69 (0.16)	0.72 (0.14)	0.67 (0.12)
LF/HF	0.56 (0.21)	0.62 (0.16)	0.64 (0.11)
RSA amplitude	0.72 (0.13)	0.68 (0.14)	0.68 (0.10)
RSA frequency	0.75 (0.07)	0.74 (0.07)	0.72 (0.07)
Breathing amplitude	0.73 (0.13)	0.73 (0.08)	0.70 (0.09)
BR	0.74 (0.07)	0.74 (0.08)	0.70 (0.07)
RSA-breathing frequency difference	0.73 (0.09)	0.76 (0.08)	0.72 (0.06)
Ratio RSA/breathing amplitude	0.69 (0.17)	0.65 (0.17)	0.64 (0.14)
PL	0.73 (0.08)	0.72 (0.08)	0.72 (0.06)
PL_{slope}	0.71 (0.12)	0.72 (0.09)	0.70 (0.07)
PLV	0.72 (0.09)	0.75 (0.08)	0.72 (0.06)
best 2*	0.73 (0.06)	0.73 (0.06)	0.70 (0.06)
best 4**	0.73 (0.07)	0.73 (0.06)	0.70 (0.08)
all 13	0.73 (0.08)	0.71 (0.07)	0.71 (0.09)

*The best two features were those with the largest average ACC over all three classification scenarios and include the RSA-breathing frequency difference and the RSA frequency.
**The best four features were the RSA-breathing frequency difference, the RSA frequency, the PLV and the BR.

Table 8.3: Emotion classification using the difference in frequency between RSA and breathing. Average classification measures (STD) over all subjects.

	liking	arousal	valence
TPR	0.83 (0.15)	0.78 (0.19)	0.80 (0.19)
FPR	0.44 (0.30)	0.36 (0.28)	0.41 (0.23)
FNR	0.16 (0.15)	0.21 (0.19)	0.19 (0.19)
TNR	0.55 (0.30)	0.63 (0.28)	0.59 (0.23)

their average performance in the classification of liking, arousal and valence as can be noted in Table 8.2.

The best features for the classification were the difference in frequency between RSA and breathing, and the PLV. These two features are related to the synchronization of the RSA and the breathing waveforms and both are affected by irregularities and sudden shift in the PL. It seems that changes to the ANS because of emotions has a particular effect on the co-regulation of these two signals.

The classification performance was better when recognizing high/positive liking, arousal and valence than when recognizing low/negative states as seen from results reported in Table 8.3. This large difference in performance might be due to imbalance in the number of instances in each class. Indeed, some subjects tended to rate the videos rather high or rather low, such that their scores were not uniformly distributed. Furthermore, contrary to theoretical considerations and intuition, using a larger number of features degrades the accuracy of the SVM classifier as observed in Table 8.2. The difference in frequency between RSA breathing achieved the highest accuracy; however, when this feature was combined with another (best two features) or several others (best four features), the accuracy dropped. This shows that is it not necessary to combine many features in order to achieve better accuracy. A single well-chosen feature performs better.

In all the classification scenarios, the labels were separated as pertaining to the two classes (high vs. low liking, high vs. low arousal and positive vs. negative valence) by placing the threshold in the middle of the rating scale. However, as the ratings were subjective, the scores were not necessarily well distributed between the two classes and might be skewed for subjects who tended to rate generally rather high or rather low on the scale. One way to circumvent this asymmetry would be to separate the classes such that they contain an equal number of instances. We chose the midscale threshold primarily to be able to compare our results to those reported in the literature for the DEAP data set.

It is incorrect to compare our results to those of other studies that used different stimuli and different subjects, thus we limit ourselves to the comparison of our method to the system presented in [281]. On the DEAP dataset, the authors used a total of 106 features extracted from the recorded peripheral physiological signals, of which 14 were related to the HR and 19 were related to breathing. They reported ACC values of 0.59, 0.57 and 0.62 for liking, arousal and valence, respectively, for the 106 features used together. These values were similar to those obtained with EEG features. In the present study, we used only two signals, namely the ECG and the breathing waveform, and we obtained much higher ACC values of 0.73, 0.76 and 0.72 for the classification of liking, arousal and valence, respectively.

There is no unique accepted way for extracting the RSA. Although the methodology employed throughout this thesis proved to be adequate for the tasks we selected, it must be noted that other methods can be used as well. In fact in [277], which was our paper used as the basis for the present chapter, the RSA was extracted using an SSA-based scheme. Although the results were slightly different than those reported in the present chapter, the overall accuracy of emotion recognition with the RSA remains similar in both cases. In [277], phase indexes were also found to be the most pertinent in relation to emotions.

8.5   Conclusion

We presented a scheme, which uses one and at most two physiological signals, namely the RSA and the breathing signals, to recognize emotions elicited by music video clips. Our methodology was based on the RSA waveform extracted from the inter-beat intervals using the local filtering scheme described in Chapter 3. We further successfully employed features based on the phase lag between the RSA and the breathing waveform (introduced in Chapter 3) to classify emotional states. This system was evaluated on a public dataset, and achieved higher accuracy

than the state-of-the-art, while employing a smaller number of physiological signals and features. This system is a good candidate for portable monitoring systems because of the ease of acquisition of the two signals, compared to other modalities conventionally used in emotion recognition, such as the EEG.

Sleep Apnea Detection with the RSA and the Breathing signals

9

Automatic screening of sleep apnea has gained interest recently with the advent of portable monitoring devices such as wearables. In the present chapter, particularities of sleep apnea events are investigated from the stand-point of the physiological changes induced by apneas on the RSA and the breathing waveforms, by using signals acquired with a smart-shirt. Elements of this chapter were presented in a conference paper [293].

9.1 Introduction

9.1.1 Sleep apnea

Sleep apnea is a common condition with many implications on health and well-being [294]. Sleep apnea is characterized by pauses in breathing or by shallow breaths during sleep. These episodes can last from a few seconds to minutes. Apnea episodes are divided into three categories according to their severity and physiological causes. The first category, obstructive sleep apnea, is caused by the blockage of the upper airway. The second category, central sleep apnea, occurs when the neural drive to the muscles involved in breathing is transiently abolished and breathing is completely ceased. The third and mildest kind, hypopnea, occurs due to a partial cessation of breathing. To classify different kinds of apnea, some criteria have been established based on the decrease of the breathing amplitude, oxygen desaturation and the duration of the event [295]. These transient instabilities of the breathing process cause restless sleep and are liked to an elevated risk of cardio-vascular disease [294].

9.1.2 Sleep apnea detection using physiological signals

The gold standard method in sleep apnea detection is polysomnography (PSG) [295]. PSG is performed at a sleep laboratory, where the subject sleeps while wearing multiple sensors to measure physiological signals. Over 20 different physiological signals such as nasal airflow, ECG and EEG among others are acquired and analyzed a posteriori in 30 seconds segments by a specialist to detect apnea events.

The bulky and uncomfortable acquisition devices, as well as the fact that the evaluation must take place in a clinical facility, hinder the routine and widespread use of this technique for sleep apnea screening over long periods of time. It is therefore of practical interest to devise methods, which use physiological signals acquired in a comfortable manner, for sleep apnea screening. A number of studies have been carried out on apnea detection using signals such as the ECG

and the breathing waveform. These signals are of interest as they can be acquired easily using wearable devices in non-laboratory conditions.

There have been many studies on the detection of sleep apnea using ECG signals. In [296], nearest neighbor classification was performed using features related to the power in several frequency bands of the HRV to detect apneas (undisclosed category) with an accuracy of 88% on a public data set of 50 subjects. In [297, 298], between 40 to 111 time-domain and spectral features were extracted from the ECG, and an SVM classifier was used to detect apnea episodes, irrespective of their kind (central apneas or hypopneas). The features included mean and standard deviations of the R-R intervals, an ECG-derived breathing waveform, and energy features related to a wavelet decomposition of the R-R intervals, among several others. Both studies used a publicly available ECG dataset containing 70 recordings, each about eight-hours long and reported an accuracy of 88% [298] and a sensitivity of 96% [297]. The breathing signal has also been used in the context of apnea detection. In [299], central apnea and hypopnea events confounded were detected using an SVM classifier with an accuracy of 96% with features derived from the amplitude and frequency of the breathing signal on proprietary data. In a recent study, the RSA, as defined by the cross-correlation between the R-R intervals series and the breathing waveform was employed to detect obstructive sleep apnea [75]. In segments of data related to obstructive sleep apnea, the cross-correlation was markedly reduced compared to normal sleep.

9.1.3 Motivation and contributions

In the present study, ECG and breathing waveforms were acquired using a smart-shirt during a night sleep. The goal of this study was to devise features with clinical relevance and interpretation, from ECG and breathing recordings obtained with a convenient recording method, to detect sleep apnea episodes. Given that the ECG and the breathing signals alone have already been investigated for apnea detection, for example in [298, 299], the present chapter focuses on the RSA and several novel aspects of its relationship with the breathing waveform as potential features for apnea detection. To this end, several indexes were extracted from each signal alone, and several were computed jointly from the two. In addition to conventional features such as the amplitude of the breathing signal, phase indexes related to the relationship between RSA and breathing were also investigated.

Data recorded with the smart-shirt were favored over existing datasets because of the ease-of-use and comfort for the subject of such acquisition devices. Indeed, several publicly available PSG datasets exist [242, 300, 301], that contain the breathing and the ECG signals among others. In conventional PSG, the breathing waveform can be acquired as the nasal airflow or chest/abdomen movements (impedance belt) or both. For example, in [299], the PSG airflow signal was used. Furthermore, there is little literature on multi-modal breathing/ECG signals to detect sleep apnea. These motivations gave rise to this chapter on apnea screening using smart-shirt-acquired cardiac and breathing signals.

9.2 Methods

9.2.1 Data

Data were recorded from 12 subjects during three nights. The subjects were all healthy adult males (age 33 ± 9.4 years, height 179 ± 4 cm, weight 75.4 ± 6.8 kg) with a minimum of 3 hours-per-week physical training. None lived in altitude or was exposed to altitude the two weeks prior to the study. In a randomized order, they slept one night at 3450 m altitude (Jungfraujoch, Switzerland), one night in simulated 3450 m altitude (hypoxic chamber, Sion, Switzerland), and one night near sea-level (500 m). Acquisition nights were spaced by at least 10 days in normal

conditions. Over the duration of each night, ECG and breathing (thoracic impedance) wave-forms, as well as conventional PSG data were collected for each subject. The ECG and breathing waveforms were acquired by an instrumented smart-shirt (model SEW, CSEM, Neuchâtel, Switzerland) [10] worn by the subjects. Sample signals are presented in Figure 9.1). The ECG was sampled at 250 Hz and the breathing waveform was sampled at 25 Hz. The protocol was approved by the institutional ethical committee (CCVEM, 051/09) and all subjects gave informed consent [1].
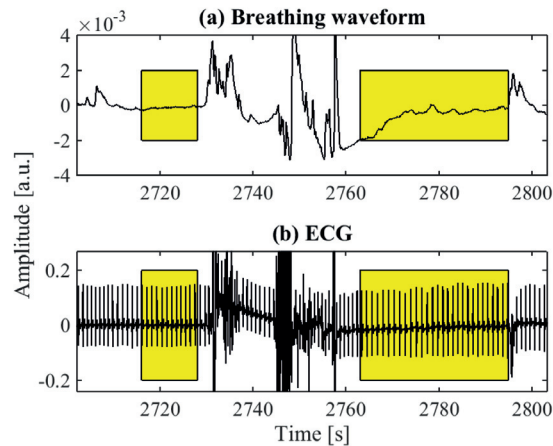
Figure 9.1: An example of the (a) breathing and (b) ECG waveforms acquired by the smart-shirt during hypopnea episodes (indicated by yellow rectangles).

Due to poor recording conditions (non-laboratory conditions) only 16 recordings over all subjects and all nights were usable and constituted a the data set for the present chapter. The PSG data were analyzed by an expert and periods of wake, central apnea, hypopnea and micro-arousals were identified and marked. The PSG data constituted the ground-truth. Table 9.1 contains the number of apnea episodes per usable recording as well as the duration of each recording. Recordings 1, 2, 4, 12, 14 and 16 were acquired in altitude. It is known that there is an alteration in the breathing pattern when one sleeps in altitude, which could account for the increased number of apneas in the recordings acquired in these conditions [302].

9.2.2 Data processing and feature extraction

Data were processed in 5-minute-long segments. The breathing waveform and ECG R-peaks were processed as described in Chapter 8 to yield the RSA and the breathing oscillation wave-forms. For several recordings, there were segments of bad quality ECG (possibly due to a loss of contact between electrodes and skin), where no R-peaks could be extracted. To avoid processing such segments further, 5-minute-long segments were marked as having poor quality, if the heart rate was lower than 30 bpm.

From the breathing signal, the instantaneous breathing rate (BR) was computed with the *NFB* algorithm (see Chapter 5). The amplitude of the breathing waveform was estimated as the half-sum of its upper and lower envelopes. The envelopes were computed by interpolating the local maxima and minima, identified in windows with lengths defined by the main period of the

Table 9.1: The number of sleep apnea episodes (c. ap.: central apnea, hypop.: hypopnea) and their average durations (STD) per recording (RC. recording).

RC.	c. ap.	dur. (s)	hypop.	dur. (s)	RC. dur. (h)
1	132	12 (1)	323	15 (5)	8.06
2	1	11	100	12 (2)	6.4
3	3	13 (2)	32	30 (17)	7.4
4	1	12	111	19 (9)	7.39
5	0	-	26	12 (1)	5.92
6	1	12	63	27 (16)	6.85
7	0	-	14	12 (3)	7.28
8	0	-	13	16 (8)	8.25
9	0	-	70	13 (3)	7.99
10	5	13 (2)	39	22 (9)	6.25
11	1	20	49	33 (27)	6.93
12	3	13 (3)	112	17 (9)	7.58
13	1	11	23	12 (2)	6.7
14	3	12 (1)	30	14 (3)	7.32
15	3	15 (3)	5	32 (36)	7.51
16	0	-	17	17 (11)	7.28

breathing oscillations. The latter was computed from the BR. An additional amplitude index was also computed to account for the change in the breathing amplitude during apneas. For each sample, a 10-s-long window centered on it was considered. The amplitude index was computed as the ratio of the maximum of the envelope of the breathing waveform in the 2 seconds preceding the 10-s to the mean envelope during the 10-s window [303] [2].

The instantaneous RSA frequency was estimated using the *NFB* algorithm similarly to BR estimation. The RSA amplitude was also computed similarly to the breathing amplitude, as described previously. The RSA power was computed by integrating its power spectral density, in a 30-second-long sliding window.

The phase lag (PL) between the RSA and the breathing waveform was computed as described in Chapter 3, Section 3.2.2. The PL slope (PL_{slope}), its variance (PLV), and synchronization (PLS), were also computed as described in Section 3.2.2.

9.2.3   Statistical analysis and classification

The features were compared during apnea episodes and during normal sleep (periods of wake and arousal were excluded) using a Mann-Whitney U-test.

Given that the duration of the apnea episodes was between 12 and 30 seconds, classification was performed on 10-s epochs, with 50% overlap. Each epoch was labeled as follows: if more than half of it was during a central apnea or hyponea episode, it was labeled as apneic. If it was not apneic, not related periods of wake and arousal and was not within a poor quality data segment, it was labeled as normal. Central apneas and hypopneas were confounded here as there were too few central apneas in the dataset for this category to be considered separately.

Classification was performed using a k-Nearest Neighbor (k-NN) scheme. This non-parametric classification scheme assigns labels based on the nearest neighbors of an instance in the training set. For $k = 1$, the classifier assigns the label of the nearest neighbor of the input in the training set. For $k > 1$, the label is assigned with majority voting. Several values were empirically

---

2. Based on an implementation by Sibylle Fallet [293].

tested for, and $k = 1$ and $k = 3$ were retained as yielding the most accurate results. For each recording, 10% of the apneic epochs and 10% of the normal epochs were retained as a test set. The remainder was used as a training set. This scheme was adopted to reflect the real ratio of normal to apneic epochs in the training and test sets, as classification of unbalanced data is notoriously problematic [304]. A 10-fold cross validation was performed to assess the classification performance.

Classification was performed and evaluated in a per-subject manner. The rationale is that such physiological features are strongly subject-dependent and vary with age, gender, and physiology in general. Moreover, apnea screening is usually performed for a person in particular, therefore, one can expect the screening method to be personalized.

The task at hand was the identification of apnea events from normal sleep. Given that the classification is actually an identification problem, reporting a classification accuracy may be misleading and insufficient to assess the performance. There were generally much more normal epochs than apneic epochs, if a classifier assigns normal labels to all epochs, a high accuracy is achieved even though no apneic episodes were actually identified. Therefore the performance is reported here with the sensitivity, specificity, precision and F-score. The sensitivity or true positive rate (TPR) is the ratio of identified apnea events and is computed as in (9.1). The precision is the fraction of the retrieved positives which are actually real positives and is computed according to (9.2). The specificity or true negative rate (TNR) is the ratio of normal sleep classified as normal sleep measured according to (9.3). The F-score is the combination of the sensitivity and precision, and is a general indicator of the accuracy of the identification measured as in (9.4) [3].

For comparison purposes, given the ratio of apneic epochs to normal epochs, the values of the classification metrics for a random guess classification were calculated for each recording. An example is given: Consider that for a recording with 100 epochs, 10 are apneic and 90 are normal. The random guess assigns an apneic label to 50 and a normal label to 50 in a random manner. If we assume that of the 10 actual apneic epochs, half are labeled as apneic, of the first 50, 5 are true positives (TP), the other 45 are false positives (FP). From the second 50, 5 are false negatives (FN) and the other 45 are true negatives (TN). Then the random guess specificity is 0.5 (half the normal sleep epochs are labeled as such), the random guess sensitivity is also 0.5 (half the apnea epochs are labeled as such), the random guess precision is 0.1 (only 10% of the labeled positives are actually apneas) and the random guess F-score is 0.16. In fact, the precision is equivalent to the proportion of apneic epochs from all epochs. This particular definition of a random guess assigns apneic labels to half the epochs. It could be conceivable to assign labels based on an a priori guess about the number of apneic epochs. For example by assuming that only 10% of all epochs should be assigned an apneic label. In this case, the precision would be even lower, given that there is a small probability that that small number of apneic labels be assigned to actual apneic epochs. Moreover, computing such probabilities are less straightforward and are therefore not considered at all here.

$$sensitivity = \frac{TP}{TP + FN} \tag{9.1}$$

$$precision = \frac{TP}{TP + FP} \tag{9.2}$$

$$specificity = \frac{TN}{TN + FP} \tag{9.3}$$

$$F\text{-}score = 2\frac{precision \times sensitivity}{precision + sensitivity} \tag{9.4}$$

---

3. Appendix A extends on the performance assessment of classification.

9.3   Results

9.3.1   Illustrative examples and statistical analysis

Most of the apneic events were hypopneas, which are the mildest kind of apnea. These events induce smaller amplitude changes compared to central and obstructive apneas. Generally, during a hypopnea episode, the breathing amplitude and consequently the RSA decreased, yielding an increase in the amplitude index. The PLV increased as a result of the disorganization of the waveforms, which can be observed visually in Figure 9.2.
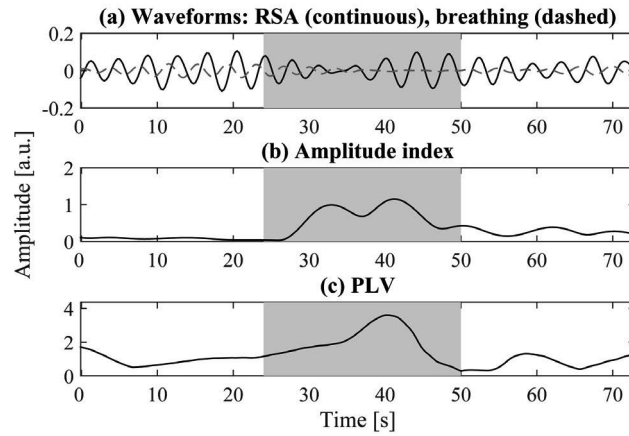
Figure 9.2: An example of the RSA and breathing waveforms, and the amplitude index and PLV during a hypopnea episode. The hypopnea episode is highlighted in gray.

Table 9.2 reports, for each feature and each condition, the number of recordings, for which there was a statistical difference ($p<0.05$), between normal sleep and each condition. The most discriminant features were the BR, breathing amplitude, amplitude index, RSA frequency, PLV and PLS.

Table 9.2: The statistical relevance of the cardiac and breathing-related features for sleep apnea detection. The number of recordings (16 total) in which there was a significant difference ($p<0.05$) between the feature for normal sleep and for specific events are reported.

	Hypopnea	Central apnea	Both confounded
BR	16	11	16
Breathing amplitude	16	9	16
Amp index	16	11	16
RSA frequency	16	11	16
RSA power	15	11	14
RSA amplitude	15	10	13
PL	13	9	12
PL_{slope}	9	7	10
PLV	16	10	15
PLS	16	10	15

The analysis of the amplitude index in hypopneas vs. normal sleep for one subject in Figure 9.3 shows this difference over one night.
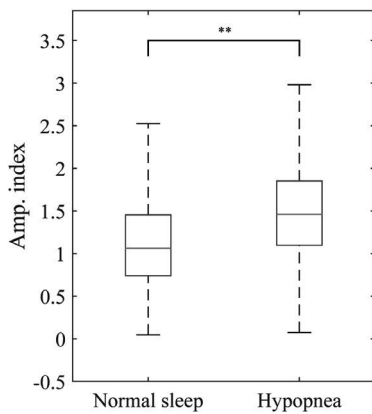
Figure 9.3: The amplitude index for normal sleep and hypopnea episodes for one subject. **p<0.05.
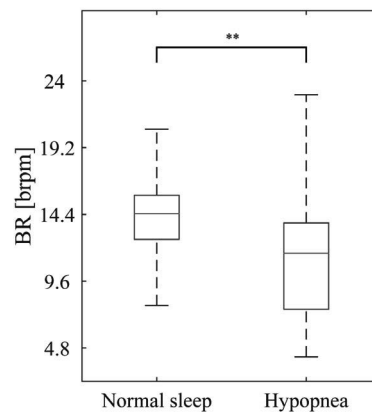
Figure 9.4: The BR for normal sleep and hypopnea episodes for one subject. **p<0.05.

As expected, the BR decreased during hypopneas as seen for one subject in Figure 9.4. The PLV increased during hypopnea episodes and the PLS decreased, as seen in Figures 9.5 and 9.6.
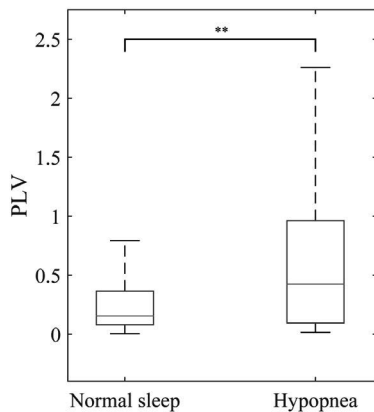
Figure 9.5: The PLV for normal sleep and hypopnea episodes for one subject. **p<0.05.
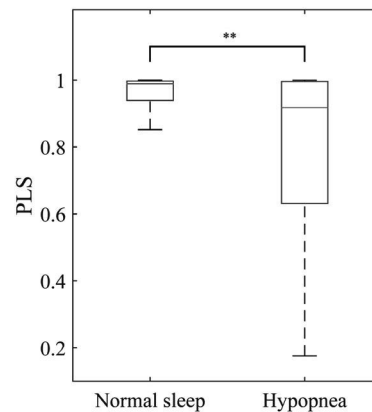
Figure 9.6: The PLS for normal sleep and hypopnea episodes for one subject. **p<0.05.

9.3.2 Classification performance

Table 9.3 reports the number of apneic and normal epochs per recording. Because of the small number of apneas in 7, 8, 13, 15 and 16, these recordings were excluded for classification. Based on the proportion of apneic epochs, the values of the classification measures for a random guess are reported as well. It can be seen that between 2% and 26% of the epochs were apneic and for most recordings, this ratio was below 10%. The random guess F-scores were between 0.03 and 0.34.

Table 9.4 reports the classification performance for each recording when using all ten fea-

Table 9.3: The number of apneic and normal epochs and random guess values for the classification performance measures.

RC.	nb apnea	nb normal	specificity	sensitivity	precision	F-score
1	980	2863	0.50	0.50	0.26	0.34
2	243	4364	0.50	0.50	0.05	0.10
3	203	5130	0.50	0.50	0.04	0.07
4	425	4896	0.50	0.50	0.08	0.14
5	65	4200	0.50	0.50	0.02	0.03
6	355	4576	0.50	0.50	0.07	0.13
9	177	5420	0.50	0.50	0.03	0.06
10	190	4075	0.50	0.50	0.04	0.08
11	332	4617	0.50	0.50	0.07	0.12
12	389	4704	0.50	0.50	0.08	0.13
14	88	5041	0.50	0.50	0.02	0.03

tures. The k-NN classifier was trained with $k = 3$. It can be seen that the classification was much better than a random guess. The sensitivity was high, often above 0.85. This means that the 3-NN classifier labeled normal sleep mostly as such. The sensitivity was mostly close to 0.5, meaning that roughly half the apnea events were identified. This is similar to a random guess. However, the precision and the F-score of the 3-NN classifier were much higher than the random guess, meaning that the former labeled a smaller number of normal epochs as apneic compared to the latter. Table 9.5 reports the same values but for a 1-NN classifier. This classifier performed with a generally lower specificity and sensitivity than the 3-NN but with a higher precision. The F-scores were not much different in the two cases.

Table 9.4: Identification of apnea epochs with a 3-NN classifier trained with all features.

RC.	specificity	sensitivity	precision	F-score
1	0.58	0.77	0.39	0.52
2	0.89	0.39	0.16	0.22
3	0.93	0.50	0.21	0.30
4	0.84	0.52	0.23	0.32
5	0.96	0.33	0.14	0.19
6	0.86	0.53	0.23	0.32
9	0.93	0.42	0.16	0.23
10	0.92	0.52	0.22	0.31
11	0.86	0.60	0.24	0.34
12	0.85	0.57	0.24	0.34
14	0.95	0.17	0.06	0.09

Table 9.6 and 9.7 report the classification performance using each feature alone for recordings 1 and 10, respectively. For recording 1, the best features were, in order, the amplitude index, the BR, the RSA frequency, and the PLS. The amplitude index yielded the same F-score as classification with all ten features. None of the other features alone was as good. For recording 10, the best features were the PLS, the amplitude index, breathing amplitude and the RSA amplitude. The F-score for the PLS and the amplitude index alone was better than that of classification with all ten features. Other features alone were not as good as all ten combined. Examination of classification with each feature alone for other recordings (see tables in Appendix D) revealed that

Table 9.5: Identification of apnea epochs with a 1-NN classifier trained with all features.

RC.	specificity	sensitivity	precision	F-score
1	0.83	0.50	0.50	0.50
2	0.96	0.23	0.23	0.23
3	0.98	0.37	0.43	0.39
4	0.94	0.34	0.32	0.33
5	0.99	0.16	0.25	0.19
6	0.95	0.33	0.35	0.34
9	0.98	0.29	0.34	0.30
10	0.98	0.28	0.37	0.32
11	0.95	0.42	0.38	0.40
12	0.95	0.32	0.34	0.33
14	0.98	0.12	0.11	0.11

for different recordings, different features were relevant but that generally, the amplitude features and the PLS were often among the most discriminant ones in apnea detection.

Table 9.6: Identification of apnea epochs with a 1-NN classifier trained with each feature alone for recording 1.

	specificity	sensitivity	precision	F-score
BR	0.80	0.40	0.40	**0.40**
Breathing amplitude	0.83	0.30	0.38	0.33
Amplitude index	0.83	0.52	0.51	**0.52**
RSA frequency	0.80	0.38	0.40	**0.38**
RSA power	0.80	0.33	0.36	0.34
RSA amplitude	0.81	0.32	0.37	0.34
PL	0.78	0.30	0.32	0.31
PL_{slope}	0.77	0.33	0.33	0.33
PLV	0.77	0.32	0.33	0.32
PLS	0.80	0.35	0.37	**0.36**

9.4 Discussion

Generally, as expected, breathing became strongly reduced and even sometimes non-existent during apneas. Indexes based on the amplitude of the breathing waveform and the RSA were the best for the identification of apnea episodes. This observation is in line with the results reported in [75], where the amplitude of the RSA, as measured by the cross-correlation between the breathing waveform and the R-R intervals series was also shown to be a discriminant feature in detecting obstructive sleep apneas. In particular, the amplitude index, measuring the evolution of the breathing amplitude was often the most discriminant feature. Indexes pertaining to the phase lag of the RSA with respect to the breathing waveform were not as good as the amplitude indexes. However, the phase lag synchronization was the best phase-related feature.

It must be noted that, given the rather small size of the dataset and the quality of the data, it was not possible to investigate differences in apnea detection between recordings related to normal or hypoxic conditions. Generally, a larger number of hypopnea episodes occurred while

Table 9.7: Identification of apnea epochs with a 1-NN classifier trained with each feature alone for recording 10.

	specificity	sensitivity	precision	F-score
BR	0.96	0.21	0.19	0.20
Breathing amplitude	0.97	0.27	0.31	**0.29**
Amplitude index	0.98	0.31	0.43	**0.35**
RSA frequency	0.97	0.16	0.18	0.17
RSA power	0.97	0.11	0.13	0.11
RSA amplitude	0.97	0.24	0.28	**0.25**
PL	0.96	0.21	0.22	0.21
PL_{slope}	0.97	0.20	0.22	0.21
PLV	0.97	0.21	0.24	0.22
PLS	0.97	0.34	0.39	**0.36**

the subjects slept at real altitude compared to when they slept in a hypoxic chamber or normally. The number of central apneas did not seem to vary notably with altitude, although the generally small number of central apneas may not allow to distinguish an effect of the altitude.

There were many limitations in the classification of apnea episodes. With one or two nights of data per subject, recorded in different conditions (altitude), one cannot realistically build a classifier. Furthermore, the number of apnea episodes per recording was very variable, which affects the training of any classifier. There was far more data pertaining to normal sleep than to apnea conditions. Typically, over a recording, apnea (mostly hypopnea) events occurred in about 5% of the recording duration. Such imbalance is notoriously difficult to handle in classification schemes and an entire branch of the machine learning field is devoted to it [304]. Last but not least, the signals were acquired with a smart-shirt, and differed considerably from typical good quality signals recorded in the framework of PSG.

Preliminary attempts to classify apnea episodes are encouraging and with more sophisticated classifiers, these features may have a potential to detect apnea episodes. It must be noted that the purpose of this chapter was merely investigative. The effect of sleep apnea on the RSA and ANS indexes was of interest and developing a robust and precise classification scheme was not a primary aim. Apnea episodes (hypopnea and central apnea confounded) were identified with a set of ten features extracted from the breathing waveform, the RSA and their relationship. Although not very high, the precision and the F-score of the classification were much larger than that of a random guess. The vast majority of the apnea episodes in the data were hypopneas, which are a mild kind of apnea, unlike central apneas and obstructive apneas. Presumably, the more distinctive effects of these sever apneas on physiological signals makes them easier to identify.

The high precision reported in [298, 299] for apnea detection with the ECG or the breathing waveform alone may be related to several factors. The quality of the signals plays an important role. Unlike the signals used in the present chapter, those used in [298, 299] were acquired in laboratory settings. Furthermore, the airflow signal used in [299] is generally a better breathing signal than that of an impedance belt, prone to movement artifacts. Furthermore, it must be noted that wearing a mask all night provides less comfort for the subject than wearing a garment with integrated sensors. The impact of the recording conditions on the results is non-negligible and for a given system to be scalable to a real situation, one must validate methods in non-laboratory conditions. The scheme for classification validation and performance measurement may also have a large effect on the performance metrics. In the present chapter, when the test set was composed of an equal number of apneic and normal epochs, the performance metrics were improved several-fold. However, this scenario is not representative of a real situation.

The dependency of sleep apneas on the activity of the autonomic nervous system (ANS) [305] may be reflected by the RSA because of its link to the ANS. In [305], it was shown that the sympathetic nervous system is influenced by the sleep cycle. In addition, different sleep stages are associated with a dominant sympathetic or parasympathetic ANS activity [306]. Further investigation on such phase relationships could reveal a link between the sympathetic regulation of breathing and the RSA. However, this aspect is purely hypothetical at this stage.

All the signal processing techniques employed in the present chapter are real-time capable. Provided a prior trained classifier, apnea detection can be performed in near-real-time as the k-NN classifier is a fast and relatively simple method.

9.5   Conclusion

In this chapter, features pertaining to the detection of sleep apnea episodes from the ECG and breathing signals acquired with a wearable smart-shirt were presented. These features were computed from the RSA and breathing waveforms and their phase relationship. In particular amplitude indexes were the most relevant for apnea detection. The synchronization of the phase lag between the RSA and the breathing waveforms was also interestingly discriminative for this task. A preliminary identification scheme to automatically label segments of data as being apneic or normal proved encouraging for the use of these indexes in conjunction with conventional ECG and breathing-related measures already accepted in literature for apnea detection.

Conclusion

10

This thesis finds its place at an intersection between physiology and medical sciences on one hand, and signal processing and information technology on the other hand.

The main focus of this thesis was the relationship, mediated by the autonomic nervous system (ANS), between cardiac and breathing activities, as analyzed using carefully selected, adapted and designed signal processing methods. Special emphasis was placed on methods with end-applications in real-life, particularly with personal health monitoring devices, such as wearables.

To begin, we described the physiological basis of the relationship between the cardiac and breathing rhythms. The regulation of the heart rate by the ANS was reviewed and the importance of studying cardiac ANS-related phenomena outlined. In particular, we underlined respiratory sinus arrhythmia (RSA) as one of the main elements of this regulation. The importance of this entity in the regulation of the cardiac and breathing rhythms, studied through heart rate variability (HRV) analysis, and its benefit to many health-related ventures were put forth through a survey of relevant literature.

We then argued several inconsistencies and shortcomings of current signal processing methodologies in the study and use of these (becoming ever more) widespread physiological phenomena. We demonstrated dilemmas involved with the fixed bandwidths employed in conventional HRV analysis and built a case to take into consideration breathing when discriminating between the various influences on the HRV. On a physiological basis, and bearing in mind health monitoring implications such as clinical interpretation and real-time processing, we introduced a methodology to define and measure the RSA and several other aspects of the relationship between cardiac and breathing rhythms. We developed and put to trial novel indexes based on this relationship using data acquired in the framework of collaborative projects. We especially investigated the particularities of autonomic modification with posture changes, ANS receptor antagonist and protagonist drugs, and altitude exposure. Our evaluations demonstrated areas in which the concepts introduced could complete and improve current techniques, as markers of the cardio-respiratory regulation in general.

On a different but related note, as a result of the relationship between cardiac and breathing rhythms, cardiac signals can be used to infer breathing information. This aspect is becoming increasingly important in the context of mobile health monitoring. Indeed, by using one type of sensor and one type of signal to measure several phenomena, there is an improvement in the cost and ease-of-use of devices. By applying a real-time capable and multi-variate algorithm developed previously in our group, we built on recent advances in the field of breathing rate estimation from cardiac activity. While answering to a major shortcoming of this existing method, namely the problem of delays in real-time processing, we designed a novel algorithm with the important requirement of minimal delays. We applied and evaluated this algorithm not only with inputs ex-

tracted from ECGs, but also using the novel imaging photoplethysmography cardiac monitoring technology. We also showed that this algorithm can be applied to estimating the instantaneous rhythm of other oscillatory signals, for example to estimate the instantaneous breathing rate from the breathing signal.

Acknowledging that such estimation of breathing parameters from cardiac recordings depends on assumptions about the acquisition conditions (mostly the body posture of the subject), we proposed a general methodology to separate breathing influences from cardiac recordings without making any kind of a priori assumptions. It must be added here that this work was triggered by a need for such specific methodology for a study being carried out by the Institute of Sport Science of the University of Lausanne (ISSUL). The ISSUL intended to analyze HRV on historical data acquired in the past, and over a number of years from high-level athletes. This data did not comprise recordings of a breathing waveform, therefore to apply breathing-aware HRV processing, there was a clear need to identify the breathing influence without a reference. We discovered that this task was non-trivial, and accordingly, devised methodology to cater to the generalized conditions.

Aside from the important application of breathing rate estimation, we applied the RSA estimation and frequency estimation algorithms developed in this thesis to other ventures. In particular, emotion recognition and sleep apnea screening using cardiac and breathing signals were chosen. Our proposals built on previous achievements in the field to take the processing one step closer to the user end of any biomedical system, by contributing to real-time processing, interpretable processing, and by introducing novel indexes based on the complexity of the relationship between cardiac and breathing rhythms.

10.1   Summary of achievements

Robust and breathing-aware RSA extraction with and without the reference breathing waveform

In Chapter 3, we extracted the RSA by filtering the heart inter-beat intervals with a time-varying IIR filter, centered on the local instantaneous breathing rate. This methodology ensures the RSA is in fact related to the real breathing rate and is not merely based on a generic assumption about the mean breathing rate in humans. The need to continuously adjust method parameters based on the study population or conditions thereby disappears. Furthermore, the filtering operation always extracts an oscillatory component due to the width of the band-pass. Therefore, this methodology also serves as a noise-removal scheme and ensures accuracy of the phase calculations. HRV parameters measured from the RSA extracted with this methodology were physiologically more relevant than those measured with conventional methods as demonstrated in Chapters 3 and 4. In addition to yielding a robust and instantaneous RSA waveform, this methodology also resulted in the creation of successful features for emotion recognition in Chapter 8 and for sleep apnea detection in Chapter 9.

On data acquired in supine and standing positions, it arose that, in such heterogeneous acquisition conditions, identifying and isolating the RSA without making use of the reference breathing waveform was not straightforward. Therefore, in Chapter 7 we proposed a methodology to decompose the heart inter-beat intervals into oscillatory constituents, and using a model, identify the one related to breathing, in other words the RSA. We performed classification using a previously validated model created from a set of independent subjects. In light of the success of this methodology, it can be applied to target historical data.

Novel markers of the relationship between cardiac and breathing rhythms

In this dissertation, we studied several aspects of the relationship between cardiac and breathing rhythms, which have remained largely unexplored until today. In particular the phase relationship between the cardiac and breathing activities was investigated in Chapters 3 and 4. Phase-based indexes were introduced in a previous thesis within our group to assess the organization of cardiac signals in relation with atrial fibrillation [192]. The stability of the phase between the dominant frequency component and the component related to its first harmonic in cardiac biosignals was demonstrated to predict atrial fibrillation therapy outcomes. In the present thesis, the phase lag between the RSA and breathing waveforms and the variations associated with this phase lag proved to carry interesting and valuable information on the regulation of cardiac and breathing rhythms. We defined two indexes based on the phase lag of the two waveforms and implemented one existing measure. These phase indexes represented synchronization aspects between the two waveforms in an instantaneous manner and showed patterns of influence under known autonomic stimuli, such as posture change and autonomic blockade as demonstrated in Chapter 3. They were also representative of ANS changes induced due to altitude exposure as seen in Chapter 4. Furthermore, these indexes showed potential in emotion recognition and sleep apnea screening with cardiac and breathing signals in Chapters 8 and 9. Through the application of these phase indexes to various situations, we observed that the phase relationship between the RSA and breathing seemed to be mostly related to the sympathetic activation of the ANS, although this connection remains hypothetical at this stage. We propose them as additional and complementary indexes to conventional markers as they report on complementary aspects of the relationship between cardiac and breathing rhythms. Furthermore, the instantaneous nature of the indexes proposed in this thesis permits to study novel aspects of the cardio-respiratory relationship, in contrast to coherence maps and synchrograms, commonplace in estimating the relationship between two signals.

Real-time breathing rate estimation from cardiac recordings

Adaptive frequency tracking schemes were the focus of two previous thesis in our group [307, 308]. In [308], it was suggested that they have a potential in estimating modulatory rhythms, such as the breathing rate from cardiac inter-beat intervals. The present thesis built on that idea and in Chapter 5, we applied a weighted multi-signal adaptive oscillator-based band pass filter (*W-OSC*) to the task of estimating the breathing rate from two breathing modulations of cardiac activity. We implemented the algorithm, including the pre-processing, conceptually in real-time. We designed the pipeline to process each new heartbeat and to update previously estimated values. To the best of our knowledge, there were no previous methods to estimate the breathing rate from the ECG beat-to-beat by using simultaneously multiple breathing modulations. In the course of the adaptation of this algorithm, we set about to further reduce de facto estimation delays of adaptive methodology. The outcome of our endeavors was a novel algorithm, based on a bank of short FIR filters, that we referred to as the *NFB* method. Indeed, the response delays of the new filters were shorter than that of the IIR filters, employed in the adaptive *W-OSC* scheme. In this new scheme, we designed a bank of similar filters to span a wide frequency band. Once filtered with all filters, the smallest output powers were indicative of filters whose central frequency was close to that of the input. To the best of our knowledge, this scheme is original. It allowed to further reduce the already short delays of the *W-OSC* method, while keeping the flexibility of introducing multiple inputs. The scheme proved to be adequate on resting state data, but also on data acquired during physical exercise, proving the robustness of the scheme. We further applied the algorithm to estimate the breathing rate from the breathing modulation of cardiac activity, as acquired by the novel imaging photoplethysmography technology in Chapter 6. This technology is based on using a video camera to sense skin tone changes in the face, which are the result

of blood volume changes occurring with every heartbeat. This technology has a potential in monitoring cardiac activity, where a close-contact sensing device cannot be used, for example in monitoring vehicle drivers or newborn infants.

Contributions to emotion recognition with cardiac and breathing signals

We tackled emotion recognition in Chapter 8 using the novel indexes introduced in Part I of the present thesis. It is increasingly important to automatically gain knowledge about the feeling of the user of a connected system, multi-media or other, to improve human-machine interactions, for example in recommendation systems. Monitoring of personality disorders and mood swings may also be a potential clinical avenue of automatic emotion recognition. We showed that the phase indexes and RSA methodology introduced in Part I of this dissertation were successful in helping to classify signals based on the emotion associated with them.

Contributions to sleep apnea screening with cardiac and breathing signals

We further investigated the indexes presented in Part I in relation to sleep apnea screening in Chapter 9. Polysomnography, the gold standard for apnea screening, takes place in a sleep clinic while the patient wears a large number of sensors and acquisition devices. A specialist then examines a large number of signals over the duration of one or several nights to identify apnea events based on their manifestation in various physiological signals. This cumbersome screening methodology prevents large-scale deployment, especially for at-risk populations such as elderly and obese people. Moreover, with the increasing incidence of certain cardiac arrhythmia, such as atrial fibrillation, and its link to sleep disorders [192], it is becoming more important to screen for sleep apnea easily. We applied novel indexes and methodology to particularly challenging data acquired with an instrumented t-shirt to detect apnea episodes. The indexes we proposed as complements to existing markers have a potential to aid in the "at home" sleep apnea screening with user-friendly devices and automated processing techniques.

10.2   Perspectives

Algorithm implementation

The methodology and algorithms developed throughout this thesis have been presented in a conceptual manner keeping in mind the end goal of mobile health monitoring applications. However, for these algorithms to be implemented on a portable device or an embedded system, they must undergo a number of adaptations. In particular, floating point computations must be revisited. Given the precision of the present methodology, floating point values are not necessary. Integer filtering can be used and quantization can be applied in many stages of the computations. Furthermore, to compute central frequencies of the filters in both the *W-OSC* scheme and the *NFB* scheme, look-up tables can be employed. It must be noted that FPGA-based algorithm implementation has received some attention recently, and algorithms as complex as the singular value decomposition have been implemented on such systems [309].

Further investigations into novel indexes describing the relationship between the cardiac and breathing rhythms

With the many uncovered enigmas about human physiology in general and ANS regulation in particular, there is much capacity for improvement and new discoveries. By taking a different point of view, we put forth previously unexplored aspects of ANS regulation. It is necessary to

further study and evaluate this methodology on additional data in other conditions. In Chapter 3, the ANS regulation and balance was artificially modified using receptor antagonist agents to suppress the sympathetic ANS activation. Parasympathetic blockade (with the injection of atropine) would bring the complimentary view to this study. Moreover, the pertinence and usability of these indexes for special populations, such as coronary disease patients should be investigated in view of the wider clinical acceptability of this methodology, for example for screening purposes.

On a different note, we hypothesized that the phase relationship between the breathing and RSA waveforms may be related to the sympathetic activation of the ANS. Further experiments are necessary to verify or to reject this hypothesis.

Catering to generalized conditions in breathing rate estimation

The application of the *W-OSC* and the *NFB* frequency estimation methods in Chapter 5 relies on the main oscillatory component of the input being related to breathing. This property holds true only in particular conditions. Resting data from sedentary subjects resulted in accurate estimations, as did data during exercise. One of the properties of all this data was the rather high breathing rate. In later stages of this thesis, in Chapter 7, we observed that in several conditions, these assumptions do not hold, in particular for individuals with naturally low resting breathing rates such as athletes. Also, with varying body postures, ANS regulation introduces further complications, which must be taken into account. The methodology for automatic RSA identification described in Chapter 7 caters especially to this problem by using a model trained on generalized data. The application of this methodology prior to breathing rate estimation with the *W-OSC* and the *NFB* methods can yield a general procedure to handle data regardless of their particular source. Furthermore, the methodology from Chapter 7 could also serve as a pre-processing stage to enhance the component of interest, similarly to the techniques applied in Chapter 6, when estimating a highly variable breathing rate from imaging photoplethysmography inter-beat intervals.

Application of the methodology for automated RSA identification

We created and validated a model to classify oscillatory constituents of a given recording of heart inter-beat intervals in Chapter 7. This model was built using data from 21 subjects with recordings in the supine and orthostatic postures. The model makes use of the decomposition of the inter-beat intervals and several attributes of the components and recording conditions. This model can now be used to identify the RSA in unseen data from independent subjects in a study of ANS particularities of high level athletes by the ISSUL.

Improving breathing rate estimation using a video camera

There are efforts in estimating the breathing rate using a video camera by monitoring breathing movements captured by the camera [248, 255]. Estimating the breathing rate in real-time from the cardiac breathing modulation of imaging photoplethysmographs presented in Chapter 6 can be used in complement with movement-based estimation to further improve robustness or accuracy.

Sport physiology signal processing

This thesis warranted several close encounters with sport physiology. The studies corresponding to the Chapters 3, 4 and 7 used data related to, or of interest for athletic training. Indeed, RSA characterization, and autonomic regulation, for example in altitude training, are of interest in sport physiology. They could help better understand and plan the effects of training and

training schedules. They could also aid in identifying, understanding, or avoiding unwanted and harmful situations for the athletes, such as fatigue and overtraining. With the increasing possibilities in portable monitoring devices, sport physiology signal processing offers many possibilities for exploration.

Appendix

Definitions A

A.1 Interpolation methods

As described in Chapter 2, the R-R intervals time series is by nature a time-series, with no naturally occurring time indexes, with unequally spaced values. In its raw format, many conventional signal processing techniques cannot be applied to it directly. It is therefore necessary to re-sample the series uniformly. Among the possible methods to do so, two have been considered in this manuscript: spline interpolation and sample-and-hold interpolation.

- Spline interpolation (linear, cubic): In spline interpolation, the interpolant is a piecewise polynomial. The polynomial is a line in the case of linear interpolation and a third-order polynomial in the case of cubic spline interpolation.
- Sample-and-hold interpolation: This technique is based on holding the interval value until the occurrence of the next value [28].

Figure A.1 illustrates the spline and sample-and-hold interpolation of an R-R intervals series. The sample-and-hold interpolation effectively introduces a delay equivalent to the first interval, as only after the occurrence of the second beat can one compute a first R-R interval. The spline interpolation introduces a second (beat of) delay, because, for linear interpolation, two interval values are necessary and for cubic interpolation two additional (interval) values are required.

The sample-and-hold interpolation introduces step-like discontinuities, requiring an extra low-pass filtering operation. After filtering with a band-pass filter, the cubic spline-interpolated and sample-and-hold-interpolated R-R interval series are very similar as illustrated in Figure A.2.
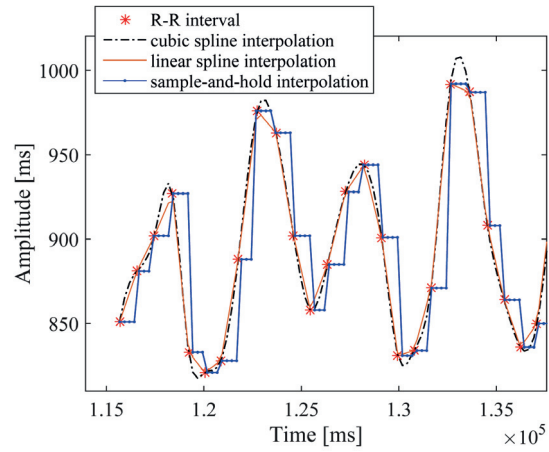
Figure A.1: Interpolation of R-R intervals.
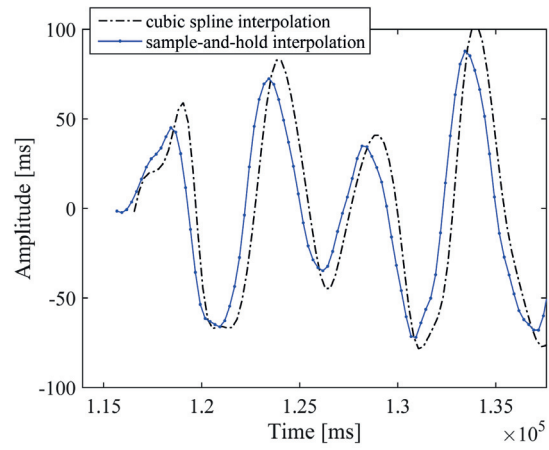
Figure A.2: Interpolation and filtering of R-R intervals.

A.2   Evaluation of a classifier

In a two-class problem, after classification of each event, given its true condition, true positives (TP), false positives (FP), true negatives (TN) and false negatives (FN) are counted. These values are then used to compute the classification performance and errors. The conventional classification measures include the true positive rate (TPR), true negative rate (TNR), accuracy (ACC), false positive rate (FPR) and false negative rate (FNR):

$$TPR = \frac{TP}{TP + FN} \tag{A.1}$$

$$TNR = \frac{TN}{TN + FP} \tag{A.2}$$

$$ACC = \frac{TP + TN}{TP + TN + FP + FN} \tag{A.3}$$

$$FPR = \frac{FP}{TN + FP} \tag{A.4}$$

$$FNR = \frac{FN}{TP + FN} \tag{A.5}$$

The TPR or sensitivity reflects the proportion of positives identified as such. The TNR or specificity similarly reflects the proportion of negatives identified as negatives. The accuracy reports the proportion of correctly identified cases. The FPR, or fall-out, indicates the proportion of negatives identified as positives, and vice-versa, the FNR or miss raten reflects the proportion of positives miss-identified as negatives.

These measures report well on the performance when the classes are rather balanced. If, on the other hand, 90% of the data belong to one class, then a high accuracy only means that the classifier identified the majority class. In an identification problem, the majority class is usually the class of the normal data. For example, in Chapter 9, the problem at hand was the identification of apnea episodes. If for one recording, apneas occurred in roughly 10% of the data, the retrieval of these events by the classifier is of interest. A high accuracy might be a consequence of a high number of TN values, meaning that in fact, normal sleep was mostly classified as such. In an identification or information retrieval problem, one might want to know that from the retrieved data, what fraction is correct. The precision reports this fraction and is defined as:

$$precision = \frac{TP}{TP + FP} \tag{A.6}$$

The counterpart of precision in an identification case is recall, which reports on the fraction of relevant instances that are actually retrieved. The F-score is a measure that reports on the identification performance. It is the harmonic mean of sensitivity (fraction of events that are retrieved) and precision (fraction of retrieved events that are correct):

$$F\text{-}score = 2\frac{precision \times sensitivity}{precision + sensitivity} \tag{A.7}$$

Characterization of the RSA and the Autonomic Balance - Further Results

B

This appendix reports further results on the characterization of the RSA and other autonomic indexes in different autonomic conditions, related to Chapter 3.

B.1   Methods - additional material
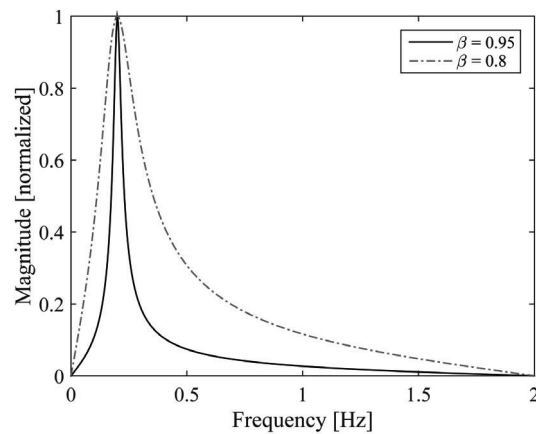
Figure B.1: The frequency response of the band-pass filter used to extract the RSA for two values of β. Smaller values of β entail a wider frequency response while larger values result in a more selective filter.

B.2   Additional results
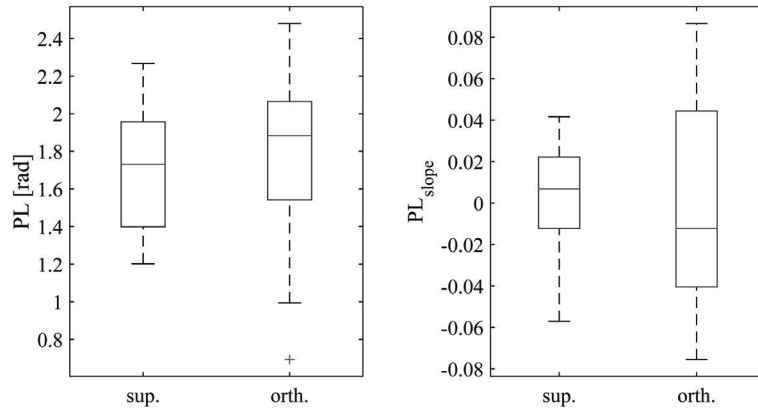
Figure B.2: PL and PL_{slope} in the supine and orthostatic positions for all 21 subjects.
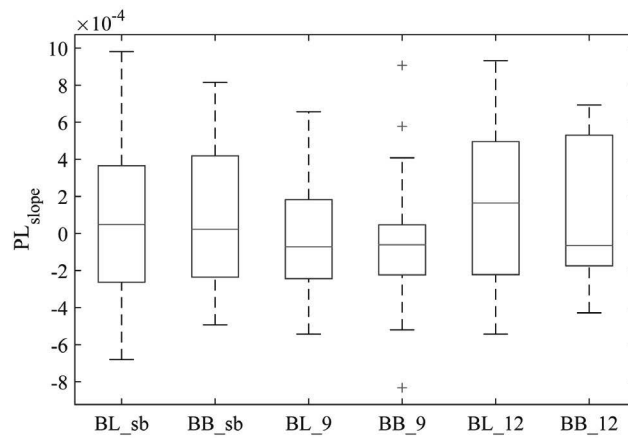
Figure B.3: PL_{slope} for the three breathing modes in the β-blocker case for all 17 subjects. BL: baseline, BB: β-blocker influence.
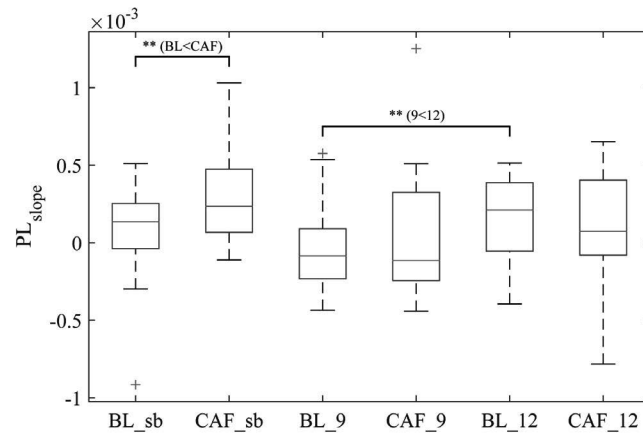
Figure B.4: PL_{slope} for the three breathing modes in the caffeine case for all 17 subjects. BL: baseline, CAF: caffeine influence. $**P < 0.05$.
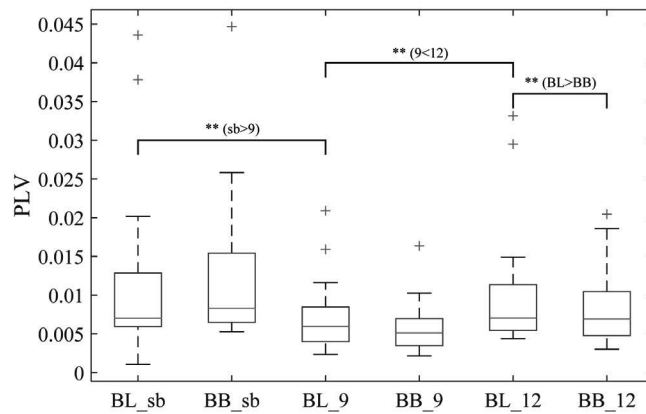
Figure B.5: PLV for the three breathing modes in the β-blocker case for all 17 subjects. BL: baseline, BB: β-blocker influence. $**P < 0.05$.
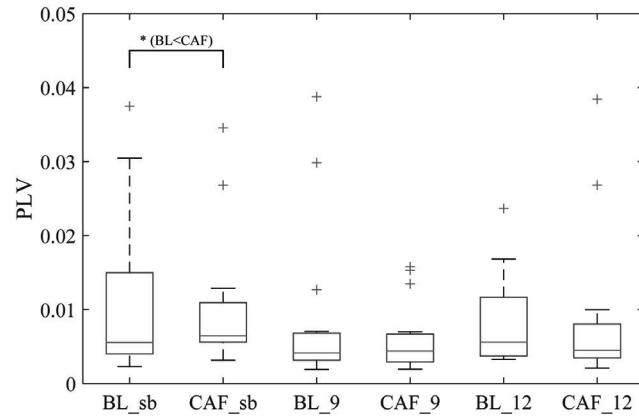
Figure B.6: PLV for the three breathing modes in the caffeine case for all 17 subjects. BL: baseline, CAF: caffeine influence. *$P < 0.1$.
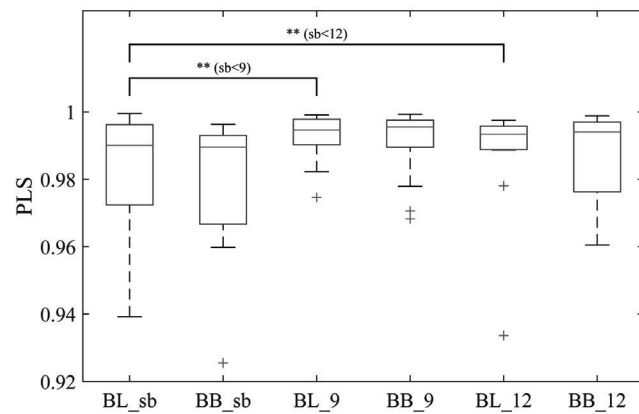
Figure B.7: PLS for the three breathing modes in the β-blocker case for all 17 subjects. BL: baseline, BB: β-blocker influence. **$P < 0.05$.
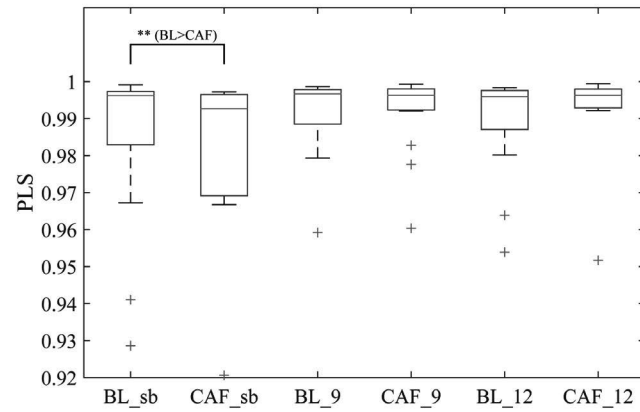
Figure B.8: PLS for the three breathing modes in the caffeine case for all 17 subjects. BL: baseline, CAF: caffeine influence. **$P < 0.05$.
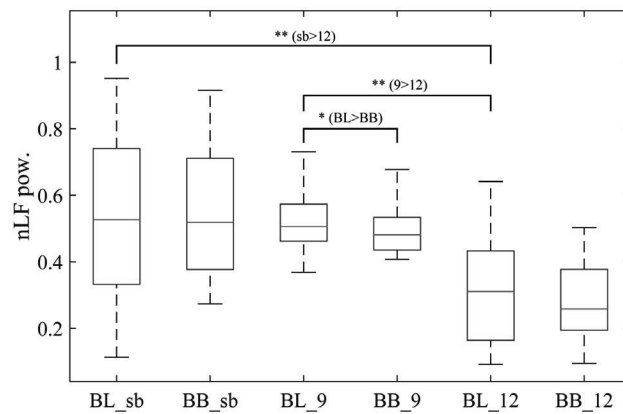
Figure B.9: nLF power for the three breathing modes in the β-blocker case for all 17 subjects. BL: baseline, BB: β-blocker influence. *$P < 0.1$; **$P < 0.05$.
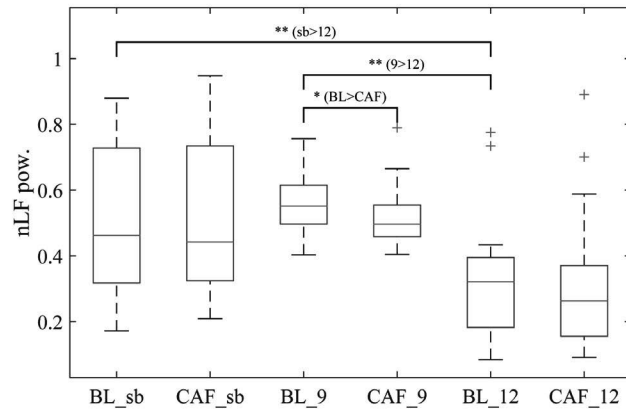
Figure B.10: nLF power for the three breathing modes in the caffeine case for all 17 subjects. BL: baseline, CAF: caffeine influence. $*P < 0.1$; $**P < 0.05$.
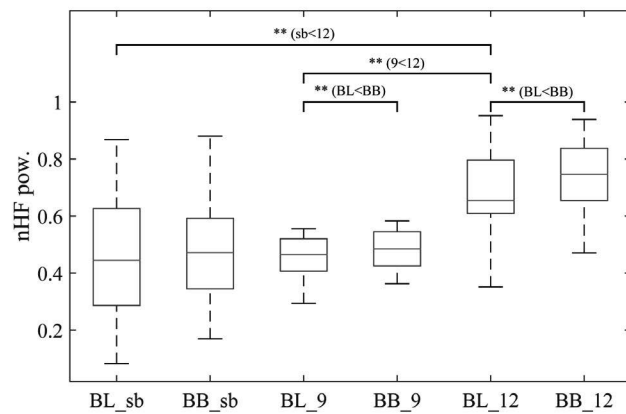
Figure B.11: nHF power for the three breathing modes in the β-blocker case for all 17 subjects. BL: baseline, BB: β-blocker influence. $**P < 0.05$.
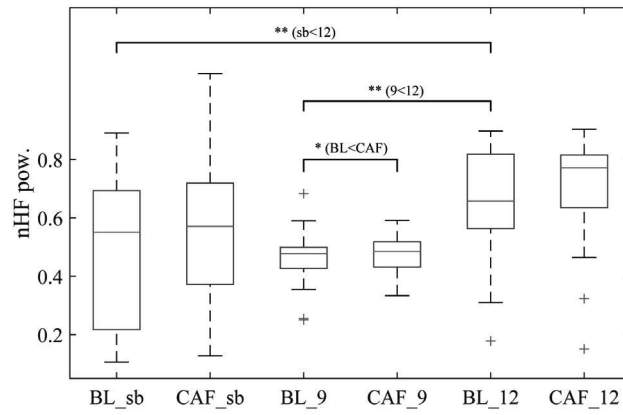
Figure B.12: nHF power for the three breathing modes in the caffeine case for all 17 subjects. BL: baseline, CAF: caffeine influence. *$P < 0.1$; **$P < 0.05$.

Characterization of the RSA upon Exposure to Altitude - Further Results

C

This appendix reports further results of the characterization of the RSA and other cardiac autonomic indexes in different autonomic conditions, related to Chapter 4.
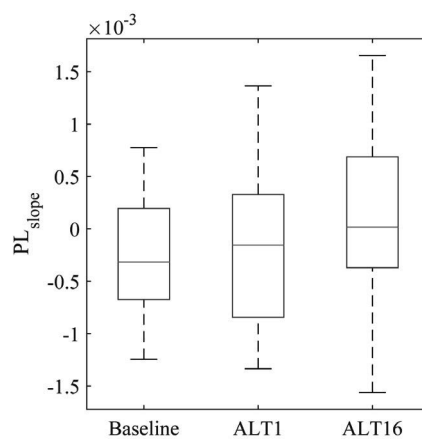
Figure C.1: The PL$_{slope}$ at baseline and after acute exposure to altitude (ALT1) and acclimatization to altitude after 16 days (ALT16).
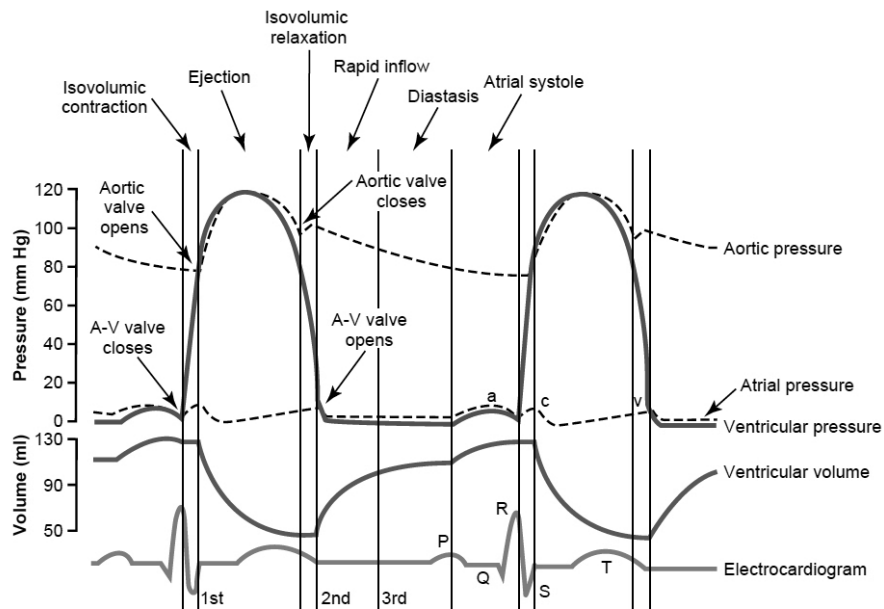
Figure C.2: The ECG and pressure recordings with the cardiac cycle. Image from [15] with permission, © Elsevier 2006.

Sleep Apnea Detection with the RSA and the Respiration - Further Results

D

This appendix reports further results on the identification of sleep apneas related to Chapter 9. Details of apnea classification with various features are reported for all recordings of the dataset, except those already presented in Chapter 9. For each recording, the best two features are reported in bold font.

Table D.1: Identification of apnea epochs with a 1-NN classifier trained with each feature alone for recording 2.

feature	specificity	sensitivity	precision	F-score
BR	0.96	0.21	0.20	0.20
Breathing amplitude	0.97	0.58	0.53	**0.55**
Amplitude index	0.96	0.25	0.27	0.26
RSA frequency	0.96	0.16	0.16	0.16
RSA power	0.96	0.17	0.19	0.18
RSA amplitude	0.97	0.33	0.36	**0.34**
PL	0.95	0.15	0.15	0.15
PL_{slope}	0.95	0.20	0.17	0.18
PLV	0.95	0.12	0.13	0.12
PLS	0.96	0.20	0.22	0.21

Table D.2: Identification of apnea epochs with a 1-NN classifier trained with each feature alone for recording 3.

feature	specificity	sensitivity	precision	F-score
BR	0.96	0.12	0.11	0.11
Breathing amplitude	0.97	0.32	0.35	**0.33**
Amplitude index	0.97	0.34	0.33	**0.33**
RSA frequency	0.96	0.12	0.11	0.11
RSA power	0.97	0.25	0.24	0.24
RSA amplitude	0.98	0.27	0.33	0.30
PL	0.97	0.17	0.19	0.17
PL_{slope}	0.97	0.24	0.23	0.23
PLV	0.97	0.15	0.16	0.16
PLS	0.97	0.33	0.29	0.30

Table D.3: Identification of apnea epochs with a 1-NN classifier trained with each feature alone for recording 4.

feature	specificity	sensitivity	precision	F-score
BR	0.94	0.23	0.25	0.24
Breathing amplitude	0.94	0.21	0.22	0.21
Amplitude index	0.96	0.45	0.49	**0.47**
RSA frequency	0.93	0.23	0.23	0.23
RSA power	0.94	0.16	0.18	0.17
RSA amplitude	0.95	0.29	0.32	0.30
PL	0.94	0.23	0.26	0.24
PL_{slope}	0.94	0.28	0.28	0.28
PLV	0.93	0.19	0.20	0.19
PLS	0.95	0.30	0.33	**0.31**

Table D.4: Identification of apnea epochs with a 1-NN classifier trained with each feature alone for recording 5.

feature	specificity	sensitivity	precision	F-score
BR	0.98	0.06	0.06	0.06
Breathing amplitude	0.99	0.04	0.05	0.04
Amplitude index	0.99	0.16	0.21	0.17
RSA frequency	0.99	0.00	Nan	0.00
RSA power	0.99	0.11	0.12	0.12
RSA amplitude	0.99	0.17	0.24	0.19
PL	0.99	0.17	0.17	0.17
PL_{slope}	0.99	0.10	0.10	0.09
PLV	0.99	0.21	0.21	**0.21**
PLS	0.99	0.21	0.34	**0.24**

Table D.5: Identification of apnea epochs with a 1-NN classifier trained with each feature alone for recording 6.

feature	specificity	sensitivity	precision	F-score
BR	0.94	0.26	0.26	0.26
Breathing amplitude	0.94	0.21	0.22	0.21
Amplitude index	0.96	0.41	0.45	**0.42**
RSA frequency	0.95	0.24	0.26	0.25
RSA power	0.94	0.24	0.25	0.24
RSA amplitude	0.95	0.33	0.34	0.33
PL	0.94	0.19	0.20	0.19
PL$_{slope}$	0.95	0.25	0.28	0.26
PLV	0.94	0.26	0.24	0.25
PLS	0.95	0.38	0.39	**0.38**

Table D.6: Identification of apnea epochs with a 1-NN classifier trained with each feature alone for recording 9.

feature	specificity	sensitivity	precision	F-score
BR	0.98	0.13	0.16	0.14
Breathing amplitude	0.97	0.19	0.21	0.19
Amplitude index	0.98	0.35	0.35	**0.35**
RSA frequency	0.97	0.11	0.12	0.11
RSA power	0.98	0.17	0.19	0.18
RSA amplitude	0.98	0.25	0.28	**0.26**
PL	0.97	0.17	0.17	0.17
PL$_{slope}$	0.98	0.12	0.14	0.13
PLV	0.97	0.14	0.14	0.14
PLS	0.98	0.24	0.24	0.24

Table D.7: Identification of apnea epochs with a 1-NN classifier trained with each feature alone for recording 11.

feature	specificity	sensitivity	precision	F-score
BR	0.95	0.26	0.26	0.26
Breathing amplitude	0.95	0.29	0.30	0.30
Amplitude index	0.96	0.44	0.43	**0.43**
RSA frequency	0.95	0.29	0.28	0.29
RSA power	0.96	0.16	0.21	0.18
RSA amplitude	0.95	0.24	0.28	0.25
PL	0.95	0.28	0.29	0.28
PL$_{slope}$	0.95	0.23	0.24	0.23
PLV	0.95	0.26	0.27	0.26
PLS	0.96	0.39	0.40	**0.39**

Table D.8: Identification of apnea epochs with a 1-NN classifier trained with each feature alone for recording 12.

feature	specificity	sensitivity	precision	F-score
BR	0.94	0.20	0.21	0.20
Breathing amplitude	0.93	0.11	0.13	0.12
Amplitude index	0.96	0.47	0.52	**0.49**
RSA frequency	0.94	0.19	0.21	0.20
RSA power	0.95	0.19	0.23	0.21
RSA amplitude	0.95	0.24	0.28	0.26
PL	0.94	0.22	0.23	0.22
PL_{slope}	0.95	0.18	0.23	0.20
PLV	0.94	0.19	0.20	0.19
PLS	0.95	0.31	0.32	**0.31**

Table D.9: Identification of apnea epochs with a 1-NN classifier trained with each feature alone for recording 14.

feature	specificity	sensitivity	precision	F-score
BR	0.99	0.10	0.15	0.11
Breathing amplitude	0.99	0.14	0.19	0.16
Amplitude index	0.99	0.52	0.48	**0.49**
RSA frequency	0.99	0.12	0.18	0.14
RSA power	0.99	0.13	0.17	0.15
RSA amplitude	0.99	0.24	0.29	**0.26**
PL	0.99	0.11	0.12	0.11
PL_{slope}	0.99	0.13	0.16	0.14
PLV	0.98	0.08	0.08	0.08
PLS	0.99	0.14	0.16	0.15

Bibliography

[1] Task force of the European Society of Cardiology and the North American Society of Pacing and Electrophysiology, "Heart rate variability standards of measurement, physiological interpretation, and clinical use," *Eur. Heart J.*, vol. 17, pp. 354–381, Mar. 1996.

[2] G. E. Billman, "The LF/HF ratio does not accurately measure cardiac sympatho-vagal balance," *Front. Physiol.*, vol. 4, p. 26, Feb 2013.

[3] L. Sidorenko, J. F. Kraemer, and N. Wessel, "Standard heart rate variability spectral analysis: does it purely assess cardiac autonomic function?" *Europace*, vol. 18, no. 7, pp. 1085–1085, Jul. 2016.

[4] A. C. Guyton and J. E. Hall, *Textbook of Medical Physiology*, 7th ed. Elsevier, 2006, ch. 10: Rhythmical Excitation of the Heart.

[5] J. A. Hirsch and B. Bishop, "Respiratory sinus arrhythmia in humans: how breathing pattern modulates heart rate," *Am. J. Physiol. Heart. Circ. Physiol.*, vol. 241, no. 4, pp. 620–629, Oct. 1981.

[6] P. Grossman and E. W. Taylor, "Toward understanding respiratory sinus arrhythmia: Relations to cardiac vagal tone, evolution and biobehavioral functions," *Biol. Psychol.*, vol. 74, no. 2, pp. 263–285, Feb. 2007.

[7] G. G. Berntson, J. T. Bigger, D. L. Eckberg, P. Grossman, P. G. Kaufmann, M. Malik, H. N. Nagaraja, S. W. Porges, J. P. Saul, P. H. Stone, and M. W. van der Molen, "Heart rate variability: origins, methods, and interpretive caveats," *Psychophysiology*, vol. 34, no. 6, pp. 623–648, Nov. 1997.

[8] H. Mamaghanian, N. Khaled, D. Atienza, and P. Vandergheynst, "Compressed sensing for real-time energy-efficient ECG compression on wireless body sensor nodes," *IEEE Trans. Biomed. Eng.*, vol. 58, no. 9, pp. 2456–2466, Sep. 2011.

[9] A. Y. Dogan, J. Constantin, M. Ruggiero, A. Burg, and D. Atienza, "Multi-core architecture design for ultra-low-power wearable health monitoring systems," in *Proceedings of the Conference on Design, Automation and Test in Europe*, 2012, pp. 988–993.

[10] O. Schleusing, P. Renevey, M. Bertschi, S. Dasen, and R. Paradiso, "Detection of mood changes in bipolar patients though monitoring of physiological and behavioral signals," in *European Conference of the International Federation for Medical and Biological Engineering*, 2011, pp. 1106–1109.

[11] D. S. Lee, T. W. Chong, and B. G. Lee, "Stress events detection of driver by wearable glove system," *IEEE Sensors J.*, vol. 17, no. 1, pp. 194–204, Jan 2017.

[12] C. Ifrim, A.-M. Pintilie, E. Apostol, C. Dobre, and F. Pop, *The Art of Advanced Healthcare Applications in Big Data and IoT Systems*.   Springer International Publishing, 2017, pp. 133–149.

[13] R. M. Buijs, "The autonomic nervous system," in *Handbook of Clinical Neurology*.   Elsevier, 2013, vol. 117, pp. 1–11.

[14] J. M. Karemaker, "How the vagus nerve produces beat-to-beat heart rate variability; experiments in rabbits to mimic in vivo vagal patterns," *J. Clin. Transl. Res.*, vol. 1, no. 3, pp. 190–204, Dec 2015.

[15] A. C. Guyton and J. E. Hall, *Textbook of Medical Physiology*, 7th ed.   Elsevier, 2006, ch. 9: Heart Muscle; The Heart as a Pump and Function of the Heart Valves.

[16] J. Hayano, F. Yasuma, A. Okada, S. Mukai, and T. Fujinami, "Respiratory sinus arrhythmia," *Circulation*, vol. 94, no. 4, pp. 842–847, Aug. 1996.

[17] F. Yasuma and J.-i. Hayano, "Respiratory sinus arrhythmia*: Why does the heartbeat synchronize with respiratory rhythm?" *Chest*, vol. 125, no. 2, pp. 683–690, Feb. 2004.

[18] A. J. Garcia III, J. E. Koschnitzky, T. Dashevskiy, and J.-M. Ramirez, "Cardiorespiratory coupling in health and disease," *Auton. Neurosci.*, vol. 175, no. 1, pp. 26–37, Apr. 2013.

[19] A. Ben-Tal, S. S. Shamailov, and J. F. R. Paton, "Central regulation of heart rate and the appearance of respiratory sinus arrhythmia: New insights from mathematical modeling," *Math. Biosci.*, vol. 255, pp. 71–82, Sep. 2014.

[20] J. M. Karemaker, "Counterpoint: Respiratory sinus arrhythmia is due to the baroreflex mechanism," *J. Appl. Physiol.*, vol. 106, no. 5, pp. 1742–1743, May 2009.

[21] D. L. Eckberg, "Point:Counterpoint: Respiratory sinus arrhythmia is due to a central mechanism vs. respiratory sinus arrhythmia is due to the baroreflex mechanism," *J. Appl. Physiol.*, vol. 106, no. 5, pp. 1740–1742, May 2009.

[22] C. O. Tan and J. A. Taylor, "Does respiratory sinus arrhythmia serve a buffering role for diastolic pressure fluctuations?" *Am. J. Physiol. Heart. Circ. Physiol.*, vol. 298, no. 5, pp. H1492–H1498, May 2010.

[23] P. T. Clemson, J. B. Hoag, A. Stefanovska, and D. L. Eckberg, "Action of the sympathetic and parasympathetic nervous system on cardiovascular dynamics revealed by blocking drugs," in *8th Conference of the European Study Group on Cardiovascular Oscillations (ESGCO)*, May 2014, pp. 197–198.

[24] M. Elstad, L. Walløe, N. L. A. Holme, E. Maes, and M. Thoresen, "Respiratory sinus arrhythmia stabilizes mean arterial blood pressure at high-frequency interval in healthy humans," *Eur. J. Appl. Physiol.*, vol. 115, no. 3, pp. 521–530, Nov. 2014.

[25] M. J. a. Parkes, "Comments on point:counterpoint: Respiratory sinus arrhythmia is due to a central mechanism vs. respiratory sinus arrhythmia is due to the baroreflex mechanism," *J. Appl. Physiol.*, vol. 106, no. 5, pp. 1745–1749, May 2009.

[26] J. M. Karemaker, "Last word on point:counterpoint: Respiratory sinus arrhythmia is due to a central mechanism vs. respiratory sinus arrhythmia is due to the baroreflex mechanism," *J. Appl. Physiol.*, vol. 106, no. 5, pp. 1750–1750, May 2009.

[27] A. T. Reisner, G. D. Clifford, and R. G. Mark, *Advanced methods and tools for ECG data analysis*. Artech House, 2007, ch. 1: The physiological basis of the electrocardiogram, pp. 1–25.

[28] R. Bailón, L. Sornmö, and P. Laguna, *Advanced Methods and Tools for ECG Data Analysis*, 1st ed. Norwood, MA, USA: Artech House, 2006, ch. 8: ECG- Derived Respiratory Frequency Estimation.

[29] T. W. Frazier, M. E. Strauss, and S. R. Steinhauer, "Respiratory sinus arrhythmia as an index of emotional response in young adults," *Psychophysiology*, vol. 41, no. 1, pp. 75–83, Jan. 2004.

[30] J. Pu, B. J. Schmeichel, and H. A. Demaree, "Cardiac vagal control predicts spontaneous regulation of negative emotional expression and subsequent cognitive performance," *Biol. Psychol.*, vol. 84, no. 3, pp. 531 – 540, Jul. 2010.

[31] J. Zhang, X. Yu, and D. Xie, "Effects of mental tasks on the cardiorespiratory synchronization," *Respir. Physiol. Neurobiol.*, vol. 170, no. 1, pp. 91–95, Jan. 2010.

[32] G. F. Lewis, S. A. Furman, M. F. McCool, and S. W. Porges, "Statistical strategies to quantify respiratory sinus arrhythmia: Are commonly used metrics equivalent?" *Biol. Psychol.*, vol. 89, no. 2, pp. 349 – 364, Feb. 2012.

[33] K. A. Sauder, E. R. Johnston, A. C. Skulas-Ray, T. S. Campbell, and S. G. West, "Effect of meal content on heart rate variability and cardiovascular reactivity to mental stress," *Psychophysiology*, vol. 49, no. 4, pp. 470–477, Apr. 2012.

[34] K. Niizeki and T. Saitoh, "Incoherent oscillations of respiratory sinus arrhythmia during acute mental stress in humans," *Am. J. Physiol. Heart. Circ. Physiol.*, vol. 302, no. 1, pp. H359–H367, Jan. 2012.

[35] L. Staton, J. B. Hinnant, J. Buckhalt, and M. El-Sheikh, "Sleep and cognitive performance: The role of income and respiratory sinus arrhythmia reactivity," *Dev. Psychobiol.*, vol. 56, no. 7, pp. 1528–1540, Nov. 2014.

[36] E. Neuhaus, R. Bernier, and T. P. Beauchaine, "Brief report: Social skills, internalizing and externalizing symptoms, and respiratory sinus arrhythmia in autism," *J. Autism Dev. Disord.*, vol. 44, no. 3, pp. 730–737, Mar. 2014.

[37] T. P. Beauchaine, "Respiratory sinus arrhythmia: A transdiagnostic biomarker of emotion dysregulation and psychopathology," *Curr. Opin. Psychol.*, vol. 3, pp. 43–47, Jun. 2015.

[38] S. Schulz, K.-J. Bär, and A. Voss, "Analyses of heart rate, respiration and cardiorespiratory coupling in patients with schizophrenia," *Entropy*, vol. 17, no. 2, pp. 483–501, Jan. 2015.

[39] J. A. Barraza, V. Alexander, L. E. Beavin, E. T. Terris, and P. J. Zak, "The heart of the story: Peripheral physiology during narrative exposure predicts charitable giving," *Biol. Psychol.*, vol. 105, pp. 138–143, Feb. 2015.

[40] J. LeMoult, K. L. Yoon, and J. Joormann, "Rumination and cognitive distraction in major depressive disorder: an examination of respiratory sinus arrhythmia," *J. Psychopathol. Behav. Assess.*, vol. 38, no. 1, pp. 20–29, Aug. 2015.

[41] M. El-Sheikh, J. B. Hinnant, and S. A. Erath, "Marital conflict, vagal regulation, and children's sleep: A longitudinal investigation," *Monogr. Soc. Res. Child Dev.*, vol. 80, no. 1, pp. 89–106, Mar. 2015.

[42] K. M. Gates, L. M. Gatzke-Kopp, M. Sandsten, and A. Y. Blandon, "Estimating time-varying RSA to examine psychophysiological linkage of marital dyads," *Psychophysiology*, vol. 52, no. 8, pp. 1059–1065, Aug. 2015.

[43] C. Arab, D. P. M. Dias, R. T. de Almeida Barbosa, T. D. de Carvalho, V. E. Valenti, T. B. Crocetta, M. Ferreira, L. C. de Abreu, and C. Ferreira, "Heart rate variability measure in breast cancer patients and survivors: A systematic review," *Psychoneuroendocrinology*, vol. 68, pp. 57 – 68, Jun. 2016.

[44] T. Skodzik, T. Zettler, M. Topper, J. Blechert, and T. Ehring, "The effect of verbal and imagery-based worry versus distraction on the emotional response to a stressful in-vivo situation," *J. Behav. Ther. Exp. Psychiatry*, vol. 52, pp. 51 – 58, Sep. 2016.

[45] L. Vazquez, J. D. Blood, J. Wu, T. M. Chaplin, R. E. Hommer, H. J. Rutherford, M. N. Potenza, L. C. Mayes, and M. J. Crowley, "High frequency heart-rate variability predicts adolescent depressive symptoms, particularly anhedonia, across one year," *J. Affect. Disord.*, vol. 196, pp. 243 – 247, May 2016.

[46] J. Koenig, A. H. Kemp, T. P. Beauchaine, J. F. Thayer, and M. Kaess, "Depression and resting state heart rate variability in children and adolescents - a systematic review and meta-analysis," *Clin. Psychol. Rev.*, vol. 46, pp. 136 – 150, Jun. 2016.

[47] D. Sinnecker, M. Dommasch, A. Steger, A. Berkefeld, P. Hoppmann, A. Müller, J. Gebhardt, P. Barthel, K. Hnatkova, K. M. Huster, K.-L. Laugwitz, M. Malik, and G. Schmidt, "Expiration-triggered sinus arrhythmia predicts outcome in survivors of acute myocardial infarction," *J. Am. Coll. Cardiol.*, vol. 67, no. 19, pp. 2213 – 2220, May 2016.

[48] D.-L. Hsieh and T.-C. Hsiao, "Respiratory sinus arrhythmia reactivity of internet addiction abusers in negative and positive emotional states using film clips stimulation," *Biomed. Eng. Online*, vol. 15, no. 1, pp. 1–18, Jul. 2016.

[49] B. Bornemann, B. E. Kok, A. Böckler, and T. Singer, "Helping from the heart: Voluntary upregulation of heart rate variability predicts altruistic behavior," *Biol. Psychol.*, vol. 119, pp. 54–63, Sep. 2016.

[50] K. Niizeki and T. Saitoh, "Analysis of cardiorespiratory phase coupling and cardiovascular autonomic responses during food ingestion," *Physiol. Behav.*, vol. 159, pp. 1–13, May 2016.

[51] A. J. Ellis, J. Shumake, and C. G. Beevers, "The effects of respiratory sinus arrhythmia on anger reactivity and persistence in major depression," *Psychophysiology*, vol. 53, no. 10, pp. 1587–1599, Oct. 2016.

[52] C. K. Fortunato, L. M. Gatzke-Kopp, and N. Ram, "Associations between respiratory sinus arrhythmia reactivity and internalizing and externalizing symptoms are emotion specific," *Cogn. Affect. Behav. Neurosci.*, vol. 13, no. 2, pp. 238–251, Dec. 2012.

[53] S. W. Porges, M. Macellaio, S. D. Stanfill, K. McCue, G. F. Lewis, E. R. Harden, M. Handelman, J. Denver, O. V. Bazhenova, and K. J. Heilman, "Respiratory sinus arrhythmia and auditory processing in autism: Modifiable deficits of an integrated social engagement system?" *Int. J. Psychophysiol.*, vol. 88, no. 3, pp. 261–270, Jun. 2013.

[54] E. Conradt, D. Degarmo, P. Fisher, B. Abar, B. M. Lester, L. L. Lagasse, S. Shankaran, H. Bada, C. R. Bauer, T. M. Whitaker, and J. A. Hammond, "The contributions of early adverse experiences and trajectories of respiratory sinus arrhythmia on the development

of neurobehavioral disinhibition among children with prenatal substance exposure," *Dev. Psychopathol.*, vol. 26, pp. 901–916, Nov. 2014.

[55] R. P. Bartsch, K. K. Liu, Q. D. Ma, and P. C. Ivanov, "Three independent forms of cardio-respiratory coupling: transitions across sleep stages," in *Computing in Cardiology (CinC)*, Sep. 2014, pp. 781–784.

[56] J. P. Mortola, D. Marghescu, and R. Siegrist-Johnstone, "Thinking about breathing: Effects on respiratory sinus arrhythmia," *Respir. Physiol. Neurobiol.*, vol. 223, pp. 28–36, Mar. 2016.

[57] M. J. Sulik, N. Eisenberg, T. L. Spinrad, and K. M. Silva, "Associations between respiratory sinus arrhythmia (RSA) reactivity and effortful control in preschool-age children," *Dev. Psychobiol.*, vol. 57, no. 5, pp. 596–606, Jul. 2015.

[58] M. M. H. E. van den Berg, J. Maas, R. Muller, A. Braun, W. Kaandorp, R. van Lien, M. N. M. van Poppel, W. van Mechelen, and A. E. van den Berg, "Autonomic nervous system responses to viewing green and built settings: Differentiating between sympathetic and parasympathetic activity," *Int. J. Environ. Res. Publ. Health.*, vol. 12, no. 12, pp. 15 860–15 874, Dec. 2015.

[59] A. J. Fisher, J. W. Reeves, and C. Chi, "Dynamic RSA: Examining parasympathetic regulatory dynamics via vector-autoregressive modeling of time-varying rsa and heart period," *Psychophysiology*, vol. 53, no. 7, pp. 1093–1099, Jul. 2016.

[60] C. P. Fagundes, L. M. Jaremka, W. B. Malarkey, and J. K. Kiecolt-Glaser, "Attachment style and respiratory sinus arrhythmia predict post-treatment quality of life in breast cancer survivors," *Psycho-Oncology*, vol. 23, no. 7, pp. 820–826, Jul. 2014.

[61] S. Tiinanen, A. Kiviniemi, M. Tulppo, and T. Seppänen, "RSA component extraction from cardiovascular signals by combining adaptive filtering and PCA derived respiration," in *Computing in Cardiology (CinC)*, Sep. 2010, pp. 73–76.

[62] D. Widjaja, E. Vlemincx, and S. Van Huffel, "Multiscale principal component analysis to separate respiratory influences from the tachogram: Application to stress monitoring," in *Computing in Cardiology (CinC)*, Sep. 2012, pp. 277–280.

[63] O. M, C. A. Swenne, L. R. Davrath, and S. Akselrod, "Phase-averaged characterization of respiratory sinus arrhythmia pattern," *Am. J. Physiol. Heart. Circ. Physiol.*, vol. 288, no. 2, pp. 504–510, Feb. 2005.

[64] R. Trobec and V. Avbelj, "A method for time-domain analysis of respiratory sinus arrhythmia," in *37th International Convention on Information and Communication Technology, Electronics and Microelectronics (MIPRO)*, May 2014, pp. 204–207.

[65] D. Sinnecker, P. Barthel, A. Müller, K.-L. Laugwitz, and G. Schmidt, "Abstract 17230: Respiratory sinus arrhythmia quantified from standard ECG for risk stratification of post-infarction patients," *Circulation*, vol. 130, no. Suppl 2, pp. A17 230–A17 230, Nov. 2014.

[66] J. Choi and R. Gutierrez-Osuna, "Removal of respiratory influences from heart rate variability in stress monitoring," *IEEE Sensors J.*, vol. 11, no. 11, pp. 2649–2656, Nov. 2011.

[67] D. Widjaja, E. Vlemincx, and S. V. Huffel, "Stress classification by separation of respiratory modulations in heart rate variability using orthogonal subspace projection," in *35th Annual International Conference of the IEEE Engineering in Medicine and Biology Society (EMBC)*, Jul. 2013, pp. 6123–6126.

[68] D. Widjaja, A. Caicedo, E. Vlemincx, I. Van Diest, and S. Van Huffel, "Separation of respiratory influences from the tachogram: A methodological evaluation," *PLoS One*, vol. 9, no. 7, pp. 1–11, Jul. 2014.

[69] P. Ataee, L. Belingard, G. A. Dumont, H. A. Noubari, and W. T. Boyce, "Autonomic-cardiorespiratory regulation: A physiology-based mathematical model," in *Annual International Conference of the IEEE Engineering in Medicine and Biology Society (EMBC)*, Aug. 2012, pp. 3805–3808.

[70] G. Lenis, M. Kircher, J. Lázaro, R. Bailón, E. Gil, and O. Doessel, "Separating the effect of respiration on the heart rate variability using Granger's causality and linear filtering," *Biomed. Signal Process. Control*, vol. 31, pp. 272 – 287, Jan. 2017.

[71] A. H. Khandoker, C. Karmakar, M. Brennan, A. Voss, and M. Palaniswami, *Poincaré Plot in Capturing Nonlinear Temporal Dynamics of HRV*.   Boston, MA: Springer US, 2013, pp. 47–68.

[72] L. Cnockaert, P. F. Migeotte, L. Daubigny, G. K. Prisk, F. Grenez, and R. C. Sá, "A method for the analysis of respiratory sinus arrhythmia using continuous wavelet transforms," *IEEE Trans. Biomed. Eng.*, vol. 55, no. 5, pp. 1640–1642, May 2008.

[73] R.-C. Peng, W.-R. Yan, X.-L. Zhou, N.-L. Zhang, W.-H. Lin, and Y.-T. Zhang, "Time-frequency analysis of heart rate variability during the cold pressor test using a time-varying autoregressive model," *Physiol. Meas.*, vol. 36, no. 3, p. 441, Feb. 2015.

[74] A. Porta, A. Marchi, V. Bari, K. Heusser, J. Tank, J. Jordan, F. Barbic, and R. Furlan, "Conditional symbolic analysis detects nonlinear influences of respiration on cardiovascular control in humans," *Phil. Trans. R. Soc. A*, vol. 373, no. 2034, p. 96, Feb. 2015.

[75] S. N. Sani and E. F. Bailey, "Using respiratory sinus arrhythmia to detect obstructive sleep apnea," *Health and Technology*, pp. 1–6, 2017.

[76] E. Gil, M. Orini, R. Bailón, J. M. Vergara, L. Mainardi, and P. Laguna, "Photoplethysmography pulse rate variability as a surrogate measurement of heart rate variability during non-stationary conditions," *Physiol. Meas.*, vol. 31, no. 9, p. 1271, 2010.

[77] J. Làzaro, E. Gil, J. M. Vergara, and P. Laguna, "Pulse rate variability analysis for discrimination of sleep-apnea-related decreases in the amplitude fluctuations of pulse photoplethysmographic signal in children," *IEEE J. Biomed. Health. Inform.*, vol. 18, no. 1, pp. 240–246, Jan 2014.

[78] R. Logier, J. D. jonckheere, A. Dassonneville, and M. Jeanne, "Comparison of pulse rate variability and heart rate variability for high frequency content estimation," in *38th Annual International Conference of the IEEE Engineering in Medicine and Biology Society (EMBC)*, Aug. 2016, pp. 936–939.

[79] E. B. Blackford, A. M. Piasecki, and J. R. Estepp, "Measuring pulse rate variability using long-range, non-contact imaging photoplethysmography," in *38th Annual International Conference of the IEEE Engineering in Medicine and Biology Society (EMBC)*, Aug 2016, pp. 3930–3936.

[80] W. Massagram, V. M. Lubecke, A. H. st Madsen, and O. Boric-Lubecke, "Assessment of heart rate variability and respiratory sinus arrhythmia via Doppler radar," *IEEE Trans. Microwave Theory Tech.*, vol. 57, no. 10, pp. 2542–2549, Oct 2009.

[81] E. Yavari, A. Rahman, J. Xu, D. P. Mandic, and O. Boric-Lubecke, "Synchrosqueezing an effective method for analyzing doppler radar physiological signals," in *38th Annual International Conference of the IEEE Engineering in Medicine and Biology Society (EMBC)*, Aug 2016, pp. 263–266.

[82] R. E. Kleiger, P. K. Stein, and J. T. Bigger, "Heart rate variability: Measurement and clinical utility," *Ann. Noninvasive Electrocardiol.*, vol. 10, no. 1, pp. 88–101, Jan. 2005.

[83] S. W. Porges, "The polyvagal perspective," *Biol. Psychol.*, vol. 74, no. 2, pp. 116 – 143, 2007.

[84] S. Reland, N. S. Ville, S. Wong, G. Carrault, and F. Carré, "Reliability of heart rate variability in healthy older women at rest and during orthostatic testing," *Aging Clin. Exp. Res.*, vol. 17, no. 4, pp. 316–321, Aug. 2005.

[85] L. T. Mainardi, "On the quantification of heart rate variability spectral parameters using time–frequency and time-varying methods," *Phil. Trans. R. Soc. A*, vol. 367, no. 1887, pp. 255–275, Jan. 2009.

[86] L. Mourot, "Could non-linear heart rate variability analysis of short RR intervals series give clinically valuable information in heart disease?" *J. Clin. Exp. Res. Cardiol.*, vol. 1, no. 1, p. 1, Sep. 2014.

[87] S. Silvilairat, P. Charoenkwan, S. Saekho, A. Tantiworawit, A. Phrommintikul, S. Srichairatanakool, and N. Chattipakorn, "Heart rate variability for early detection of cardiac iron deposition in patients with transfusion-dependent thalassemia," *PLoS One*, vol. 11, no. 10, p. e0164300, Oct. 2016.

[88] S. Yoshida, H. Tanaka, R. Nakao, N. Okamoto, M. Kajiura, Y. Kanbara, S. Azuma, and H. Tamai, "Variant cardiovascular regulation in children with postural tachycardia syndrome," *Pediatr. Int.*, vol. 56, no. 3, pp. 328–335, Jun. 2014.

[89] T. M. Cooper, P. S. McKinley, T. E. Seeman, T.-H. Choo, S. Lee, and R. P. Sloan, "Heart rate variability predicts levels of inflammatory markers: Evidence for the vagal anti-inflammatory pathway," *Brain Behav. Immun.*, vol. 49, pp. 94–100, Oct. 2015.

[90] D. S. Quintana, M. Elstad, T. Kaufmann, C. L. Brandt, B. Haatveit, M. Haram, M. Nerhus, L. T. Westlye, and O. A. Andreassen, "Resting-state high-frequency heart rate variability is related to respiratory frequency in individuals with severe mental illness but not healthy controls," *Scientific Reports*, vol. 6, p. 37212, Nov. 2016.

[91] E. Ramírez, A. R. Ortega, and G. A. Reyes Del Paso, "Anxiety, attention, and decision making: The moderating role of heart rate variability," *Int. J. Psychophysiol.*, vol. 98, no. 3, Part 1, pp. 490–496, Dec. 2015.

[92] E.-H. Kim, J.-H. Park, S. M. Lee, M.-S. Gwak, G.-S. Kim, and M.-H. Kim, "Preoperative depressed mood and perioperative heart rate variability in patients with hepatic cancer," *J. Clin. Anesth.*, vol. 35, pp. 332–338, Dec. 2016.

[93] J. M. Pyne, J. I. Constans, M. D. Wiederhold, D. P. Gibson, T. Kimbrell, T. L. Kramer, J. A. Pitcock, X. Han, D. K. Williams, D. Chartrand, R. N. Gevirtz, J. Spira, B. K. Wiederhold, R. McCraty, and T. R. McCune, "Heart rate variability: Pre-deployment predictor of post-deployment PTSD symptoms," *Biol. Psychol.*, vol. 121, Part A, pp. 91–98, Dec. 2016.

[94] M. J. Peltola, T. Mäkelä, E. J. Paavonen, E. Vierikko, O. Saarenpää-Heikkilä, T. Paunio, J. K. Hietanen, and A. Kylliäinen, "Respiratory sinus arrhythmia moderates the impact of maternal prenatal anxiety on infant negative affectivity," *Dev. Psychobiol.*, pp. n/a–n/a, Oct. 2016.

[95] N. Gueron-Sela, C. B. Propper, N. J. Wagner, M. Camerota, K. P. Tully, and G. A. Moore, "Infant respiratory sinus arrhythmia and maternal depressive symptoms predict toddler sleep problems," *Dev. Psychobiol.*, pp. n/a–n/a, Oct. 2016.

[96] K. W. Murdock and C. P. Fagundes, "Attachment orientations, respiratory sinus arrhythmia, and stress are important for understanding the link between childhood socioeconomic status and adult self-reported health," *Ann. Behav. Med.*, pp. 1–10, Sep. 2016.

[97] M. Ardizzi, M. A. Umiltà, V. Evangelista, A. D. Liscia, R. Ravera, and V. Gallese, "Less empathic and more reactive: The different impact of childhood maltreatment on facial mimicry and Vagal regulation," *PLoS One*, vol. 11, no. 9, pp. 1–15, Sep. 2016.

[98] P. Graziano and K. Derefinko, "Cardiac vagal control and children's adaptive functioning: A meta-analysis," *Biol. Psychol.*, vol. 94, no. 1, pp. 22 – 37, Sep. 2013.

[99] W. Lu and Z. Wang, "Physiological adaptation to recurrent social stress of extraversion," *Psychophysiology*, pp. n/a–n/a, Oct. 2016.

[100] M. El-Sheikh, D. D. Arsiwalla, J. B. Hinnant, and S. A. Erath, "Children's internalizing symptoms: The role of interactions between cortisol and respiratory sinus arrhythmia," *Physiol. Behav.*, vol. 103, no. 2, pp. 225–232, May 2011.

[101] C. D. Aults, P. J. Cooper, R. E. Pauletti, N. A. Jones, and D. G. Perry, "Child sex and respiratory sinus arrhythmia reactivity as moderators of the relation between internalizing symptoms and aggression," *Appl. Psychophysiol. Biofeedback*, vol. 40, no. 4, pp. 269–276, Jul. 2015.

[102] M. J. Sulik, N. Eisenberg, K. M. Silva, T. L. Spinrad, and A. Kupfer, "Respiratory sinus arrhythmia, shyness, and effortful control in preschool-age children," *Biol. Psychol.*, vol. 92, no. 2, pp. 241 – 248, Feb. 2013.

[103] M. Orini, R. Bailón, R. Enk, S. Koelsch, L. Mainardi, and P. Laguna, "A method for continuously assessing the autonomic response to music-induced emotions through HRV analysis," *Med. Biol. Eng. Comput.*, vol. 48, no. 5, pp. 423–433, May 2010.

[104] J. E. Stellar, A. Cohen, C. Oveis, and D. Keltner, "Affective and physiological responses to the suffering of others: Compassion and vagal activity," *J. Pers. Soc. Psychol.*, vol. 108, no. 4, pp. 572–585, Apr. 2015.

[105] C. P. Fagundes, L. M. Diamond, and K. P. Allen, "Adolescent attachment insecurity and parasympathetic functioning predict future loss adjustment," *Pers. Soc. Psychol. Bull.*, vol. 38, no. 6, pp. 821–832, Jun. 2012.

[106] R. H. Gramzow, G. Willard, and W. B. Mendes, "Big tales and cool heads: Academic exaggeration is related to cardiac vagal reactivity," *Emotion*, vol. 8, no. 1, pp. 138–144, Feb. 2008.

[107] T. J. Overbeek, A. van Boxtel, and J. H. Westerink, "Respiratory sinus arrhythmia responses to induced emotional states: Effects of RSA indices, emotion induction method, age, and sex," *Biol. Psychol.*, vol. 91, no. 1, pp. 128 – 141, Sep. 2012.

[108] S. Messerotti Benvenuti, R. Mennella, G. Buodo, and D. Palomba, "Dysphoria is associated with reduced cardiac vagal withdrawal during the imagery of pleasant scripts: Evidence for the positive attenuation hypothesis," *Biol. Psychol.*, vol. 106, pp. 28–38, Mar. 2015.

[109] Z. E. Taylor, N. Eisenberg, and T. L. Spinrad, "Respiratory sinus arrhythmia, effortful control, and parenting as predictors of children's sympathy across early childhood," *Dev. Psychol.*, vol. 51, no. 1, pp. 17–25, Jan. 2015.

[110] S. L. Mann, E. A. Selby, M. E. Bates, and R. J. Contrada, "Integrating affective and cognitive correlates of heart rate variability: A structural equation modeling approach," *Int. J. Psychophysiol.*, vol. 98, no. 1, pp. 76–86, Oct. 2015.

[111] A. Gračanin, I. Kardum, and J. Hudek-Kneˇvević, "Parasympathetic concomitants of habitual, spontaneous, and instructed emotional suppression," *J. Psychophysiol.*, vol. 0, no. 0, pp. 1–12, Sep. 2016.

[112] R. P. Bartsch, A. Y. Schumann, J. W. Kantelhardt, T. Penzel, and P. C. Ivanov, "Phase transitions in physiologic coupling," *Proc. Natl. Acad. Sci.*, vol. 109, no. 26, pp. 10 181–10 186, Jun. 2012.

[113] R. Trimer, R. Cabiddu, R. G. Mendes, F. S. M. Costa, A. D. Oliveira, A. Borghi-Silva, and A. M. Bianchi, "Heart rate variability and cardio-respiratory coupling during sleep in patients prior to bariatric surgery," *Obes. Surg.*, vol. 24, no. 3, pp. 471–477, Jan. 2014.

[114] D. Shepherd, J. Mulgrew, and M. J. Hautus, "Exploring the autonomic correlates of personality," *Auton. Neurosci.*, vol. 193, pp. 127–131, Dec. 2015.

[115] M. A. Patriquin, A. Scarpa, B. H. Friedman, and S. W. Porges, "Respiratory sinus arrhythmia: A marker for positive social functioning and receptive language skills in children with autism spectrum disorders," *Dev. Psychobiol.*, vol. 55, no. 2, pp. 101–112, Mar. 2013.

[116] M. Pace, L. Dumortier, A. Favre-Juvin, M. Guinot, and V.-A. Bricout, "Heart rate variability during sleep in children with autism spectrum disorders," *Physiol. Behav.*, vol. 167, pp. 309–312, Dec. 2016.

[117] E. Cherland, "The Polyvagal Theory: Neurophysiological foundations of emotions, attachment, communication, self-regulation," *J. Can. Acad. Child Adolesc. Psychiatry*, vol. 21, no. 4, pp. 313–314, Nov. 2012.

[118] J. G. Miller, J. N. Nuselovici, and P. D. Hastings, "Nonrandom acts of kindness: Parasympathetic and subjective empathic responses to sadness predict children's prosociality," *Child Dev.*, vol. 87, no. 6, pp. 1679–1690, Nov. 2016.

[119] N. Kim, T. L. Hughes, C. G. Park, L. Quinn, and I. D. Kong, "Altered autonomic functions and distressed personality traits in male adolescents with Internet gaming addiction," *Cyberpsychol. Behav. Soc. Netw.*, vol. 19, no. 11, pp. 667–673, Nov. 2016.

[120] J. L. Abaied, C. Wagner, N. L. Breslend, and M. Flynn, "Respiratory sinus arrhythmia as a predictor of eating disorder symptoms in college students: Moderation by responses to stress and parent psychological control," *Eat. Behav.*, vol. 21, pp. 109 – 115, Apr. 2016.

[121] J. L. Helm, D. A. Sbarra, and E. Ferrer, "Coregulation of respiratory sinus arrhythmia in adult romantic partners," *Emotion*, vol. 14, no. 3, pp. 522–531, Jun. 2014.

[122] V. Müller and U. Lindenberger, "Cardiac and respiratory patterns synchronize between persons during choir singing," *PLoS One*, vol. 6, no. 9, p. e24893, Sep. 2011.

[123] H. K. Lackner, I. Papousek, J. J. Batzel, A. Roessler, H. Scharfetter, and H. Hinghofer-Szalkay, "Phase synchronization of hemodynamic variables and respiration during mental challenge," *Int. J. Psychophysiol.*, vol. 79, no. 3, pp. 401– 409, 2011.

[124] A. B. Forman-Alberti and J. B. Hinnant, "Links between autonomic activity and implicit learning," *Int. J. Psychophysiol.*, pp. 75–80, Dec. 2016.

[125] V. F. Gladwell, D. K. Brown, J. L. Barton, M. P. Tarvainen, P. Kuoppa, J. Pretty, J. M. Suddaby, and G. R. H. Sandercock, "The effects of views of nature on autonomic control," *Eur. J. Appl. Physiol.*, vol. 112, no. 9, pp. 3379–3386, Jan. 2012.

[126] D. K. Brown, J. L. Barton, and V. F. Gladwell, "Viewing nature scenes positively affects recovery of autonomic function following acute-mental stress," *Environ. Sci. Technol.*, vol. 47, no. 11, pp. 5562–5569, Jun. 2013.

[127] T. Udo, A. H. Weinberger, C. M. Grilo, K. D. Brownell, R. J. DiLeone, R. Lampert, S. L. Matlin, K. Yanagisawa, and S. A. McKee, "Heightened vagal activity during high-calorie food presentation in obese compared with non-obese individuals—Results of a pilot study," *Obes. Res. Clin. Pract.*, vol. 8, no. 3, pp. 258–265, May 2014.

[128] C. C. Grant, M. Viljoen, D. Janse van Rensburg, and P. S. Wood, "Heart rate variability assessment of the effect of physical training on autonomic cardiaccontrol," *Ann. Noninvasive Electrocardiol.*, vol. 17, no. 3, pp. 219–229, Jul. 2012.

[129] R. Hainsworth, M. J. Drinkhill, and M. Rivera-Chira, "The autonomic nervous system at high altitude," *Clin. Auton. Res.*, vol. 17, no. 1, pp. 13–19, Feb. 2007.

[130] M. Wille, K. Mairer, H. Gatterer, M. Philippe, M. Faulhaber, and M. Burtscher, "Changes in cardiac autonomic activity during a passive 8 hour acute exposure to 5500 m normobaric hypoxia are not related to the development of acute mountain sickness," *Int. J. Sports Med.*, vol. 33, no. 3, pp. 186–191, Mar. 2012.

[131] G. Bhaumik, D. Dass, D. Bhattacharyya, Y. K. Sharma, and S. B. Singh, "Heart rate variabilty changes during first week of acclimatization to 3500 m altitude in Indian military personnel." *Indian J. Physiol. Pharmacol.*, vol. 57, no. 1, pp. 16–22, Jan. 2013.

[132] S. Brown, M. J. Barnes, and T. Mündel, "Effects of hypoxia and hypercapnia on human HRV and respiratory sinus arrhythmia," *Acta Physiol. Hung.*, vol. 101, no. 3, pp. 263–272, Sep. 2014.

[133] D. Zhang, J. She, Z. Zhang, and M. Yu, "Effects of acute hypoxia on heart rate variability, sample entropy and cardiorespiratory phase synchronization," *Biomed. Eng. Online*, vol. 13, p. 73, Jun. 2014.

[134] Z. Taralov, K. Terziyski, P. Dimov, B. Marinov, M. P. Tarvainen, R. Perini, and S. Kostianev, "Assessment of the acute impact of normobaric hypoxia as a part of an intermittent hypoxic training on heart rate variability," *Cor Vasa*, vol. 57, no. 4, pp. 251–256, Aug. 2015.

[135] C. Lizamore, Y. Kathiravel, J. Elliott, J. Hellemans, and M. Hamlin, "The effect of short-term intermittent hypoxic exposure on heart rate variability in a sedentary population," *Acta Physiol. Hung.*, vol. 103, no. 1, pp. 75–85, Mar. 2016.

[136] H. M. Karinen, A. Uusitalo, H. Vähä-Ypyä, M. Kähönen, J. E. Peltonen, P. K. Stein, J. Viik, and H. O. Tikkanen, "Heart rate variability changes at 2400 m altitude predicts acute mountain sickness on further ascent at 3000-4300 m altitudes," *Front. Physiol.*, vol. 3, Aug. 2012.

[137] A. Hadefi, C. Dedobbeleer, F. Villafuerte, J. L. Macarlupu, A. Pichon, R. Naeije, and P. Unger, "Heart rate variability in recently acclimatized lowlanders, in healthy highlanders and in patients with chronic mountain sickness at the altitude of 4,350 m," *Circulation*, vol. 126, no. Suppl 21, pp. A17 085–A17 085, Nov. 2012.

[138] C. Orphanidou, S. Fleming, S. A. Shah, and L. Tarassenko, "Data fusion for estimating respiratory rate from a single-lead ECG," *Biomed. Signal Process. Control*, vol. 8, no. 1, pp. 98–105, Jan. 2013.

[139] J. Lázaro, Y. Nam, E. Gil, P. Laguna, and K. H. Chon, "Respiratory rate derived from smartphone-camera-acquired pulse photoplethysmographic signals," *Physiol. Meas.*, vol. 36, no. 11, p. 2317, Oct. 2015.

[140] L. Mirmohamadsadeghi, N. Bourdillon, G. P. Millet, and J.-M. Vesin, "Cardio-respiratory characterization of the autonomic balance," in *Computing in Cardiology (CinC)*, Sep. 2016.

[141] J. F. Thayer, *Heart Rate Variability*. New York, NY: Springer New York, 2013, pp. 952–953.

[142] B. Tavernier and M. Jeanne, *Heart Rate Variability*. New York, NY: Springer New York, 2014, pp. 109–115.

[143] G. A. Reyes del Paso, W. Langewitz, L. J. M. Mulder, A. van Roon, and S. Duschek, "The utility of low frequency heart rate variability as an index of sympathetic cardiac tone: A review with emphasis on a reanalysis of previous studies," *Psychophysiology*, vol. 50, no. 5, pp. 477–487, May 2013.

[144] F. Rahman, S. Pechnik, D. Gross, L. Sewell, and D. S. Goldstein, "Low frequency power of heart rate variability reflects baroreflex function, not cardiac sympathetic innervation," *Clin. Auton. Res.*, vol. 21, no. 3, pp. 133–141, Jan. 2011.

[145] C. Julien, "The enigma of Mayer waves: Facts and models," *Cardiovasc. Res.*, vol. 70, no. 1, pp. 12–21, Apr. 2006.

[146] M. Pagani, F. Lombardi, S. Guzzetti, G. Sandrone, O. Rimoldi, G. Malfatto, S. Cerutti, and A. Malliani, "Power spectral density of heart rate variability as an index of sympatho-vagal interaction in normal and hypertensive subjects." *J. Hypertens. Suppl.*, vol. 2, no. 3, pp. S383–5, 1984.

[147] B. Pomeranz, R. J. Macaulay, M. A. Caudill, I. Kutz, D. Adam, D. Gordon, K. M. Kilborn, A. C. Barger, D. C. Shannon, R. J. Cohen, and others, "Assessment of autonomic function in humans by heart rate spectral analysis," *Am. J. Physiol. Heart. Circ. Physiol.*, vol. 248, no. 1, pp. H151–H153, Jan. 1985.

[148] K. Howorka, J. Pumprla, A. Jirkovska, S. Lacigova, and J. Nolan, "Modified orthostatic load for spectral analysis of short-term heart rate variability improves the sensitivity of autonomic dysfunction assessment," *J. Diabetes Complications*, vol. 24, no. 1, pp. 48–54, Jan. 2010.

[149] G. A. d. P. Vidigal, B. S. Tavares, D. M. Garner, A. A. Porto, L. Carlos de Abreu, C. Ferreira, and V. E. Valenti, "Slow breathing influences cardiac autonomic responses to postural maneuver: Slow breathing and HRV," *Complement Ther. Clin. Pract.*, vol. 23, pp. 14–20, May 2016.

[150] P. D. Larsen, Y. C. Tzeng, P. Y. W. Sin, and D. C. Galletly, "Respiratory sinus arrhythmia in conscious humans during spontaneous respiration," *Respir. Physiol. Neurobiol.*, vol. 174, no. 1, pp. 111–118, Nov. 2010.

[151] M. Malik, R. Sassi, S. Cerutti, F. Lombardi, H. V. Huikuri, C.-K. Peng, G. Schmidt, and Y. Yamamoto, "Assessing cardiac autonomic function via heart rate variability analysis requires monitoring respiration: reply," *Europace*, vol. 18, no. 8, pp. 1280–1281, Aug. 2016.

[152] T. Stankovski, W. H. Cooke, L. Rudas, A. Stefanovska, and D. L. Eckberg, "Time-frequency methods and voluntary ramped-frequency breathing: A powerful combination for exploration of human neurophysiological mechanisms," *J. Appl. Physiol.*, vol. 115, no. 12, pp. 1806–1821, Dec. 2013.

[153] H. Kobayashi, "Does paced breathing improve the reproducibility of heart rate variability measurements?" *J. Physiol. Anthropol.*, vol. 28, no. 5, pp. 225–230, Oct. 2009.

[154] V. V. Trubachev, A. V. Gorbunov, V. S. Trubacheva, M. S. Nemtseva, and M. S. Ogorodnikova, "Plasticity of heart rate modulation at different paced respiration frequencies in young adults," *Neurosci. Behav. Physiol.*, vol. 45, no. 7, pp. 743–749, Aug. 2015.

[155] W. H. Cooke, J. F. Cox, A. M. Diedrich, J. A. Taylor, L. A. Beightol, J. E. Ames, J. B. Hoag, H. Seidel, and D. L. Eckberg, "Controlled breathing protocols probe human autonomic cardiovascular rhythms," *Am. J. Physiol. Heart. Circ. Physiol.*, vol. 274, no. 2, pp. H709–H718, Feb. 1998.

[156] A. Guillén-Mandujano and S. Carrasco-Sosa, "Additive effect of simultaneously varying respiratory frequency and tidal volume on respiratory sinus arrhythmia," *Auton. Neurosci.*, vol. 186, pp. 69–76, Dec. 2014.

[157] J. A. Taylor, C. W. Myers, J. R. H., H. Seidel, and D. L. Eckberg, "Sympathetic restraint of respiratory sinus arrhythmia: implications for vagal-cardiac tone assessment in humans," *Am. J. Physiol. Heart Circ. Physiol.*, vol. 280, no. 6, pp. 2804–2814, Jun. 2001.

[158] K. H. Bendixen, A. J. Terkelsen, L. Baad-Hansen, B. E. Cairns, and P. Svensson, "Effect of propranolol on hypertonic saline-evoked masseter muscle pain and autonomic response in healthy women during rest and mental arithmetic task," *J. Orofac. Pain*, vol. 27, no. 3, pp. 243–255, 2013.

[159] C. Médigue, A. Girard, D. Laude, A. Monti, M. Wargon, and J.-L. Elghozi, "Relationship between pulse interval and respiratory sinus arrhythmia: a time- and frequency-domain analysis of the effects of atropine," *Pflügers Archiv*, vol. 441, no. 5, pp. 650–655, Jan. 2001.

[160] T. Richardson, A. Rozkovec, P. Thomas, J. Ryder, C. Meckes, and D. Kerr, "Influence of caffeine on heart rate variability in patients with long-standing type 1 diabetes," *Diabetes Care*, vol. 27, no. 5, pp. 1127–1131, May 2004.

[161] R. Corti, C. Binggeli, I. Sudano, L. Spieker, E. Hänseler, F. Ruschitzka, W. F. Chaplin, T. F. Lüscher, and G. Noll, "Coffee acutely increases sympathetic nerve activity and blood pressure independently of caffeine content," *Circulation*, vol. 106, no. 23, pp. 2935–2940, Dec. 2002.

[162] K. Bunsawat, D. W. White, R. M. Kappus, and T. Baynard, "Caffeine delays autonomic recovery following acute exercise," *Eur. J. Prev. Cardiol.*, vol. 22, no. 11, pp. 1473–1479, Nov. 2015.

[163] A. Nehlig, J.-L. Daval, and G. Debry, "Caffeine and the central nervous system: Mechanisms of action, biochemical, metabolic and psychostimulant effects," *Brain Res. Rev.*, vol. 17, no. 2, pp. 139–170, May 1992.

[164] A. C. Guyton and J. E. Hall, *Textbook of Medical Physiology*, 7th ed.   Elsevier, 2006, ch. 17: Local and Humoral Control of Blood Flow by the Tissues.

[165] T. P. Zahn and J. L. Rapoport, "Autonomic nervous system effects of acute doses of caffeine in caffeine users and abstainers," *Int. J. Psychophysiol.*, vol. 5, no. 1, pp. 33–41, May 1987.

[166] I. Höfer and K. Bättig, "Cardiovascular, behavioral, and subjective effects of caffeine under field conditions," *Pharmacol. Biochem. Behav.*, vol. 48, no. 4, pp. 899–908, Aug. 1994.

[167] R. J. Barry, A. R. Clarke, S. J. Johnstone, and J. A. Rushby, "Timing of caffeine's impact on autonomic and central nervous system measures: Clarification of arousal effects," *Biol. Psychol.*, vol. 77, no. 3, pp. 304–316, Mar. 2008.

[168] M. Monda, A. Viggiano, C. Vicidomini, A. Viggiano, T. Iannaccone, D. Tafuri, and B. D. Luca, "Expresso coffee increases parasympathetic activity in young, healthy people," *Nutr. Neurosci.*, vol. 12, no. 1, pp. 43–48, Feb. 2009.

[169] A. Hernando, J. Lázaro, E. Gil, A. Arza, J. M. Garzón, R. López-Antón, C. de la Cámara, P. Laguna, J. Aguiló, and R. Bailón, "Inclusion of respiratory frequency information in heart rate variability analysis for stress assessment," *IEEE J. Biomed. Health. Inform.*, vol. 20, no. 4, pp. 1016–1025, July 2016.

[170] N. Wessel, L. Sidorenko, J. F. Kraemer, C. Schoebel, and G. Baumann, "Assessing cardiac autonomic function via heart rate variability analysis requires monitoring respiration," *Europace*, vol. 18, no. 8, pp. 1280–1280, Aug. 2016.

[171] G. Valenza, L. Citi, and R. Barbieri, "Disentanglement of sympathetic and parasympathetic activity by instantaneous analysis of human heartbeat dynamics," in *38th Annual International Conference of the IEEE Engineering in Medicine and Biology Society (EMBC)*, Aug 2016, pp. 932–935.

[172] D. Saboul, V. Pialoux, and C. Hautier, "The breathing effect of the LF/HF ratio in the heart rate variability measurements of athletes," *Eur. J. Sport Sci.*, vol. 14, no. sup1, pp. S282–S288, 2012.

[173] M. A. Cretikos, R. Bellomo, K. Hillman, J. Chen, S. Finfer, and A. Flabouris, "Respiratory rate: the neglected vital sign," *Med. J. Aust.*, vol. 188, no. 11, p. 657, 2008.

[174] R. Bailón, L. Mainardi, M. Orini, L. Sörnmo, and P. Laguna, "Analysis of heart rate variability during exercise stress testing using respiratory information," *Biomed. Signal Process. Control*, vol. 5, no. 4, pp. 299–310, Oct. 2010.

[175] L. Bernardi, J. Wdowczyk-Szulc, C. Valenti, S. Castoldi, C. Passino, G. Spadacini, and P. Sleight, "Effects of controlled breathing, mental activity and mental stress with or without verbalization on heart rate variability," *J. Am. Coll. Cardiol.*, vol. 35, no. 6, pp. 1462–1469, May 2000.

[176] G. Carrault, A. Beuchee, P. Pladys, L. Senhadji, and A. Hernandez, "Time-frequency relationships between heart rate and respiration: A diagnosis tool for late onset sepsis in sick premature infants," in *Computers in Cardiology (CinC)*, Sep. 2009, pp. 369–372.

[177] H. K. Lackner, I. Papousek, J. J. Batzel, A. Roessler, H. Scharfetter, and H. Hinghofer-Szalkay, "Phase synchronization of hemodynamic variables and respiration during mental challenge," *Int. J. Psychophysiol.*, vol. 79, no. 3, pp. 401–409, Mar. 2011.

[178] N. Mitrou, A. Laurin, T. Dick, and J. Inskip, "A peak detection method for identifying phase in physiological signals," *Biomed. Signal Process. Control*, vol. 31, pp. 452–462, Jan. 2017.

[179] P. Y. W. Sin, D. C. Galletly, and Y. C. Tzeng, "Influence of breathing frequency on the pattern of respiratory sinus arrhythmia and blood pressure: Old questions revisited," *Am. J. Physiol. Heart. Circ. Physiol.*, vol. 298, no. 5, pp. H1588–H1599, May 2010.

[180] K. Kotani, K. Takamasu, Y. Jimbo, and Y. Yamamoto, "Postural-induced phase shift of respiratory sinus arrhythmia and blood pressure variations: Insight from respiratory-phase domain analysis," *Am. J. Physiol. Heart. Circ. Physiol.*, vol. 294, no. 3, pp. H1481–H1489, Mar. 2008.

[181] S. Ahn, J. Solfest, and L. L. Rubchinsky, "Fine temporal structure of cardiorespiratory synchronization," *Am. J. Physiol. Heart. Circ. Physiol.*, vol. 306, no. 5, pp. 755–763, Mar. 2014.

[182] J. Solà-Soler, B. F. Giraldo, J. A. Fiz, and R. Jané, "Study of phase estimation methods to analyse cardiorespiratory synchronization in OSA patients," in *38th Annual International Conference of the IEEE Engineering in Medicine and Biology Society (EMBC)*, Aug 2016, pp. 4280–4283.

[183] D. Benitez, P. A. Gaydecki, A. Zaidi, and A. P. Fitzpatrick, "The use of the Hilbert transform in ECG signal analysis," *Comput. Biol. Med.*, vol. 31, no. 5, pp. 399–406, Sep. 2001.

[184] M. Chavez, M. Besserve, C. Adam, and J. Martinerie, "Towards a proper estimation of phase synchronization from time series," *J. Neurosci. Methods*, vol. 154, no. 1-2, pp. 149–160, Jun. 2006.

[185] N. E. Huang and Z. Wu, "A review on Hilbert-Huang transform: Method and its applications to geophysical studies," *Rev. Geophys.*, vol. 46, no. 2, Jun. 2008.

[186] N. E. Huang and S. S. P. Shen, *Hilbert-Huang Transform and its Applications*, 2nd ed., ser. Interdisciplinary Mathematical Sciences- Vol. 16. World Scientific Publishing Co. Pte. Ltd., 2014, ch. 1: Introduction to the Hilbert-Huang Transform and its Related Mathematical Problems.

[187] S. Rzeczinski, N. B. Janson, A. G. Balanov, and P. V. E. McClintock, "Regions of cardiorespiratory synchronization in humans under paced respiration," *Phys. Rev. E*, vol. 66, no. 5, p. 051909, Nov. 2002.

[188] A. Buttu, E. Pruvot, J. Van Zaen, A. Viso, A. Forclaz, P. Pascale, S. M. Narayan, and J. M. Vesin, "Adaptive frequency tracking of the baseline ECG identifies the site of atrial fibrillation termination by catheter ablation," *Biomed. Signal Process. Control*, vol. 8, pp. 969–980, Nov. 2013.

[189] M. Stridh, D. Husser, A. Bollmann, and L. Sörnmo, "Waveform characterization of atrial fibrillation using phase information," *IEEE Trans. Biomed. Eng.*, vol. 56, no. 4, pp. 1081–1089, Apr. 2009.

[190] T. D. Timmins and D. H. Saunders, "Effect of caffeine ingestion on maximal voluntary contraction strength in upper- and lower-body muscle groups," *J. Strength Cond. Res.*, vol. 28, no. 11, pp. 3239–3244, Nov. 2014.

[191] H.-Y. Chen, H.-S. Wang, K. Tung, and H.-H. Chao, "Effects of gender difference and caffeine supplementation on anaerobic muscle performance," *Int. J. Sports Med.*, vol. 36, no. 12, pp. 974–978, Aug. 2015.

[192] A. Buttu, "Novel ECG and intracardiac electrograms signal processing schemes for predicting the outcome of atrial fibrillation catheter ablation," Ph.D. dissertation, Ecole Polytechnique Fédérale de Lausanne, 2015.

[193] B. D. Levine, "Intermittent hypoxic training: Fact and fancy," *High Alt. Med. Biol.*, vol. 3, no. 2, pp. 177–193, Jul. 2002.

[194] C. C. J. Farinelli, B. Kayser, T. Binzoni, P. Cerretelli, and L. Girardier, "Autonomic nervous control of heart rate at altitude (5050 m)," *Eur. J. Appl. Physiol.*, vol. 69, no. 6, pp. 502–507, Dec. 1994.

[195] R. Perini, S. Milesi, L. Biancardi, and A. Veicsteinas, "Effects of high altitude acclimatization on heart rate variability in resting humans," *Eur. J. Appl. Physiol.*, vol. 73, no. 6, pp. 521–528, Jul. 1996.

[196] R. L. Hughson, Y. Yamamoto, R. E. McCullough, J. R. Sutton, and J. T. Reeves, "Sympathetic and parasympathetic indicators of heart rate control at altitude studied by spectral analysis," *J. Appl. Physiol.*, vol. 77, no. 6, pp. 2537–2542, Dec. 1994.

[197] L. Bernardi, C. Passino, G. Spadacini, A. Calciati, R. Roberts, R. Greene, E. Martignoni, I. Anand, and O. Appenzeller, "Cardiovascular autonomic modulation and activity of carotid baroreceptors at altitude," *Clin. Sci.*, vol. 95, no. 5, pp. 565–573, Nov. 1998.

[198] K. Sevre, B. Bendz, E. Hanko, A. R. Nakstad, A. Hauge, J. I. Kasin, J. D. Lefrandt, A. J. Smit, I. Eide, and M. Rostrup, "Reduced autonomic activity during stepwise exposure to high altitude," *Acta Physiol. Scand.*, vol. 173, no. 4, pp. 409–417, Dec. 2001.

[199] M. Kanai, F. Nishihara, T. Shiga, H. Shimada, and S. Saito, "Alterations in autonomic nervous control of heart rate among tourists at 2700 and 3700 m above sea level," *Wilderness Environ. Med.*, vol. 12, no. 1, pp. 8–12, Mar. 2001.

[200] Y.-C. Chen, F.-C. Lin, G.-M. Shiao, and S.-C. Chang, "Effect of rapid ascent to high altitude on autonomic cardiovascular modulation," *Am. J. Med. Sci.*, vol. 336, no. 3, pp. 248–253, Sep. 2008.

[201] H.-H. Huang, C.-Y. Tseng, J.-S. Fan, D. H.-T. Yen, W.-F. Kao, S.-C. Chang, T. B. J. Kuo, C.-I. Huang, and C.-H. Lee, "Alternations of heart rate variability at lower altitude in the predication of trekkers with acute mountain sickness at high altitude," *Clin. J. Sport. Med.*, vol. 20, no. 1, pp. 58–63, Jan. 2010.

[202] C. Povea, L. Schmitt, J. Brugniaux, G. Nicolet, J.-P. Richalet, and J.-P. Fouillot, "Effects of intermittent hypoxia on heart rate variability during rest and exercise," *High Alt. Med. Biol.*, vol. 6, no. 3, pp. 215–225, Sep. 2005.

[203] L. A. Lipsitz, F. Hashimoto, L. P. Lubowsky, J. Mietus, G. B. Moody, O. Appenzeller, and A. L. Goldberger, "Heart rate and respiratory rhythm dynamics on ascent to high altitude." *Br. Heart J.*, vol. 74, no. 4, pp. 390–396, Oct. 1995.

[204] M. Di Rienzo, P. Castiglioni, F. Rizzo, A. Faini, P. Mazzoleni, C. Lombardi, P. Meriggi, G. Parati, and on behalf of the HIGHCARE investigators, "Linear and fractal heart rate dynamics during sleep at high altitude: Investigation with textile technology," *Methods Inf. Med.*, vol. 49, no. 5, pp. 521–525, Jun. 2010.

[205] Q. Jun, H. Lan, T. Kaixin, Y. Shiyong, Y. Yang, and L. Min, "Changes of autonomic nervous system function in healthy young men during initial phase at acute high-altitude exposure," *J. Med. Coll. PLA*, vol. 23, no. 5, pp. 270–275, Oct. 2008.

[206] G. P. Millet, R. Faiss, and V. Pialoux, "Point: Counterpoint: Hypobaric hypoxia induces/-does not induce different responses from normobaric hypoxia," *J. Appl. Physiol.*, vol. 112, no. 10, pp. 1783–1784, May 2012.

[207] R. Heinzer, J. Saugy, N. Tobback, T. Rupp, J. Haba-Rubio, and G. Millet, "Effects of real vs simulated altitude on sleep and sleep disordered breathing," *Sleep Medicine*, vol. 14, Supplement 1, p. e285, Dec. 2013.

[208] C. Guger, S. Krausert, W. Domej, G. Edlinger, and M. Tannheimer, "EEG, ECG and oxygen concentration changes from sea level to a simulated altitude of 4000 m and back to sea level," *Neurosci. Lett.*, vol. 442, no. 2, pp. 123–127, Sep. 2008.

[209] A. W. Subudhi, N. Bourdillon, J. Bucher, C. Davis, J. E. Elliott, M. Eutermoster, O. Evero, J.-L. Fan, S. J.-V. Houten, C. G. Julian, J. Kark, S. Kark, B. Kayser, J. P. Kern, S. E. Kim, C. Lathan, S. S. Laurie, A. T. Lovering, R. Paterson, D. M. Polaner, B. J. Ryan, J. L. Spira, J. W. Tsao, N. B. Wachsmuth, and R. C. Roach, "AltitudeOmics: The integrative physiology of human acclimatization to hypobaric hypoxia and its retention upon reascent," *PLoS One*, vol. 9, no. 3, pp. 1–11, Mar. 2014.

[210] L. Mirmohamadsadeghi and J.-M. Vesin, "Respiratory rate estimation from multi-lead ECGs using an adaptive frequency tracking algorithm," in *Computing in Cardiology (CinC)*, Sep. 2014.

[211] ——, "Respiratory rate simultaneous estimation from two ECG-derived respiratory waveforms using an adaptive frequency tracking algorithm," in *International Congress on Electrocardiology*, Jun. 2014.

[212] ——, "Respiratory rate estimation from the ECG using an instantaneous frequency tracking algorithm," *Biomed. Signal Process. Control*, vol. 14, no. 0, pp. 66–72, Nov. 2014.

[213] ——, "Estimating the real-time respiratory rate from the ECG with a bank of notch filters," in *Computing in Cardiology (CinC)*, Sep. 2015.

[214] ——, "Real-time multi-signal frequency tracking with a bank of notch filters to estimate the respiratory rate from the ECG," *Physiol. Meas.*, vol. 37, no. 9, pp. 1573–1587, Aug. 2016.

[215] D. Sinnecker, M. Dommasch, P. Barthel, A. Müller, R. J. Dirschinger, A. Hapfelmeier, K. M. Huster, K.-L. Laugwitz, M. Malik, and G. Schmidt, "Assessment of mean respiratory rate from ECG recordings for risk stratification after myocardial infarction," *J. Electrocardiol.*, vol. 47, no. 5, pp. 700–704, Sep. 2014.

[216] T. J. Moss, M. T. Clark, J. F. Calland, K. B. Enfield, G. Kim, M. A. Lynch, M. I. Blatt, D. E. Lake, and J. R. Moorman, "Electrocardiography-derived respiratory rate detects clinical deterioration in acute care patients with cardiovascular disease," *Circulation*, vol. 134, no. Suppl 1, pp. A13 937–A13 937, Nov. 2016.

[217] L. Brochard, G. S. Martin, L. Blanch, P. Pelosi, F. J. Belda, A. Jubran, L. Gattinoni, J. Mancebo, V. M. Ranieri, J.-C. M. Richard *et al.*, "Clinical review: Respiratory monitoring in the ICU-a consensus of 16," *Crit. Care*, vol. 16, no. 2, p. 219, Apr. 2012.

[218] P. H. Charlton, M. Villarroel, and F. Salguiero, "Waveform analysis to estimate respiratory rate," in *Secondary Analysis of Electronic Health Records*. Springer, 2016, pp. 377–390.

[219] P. H. Charlton, T. Bonnici, L. Tarassenko, D. A. Clifton, R. Beale, and P. J. Watkinson, "An assessment of algorithms to estimate respiratory rate from the electrocardiogram and photoplethysmogram," *Physiol. Meas.*, vol. 37, no. 4, p. 610, Mar. 2016.

[220] A. Schäfer and K. Kratky, "Estimation of breathing rate from respiratory sinus arrhythmia: Comparison of various methods," *Ann. Biomed. Eng.*, vol. 36, no. 3, pp. 476–485, Mar. 2008.

[221] D. Cysarz, R. Zerm, H. Bettermann, M. Frühwirth, M. Moser, and M. Kröz, "Comparison of respiratory rates derived from heart rate variability, ECG amplitude, and nasal/oral airflow," *Ann. Biomed. Eng.*, vol. 36, no. 12, pp. 2085–2094, Dec. 2008.

[222] D. R. Bach, S. Gerster, A. Tzovara, and G. Castegnetti, "A linear model for event-related respiration responses," *J. Neurosci. Methods*, vol. 270, pp. 147–155, Sep. 2016.

[223] F. Schrumpf, M. Sturm, G. Bausch, and M. Fuchs, "Derivation of the respiratory rate from directly and indirectly measured respiratory signals using autocorrelation," *Curr. Dir. Biomed. Eng.*, vol. 2, no. 1, pp. 241–245, Sep. 2016.

[224] N. N. Lepine, T. Tajima, T. Ogasawara, R. Kasahara, and H. Koizumi, "Robust respiration rate estimation using adaptive Kalman filtering with textile ECG sensor and accelerometer," in *38th Annual International Conference of the IEEE Engineering in Medicine and Biology Society (EMBC)*, Aug. 2016, pp. 3797–3800.

[225] A. Vehkaoja, M. Peltokangas, and J. Lekkala, "Extracting the respiration cycle lengths from ECG signal recorded with bed sheet electrodes," in *J. Phys.: Conf. Series*, vol. 459, no. 1. IOP Publishing, 2013, p. 012015.

[226] B. Boashash, "Estimating and interpreting the instantaneous frequency of a signal I Fundamentals," *Proc. IEEE*, vol. 80, no. 4, pp. 520–538, Apr 1992.

[227] A. Potamianos and P. Maragos, "A comparison of the energy operator and the Hilbert transform approach to signal and speech demodulation," *Signal Process.*, vol. 37, no. 1, pp. 95–120, May 1994.

[228] N. E. Huang, Z. Shen, S. R. Long, M. C. Wu, H. H. Shih, Q. Zheng, N.-C. Yen, C. C. Tung, and H. H. Liu, "The empirical mode decomposition and the Hilbert spectrum for nonlinear and non-stationary time series analysis," *Phil. Trans. R. Soc. A*, vol. 454, no. 1971, pp. 903–995, Nov. 1998.

[229] M. Aboy, O. W. Marquez, J. McNames, R. Hornero, T. Tran, and B. Goldstein, "Adaptive modeling and spectral estimation of nonstationary biomedical signals based on Kalman filtering," *IEEE Trans. Biomed. Eng.*, vol. 52, no. 8, pp. 1485–1489, Aug 2005.

[230] R. Punchalard, A. Lorsawatsiri, W. Loetwassana, J. Koseeyaporn, P. Wardkein, and A. Roeksabutr, "Direct frequency estimation based adaptive algorithm for a second-order adaptive FIR notch filter," *Signal Process.*, vol. 88, no. 2, pp. 315–325, Feb. 2008.

[231] R. Punchalard, J. Koseeyaporn, and P. Wardkein, "Indirect frequency estimation based on second-order adaptive FIR notch filter," *Signal Process.*, vol. 89, no. 7, pp. 1428–1435, Jul. 2009.

[232] X. Tan and H. Zhang, "A novel adaptive IIR notch filter for frequency estimation and tracking," in *3rd IEEE International Conference on Computer Science and Information Technology (ICCSIT)*, vol. 5, Jul 2010, pp. 259–263.

[233] Y. Prudat and J.-M. Vesin, "Multi-signal extension of adaptive frequency tracking algorithms," *Signal Process.*, vol. 89, no. 6, pp. 963–973, Jun. 2009.

[234] J. Van Zaen, L. Uldry, C. Duchêne, Y. Prudat, R. A. Meuli, M. M. Murray, and J.-M. Vesin, "Adaptive tracking of EEG oscillations," *J. Neurosc. Meth.*, vol. 186, no. 1, pp. 97–106, Jan. 2010.

[235] S. G. Fleming and L. Tarassenko, "A comparison of signal processing techniques for the extraction of breathing rate from the photoplethysmogram," *Int. J. Biol. Med. Sci.*, vol. 2, no. 4, pp. 232–236, 2007.

[236] D. Gabor, "Theory of communication. part 1: The analysis of information," *J. Instit. Elec. Engineers-Part III: Radio Commun. Eng.*, vol. 93, no. 26, pp. 429–441, 1946.

[237] G. Rilling, P. Flandrin, and P. Gonçalvés, "On empirical mode decomposition and its algorithms," in *IEEE-EURASIP Workshop on Nonlin. Sig. Image Process.*, vol. 3, 2003, pp. 8–11.

[238] H. C. So, "A comparative study of three recursive least-squares algorithms for single-tone frequency tracking," *Signal Process.*, vol. 83, no. 9, pp. 2059–2062, Sep. 2003.

[239] S. L. Marple, *Digital Spectral Analysis with Applications*, ser. Digital Spectral Analysis with Applications. Englewood Cliffs, NJ, Prentice-Hall, Inc., 1987, ch. 11: Prony's Method.

[240] L. B. Fertig and J. H. McClellan, "Instantaneous frequency estimation using linear prediction with comparisons to the DESAs," *IEEE Signal Process. Lett.*, vol. 3, pp. 54–56, Feb 1996.

[241] N. Iyengar, C. K. Peng, R. Morin, A. Goldberger, and L. A. Lipsitz, "Age-related alterations in the fractal scaling of cardiac interbeat interval dynamics," *Am. J. Physiol.*, vol. 271, no. 4, pp. 1078–1084, Oct. 1996.

[242] A. L. Goldberger, L. A. Amaral, L. Glass, J. M. Hausdorff, P. C. Ivanov, R. G. Mark, J. E. Mietus, G. B. Moody, C.-K. Peng, and H. E. Stanley, "PhysioBank, PhysioToolkit, and PhysioNet: components of a new research resource for complex physiologic signals," *Circulation*, vol. 101, no. 23, pp. 215–220, Jun. 2000.

[243] X.-R. Ding, Y.-T. Zhang, H. K. Tsang, and W. Karlen, "A pulse transit time based fusion method for the noninvasive and continuous monitoring of respiratory rate," in *38th Annual International Conference of the IEEE Engineering in Medicine and Biology Society (EMBC)*, Aug. 2016, pp. 4240–4243.

[244] L. Mirmohamadsadeghi, S. Fallet, V. Moser, F. Braun, and J.-M. Vesin, "Real-time respiratory rate estimation using imaging photoplethysmography inter-beat intervals," in *Computing in Cardiology (CinC)*, 2016.

[245] J. Allen, "Photoplethysmography and its application in clinical physiological measurement," *Physiol. Meas.*, vol. 28, no. 3, p. R1, Feb. 2007.

[246] F. P. Wieringa, F. Mastik, and A. F. W. van der Steen, "Contactless multiple wavelength photoplethysmographic imaging: A first step toward SpO2," *Ann. Biomed. Eng.*, vol. 33, no. 8, pp. 1034–1041, Aug. 2005.

[247] W. Verkruysse, L. O. Svaasand, and J. S. Nelson, "Remote plethysmographic imaging using ambient light," *Opt Express*, vol. 16, no. 26, pp. 21 434–21 445, Dec. 2008.

[248] L. Tarassenko, M. Villarroel, A. Guazzi, J. Jorge, D. A. Clifton, and C. Pugh, "Non-contact video-based vital sign monitoring using ambient light and auto-regressive models," *Physiol. Meas.*, vol. 35, no. 5, pp. 807–831, May 2014.

[249] S. Fallet, , V. Moser, F. Braun, and J. M. Vesin, "Imaging photoplethysmography: What are the best locations on the face to estimate heart rate?" in *Computing in Cardiology*, 2016.

[250] K. H. Chon, S. Dash, and K. Ju, "Estimation of respiratory rate from photoplethysmogram data using time-frequency spectral estimation," *IEEE Trans. Biomed. Eng.*, vol. 56, no. 8, pp. 2054–2063, Aug. 2009.

[251] S. Dash, K. H. Shelley, D. G. Silverman, and K. H. Chon, "Estimation of respiratory rate from ECG, photoplethysmogram, and piezoelectric pulse transducer Signals: A comparative study of time-frequency methods," *IEEE Trans. Biomed. Eng.*, vol. 57, no. 5, pp. 1099–1107, May 2010.

[252] P. S. Addison, J. N. Watson, M. L. Mestek, and R. S. Mecca, "Developing an algorithm for pulse oximetry derived respiratory rate (RRoxi): a healthy volunteer study," *J. Clin. Monit. Comput.*, vol. 26, no. 1, pp. 45–51, Jan. 2012.

[253] W. Karlen, S. Raman, J. M. Ansermino, and G. A. Dumont, "Multiparameter respiratory rate estimation from the photoplethysmogram," *IEEE Trans. Biomed. Eng.*, vol. 60, no. 7, pp. 1946–1953, Jul. 2013.

[254] D. Wertheim, C. Olden, L. Symes, H. Rabe, and P. Seddon, "Monitoring respiration in wheezy preschool children by pulse oximetry plethysmogram analysis," *Med. Biol. Eng. Comput.*, vol. 51, no. 9, pp. 965–970, Apr. 2013.

[255] W. Karlen, A. Garde, D. Myers, C. Scheffer, J. Ansermino, and G. Dumont, "Estimation of respiratory rate from photoplethysmographic imaging videos compared to pulse oximetry," *IEEE J. Biomed. Health. Inform.*, vol. 19, no. 4, pp. 1331–1338, 2015.

[256] M. Z. Poh, D. J. McDuff, and R. W. Picard, "Advancements in noncontact, multiparameter physiological measurements using a webcam," *IEEE Trans. Biomed. Eng.*, vol. 58, no. 1, pp. 7–11, Jan. 2011.

[257] S. Fallet, L. Mirmohamadsadeghi, V. Moser, F. Braun, and J. M. Vesin, "Real-time approaches for heart rate monitoring using imaging photoplethysmography," in *Computing in Cardiology*, Vancouver, BC, Canada, 2016.

[258] R. Vautard, P. Yiou, and M. Ghil, "Singular-spectrum analysis: A toolkit for short, noisy chaotic signals," *Physica D.*, vol. 58, no. 1-4, pp. 95–126, Sep. 1992.

[259] S. Sanei and H. Hassani, in *Singular Spectrum Analysis of Biomedical Signals*. CRC Press, 2015, ch. Singular Spectrum Analysis.

[260] R. Wang, H.-G. Ma, G.-Q. Liu, and D.-G. Zuo, "Selection of window length for singular spectrum analysis," *J. Franklin Inst.*, vol. 352, no. 4, pp. 1541–1560, Apr. 2015.

[261] R. Badeau, G. Richard, and B. David, "Sliding window adaptive SVD algorithms," *IEEE Trans. Signal Process.*, vol. 52, no. 1, pp. 1–10, Jan. 2004.

[262] R. L. Horner, D. Brooks, L. F. Kozar, K. Gan, and E. A. Phillipson, "Respiratory-related heart rate variability persists during central apnea in dogs: mechanisms and implications," *J Appl Physiol*, vol. 78, no. 6, pp. 2003–2013, June 1995.

[263] A. P. Prathosh, P. Praveena, L. K. Mestha, and S. Bharadwaj, "Estimation of respiratory pattern from video using selective ensemble aggregation," *arXiv preprint*, Nov. 2016.

[264] F. Braun, A. Lemkaddem, V. Moser, D. S., and O. Grossenbacher, "Camera-based respiration monitoring," in *"Dreiländertagung" Swiss, Austrian and German Societies for Biomedical Engineering*, Basel, Switzerland, Oct. 2016.

[265] M. van Gastel, S. Stuijk, and G. de Haan, "Robust respiration detection from remote photoplethysmography," *Biomed. Opt. Express*, vol. 7, no. 12, pp. 4941–4957, Dec 2016.

[266] F.-X. Gamelin, G. Baquet, S. Berthoin, and L. Bosquet, "Validity of the Polar S810 to measure R-R intervals in children," *Int. J. Sports Med.*, vol. 29, no. 2, pp. 134–138, Feb. 2008.

[267] D. Widjaja, C. Varon, D. Testelmans, B. Buyse, L. Faes, and S. V. Huffel, "Separating respiratory influences from the tachogram: Methods and their sensitivity to the type of respiratory signal," in *Computing in Cardiology (CinC)*, Sep. 2014, pp. 609–612.

[268] S. Tiinanen, M. Tulppo, and T. Seppänen, "RSA component extraction from heart rate signal by independent component analysis," in *Computing in Cardiology (CinC)*, Sep. 2009, pp. 161–164.

[269] R. Bailón, P. Laguna, L. Mainardi, and L. Sörnmo, "Analysis of heart rate variability using time-varying frequency bands based on respiratory frequency," in *29th Annual International Conference of the IEEE Engineering in Medicine and Biology Society*, Aug. 2007, pp. 6674–6677.

[270] H. G. Ma, R. Lei, X. Y. Kong, Z. Q. Liu, and Q. B. Jiang, "Determine a proper window length for singular spectrum analysis," in *IET International Conference on Radar Systems (Radar 2012)*, Oct. 2012, pp. 1–6.

[271] J. Harmouche, D. Fourer, F. Auger, P. Borgnat, and P. Flandrin, "Une ou deux composantes: la réponse de l'analyse spectrale singulière," in *GRETSI*, 2015.

[272] A. Guillén-Mandujano and S. Carrasco-Sosa, "Additive effect of simultaneously varying respiratory frequency and tidal volume on respiratory sinus arrhythmia," *Auton. Neurosci.*, vol. 186, pp. 69–76, Dec. 2014.

[273] J. Kim and E. André, "Emotion recognition based on physiological changes in music listening," *IEEE Trans. Pattern Anal. Mach. Intell.*, vol. 30, no. 12, pp. 2067–2083, Dec. 2008.

[274] A. Konar, A. Halder, and A. Chakraborty, *Introduction to Emotion Recognition*. John Wiley and Sons, Inc., 2015, pp. 1–45.

[275] A. Yazdani, "Brain-computer interface in multimedia systems," Ph.D. dissertation, Ecole Polytechnique Fédérale de Lausanne, 2012.

[276] S. Balters and M. Steinert, "Capturing emotion reactivity through physiology measurement as a foundation for affective engineering in engineering design science and engineering practices," *J. Intell. Manuf.*, pp. 1–23, Sep. 2015.

[277] L. Mirmohamadsadeghi, A. Yazdani, and J.-M. Vesin, "Using cardio-respiratory signals to recognize emotions elicited by watching music video clips," in *IEEE Workshop on Multimedia Signal Processing (MMSP 2016)*. IEEE, 2016.

[278] K. R. Scherer, "What are emotions? and how can they be measured?" *Soc. Sci. Inf.*, vol. 44, no. 4, pp. 695–729, Dec. 2005.

[279] J. Posner, J. A. Russel, and B. S. Peterson, "The circumplex model of affect: An integrative approach to affective neuroscience, cognitive development, and psychopathology," *Dev. Psychopathol.*, vol. 17, pp. 715–734, Sep. 2005.

[280] R. W. Levenson, "The autonomic nervous system and emotion," *Emot. Rev.*, vol. 6, no. 2, pp. 100–112, Apr. 2014.

[281] S. Koelstra, C. Muhl, M. Soleymani, J.-S. Lee, A. Yazdani, T. Ebrahimi, T. Pun, A. Nijholt, and I. Patras, "DEAP: A database for emotion analysis; using physiological signals," *IEEE Trans. Affective Comput.*, vol. 3, no. 1, pp. 18–31, Jan. 2012.

[282] R. Jenke, A. Peer, and M. Buss, "Feature extraction and selection for emotion recognition from EEG," *IEEE Trans. Affective Comput.*, vol. 5, no. 3, pp. 327–339, Jul. 2014.

[283] R. D. Lane, K. McRae, E. M. Reiman, K. Chen, G. L. Ahern, and J. F. Thayer, "Neural correlates of heart rate variability during emotion," *NeuroImage*, vol. 44, no. 1, pp. 213 – 222, Jan. 2009.

[284] S. D. Kreibig, "Autonomic nervous system activity in emotion: A review," *Biol. Psychol.*, vol. 84, no. 3, pp. 394–421, Jul. 2010.

[285] G. Valenza, L. Citi, A. Lanatá, E. P. Scilingo, and R. Barbieri, "Revealing real-time emotional responses: A personalized assessment based on heartbeat dynamics," *Sci. Rep.*, vol. 4, May 2014.

[286] F. Agrafioti, D. Hatzinakos, and A. Anderson, "ECG pattern analysis for emotion detection," *IEEE Trans. Affective Comput.*, vol. 3, no. 1, pp. 102–115, Jan. 2012.

[287] A. Goshvarpour, A. Abbasi, and A. Goshvarpour, "Affective visual stimuli: Characterization of the picture sequences impacts by means of nonlinear approaches," *Basic Clin. Neurosci.*, vol. 6, no. 4, pp. 209–222, Oct. 2015.

[288] C.-K. Wu, P.-C. Chung, and C.-J. Wang, "Representative segment-based emotion analysis and classification with automatic respiration signal segmentation," *IEEE Trans. Affective Comput.*, vol. 3, no. 4, pp. 482–495, Jun. 2012.

[289] G. Valenza, A. Lanatá, and E. P. Scilingo, "Improving emotion recognition systems by embedding cardiorespiratory coupling," *Physiol. Meas.*, vol. 34, no. 4, p. 449, Mar. 2013.

[290] A. Betella, R. Zucca, R. Cetnarski, A. Greco, A. Lanatá, D. Mazzei, A. Tognetti, X. D. Arsiwalla, P. Omedas, D. De Rossi, and P. F. M. J. Verschure, "Inference of human affective states from psychophysiological measurements extracted under ecologically valid conditions," *Front. Neurosci.*, vol. 8, p. 286, Sep. 2014.

[291] W. Wen, G. Liu, N. Cheng, J. Wei, P. Shangguan, and W. Huang, "Emotion recognition based on multi-variant correlation of physiological signals," *IEEE Trans. Affective Comput.*, vol. 5, no. 2, pp. 126–140, Apr. 2014.

[292] B. Whitman, "How music recommendation works- and doesn't work," 2012. [Online]. Available: http://notes.variogr.am/

[293] L. Mirmohamadsadeghi, S. Fallet, A. Buttu, J. Saugy, T. Rupp, R. Heinzer, J.-M. Vesin, and G. P. Millet, "Sleep apnea detection using features from the respiration and the ECG recorded with smart-shirts," in *IEEE Biomedical Circuits and Systems (BioCAS) Proceedings*, Oct. 2014, pp. 61–64.

[294] S. R. Pandi-Perumal and D. Leger, *Sleep Disorders: Their Impact on Public Health*. Taylor & Francis, 2006.

[295] A. A. of Sleep Medicine Task Force, "Sleep-related breathing disorders in adults: Recommendations for syndrome definition and measurement techniques in clinical research. editorials," *Sleep*, vol. 22, no. 5, pp. 662–689, Aug. 1999.

[296] A. M. Bianchi, M. O. Mendez, and S. Cerutti, "Processing of signals recorded through smart devices: Sleep-quality assessment," *IEEE Trans. Inf. Technol. Biomed.*, vol. 14, no. 3, pp. 741–747, May 2010.

[297] M. Bsoul, H. Minn, and L. Tamil, "Apnea MedAssist: Real-time sleep apnea monitor using single-lead ECG," *IEEE Trans. Inf. Technol. Biomed.*, vol. 15, no. 3, pp. 416–427, May 2011.

[298] Y. W. Tu, X. M. Yu, H. Chen, and S. M. Ye, "A novel method for the detection of sleep apnea syndrome based on single-lead ECG signal," *Appl. Mech. Mater.*, vol. 239, pp. 1079–1083, 2013.

[299] B. Koley and D. Dey, "Real-time adaptive apnea and hypopnea event detection methodology for portable sleep apnea monitoring devices," *IEEE Trans. Biomed. Eng.*, vol. 60, no. 12, pp. 3354–3363, Dec. 2013.

[300] Y. Ichimaru and G. Moody, "Development of the polysomnographic database on CD-ROM," *Psychiatry Clin. Neurosci.*, vol. 53, no. 2, pp. 175–177, Apr. 1999.

[301] "St. vincent's university hospital / university college dublin sleep apnea database," https://physionet.org/physiobank/database/ucddb/.

[302] A. Salvaggio, G. Insalaco, O. Marrone, S. Romano, A. Braghiroli, P. Lanfranchi, V. Patruno, D. C.F., and G. Bonsignore, "Effects of high-altitude periodic breathing on sleep and arterial oxyhaemoglobin saturation," *Euro. Respiratory J.*, vol. 12, pp. 408–413, 1998.

[303] L. Poupard, M. Mathieu, M. Goldman, F. Chouchou, and F. Roche, "Multi-modal ECG holter system for sleep-disordered breathing screening," *Sleep Breath.*, vol. 16, pp. 685–693, Sep. 2012.

[304] G. Menardi and N. Torelli, "Training and assessing classification rules with imbalanced data," *Data Min. Knowl. Discov.*, vol. 28, no. 1, pp. 92–122, Jan. 2014.

[305] H. J. Burgess, J. Trinder, Y. Kim, and D. Luke, "Sleep and circadian influences on cardiac autonomic nervous system activity," *Am. J. Physiol. Heart. Circ. Physiol.*, vol. 273, no. 4, pp. 1761–1768, Oct. 1997.

[306] A. Domingues, T. Paiva, and J. M. Sanches, "Hypnogram and sleep parameter computation from activity and cardiovascular data," *IEEE Trans. Biomed. Eng.*, vol. 61, no. 6, pp. 1711–1719, Jun. 2014.

[307] Y. Prudat, "Adaptive frequency tracking and application to biomedical signals," Ph.D. dissertation, Ecole Polytechnique Fédérale de Lausanne, 2009.

[308] J. Van Zaen, "Efficient schemes for adaptive frequency tracking and their relevance for EEG and ECG," Ph.D. dissertation, Ecole Polytechnique Fédérale de Lausanne, 2012.

[309] M. Rahmati, M. S. Sadri, and M. A. Naeini, "FPGA based singular value decomposition for image processing applications," in *Proceedings of the 2008 International Conference on Application-Specific Systems, Architectures and Processors*, ser. ASAP '08, 2008, pp. 185–190.

Leila Mirmohamadsadeghi

Birth date : 08.05.1988
Nationality : Swiss/Iranian
leila.mirmo(at)gmail.com

Education

Ecole Polytechnique Fédérale de Lausanne (EPFL), Lausanne, Switzerland
2017   Ph.D. in Electrical Engineering focused in biomedical signal processing.
Thesis: *Signal processing approaches for cardio-respiratory biosignals with an emphasis on mobile health applications.*

EPFL
2011   Master of Science in Electrical and Electronics Engineering.
Major: Information technology, Minor: Space technologies.
Thesis: *Feature extraction and classification for palm vein recognition.*

EPFL
2009   Bachelor of Science in Electrical and Electronics Engineering.
One year exchange abroad: Iowa State University, Ames, IA, USA.

Bent-ol-Hoda High school, Saveh, Iran
2005   High school diploma in mathematics and physics.

Main Experience

Ferring Pharmaceuticals, Saint-Prex, Switzerland
2017-pr   Junior Medical Scientist Gastroenterology- Global Medical Affairs

Ferring Pharmaceuticals, Saint-Prex, Switzerland
2016-17   Intern- Global Medical Affairs

Applied Signal Processing Group, EPFL
2013-16   Researcher, teaching assistant for master-level courses

LIDIAP laboratory, EPFL
2011-13   Researcher

Laboratory for computer communications and applications, EPFL
2010   Intern

Other experience

2011-pr.   **State of Vaud, Switzerland**: French/Persian translator/interpreter for the police and justice departments.

2014-16. **EPFL astronomy club Callista:** Secretary, link with school administration, event organization.

2011 **Forum EPFL**: hospitality staff.

2010-11 **EPFL**: teaching-assistant for bachelor-level courses.

2009 **Department of World Languages and Cultures, Iowa State University**: Tutor for French classes.

2007 **EPFL yearbook:** member, took photos and made layouts.

Languages

English: mother tongue.

French: fluent (C1, written and spoken).

Persian: father tongue, school.

German: intermediate beginner (A2/B1, written and spoken).

Awards

Finalist in the EPFL "My Thesis in 180 seconds", Lausanne, Switzerland, Oct. 2016

First place in the Nano-Tera "My Thesis in 180 seconds", Lausanne, Switzerland, Apr. 2016.

Best poster award at the computing in cardiology conference, Boston, USA, Sep. 2014

Best student paper award at the International congress on electrophysiology, Bratislava, Slovakia, Jun. 2014.

Best EPFL Human and Social Sciences project award, Switzerland, Jul. 2011.

Computer skills

LaTex, Office, Matlab/Python, C++, JAVA, Adobe Photoshop/Indesign.

Hobbies

Pottery, Astronomy, Travelling, Ultimate Frisbee.

Publications

Journal Papers

L. Mirmohamadsadeghi, and J.-M. Vesin, "Respiratory rate estimation from the ECG using an instantaneous frequency tracking algorithm," *Biomedical Signal Processing and Control*, vol. 14 no 0, pp. 66–72, 2014

L. Mirmohamadsadeghi, and J.-M. Vesin, "Real-time multi-signal frequency tracking with a bank of notch filters to estimate the respiratory rate from the ECG," *Physiological Measurement*, vol. 37 no 9, pp. 1573–1787, 2016

L. Mirmohamadsadeghi, N. Bourdillon, G. P. Millet, and J.-M. Vesin, "Identification and removal of the respiratory influence from the heart inter-beat intervals without using a reference respiration signal," *in preparation to be submitted to Medical & Biological Engineering & Computing*.

Conference Papers

L. Mirmohamadsadeghi, N. Bourdillon, G. P. Millet, and J.-M. Vesin, "Cardio-respiratory characterization of the autonomic balance," *Computing in Cardiology (CinC)*, Vancouver, BC, Canada, September 2016.

L. Mirmohamadsadeghi, S. Fallet, V. Moser, F. Braun, and J.-M. Vesin, "Real-Time Respiratory Rate Estimation using Imaging Photoplethysmography Inter-Beat Intervals," *Computing in Cardiology (CinC)*, Vancouver, BC, Canada, September 2016.

S. Fallet, L. Mirmohamadsadeghi, V. Moser, F. Braun, and J.-M. Vesin, "Real-time approaches for heart rate monitoring using imaging photoplethysmography," *Computing in Cardiology (CinC)*, Vancouver, BC, Canada, September 2016.

J.-M. Vesin, S. Yazdani, L. Mirmohamadsadeghi and N. Bourdillon, "Extraction and Analysis of Short-Time Excursion in RR-interval Time Series," *Computing in Cardiology (CinC)*, Vancouver, BC, Canada, September 2016.

L. Mirmohamadsadeghi, A. Yazdani, and J.-M. Vesin, "Using Cardio-Respiratory Signals to Recognize Emotions Elicited by Watching Music Video Clips," *IEEE Workshop on Multimedia*

Signal Processing (MMSP), Montreal, QC, Canada, September 2016.

L. Mirmohamadsadeghi, and J.-M. Vesin, "Estimating the real-time respiratory rate from the ECG with a bank of notch filters," *Computing in Cardiology (CinC)*, Nice, France, September 2015.

L. Mirmohamadsadeghi, J.-M. Vesin, M. Lemay and O. Dériaz, "The respiration pattern as an indicator of the anaerobic threshold," *37th Annual International Conference of the IEEE Engineering in Medicine and Biology Society (EMBC)*, Milan, Italy, August 2015.

L. Mirmohamadsadeghi, S. Fallet, A. Buttu, J. Saugy, T. Rupp, R. Heinzer, J.-M. Vesin, and G. P. Millet, "Sleep apnea detection using features from the respiration and the ECG recorded with smart-shirts," *IEEE Biomedical Circuits and Systems Conference (BioCAS)*, Lausanne, Switzerland, October 2014.

L. Mirmohamadsadeghi, and J.-M. Vesin, "Respiratory Rate Estimation from Multi-Lead ECGs using an Adaptive Frequency Tracking Algorithm," *Computing in Cardiology (CinC)*, Boston, MA, USA, September 2014.

L. Mirmohamadsadeghi, and J.-M. Vesin, "Respiratory rate simultaneous estimation from two ECG-derived respiratory waveforms using an adaptive frequency tracking algorithm," *International Congress on Electrocardiology*, Bratislava, Slovakia, June 2014.